



National and Kapodistrian University of Athens
School of Science
Faculty of Geology and Geoenvironment
Department of Geophysics -Geothermics

**Evaluation Of The Nature Of Seismogenetic Systems Along
The North-Western Rim Of The Circum-Pacific Belt, Based
On (Non-Extensive) Statistical Physics And Complexity
Science Methods**

Master Thesis

Evangelia K. Tripoliti

Athens, 2017

ΕΘΝΙΚΟ ΚΑΙ ΚΑΠΟΔΙΣΤΡΙΑΚΟ ΠΑΝΕΠΙΣΤΗΜΙΟ ΑΘΗΝΩΝ



**ΣΧΟΛΗ ΘΕΤΙΚΩΝ ΕΠΙΣΤΗΜΩΝ
ΤΜΗΜΑ ΓΕΩΛΟΓΙΑΣ ΚΑΙ ΓΕΩΠΕΡΙΒΑΛΛΟΝΤΟΣ
ΤΟΜΕΑΣ ΓΕΩΦΥΣΙΚΗΣ ΓΕΩΘΕΡΜΙΑΣ**

**ΜΕΛΕΤΗ ΤΩΝ ΣΕΙΣΜΟΤΕΚΤΟΝΙΚΩΝ ΧΑΡΑΚΤΗΡΙΣΤΙΚΩΝ
ΣΤΗΝ ΠΕΡΙΟΧΗ ΤΗΣ ΒΔ ΠΕΡΙ-ΕΙΡΗΝΙΚΗΣ ΖΩΝΗΣ ΜΕ
ΜΕΘΟΔΟΥΣ ΜΗ-ΕΚΤΑΤΙΚΗΣ ΣΤΑΤΙΣΤΙΚΗΣ ΦΥΣΙΚΗΣ.**

ΜΕΤΑΠΤΥΧΙΑΚΗ ΔΙΑΤΡΙΒΗ ΕΙΔΙΚΕΥΣΗΣ

ΕΥΑΓΓΕΛΙΑ Κ. ΤΡΙΠΟΛΙΤΗ

A.M: 21420

**ΑΝΔΡΕΑΣ ΤΖΑΝΗΣ, ΑΝΑΠΛΗΡΩΤΗΣ ΚΑΘΗΓΗΤΗΣ (ΕΠΒΛΕΠΩΝ)
ΝΙΚΟΛΑΟΣ ΒΟΥΛΓΑΡΗΣ, ΚΑΘΗΓΗΤΗΣ
ΦΙΛΙΠΠΟΣ ΒΑΛΛΙΑΝΑΤΟΣ, ΚΑΘΗΓΗΤΗΣ**

**ΙΟΥΝΙΟΣ, 2017
ΑΘΗΝΑ**

ΔΗΛΩΣΗ ΠΕΡΙ ΜΗ ΠΡΟΣΒΟΛΗΣ ΠΝΕΥΜΑΤΙΚΗΣ ΙΔΙΟΚΤΗΣΙΑΣ

Προσβολή πνευματικής ιδιοκτησίας θεωρείται η ολική ή η μερική αναπαραγωγή του έργου άλλου προσώπου ή η παρουσίαση του έργου κάποιου άλλου ως προσωπικού του γράφοντος. Το Τμήμα Γεωλογίας και Γεωπεριβάλλοντος λαμβάνει πολύ σοβαρά υπόψη και καταδικάζει την προσφυγή σε τέτοιου είδους πρακτικές από τους Μεταπτυχιακούς Φοιτητές. Σε περιπτώσεις πρόδηλης ή εκ προθέσεως προσβολής πνευματικής ιδιοκτησίας, τα αρμόδια όργανα του Τμήματος δύνανται να επιβάλουν ως κύρωση έως και την οριστική διαγραφή από το ΠΜΣ. Κατά την εκπόνηση Διπλωματικής Εργασίας Ειδίκευσης οι Μεταπτυχιακοί Φοιτητές οφείλουν να τηρούν τις ακόλουθες κατευθυντήριες οδηγίες:

1. Η Διπλωματική Εργασία Ειδίκευσης πρέπει να αποτελεί έργο του υποβάλλοντος αυτήν φοιτητή.
2. Η αντιγραφή ή η παράφραση έργου τρίτου προσώπου αποτελεί προσβολή πνευματικής ιδιοκτησίας και συνιστά σοβαρό αδίκημα. Στο αδίκημα αυτό περιλαμβάνεται τόσο η προσβολή πνευματικής ιδιοκτησίας άλλου φοιτητή όσο και η αντιγραφή από δημοσιευμένες πηγές, όπως βιβλία, εισηγήσεις ή επιστημονικά άρθρα. Το υλικό που συνιστά αντικείμενο λογοκλοπής μπορεί να προέρχεται από οποιαδήποτε πηγή. Η αντιγραφή ή χρήση υλικού προερχόμενου από το διαδίκτυο ή από ηλεκτρονική εγκυκλοπαίδεια είναι εξίσου σοβαρή με τη χρήση υλικού προερχόμενου από τυπωμένη πηγή ή βάση δεδομένων.
3. Η χρήση αποσπασμάτων από το έργο τρίτων είναι αποδεκτή εφόσον, αναφέρεται η πηγή του σχετικού αποσπάσματος. Σε περίπτωση αυτολεξεί μεταφοράς αποσπάσματος από το έργο άλλου, η χρήση εισαγωγικών ή σχετικής υποσημείωσης είναι απαραίτητη, ούτως ώστε η πηγή του αποσπάσματος να αναγνωρίζεται.
4. Η παράφραση κειμένου, αποτελεί προσβολή πνευματικής ιδιοκτησίας.
5. Οι πηγές των αποσπασμάτων που χρησιμοποιούνται θα πρέπει να καταγράφονται πλήρως σε πίνακα βιβλιογραφίας στο τέλος της εργασίας.
6. Η προσβολή πνευματικής ιδιοκτησίας επισύρει την επιβολή κυρώσεων. Κατά την απόφαση επί των ενδεδειγμένων κυρώσεων, τα αρμόδια όργανα του Τμήματος θα λαμβάνουν υπόψη παράγοντες όπως το εύρος και το μέγεθος του τμήματος της εργασίας που οφείλεται σε προσβολή πνευματικής ιδιοκτησίας. Οι κυρώσεις θα επιβάλλονται σύμφωνα με το Άρθρο 7 Παράγραφος 7 του Κανονισμού Σπουδών.

Βεβαιώνω ότι η Διπλωματική Εργασία Ειδίκευσης, την οποία υποβάλλω, δεν περιλαμβάνει στοιχεία προσβολής πνευματικής ιδιοκτησίας, όπως αυτά προσδιορίζονται από την παραπάνω δήλωση, τους όρους της οποίας διάβασα και αποδέχομαι.

Παρέχω τη συναίνεσή μου, ώστε ένα ηλεκτρονικό αντίγραφο της διπλωματικής εργασίας μου να υποβληθεί σε ηλεκτρονικό έλεγχο για τον εντοπισμό τυχόν στοιχείων προσβολής πνευματικής ιδιοκτησίας.

20/06/2017

Τριπολίτη Ευαγγελία

ACKNOWLEDGEMENT

I would first like to thank my thesis advisor Associate Professor Andreas Tzanis of the Faculty of Geology-Department of Geophysics-of the National and Kapodistrian University of Athens, for his advice, guidance and support throughout this work, who steered me in the right direction whenever he thought I needed it. I would also like to thank the members of my Master's committee, Professor Nikolaos Voulgaris of the Faculty of Geology-Department of Geophysics-of the National and Kapodistrian University of Athens, and Professor Filippos Vallianatos of the School of Natural Resources & Environment, Department of Geoenvironment-Laboratory of Geophysics & Seismology- of the Technological Educational Institute of Crete. Many thanks, to the PhD candidate Ageliki Efstathiou for her advice and help.

I want to express my very profound gratitude to my parents, my sister and my brother for providing me with unfailing support and continuous encouragement throughout my years of studies (undergraduate and graduate). This accomplishment would not have been possible without them. Thank you for making this possible.

ABSTRACT

The Thesis examines the nature of seismogenetic systems along the north-western rim of the Circum-Pacific belt by searching for evidence of complexity and non-extensivity in the earthquake record. The objective is to determine whether earthquakes are generated by a self-excited Poisson process, in which case they obey Boltzmann-Gibbs thermodynamics, or by a Critical process, in which long-range interactions in non-equilibrium states are expected (correlation) and the thermodynamics deviate from the Boltzmann-Gibbs formalism. Emphasis is given to background seismicity since it is generally agreed that aftershock sequences comprise correlated sets. Because the study area features convergent plate boundaries that include both crustal (in the lithosphere), and *sub-crustal* (in the Wadati-Benioff zones) earthquakes, the analysis was carried out by roughly separating *crustal* and *sub-crustal* seismicity according to the depth of the Mohorovičić discontinuity, in an attempt to inquire whether environmental conditions (e.g. temperature, pressure), or/and boundary conditions (free at the surface vs. fixed at depth), affect the dynamic expression and evolution of seismogenetic fault networks.

The analysis uses the complete and homogeneous Unified Seismic Catalogue of Japan, obtained from the earthquake data used in the study span the time period 1/1/2002 – 31/5/2016 and was provided by the National Research Institute for Earth Science and Disaster Resilience, the Japan Meteorological Agency, Hokkaido University, Hirosaki University, Tohoku University, the University of Tokyo, Nagoya University, Kyoto University, Kochi University, Kyushu University, Kagoshima University, the National Institute of Advanced Industrial Science and Technology, the Geographical Survey Institute, Tokyo Metropolis, Shizuoka Prefecture, Hot Springs Research Institute of Kanagawa Prefecture, Yokohama City, and Japan Agency for Marine-Earth Science and Technology. The earthquake catalogue is available in the website of the *National Research Institute for Earth Sciences and Disaster Prevention* (NIED). The analysis examined *multivariate* cumulative frequency distributions of earthquake magnitude, interevent time and interevent distance in the context of Non-Extensive Statistical Physics, which is a generalization of extensive Boltzmann-Gibbs thermodynamics to non-equilibrating (non-extensive) systems. It follows that the results are obtained through a physics-based approach and *not* through any type of model-based (or model-driven) consideration, as usually is the case in earthquake statistical studies. The analysis was applied to different catalogue realizations in which aftershocks were either included, or had been removed by a stochastic declustering procedure.

The results provide evidence that in the seismogenetic systems of the NW Circum-Pacific belt, background seismicity is complex sub-extensive of nature, although it exhibits significant differences between systems (plates): Complexity is certainly prominent in the Okhotsk and Pacific plates and definitely less evident in the Eurasia and Philippine plates where the systems appear to verge on randomness. In the Okhotsk and Pacific plates background seismicity exhibits strong long-range interaction as evident by the overall high correlation observed in highly declustered catalogues and, primarily, in the long-range interaction observed in earthquake groups separated by long interevent distances. The increase in the level of complexity after declustering can be neatly explained by the exposition of long range interactions after curtailing the effect of short-range interactions associated with aftershock sequences. It is also highly probable –but was not be investigated herein– that the elevated

complexity (sub-extensivity) of the Okhotsk and Pacific seismicity is closely related to the 2011 M9 Tohoku mega-earthquake, whose preparation phase and aftermath has organized the seismogenetic systems over long ranges.

Criticality is a likely explanation for the complexity observed in the background seismicity of Okhotsk and Pacific plates, inasmuch as power-laws and long-range interaction are its hallmarks. However, the question is still very far from having been answered as there may be alternative (albeit less likely) mechanisms by which complexity and power-laws may arise. It is therefore clear that additional work is required before the complexity mechanism of background seismicity can be proposed with confidence.

TABLE OF CONTENTS

ACKNOWLEDGEMENT	3
ABSTRACT	4
INTRODUCTION	ERROR! BOOKMARK NOT DEFINED.
1. STATISTICAL PHYSICS AND COMPLEXITY- REVIEW	8
1.1 EARTHQUAKE STATISTICS	14
1.1.1 THE STANDARD PARADIGM: SEISMOGENESIS AS A RANDOM (POINT) PROCESS	14
1.1.2 THE EMERGENT PARADIGM: SEISMOGENESIS AND SELF-ORGANIZED CRITICALITY	15
1.2. THE STATNDARD VS THE EMERGENT PARADIGMS	19
1.3 STATISTICAL PHYSICS – AN OVERVIEW	20
1.3.1 ADDITIVE OR EXTENSIVE STATISTICAL PHYSICS (BOLTZMANN-GIBBS)	20
1.3.2 NON – EXTENSIVITY	20
1.3.2. i. Non-additive or non-extensive statistical physics (Tsallis)	20
1.3.2. ii. The q-exponential distribution	22
1.3.2. iii. The q-gaussian distribution	23
1.3.3 NON-EXTENSIVITY AND SEISMOLOGY	24
2. METHODOLOGY AND DATA ANALYSIS PROCEDURES	26
2.1 OVERVIEW	26
2.2 BIVARIATE FREQUENCY-MAGNITUDE-INTEREVENT TIME DISTRIBUTIONS: CONSTRUCTION	28
2.3 IMPLEMENTATION	30
2.4 MOHOROVICIÇ DISCONTINUITY	33
2.5 DECLUSTERING	35
3. GEOLOGY AND SEISMICITY OF THE STUDY AREA	37
3.1 GEOLOGY AND TECTONICS OF THE STUDY AREA	37
3.2 SEISMIC NETWORK AND EARTHQUAKE MONITORING	41
3.2.1 HYPOCENTER DETERMINATION	43
3.2.2 MAGNITUDE DETERMINATION	44
3.3 EARTHQUAKE CATALOGUE	45
3.3.1 CATALOGUE DECLUSTERING	51
4. DETERMINATION AND ANALYSIS OF ENTROPIC INDICES FOR RAW AND DECLUSTERED CATALOGUES AND B – VALUE ANALYSIS	55

4.1 RAW CATALOGUE ANALYSIS	55
4.1.1 EURASIAN PLATE.	55
4.1.2. OKHOTSK PLATE	58
4.1.3. PACIFIC PLATE	64
4.1.4. PHILIPPINE PLATE	66
4.2 DECLUSTERED CATALOGUE ANALYSIS	68
4.2.1 EURASIA PLATE	68
4.2.2 OKHOTSK PLATE	73
4.2.3 PACIFIC PLATE	78
4.2.4 PHILIPPINE PLATE	80
4.3 B-VALUE ANALYSIS	83
4.3.1 EURASIAN PLATE.	84
4.3.2 OKHOTSK PLATE.	86
4.3.3 PACIFIC PLATE.	89
4.3.4 PHILIPPINE PLATE.	89
<u>5. TIME DEPENDENCE OF ENTROPIC INDICES VARIATIONS AND B-VALUES</u>	<u>91</u>
5.1 EURASIAN PLATE	91
5.2 OKHOTSK PLATE.	95
5.3 PACIFIC PLATE.	98
5.4 PHILIPPINE PLATE.	100
<u>6 .DISCUSION AND CONCLUSIONS</u>	<u>104</u>
<u>BIBLIOGRAPHY</u>	<u>112</u>

INTRODUCTION

At a given active fault system (seismogenetic area), the observed seismicity consists of a *background process* that expresses the continuum of tectonic deformation, draped by a large population of prolific short-term activity in the form of earthquake swarms, clusters and aftershock sequences (*foreground process*). Although, progress has been made towards understanding the foreground process using statistical methods (statistical seismology), the statistical physics of background seismicity, hence the way in which seismicity and tectonic deformation evolve, has not been clarified with significant repercussions on problems pertaining to hazard analysis and long-term forecasting.

The development of theoretical and empirical models that combine the statistics or/and physics of seismogenesis has led to two general viewpoints regarding the nature of background seismicity. The first and presently more influential postulates that the background process is Poissonian in time and space (point process), ergo consistent with Boltzmann-Gibbs thermodynamics. The second posits that seismogenesis is a complex process that involves some form of criticality, (e.g. stationary or self-organized vs. evolutionary or self-organizing), although non-critical models which maintain the seismogenetic system in a perennial state of non-equilibrium have also been proposed.

The primary example of the “Poissonian viewpoint” is the ETAS model (Episodic Type Aftershock Sequence) introduced by Ogata (1988, 1998); for additional information see Zhuang et al, (2002), Helmstetter and Sornette, (2003), Touati et al, (2009); Segou et al, (2013). This is an empirical construct based on the self-excited conditional Poisson process (Hawkes, 1972; Hawkes and Adamopoulos, 1973; Hawkes and Oakes, 1974). The Poissonian viewpoint rests on the assumption that background earthquakes are statistically independent and that their individual occurrence does not contribute to the evolution of seismicity (memoryless process). According to ETAS for instance, *random* background events trigger aftershock sequences in which aftershocks trigger their own sub-sequences thus leading to short-term spatiotemporal clustering of multiple generations of foreground events whose overall time dependence is described by a power law known as the Omori-Utsu law of aftershocks (e.g. Utsu et al., 1995). It is also important to note that the Poissonian view of seismicity is mainly concerned with the statistics of time and distance between earthquakes; the size (magnitude) distribution of both background and foreground processes is still thought to be governed by the time-honoured frequency–magnitude (F-M) relationship of Gutenberg and Richter. The assumptions on which ETAS is based cause it to exhibit *significant internal inconsistencies*: the Omori-Utsu and Gutenberg-Richter laws are *power-law distributions* that *cannot* be derived from the Boltzmann-Gibbs formalism. Point process models have also been developed to address the problem of intermediate to long-term clustering such as the EEPAS (Each Earthquake is a Precursor According to Scale, e.g. Rhoades, 2007) and the PPE (Proximity to Past Earthquakes, e.g. Marzocchi and Lombardi, 2008).

The “Complexity viewpoint” is also model-driven. A well-studied class of models (Bak and Tang, 1989; Sornette and Sornette, 1989; Olami et al., 1992; Bak et al., 2002; Bakar and Tirnakli, 2009; many others) suggests that seismicity expresses a non-equilibrating fractal fault system that continuously evolves toward a *stationary* critical condition with no characteristic

spatiotemporal scale (Self Organized Criticality – SOC). In this view, all earthquakes belong to, or evolve towards the same global population and participate in forming a non-equilibrium state in which events develop spontaneously and any small instability has a finite probability of escalating into a large earthquake. A second class of models which have been rather influential during the late 1990's and early 2000's, suggest that the evolution of seismicity prior to large events expresses a Critical Point (or Self-Organizing Critical) process (e.g. Sornette and Sammis, 1995; Rundle et al., 2000; Sammis and Sornette, 2001; many others). In this view, a large earthquake terminates a cycle by moving parts of its associated fault network out of the critical state. Once this happens, a new cycle begins as tectonic loading and stress transfer re-establish long-range stress correlation and produce acceleration of energy release rates in a power-law fashion. The next large event is possible when the network has reached a critical state in which highly stressed patches are correlated at the scale of the network so that local events can grow by rupturing through geometrical and rheological barriers. Complex critical systems evolving in a fractal-like space-time are characterized by long-range interaction and long-term memory (*correlation*) which should be evident as power-law distributions of the collective behaviour of energy release, temporal dependence and spatial dependence.

In addition to the SOC/CP models, alternative complexity mechanisms have been proposed, that do not involve criticality yet maintain the fault network in a state of non-equilibrium: a useful discussion can be found in Sornette and Werner (2009). In exploring the possibility of external stresses acting coherently onto all elements of a fault network without having any direct interaction with them, Celikoglu et al. (2010) applied the Coherent Noise Model of Newman (1996) and found that it generates power-law interevent time distributions. A weak point in this model is that it does not include some geometric configuration of the faults and it is not known how this would affect the behaviour of the network. In another example, Mignan (2008) formulated the “non-critical Precursory Accelerating Seismicity Theory”, which behaves just like a CP process; in this context, stress correlation is a result of stress shadow shrinking by top-down tectonic loading as part of a large-scale preparation process and not by scaling-up (or bottom-up triggering) as predicted by the CP theory.

Both Poissonian and Criticality viewpoints agree that foreground processes (swarms, aftershock sequences) comprise sets of dependent events, but the former assigns only local significance to this dependence whereas the latter considers them to be an integral part of the seismogenetic process. Besides theory, the practical fundamental difference between the Poissonian and Criticality viewpoints is their understanding of the background process. The former implicitly assumes that there is no correlation (interaction) between background events, meaning that the statistical description of parameters pertaining to their temporal and spatial evolution should be consistent with Boltzmann-Gibbs thermodynamics. The latter requires short and long-range interactions (correlation) in a non-equilibrium state, between background/background, background/foreground and foreground/foreground events that induce power-law behaviour with long (fat) tails on the statistical distributions of the parameters relevant to its temporal and spatial evolution. Moreover, non-critical complexity models cannot develop power-law distributions unless they evolve in non-equilibrium states, meaning even in this case, correlations between the elements of the fault system are unavoidable.

A natural conclusion of the above discussion is that if it would be possible to identify and remove the foreground process (aftershocks), it might also be possible to inquire the properties of the background process by examining its spatiotemporal characteristics for the existence of correlation. It should be apparent that in order to successfully carry out this inquiry one must have: **a)** a self-consistent theoretical context to serve as a *natural* (and not model-based) general basis on which to search for the existence of correlation; **b)** effective measures of correlation in the temporal and spatial expression of seismicity and, finally, **c)** effective ways to distinguish between the background and foreground processes. As it turns out, there are satisfactory (or nearly satisfactory) answers to all three prerequisites, as will be discussed below.

The Boltzmann-Gibbs (BG) formalism of thermodynamics *cannot* satisfy the first requirement. The cardinal property of BG entropy is *additivity (extensivity)*, namely proportionality with the number of elements of the thermodynamic system. BG entropy satisfies this prescription if the elements are statistically (quasi)independent, or typically if the correlations within the system are generically local. This, in turn, leads to the fundamental notion of *ergodicity*, which means that the long-term average and ensemble average of physical parameters are identical (the expectation value of the parameter is time-invariant). However, if a system is out of equilibrium, or if its component states are strongly interdependent, additivity and ergodicity break down and the BG formalism can no longer serve as a basis of appropriate and viable statistical descriptions of its parameters. As noted by Abe et al. (2005), the concept of ergodicity does not apply to seismicity due to the absence of the notion of ensemble. As also noted above, the Omori-Utsu and Gutenberg-Richter laws are power-law distributions strongly indicative of non-equilibrium in active fault networks.

The emergence of Non-Extensive Statistical Physics (NESP) has provided a theoretical framework appropriate for the study of *non-additive* (non-equilibrating) physical and natural systems. NESP has been developed by Tsallis (1988, 2009) as a generalization of the BG formalism and is suitable for the analysis of complexity evolving in a fractal-like space-time and exhibiting scale invariance, long-range interactions and long-term memory (e.g. Gell'mann and Tsallis, 2004). NESP predicts power-law cumulative probability distributions for non-additive (non-extensive) dynamic systems, which reduce to the exponential cumulative distribution in the limiting case of additive (extensive/random/point) processes. NESP has been applied to the statistical description of earthquake occurrence with notable results; for details see Chapter 1.3.3). Very importantly, NESP has been shown to generate the Gutenberg-Richter frequency-magnitude distribution from first principles (e.g. Sotolongo-Costa and Posadas, 2004; Silva, 2006; Telesca, 2011, 2012). Thus, NESP provides a general, complete, consistent and *model-independent* theoretical context in which to investigate the nature and dynamics of the background and foreground seismogenetic processes.

With respect to the second requirement above, a definite indicator of correlation (interaction) between faults in a network is the lapse between consecutive earthquakes above a magnitude threshold and over a given area: this is variably called *interevent time*, *waiting time*, *calm time*, or *recurrence time*. The properties (statistics) of the earthquake frequency – interevent time (F-T) distributions are key to understanding the dynamics of seismogenetic systems. Accordingly, they have been studied by several researchers. The empirical F-T distributions generally

exhibit power-law behaviour and in the context of Statistical Seismology they have been investigated with standard tailed statistical models reducible to power laws in some way. Examples of such models are the gamma distribution and the Weibull distribution (e.g. Bak et al., 2002; Davidsen and Gold, 2004; Corral, 2004; Martinez et al., 2005; Talbi and Yamazaki, 2010). Corral (2004) has applied the gamma distribution and has suggested universality analogous to the Gutenberg–Richter F-M distribution. This has been refuted by other investigators, some of whom proposed *ad hoc* mechanisms for the generation of *apparent* power laws by combination of correlated foreground and uncorrelated background processes (e.g. Saichev and Sornette, 2013; Hainzl et al., 2006; Touati et al., 2009). Molchan (2005) has shown that for a stationary point process, if there is a universal distribution of interevent times, then it must be exponential! Investigations performed in the context of Non Extensive Statistical Physics will be reviewed in 1.3.3. It is also important to note that almost all hitherto studies have generally focused on the mixed background/foreground processes and not on the background process independently. An analogous measure of fault interaction is the *hypocentral distance* between consecutive earthquakes, above a magnitude threshold and over a given area (*interevent distance*). The statistical properties of the earthquake frequency – interevent distance (F-D) distributions should be related to the *range of interaction* over that area. Unfortunately, with only a few known attempts to investigate it, (e.g. Eneva and Pavlis, 1991; Abe and Suzuki, 2003; Batac and Kantz, 2014; Shoenball et al., 2015), the statistics of F-D distributions is rather inadequately understood. Finally, a common criterion of scaling in earthquake size is the Gutenberg–Richter F-M distribution which expresses the scale-free hierarchical grading of a fractal active fault system. The F-M distribution is *static* and does not say anything about correlation in energy release, since it does not relate the energy released by an earthquake to the energy released by its preceding and following events. Nevertheless, it is undisputable and may serve as a standard by which to compare physical and statistical descriptions of the relationship between earthquake size and frequency.

With respect to the third requirement above, the discrimination between background and foreground processes is commonly referred to as *declustering*. In Statistical Seismology, a background event is one that has not been induced (or triggered) by a preceding event and is purely an effect of tectonic loading. The discrimination between foreground (dependent) and background events is based on their spatiotemporal proximity to preceding earthquakes on the fact that they occur at rates higher than the long-term average (background) seismicity rate. Therefore, in order to relate an aftershock (filial event) with a parental (main) event, one must define a measure of the space-time distance between the two and some statistical criterion based on this measure. Methods of declustering have evolved from deterministic (e.g. Gardner and Knopoff, 1974; Reasenber, 1985) to stochastic (e.g. Zhuang et al, 2002; Marsan and Lengliné, 2008). A very comprehensive review is provided by van Stiphout et al., (2012). Deterministic methods attempt to aftershocks by using space-and-time windows usually defined as functions of the main shock magnitude while ignoring higher order aftershocks (aftershocks of aftershocks). The latter allow for aftershock triggering within a sequence and use Omori’s law as a measure of the temporal dependence of aftershock activity. Both approaches ignore fault elongation for larger magnitude events, assuming circular (isotropic) spatial windows. Stochastic declustering was pioneered by Zhuang et al. (2002) and is based on space-time branching formulations to describe how each event triggers its filial sequences and

optimizing the choice of space-time window by fitting an ETAS model to the earthquake data. Moreover, instead of unitarily associating one aftershock with one main shock, each earthquake is assigned with a probability that it is an aftershock of its predecessor. This means that *all* earthquakes are possible main shocks to their short-term aftermath. Marsan and Lengliné (2008) carried stochastic declustering one step forward by introducing a generalized triggering process free of any underlying earthquake occurrence model, although they still assume that background earthquakes occur at constant and spatially uniform rate.

Herein the stochastic declustering method of Zhuang et al. (2002) will be implemented. As will further be elaborated in Chapters 2 and 4, this has an additional for the objectives of this thesis advantage: the Zhuang et al. algorithm comprises a *paradigmatic* realization of the self-excited Poisson process. If the background seismicity obeys Boltzmann-Gibbs statistics, then this method will extract a nearly random background process. If it does not, the argument for a Critical background will be stronger. Note, also, that being stochastic, the Zhuang et al. algorithm does not return a binary answer as to whether an event belongs to the background or foreground process. Rather, it assigns each event with a *probability* of being background. As a general rule, events with probability less than 50% are considered to be foreground. Since the output of stochastic declustering is not unique, it is useful to generate different realizations of the declustered catalogue at different probability levels and use them to test hypotheses associated with background seismicity. The analysis reported herein will be based on the assumption that *only* events with probability greater than $\geq 70\%$ are likely to be background and will examine catalogue realizations at probability levels $\geq 70\%$, $\geq 80\%$ and $\geq 90\%$ to be background.

The present study attempts to examine the dynamics of seismogenetic systems by implementing the generalized NESP formalism and searching for signs of randomness or complexity/criticality in time and in space. The analysis will emphasize on the bivariate Frequency – Magnitude – Interevent Time (F-M-T) distribution while using interevent distances as spatial constraints or spatial filters in appraising the spatial dependence of the energy and time dynamics of seismogenetic systems along the NW stretch of the Circum-Pacific Rim (Belt). The area extends between the coordinates (130°W , 164°E) and (20°S , 54°N) and includes four major lithospheric plates (Pacific, Okhotsk, Eurasia and Philippine) and their convergent boundaries/ associated seismogenetic systems: The Philippine Sea Plate is being subducted beneath the southern part of northeast Japan and beneath southwest Japan. The convergence directions and rates are north – north-westward and 4 to 6 cm/yr at the Suruga – Nankai trough and the Ryukyu trench. The Pacific plate is being subducted beneath northeast Japan west – north – westward at the Kuril and Japan trenches at the rate of about 8 cm/yr and beneath the Philippine Sea plate west – north – westward at the Izu Bonin trench at the rate of about 6 cm/yr. More information about these major structural units and their geodynamic characteristics is given in Chapter 3.

The earthquake data used in the study span the time period 1/1/2002 – 31/5/2016 and was provided by the National Research Institute for Earth Science and Disaster Resilience, the Japan Meteorological Agency, Hokkaido University, Hirosaki University, Tohoku University, the University of Tokyo, Nagoya University, Kyoto University, Kochi University, Kyushu University, Kagoshima University, the National Institute of Advanced Industrial Science and Technology,

the Geographical Survey Institute, Tokyo Metropolis, Shizuoka Prefecture, Hot Springs Research Institute of Kanagawa Prefecture, Yokohama City, and Japan Agency for Marine-Earth Science and Technology. The earthquake catalogue is available in the website of the *National Research Institute for Earth Sciences and Disaster Prevention* (NIED), <http://www.hinet.bosai.go.jp/> . Details about the earthquake catalogue are given in Chapter 1.3.

Inasmuch as the study area is vast and contains more than one distinct geodynamic features, the earthquake catalogue was not treated as a single entity. Instead, it was divided into four sub-catalogues, each corresponding to one of the four major lithospheric plates. Because the seismicity of the convergent boundaries in all four plates is both crustal (in the lithosphere), and *sub-crustal* (in the Wadati-Benioff zone), the analysis will proceed by roughly separating *crustal* and *sub-crustal* earthquakes according to the depth of the Mohorovičić discontinuity. This type of differential study may also provide an opportunity to inquiry as to whether environmental conditions (e.g. temperature, pressure), or/and boundary conditions (free at the surface vs. fixed at depth), have a role in the dynamic expression and evolution of a seismogenetic fault network. Comparison of results from such exercises may afford some evidence as to the existence of differences between crustal and sub-crustal seismogenesis. As a result of this reasoning, a total of 32 subset earthquake catalogues will be analysed: One crustal and one sub-crustal for each plate as well as their respective declustered realizations at the 70%, 80% and 90% probability levels.

The remaining of this study is organized in six chapters. Chapter One will review the fundamental laws and principles on which the analysis is based. Chapter Two exposes the analytical techniques and methodology applied to the data. Chapter Three introduces the geology and geodynamics of the study area (Ch. 3.1) and provides a detailed overview of the earthquake catalogue and data. Chapters Four and Five present and discuss/comment on the results of the analysis. Finally, Chapter Six provides a recapitulation of the results and discusses their significance with respect to the objectives of the Thesis.

1. STATISTICAL PHYSICS AND COMPLEXITY- REVIEW

1.1 EARTHQUAKE STATISTICS

Seismogenesis system is generally thought to comprise a mixture of processes that express the continuum of tectonic deformation (*background process*) and a large population of aftershocks that express the short-term activity associated with the occurrence of significant earthquakes (foreground process). Over the years there have been many attempts to interpret the statistical nature of seismogenesis and seismicity theoretical models and simulations. The currently and most influential viewpoint postulates that the background process is Poissonian in time and space, and obeys Boltzmann–Gibbs thermodynamics. The second holds that seismogenesis at large is a Complex process that involves some form of criticality, (e.g. stationary or self-organized vs. evolutionary or self-organizing), although non-critical models have also been proposed.

1.1.1 THE STANDARD PARADIGM: SEISMOGENESIS AS A RANDOM (POINT) PROCESS

Principal example of the “Poissonian viewpoint” is the ETAS model (Episodic Type Aftershock Sequence, e.g. Ogata, 1988, 1998; Zhuang et al, 2002; Helmstetter and Sornette, 2003; Touati et al, 2009; Segou et al, 2013). This is an ad hoc construct that essentially expresses a self-excited conditional Poisson process (Hawkes, 1972; Hawkes and Adamopoulos, 1973; Hawkes and Oakes, 1974). According to ETAS, random background parental events trigger filial foreground (aftershock) sequences in which parental aftershocks trigger their own filial sub-sequences, thereby spawning short-term spatiotemporal clustering of multiple generations of foreground events that depend on each other and their decay in time is described by the Omori-Utsu law of aftershocks (e.g. Utsu et al., 1995). Point process models have also been developed to address the problem of intermediate to long-term clustering such as the EEPAS (Each Earthquake is a Precursor According to Scale, e.g. Rhoades, 2007) and the PPE (Proximity to Past Earthquakes, e.g. Marzocchi and Lombardi, 2008).

In any case, point processes are memoryless, therefore the Poissonian viewpoint rests on the assumption that background earthquakes are statistically independent and although it is possible for one event to trigger another (smaller or larger), this occurs in an unstructured random fashion and does not contribute to the long-term evolution of seismicity. It is therefore important to emphasize that the Poissonian viewpoint is mainly concerned with the statistics of time and the distance between *background* earthquake events. The size (magnitude) distribution of both background and foreground processes is still thought to be governed by the well-established frequency-magnitude (F-M) relationship of Gutenberg and Richter (1944), which is essentially a power law, and the time dependence (decay) of earthquake frequency in aftershock sequences is described by yet another power law, namely the Omori-Utsu law of aftershocks.

The Gutenberg – Richter frequency magnitude law states that

$$\log N(M) = a - bM \tag{1.1}$$

where M is earthquake magnitude and $N(M)$ is the frequency of earthquakes with magnitude greater than M occurring in a specified area. The constant b , so called ‘ b -value’, is a scale factor

indicating the rate at which event sizes grow in a given area and has a global value of unity although it exhibits considerable local and regional variation: the b -value of has been observed to change from one geographical region to another (1.8-1.0 for oceanic ridges, 1.0-0.7 for interplate seismicity and 0.7-0.4 for intraplate seismicity). The constant a is a measure of the regional level of seismicity and describes the *seismic productivity* of an area. Owing to the log-linear relationship between seismic energy released and the magnitude of the earthquake, there is another form of the Gutenberg-Richter law stated as

$$N(\varepsilon) \sim \varepsilon^{-\alpha} \quad (1.2)$$

where $N(\varepsilon)$ is defined in analogy to the previous form but for events which release energy greater than ε . This is due to the fact that usually magnitude is defined in terms of the logarithm of a seismogram's amplitude and hence bears a log-linear relationship with energy.

Omori (1894a, b) studied the decrease of half-day and monthly frequencies of felt aftershocks with time following the 1891 Nobi (Mino-Owari), central Japan, earthquake and two other earthquakes in Japan. He showed that the frequency of aftershocks per unit time interval $n(t)$ at time t is well represented by

$$n(t) = K(t + c)^{-1} \quad (1.3)$$

where K and c are constants. Omori used the letter h in place of c , but we use c since it is commonly used in recent years. It is also common for t to be measured from the origin time of the main shock, but Omori used a different time origin in his papers, where $t = 0$, $t = 1$, corresponds to the first, second, unit time intervals, respectively. The original Omori formula predicts a constant slope K for large t , because $N(t)$ for eq. (1.3) takes the form

$$N(t) = \int_0^t n(s) ds = K \ln \left(\frac{t}{c} + 1 \right) \quad (1.4)$$

Utsu (1957) showed that the occurrence rate of aftershock fits the equation

$$n(t) = Kt^{-p} \quad (1.5)$$

With p around 1.4. Since this function diverges at $t = 0$, he recommended the use of the form

$$n(t) = K(t + c)^{-p} \quad (1.6)$$

with an additional small positive constant c . The cumulative number $N(t)$ for this equation is

$$N(t) = \frac{K\{c^{1-p} - (t+c)^{1-p}\}}{p-1} \quad (1.7)$$

For $p \neq 1$. When $p > 1$, $N(t)$ tends to a constant level $N_\infty = K/\{p - 1\}c^{p-1}$ as $t \rightarrow \infty$. When $p \leq 1$, $N(t) \rightarrow \infty$ as $t \rightarrow \infty$. Utsu (1961) called Eq. 1.7 the modified Omori formula and estimated p and c values for 41 aftershock sequences mostly in Japan.

1.1.2 THE EMERGENT PARADIGM: SEISMOGENESIS AND SELF-ORGANIZED CRITICALITY

A system is said to be in a state of self-organized critically if it is maintained near a critical point (Bak et al., 1988). According to this concept a natural system is in a marginally stable state; when perturbed from this state it will evolve naturally back to the state of marginal stability. In the critical state there is no longer a natural length scale so that fractal statistics are applicable. One usually measures the complexity of a physical system by the number of degrees of freedom the system possesses. However, it is possible for the many nominal degrees of freedom that make up the complex system to be combined into a few effective degrees of freedom. This

collective behaviour, which in linear systems would be called normal modes, is more generally termed self-organization.

The discovery of the Self-Organized Criticality (SOC) is one of ground-breaking achievements of statistical physics in the last couple of decades. Self-organized criticality is a very rich phenomenon as it combines self-organization and criticality to describe complexity. This concept was first introduced by Per Bak and co-workers in their seminal paper of 1988 (Bak et al., 1988).

A commonly used, intuitive example calls for the process of creating a pile of sand. Suppose that sand being added one grain at a time to a sandbox. At first, the grains land on the stable slope of a proto-sand pile. As more grains are added, the slope of the pile increases. Eventually, the slope locally reaches a critical value such that the addition of one more grain results in an "avalanche". The avalanche hills in empty areas of the sandbox. With the addition of still more grains, the sandbox will overflow. Sand is thus added and lost from the system. When the count of grains added equals the count of grains lost (on average) then, according to the theory, the sand pile has self-organized to a critical state (Turcotte, 1997).

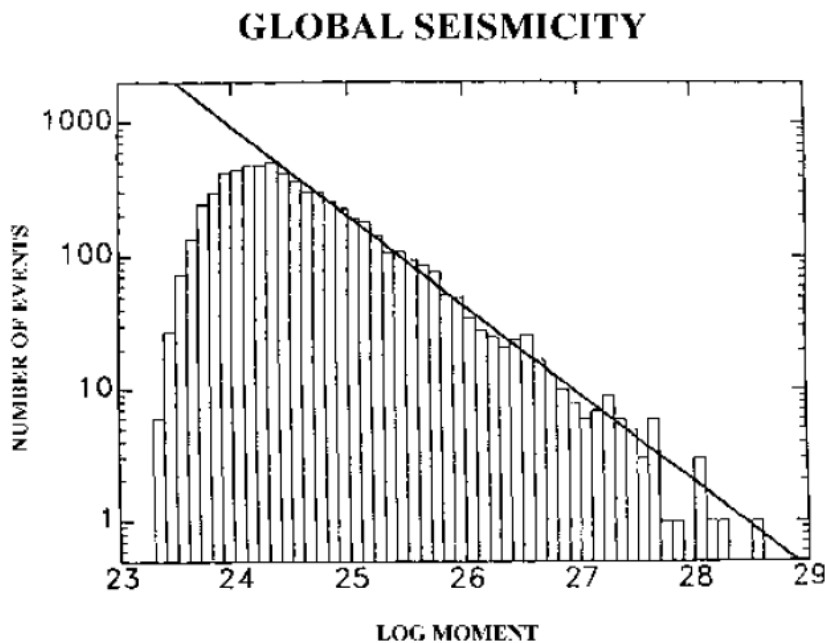


Figure 1.1: Log-log plot of global occurrence of earthquakes from 1977- 1995. Seismic moment (used to determine magnitude) is plotted vs. number of events. The distribution follows a power law relationship (Lay and Wallace, 1995).

Consider a two dimensional array of blocks. Each block is connected by springs to its nearest neighbour, as well as to a driving plate (Fig. 1.2). This system is analogous to a "sand pile" in that the local addition of slope to the sand pile:

$$z(x, y) - z(x, y) + 1$$

Is like adding stress to the "fault plane". The addition of stress (sand) eventually causes a block to fail and an earthquake (avalanche) occurs:

$$z(x, y) - z(x, y) - 4$$

$$z(x \pm 1, y) - z(x, y \pm 1) + 1$$

$$z(x, y \pm 1) - z(x, y) + 1$$

If the subsequent redistribution of stress or "stress drop" causes a nearby block to exceed the critical stress value, then it too will fail. Thus, earthquakes can range in size from the failure of a single block to failures which encompass nearly the entire system. As with computer models of sand piles, this simple set of rules produces computer-earthquakes which follow a power law distribution.

The idea of using spring-slider block models (Fig. 1.2) to generate synthetic seismicity has a long history in Seismology. Burridge and Knopoff (1967) made similar simulations both in the laboratory and on the computer. These simulations generated power law distributions as well. In this sense, simple SOC models bring nothing new to Seismology.

Lomnitz-Adler (1993) did, however, extend the Burridge-Knopoff model. Their work took the interactions of $z(x,y)$ as shown above and modified them to more closely simulate current, competing theories of earthquake rupture physics. There are currently two competing models used to describe earthquake rupture physics. The first, typically described as the Heaton pulse model (Heaton, 1992), states that earthquakes have a rupture front which is closely followed by a healing front. The rupture front breaks the rock, and displacement occurs directly behind the rupture front. Displacement at a particular point ceases when a healing front (closely following the rupture front) passes the point. The healing front prevents a complete stress drop on the fault plane. The Heaton pulse model is thus also known as a partial stress drop model.

The second model used to describe earthquake rupture physics is that of the classical crack. The crack model has no healing front. Displacement initiates with the passage of a rupture front and continues until the earthquake itself stops. Lomnitz-Adler modified the Burridge-Knopoff model in order to compare the crack model to the partial stress drop model. He further modified the Burridge-Knopoff model to test other key parameters of earthquake rupture physics including frictional and stress loading relationships. The criteria for the model tests were whether or not the said rupture physics could produce a power law distribution. His results indicate (with a few exceptions) that only partial stress drop models can produce power law distributions.

Using these modifications on the classical Burridge-Knopoff model to constrain the rupture physics of earthquakes can, however, lead to spurious results. The principle criticism of the Burridge-Knopoff (and hence the SOC) models is that they fail to properly model elasticity. In the SOC models the amount of displacement experienced by a fault block is the same whether the earthquake involves one block (magnitude 1) or 100,000,000 blocks (magnitude 8). In an elastic solid, however, the displacement experienced is a function of the size of the earthquake. In practical terms, a magnitude 8 earthquake with a fault area on the order of hundreds of square kilometers may locally produce tens of meters of displacement: it is impossible for a magnitude 2 earthquake, with a fault area on the order of a few square meters, to produce tens of meters of slip.

SPRING-SLIDER BLOCK MODEL

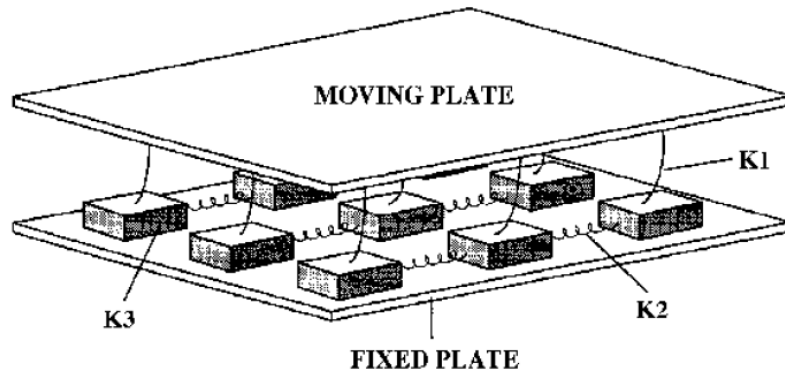


Figure 1.2: Conceptual drawing of a two-dimensional spring-slider block model. Leaf springs (K1) connect a moving plate to an array of smaller sliding blocks. These blocks are in turn connected to their nearest neighbours via coil springs (K2, K3). Sliding blocks also have a frictional contact with a fixed plate (Bak, 1996).

Lately, a well-studied class of models (Bak and Tang, 1989; Sornette and Sornette, 1989; Olami et al., 1992; Bak et al., 2002; Bakar and Tirnakli, 2009; many others) suggests that seismicity expresses a non-equilibrating fractal fault system that continuously evolves toward a stationary critical condition with no characteristic spatiotemporal scale (Self Organized Criticality – SOC). In this view, all earthquakes belong to, or evolve towards the same global population and participate in shaping a non-equilibrium state in which events develop spontaneously and any small instability has a chance of cascading into a large shock. A second class of models which have been rather influential during the late 90's and early 2000's, suggest that large events comprise Critical Points in the evolution of seismicity (Self-Organizing Critical process, e.g. Sornette and Sammis, 1995; Rundle et al., 2000; Sammis and Sornette, 2001; many others). In this context, a large earthquake terminates a cycle by moving parts of its associated fault network out of the critical state and destroying stress correlation, thereby creating a “stress shadow”. At the same time, a new cycle begins as tectonic loading combined with stress transfer from smaller events re-establishes long range stress-stress correlation and accelerates energy release rates in a power-law fashion. The next large event is possible when the network has reached a critical state, in which highly stressed patches are correlated at the scale of the fault network so that a local event can grow by rupturing through geometrical and rheological barriers. In any case, critical complex systems evolving in a fractal-like space-time are characterized by long-range interactions and long-term memory which, at a regional scale, should be manifested by correlations and power-law distributions observable in the statistics of energy release, temporal dependence and spatial dependence.

In addition to the SOC/CP models, a few authors have investigated models with alternative complexity mechanisms that do not involve criticality, yet maintain the fault system in a state of non-equilibrium: a useful discussion can be found in Sornette and Werner (2009). More recently, Celikoglu et al, (2010) applied the Coherent Noise Model (Newman, 1996) based on the notion of external stress acting coherently onto all agents of the system without having any direct interaction with them and is shown to generate power-law interevent time distributions. A weak point in this model is that it does not include some geometric configuration of the

agents and it is not known how this would influence the behaviour of the system. In another example, Mignan (2008) has formulated a non-critical model, the “non-critical Precursory Accelerating Seismicity Theory”, which behaves similarly to a CP process; in this context, stress correlation is a result of stress shadow shrinking by top-down tectonic loading as part of a large-scale preparation process and not by scaling-up (or bottom-up triggering) as predicted by the CP theory.

1.2. THE STANDARD VS THE EMERGENT PARADIGMS

The common characteristic of SOC and Poisson models is that they both consider the seismic events of an aftershock sequence dependent, whilst their main difference is in their perception of background seismogenesis. In Poisson models there're no interaction (correlation) between background events and their parameters are consistent with the BG thermodynamics, whereas, in Complex/Critical models we have the presence of long-range interactions and long-term memory.

An important point to consider is that the scale-free grading between earthquake frequency and magnitude implied by the Gutenberg-Richter relationship law is a power-law that *cannot* be derived from the Boltzmann-Gibbs formalism. This, in turn, implies that while the temporal and spatial expression of background seismicity is consistent with Boltzmann-Gibbs thermodynamics, the carriers of this expression (faults) are not! Advocates of Non-Poissonian models of seismogenesis point to this fact as best evidence (finger print) for the existence of SOC. Likewise, the Omori-Utsu power law *cannot* be derived from Boltzmann-Gibbs thermodynamics – being a power law it implies that foreground earthquakes (aftershock sequences) are generated by a dynamic system *with* memory, therefore with interaction between its elements and not random – as analyzed in Par.1.1.1.

The non-compliance of the Gutenberg-Richter and Omori-Utsu laws with Boltzmann-Gibbs thermodynamics has a significant repercussion: It implies that the Poissonian viewpoint of seismogenesis postulates that the same effect (seismicity) has two different physical causes: one whose entropy generates random spatiotemporal distributions of background events from non-random spatial distributions of agents (faults) and one whose entropy generates non-random temporal distributions of foreground events from non-random spatiotemporal distributions of agents.

These are logical inconsistencies with no theoretical resolution. In addition, although in principle (and at the current level of understanding) such a dual mode of seismogenesis cannot be ruled out, it nevertheless violates the *lex parsimoniae* (or Occam's razor) and is therefore philosophically not appealing. In fact, Poissonian seismicity models effectively are *ad hoc* conceptual constructs that try to reconcile an (inherited) Poissonian worldview of dynamic systems with the apparently non-Poissonian geometry and dynamics of fault formation and clustering.

SOC models obey the NESP formalism which has recently been applied to the statistical description of earthquake occurrence with notable results, and has also been shown to generate the Gutenberg-Richter frequency-magnitude distribution, which is a power-law, from first principles (e.g. Sotolongo-Costa and Posadas, 2004; Silva, 2006; Telesca, 2011, 2012). Thus, it provides a general, complete, consistent and *model-independent* theoretical context in which to investigate the nature and dynamics of the background and foreground seismogenetic processes.

1.3 STATISTICAL PHYSICS – AN OVERVIEW

1.3.1 Additive or Extensive Statistical Physics (Boltzmann-Gibbs)

The concept of entropy is fundamental in statistical physics. It first appeared in thermodynamics through the second law of thermodynamics. The notion of entropy has been broadened by the advent of statistical mechanics and has been still further broadened by the later advent of information theory. As we know, almost all the systems treated in statistical mechanics with Boltzmann-Gibbs (BG) entropy have usually been extensive and this property holds for the systems with short-range interparticle forces. Entropy as a physical property was introduced by the German physicist Rudolf Clausius in the mid-1860s to explain the maximum energy available for useful work in heat engines. Clausius was also the first to restate the second law of thermodynamics in terms of entropy, by saying that the entropy, or disorder, of an isolated system will always increase, and that the entropy of the universe will tend to a maximum. It was not until the work of Boltzmann in the late 1870s, however, that entropy became clearly defined according to the famous formula. Boltzmann entropy is defined for a macroscopic state of a system while Gibbs entropy is defined over an ensemble that is over the probability distribution of macrostates. Both Boltzmann and Gibbs entropies are, in fact, the pillars of the foundation of statistical mechanics and are the basis of all the entropy concepts in modern physics.

A lot of work on the mathematical analysis and practical applications of both Boltzmann and Gibbs entropies has been done (Wehrl, 1978), yet the subject is not closed but is awaiting additional effort for their characterization, interpretation, and generalization. The measure of disorder first provided by Boltzmann principle (known as Boltzmann entropy) is given by

$$S_B = K_B \ln W \quad (1.8)$$

where K is the thermodynamic unit of measurement of entropy and is known as Boltzmann constant. $K=1.33 \times 10^{-16} \text{erg}/^\circ\text{C}$. W , called thermodynamic probability or statistical weight, is the total number of microscopic complexions compatible with the macroscopic state of the system. We avoid the name thermodynamic probability for the term 'W' as it leads to much confusion (Lavenda H. B., 1991). Following Carnap (Carnap R., 1977) the quantity 'W' is called the 'degree of disorder'.

1.3.2 NON - EXTENSIVITY

1.3.2. i. Non-additive or non-extensive statistical physics (Tsallis)

One of the crucial properties of entropy in the context of classical thermodynamics is extensivity, namely, its directly proportional relationship to the number of elements N in the system (eq 1.8). If strong interactions among i different microstates of a system exist, the probabilities p_i , are interrelated and the occurrence of one microstate strongly depends on the occurrence of another. Some microstates are favoured, while some others are ignored. For instance, water molecules in the presence of a whirlpool do not take any path but only those paths that resemble a vortex, due to correlations in the molecules' motions (Cartwright, 2014). In this case, the number of possible microstates, W , no longer increases exponentially with N , so SBG is no longer proportional to N (see eq 1.1) and extensivity is violated. The BG entropy satisfies this prescription if the subsystems are statistically (quasi -)independent, or typically if

the correlations within the system are generically local. In such cases the system is called extensive (Caruso and Tsallis, 2008).

In general, however, the situation is not always of this type and correlations may be far from negligible. In such cases the BG entropy (of the entire system or a large part of it) may be non-extensive. Nonetheless, for an important class of such systems an entropy exists that is extensive in terms of microscopic probabilities. The additive BG entropy can be generalized into the non-additive q -entropy (Tsallis and Gell'mann, 2005).

During the past several years, the concept of non-additive (non-extensive, or Tsallis, statistical physics, henceforth NESP for brevity), based on Tsallis' formulation of non-additive entropy, has been proposed as a generalization of BG statistics. This new statistics is attracting considerable attention since it has been developed as a tool for use in the statistical description of complex systems whose description is beyond the capacity of BG statistics due, for instance, to long-range interactions (Gell'mann and Tsallis, 2004; Abe and Okamoto, 2001; Boon and Tsallis, 2005; Tsallis, et al, 2005; Tamarit and Anteneodo, 2005; Abe, et al, 2005; Plastino, 2005).

The Tsallis entropy, S_q , is claimed to be useful in cases where there are strong correlations between the different microstates in a system and is defined as

$$S_q = \frac{1}{q-1} (1 - \sum_i p_i^q), \quad q \in \mathbb{R}, \quad (1.9)$$

where the index i runs over the microstates of a system, each of which has its own probability of occurrence p_i , and, q is a measure of how strong the correlations are. The value of q is either greater or smaller less than unity, but in the limit where $q \rightarrow 1$, the Tsallis entropy reduces to the Boltzmann-Gibbs entropy (Tsallis, 1994). The parameter q is called the Tsallis *entropic index*.

Let X be a dynamic parameter of a complex system and $p(X)dX$ the probability of finding its value in $[X, X+dX]$, such that $\int_0^\infty p(X)dX = 1$. In seismogenetic systems X can be the interevent time, interevent distance, fault and fragment surface, energy etc. Non-equilibrium states in systems with complex behaviour can be described by the Tsallis (1988) entropic functional.

$$S_q = k \frac{1}{q-1} [1 - \int_0^\infty p^q(X)dX] \quad (1.10)$$

Where k is the Boltzmann constant. As mentioned above, q is a measure of the non-extensivity of the system and for the particular case $q = 1$ equation (3) reduces to the Boltzmann-Gibbs entropy

$$S_{BG} = -k \int_0^\infty p(X) \ln(p(X)) dX \quad (1.11)$$

The Tsallis entropy shares properties with the Boltzmann-Gibbs entropy, including concavity and fulfilment of the H -theorem (e.g. Biro and Kaniadakis, 2005 pp.3). However, it is pseudo-additive in the sense that it is not proportional to the number of the elements of the system as S_{BG} . Thus, for a composite of two statistically independent systems, A and B, $S_q(A, B) = S_q(A) + S_q(B) + (1-q) S_q(A) S_q(B)$, leading to *super-additivity (super extensivity)* for $q < 1$, *additivity (extensivity)* for $q = 1$, that is Gibbs-Boltzmann statistics, and *sub-additivity (sub extensivity)* for $q > 1$ (Tsallis, 1988). Accordingly, the entropic index is a measure of non-extensivity in the system. It should now be pointed out that the terms "extensive" and "extensivity" has been

introduced by Tsallis (1988) in order to designate systems that are equilibrating (full or complete according to Merriam-Webster's definition), as opposed to systems that are not equilibrating (incomplete, i.e. non-extensive). The terms "additive" and "non-additive" are probably more appropriate but for the sake of consistency with the literature, I shall henceforth use the terminology of Tsallis. The difference between additivity and extensivity is that the former depends only on the mathematical definition of entropy; therefore S is additive, whilst $S_q (q \neq 1)$ is non-additive. Extensivity is more subtle, since it also depends on the specific system (Caruso and Tsallis, 2008).

1.3.2 ii. The q -exponential distribution

Maximization of the Tsallis entropy yields the q -exponential distribution

$$p(X) = \frac{1}{Z_q} \exp_q \left[-\frac{\lambda}{I_q} (X - \langle X \rangle_q) \right] \quad (1.12)$$

where, $\langle X \rangle_q = \int_0^\infty X \cdot p_q(X) dX$ is the q -expectation value of X , λ is an appropriate Lagrange multiplier, $Z_q = \int_0^\infty dX \exp[-\lambda \cdot I_q^{-1} \cdot (X - \langle X \rangle_q)]$ is a generalized canonical partitioning function and $I_q = \int_0^\infty dX [p(X)]^q$. In Eq. 1.12, the function $\exp_q(\cdot)$ represents the q -exponential function (see Tsallis, 2009 and references therein).

$$\exp(X) = \begin{cases} (1 + (1 - q)X)^{\frac{1}{1-q}} & 1 + (1 - q)X > 0 \\ 0 & 1 + (1 - q)X \leq 0 \end{cases} \quad (1.13)$$

and comprises a generalization of the exponential function: for $q=1$, $\exp_1(X) = e^x$. As evident from Eq. 1.12 and 1.13, the probability $p(X)$ is a power-law with a long tail if $q > 1$, corresponding to sub-additivity, an exponential distribution if $q = 1$, corresponding to additivity, and a cut-off if $0 < q < 1$, corresponding to super-additivity. The cut-off appears at $X_c = X_0(1-q)^{-1}$, with $X_0 = (1-q) \cdot \langle X \rangle_q + \lambda/I_q$. If the empirical distribution of X is $P_q(X)$, which is called the escort probability, then the cumulative probability function (CDF) derived from the above analysis is

$$P(> X) = \int_X^\infty dX P_q(X) \quad (1.14)$$

The escort probability distribution (Tsallis, 2009) is defined as

$$P_q(X) = \frac{p^q(X)}{\int_0^\infty p^q(X) dX}, \text{ with } \int_0^\infty P_q(X) dX = 1 \quad (1.15)$$

In the case of $q > 1$ and $X \in [0, \infty)$, the CDF becomes

$$P(> X) = \exp\left(-\frac{X}{X_0}\right) = \left[1 - (1 - q)\frac{X}{X_0}\right]^{\frac{1}{1-q}} \quad (1.16)$$

which is a q -exponential distribution. When $q > 1$ the CDF exhibits a long tail, which becomes longer with increasing q ; the system experiences long-range correlations and has long-term memory. When $q = 1$, the q -exponential distribution reduces to the common exponential distribution: the system is a random process (uncorrelated and memory-less). When $q < 1$, the distribution exhibits a cut-off, i.e. $P(>X) = 0$ whenever the argument becomes negative and is characterized by a bounded correlation radius. The q -exponential function for various values of q is shown in figure 1.3.

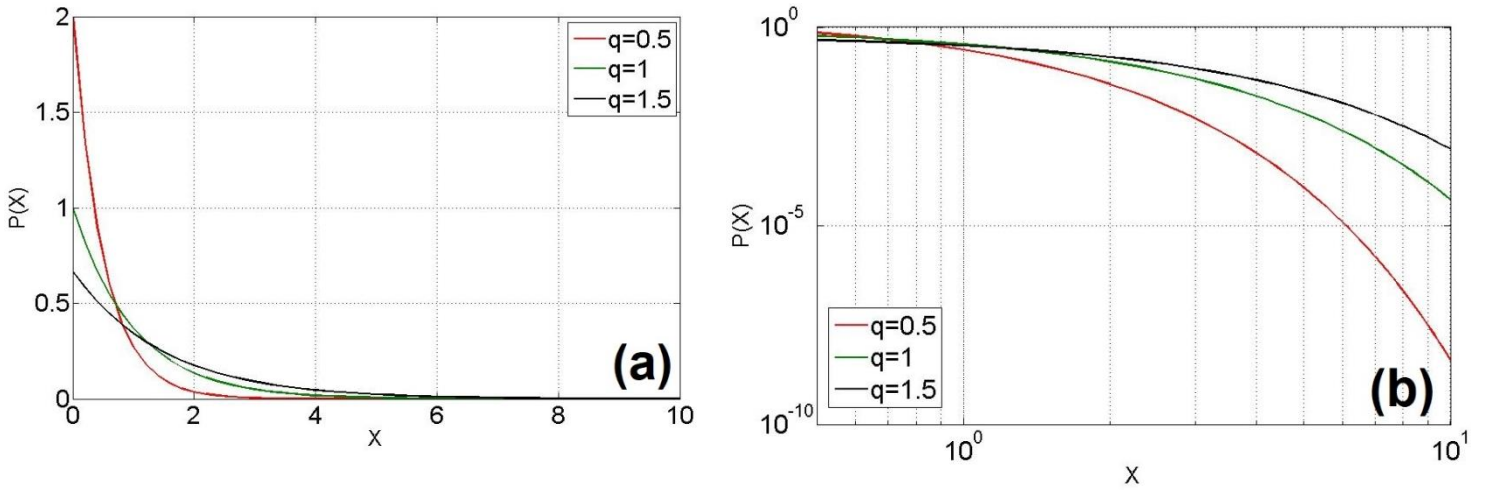


Figure 1.3: The q -exponential function $\exp_q(X)$ for various values of q and λ in (a) linear and (b) logarithmic scales.

1.3.2. iii. The q -Gaussian distribution

Probability distributions emerge from the non-extensive formalism - also called q -distributions - and have been applied to a variety of problems in diverse research areas including the interdisciplinary field of complex systems. Here we focus on q - Gaussian distributions. The maximization of the Tsallis entropy (S_q) under the constraints

$$\int f(x)dx = 1, \quad \frac{\int x^2 f(x)^2 dx}{\int f(y)^q dy} = \sigma^2 \quad (1.17)$$

Yields the so-called q -Gaussian probability density function

$$f(x) = \frac{\exp_q(-\beta_q x^2)}{\int \exp_q(-\beta_q y^2) dy} \propto [1 + (1 - q)(-\beta_q x^2)]^{\frac{1}{1-q}} \quad (1.18)$$

where $\exp_q(x)$ is the q -exponential function and β_q is a positive constant related to σ (standard deviation) and q (Tsallis et. al, 1996; Prato and Tsallis 2000). The q -Gaussian distribution is a generalization of the Gaussian, arising directly from Tsallis's entropy, which is a generalization of standard Boltzmann-Gibbs entropy. The normal Gaussian distribution is recovered when $q \rightarrow 1$ (Boltzmann - Gibbs Thermodynamics).

The probability density function (PDF), $p(X)$, of a continuous random variable, is a function that describes the relative likelihood for this random variable to take a given value. The probability of the random variable falling within a particular range is given by the integral of this variable's density over that range, i.e. by the area under the density function but above the abscissa and between the lowest and supremum of the range. The probability density function is non-negative everywhere, and its integral ad infinitum is equal to one. Let X be a continuous random vector. Then a probability distribution or probability density function of X is a function $f(x)$ such that for any two numbers a and b with $a \leq b$.

$$P(a \leq X \leq b) = \int_a^b f(x)dx \quad (1.19)$$

That is, the probability that X takes on a value in the interval $[a, b]$ is the area above this interval and under the graph of the density function. The graph of $f(x)$ is often referred to as the density curve.

The power form of the q -Gaussian (eq. 1.18) has been found to be befitting to the description of physical systems that cannot be systematically studied in the context of Boltzmann-Gibbs statistical mechanics (Tsallis et. al, 2001 and 2004). The distribution is often favoured for its heavy tails in comparison to the Gaussian for $1 < q < 3$. For $q < 1$ the q -Gaussian distribution is the PDF of a bounded random variable (Fig. 1.4).

In the heavy tail region, the distribution is equivalent to the Student t distribution with a direct mapping between q and the degrees of freedom. For $q < 1$ the system is sub - additive and for $q > 1$ is super - additive. The Student t distribution is any member of a family of continuous probability distributions that arises when estimating the mean of a normally distributed population in situations where the sample size is small and population is unknown.

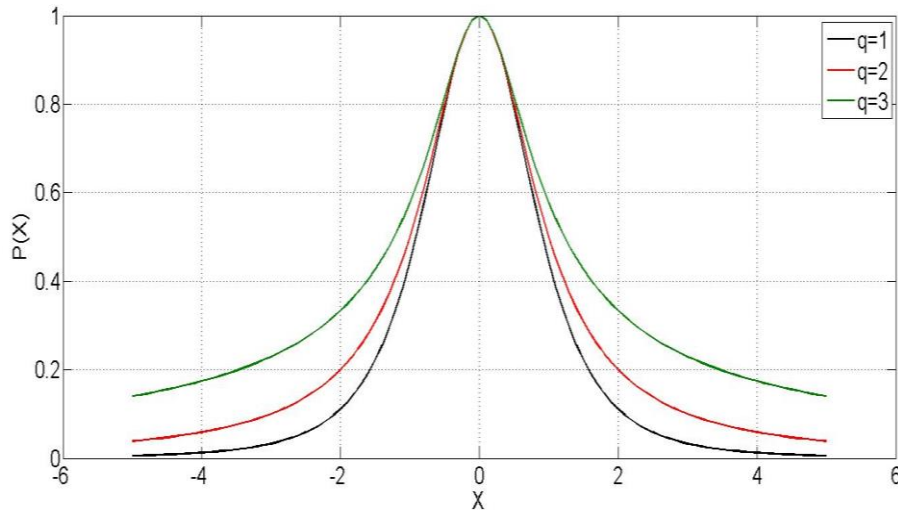


Figure 1.3: The q -Gaussian distribution for various values of q .

1.3.3 NON-EXTENSIVITY AND SEISMOLOGY

The frequency-magnitude (F-M) distribution has been approximated with a number of NESP-compatible models by Sotolongo-Costa and Posadas, (2004); Silva et al., (2006), Telesca (2011, 2012) and others. All these researchers consider the interaction of two rough fault walls (asperities) and the fragments filling space between them, which is considered to control earthquake triggering (the fragment-asperity model). However, they differ in their assumption of how energy is stored in the asperities and fragments.

Sotolongo-Costa and Posadas (2004) assume that the energy stored in the asperities and fragments scales with their linear characteristic dimension ($E \propto r \Rightarrow E \propto \sigma^{1/2}$), and that the magnitude scales with the logarithm of the energy as $M \propto \log(E)$. Using the definitions of x_0 from Eq. 1.13 and the q -exponential distribution (Eq. 1.15) the probability $\hat{p}(x)$ can be expressed as

$$\hat{p}(X) = \frac{\exp_q\left(\frac{X}{x_0}\right)}{\int_0^\infty \exp_q\left(\frac{X}{x_0}\right) dx} \quad (1.19)$$

Silva et al. (2006) revisited the fragment-asperity model and expressed Eq. 1.19 as

$$\hat{p}(\sigma) = \left[1 - \frac{1-q}{2-q}(\sigma - \langle\sigma\rangle_q)\right]^{\frac{1}{1-q}} \quad (1.20)$$

On assuming that the energy scales with the characteristic volume of the fragments ($E \propto r^3$), so that $E \propto \sigma^{3/2}$ because σ scales with r^2 , it is easy to see that $(\sigma - \langle \sigma \rangle_q) = (E/\alpha)^{2/3}$ with α being a proportionality constant between E and r . This yields the energy density function (EDF)

$$\hat{p}(E) = \left(\frac{2}{3} \cdot \frac{E^{-1/3}}{\alpha^{2/3}} \right) \cdot \left[1 - \frac{(1-q) E^{2/3}}{(2-q) \alpha^{2/3}} \right]^{-\frac{1}{1-q}} \quad (1.21)$$

The corresponding CDF is then,

$$\hat{P}(> E) = \frac{N(>E)}{N_0} = \int_E^\infty \hat{p}(E) dE \quad (1.22)$$

where $N(>E)$ is the number of events with energy greater than E normalized by the total number of earthquakes N_0 . On assuming that the magnitude scales with the logarithm of energy as $M \propto \frac{1}{3} \log(E)$, for $q > 1$, Telesca (2011,2012) introduced a modified version of Eq. 1.22:

$$P(> M) = \log \frac{N(>M)}{N(M=0)} = \left(\frac{2-q_M}{1-q_M} \right) \log \left(1 - \left[\frac{1-q_M}{2-q_M} \right] \left[\frac{10^M}{\alpha^{\frac{2}{3}}} \right] \right) \quad (1.23)$$

This relationship describes from first principles and in NESP formalism, the cumulative distribution of the number of earthquakes N with magnitude greater than a threshold M in a seismic region, normalized by the total number of earthquakes. The constant α expresses the proportionality between the released energy E and the fragment size r and q_M is the entropic index. This model has been recently applied to regional seismicity, covering diverse tectonic regions (Telesca, 2010a,b; Telesca and Chen, 2010; Scherrer et al., 2015).

The CDF expressed by Eq.1.16 is the only NESP formulation proposed for the one-dimensional distributions frequency - interevent time distributions F-T (Abe and Suzuki, 2005) and F-D (Abe and Suzuki, 2003). Moreover, the empirical application of NESP to interevent times has been taken up by only a handful of authors. Abe and Suzuki (2005) investigated the temporal properties of the seismicity in California and Japan; Carbone et al (2005) investigated the Italian seismicity; more recently, Vallianatos et al. (2012) investigated the spatiotemporal properties of the 1996 Aigion (Greece) aftershock sequence; Vallianatos et al. (2013) the temporal behaviour of the 2011-2012 seismicity crisis in the Santorini volcanic complex (Greece); Vallianatos and Sammonds (2013) the behaviour of global seismicity prior to the 2004 Sumatran and 2011 Honshu mega-earthquakes. In these studies, the F-T distribution $P(> \Delta t)$ was all nicely fitted with an one-dimensional q -exponential distribution of the form (1.16). In addition, Tzanis et al., (2013) analyzed the interdependence of magnitude, interevent time and interevent distance in North California, Efstathiou et al. (2015) searched for evidence of non-extensivity in the evolution of seismicity along the San Andreas Fault, California, USA and Efstathiou et al., (2016) looked into the nature and dynamics of the seismogenetic systems of North California, USA.

2. METHODOLOGY AND DATA ANALYSIS PROCEDURES

2.1 OVERVIEW

The complexity and self-organization, that may characterize the seismogenetic system, are associated with long range interactions and long term memory effects. These properties are collectively referred to as *correlation*. The entropic indices are a measure of a correlation in the sense that index values approaching unity indicate low correlation (or randomness) while index values diverging from unity indicate correlation in a complex system. As frequently mentioned in the foregoing, objective of this research is to use the NESP formalism in order to search for correlation in the temporal, spatial and size manifestations of the seismicity observed in the broader area of Japan. This objective will be realized by determining the values and variation of the relevant entropic indices q_M and q_T .

Given the objective specified above, the earthquake occurrence model implemented herein will be based on multivariate frequency distributions that express the joint probability of observing an earthquake larger than a given magnitude, after a given lapse time and beyond a given distance. However, this would require the construction and analysis of tri-variate F-M-T-D distributions (frequency-magnitude-interevent time-interevent distance) which would arguably be harder to handle and interpret. Instead, it was decided to use the easier to study bivariate F-M-T distributions so as to search for correlation in earthquake size and time of occurrence. This, nonetheless, will not extract direct information about the range of correlation and as a way around this problem we will use the interevent distance as a spatial filter by which to separate and study the temporal correlation of proximal and distal earthquakes: the premise is that if distal earthquakes are correlated in time, then they have to be correlated in space via long-distance interaction and vice versa. The technical details of this approach will be specified in Sections 2.2 and 2.3.

Japan and its island possessions lie across four major tectonic plates: Pacific plate; North America (Okhotsk) plate; Eurasia plate; and Philippine Sea plate. The Pacific plate is subducted into the mantle, beneath Hokkaido and northern Honshu, along the eastern margin of the Okhotsk microplate, a proposed subdivision of the North America plate (Bird, 2003). Farther south, the Pacific plate is subducted beneath volcanic islands along the eastern margin of the Philippine Sea plate. This 2,200 km-long zone of subduction of the Pacific plate is responsible for the creation of the deep offshore Japan Trench as well as parallel chains of islands and volcanoes, typical of Circumpacific island arcs. Similarly, the Philippine Sea plate is itself subducting under the Eurasia plate along a zone, extending from Taiwan to southern Honshu that comprises the Ryukyu Islands (Fig. 3.2).

Subduction zones at the Japanese island arcs are geologically complex and produce numerous earthquakes from multiple sources. Deformation of the overriding plates generates shallow crustal earthquakes, whereas slip at the interface of the plates generates interplate earthquakes that extend from near the base of the trench to depths of 40 to 60 km. At greater depths, Japanese arc earthquakes occur within the subducting Pacific and Philippine Sea plates and can reach depths of nearly 700 km (mantle/ sub-crustal earthquakes).

Due to the differences between the tectonic plates, it was considered essential to divide the seismic catalogue into four smaller, each referring to a different tectonic setting. As already mentioned, the process of seismogenesis in the crust differs from that in the mantle. Crustal earthquakes are those whose epicentre is located above the Mohorovicic discontinuity and are generated by crust deformations (faults). Sub-crustal earthquakes are those that occur in the mantle, due to the subduction process. The submerged tectonic plates (in this case the Pacific and Philippine) are generating earthquakes due to their interaction with the continental plates (Eurasia and Okhotsk). Crustal and sub-crustal earthquakes have different characteristics, different seismic parameters and different mechanisms. For the purposes of this analysis it was necessary to further separate the seismic catalogues of each plate into crustal and sub-crustal.

The Mohorovicic discontinuity and upper mantle structures in and around Japan have been well investigated both with active and passive seismic studies, including marine expeditions. Earlier results on this topic (1960–1970s) were mainly based on seismic refraction experiments (Yoshii, 1994). The advances in data acquisition and processing technologies introduced in the 80's and 90's have afforded a large amount of high quality seismic data (Yoshii, 1994; Iwasaki et al., 2002). In active source experiments, receiver spacing became much denser (less than 2–3 km) enabling the identification of many seismic phases such as reflections from the Moho (PmP phase) and improving the estimation of the location and nature of the Moho boundary. After the 1995 Kobe earthquake, a new and denser seismic network was established in Japan and was subsequently used to carry out detailed tomographic and receiver function investigations that provided constraints on the lateral variations of the discontinuity. Given the above, the surface of the Moho discontinuity was reconstructed by combining information from the studies of Yoshimoto et al., (2004), Iwasaki et al., (2013), Shiomi et al., (2006), Nakamura et al., (2003) and Nakamura and Umedu, (2009). It was subsequently mapped onto a regular grid using natural neighbour interpolation. The result shows that the depth of the discontinuity varies along the entire area. In the oceanic plates the discontinuity is in less than 10 km depth, whilst, within continental areas and under mountain chains it ranges between 30 – 44 km (Fig. 2.).

A primary objective of this study is to investigate whether background seismicity is generated by non-Poissonian dynamic processes. The first attempts to define whether an earthquake catalogue is Poissonian or not were made by Aki (1956) and Knopoff (1964) who found that earthquake catalogue do not generally fit a Poisson distribution. Knopoff (1964) probably introduced for the first time a kind of declustering algorithm by excluding the aftershocks from the analysis. They counted earthquakes in successive ten-day bins and found a histogram showing many feature of a Poisson distribution. As background seismic events we typically define earthquakes that have not been triggered by another; thought to be the result of tectonic loading. Alternatively, in seismic hazard assessment may refer to an earthquake not associated with a particular fault. Background seismic catalogues can be derived from the raw catalogues through a declustering process that removes nonessential earthquake data (aftershock sequences or events that are considered to be triggered). In this study three probability levels are examined for each event of the background catalogues that are greater of equal to $\varphi_j=70\%$, $\varphi_j=80\%$ and $\varphi_j=90\%$.

The goal of seismicity declustering is to separate earthquakes in the seismicity catalogue into independent and dependent earthquakes. Aftershocks, which are dependent earthquakes, cannot be distinguished by any particular, outstanding feature in their waveforms. They can thus only be selected on the basis of their spatiotemporal proximity to other, previous earthquakes, and/or by the fact that they occur at rates greater than the seismicity rate averaged over long durations. To relate an aftershock to a mainshock therefore requires defining a measure of the space-time distance between the two, and a criterion based on this measure that needs to be met. All declustering methods follow this general scheme.

So far, the algorithms used for seismic declustering have been deterministic, i.e., each earthquake is classified either as a mainshock or as an aftershock (Reasenber, 1985; Molchan and Dmitrieva, 1992; Gardner and Knopoff, 1974). Another class of seismicity declustering algorithm came with the stochastic model of Zhuang et al. (2002) which is based on a space-time branching process model (van Stiphout et al, 2012) to describe how each event generates offspring events. This approach generalizes and improves previous methods in two ways: (1) the choice of the space-time distance is optimized in order to best model the earthquake dataset, within the limits of the ETAS model. As such, there is no need to assume arbitrary values for the parameters that enter the space-time distance, although the parameterized form of the distance is imposed a priori. This comes with a cost: this optimization can sometimes be time-consuming and delicate to perform. (2) Instead of binary linking an aftershock to only one mainshock, this method gives, for each earthquake, the associated probabilities that it is an aftershock of each preceding earthquake (i.e., all preceding earthquakes are thus potential mainshocks). This makes for a much more sophisticated approach: if the space-time distance is roughly the same between A and C and between B and C, then instead of only keeping either A or B as the mainshock of C, this method keeps both earthquakes as mainshocks of C with roughly equal probability, reflecting the difficulty to make a clear decision in such a case. A limit to this method stems from the use of the ETAS model, as it imposes the parameterized form of the space-time distance. While this is appropriate for the temporal dependence, given the ubiquity of the Omori-Utsu law for describing the decaying influence of a mainshock, this is not the case anymore when considering the spatial dependence, or the space-time coupling (i.e., change with time of the spatial dependence) as no firm consensus exists on these yet.

For the purposes of this study, the space-time ETAS model was used (Zhuang 2002; Zhuang et al., 2004, 2008; Helmstetter and Sornette, 2003; Hainzl and Ogata, 2005; Lombardi et al., 2010). In a few words, what this algorithm basically does, is to identify events that are considered first order events that are parental to second order, third order and so on, earthquake sequences. To simplify it even more, it identifies events which, at a certain probability level have triggered earthquake sequences. According to ETAS and the Poisson worldview of seismicity, triggering (background) events may not be major at all (e.g an earthquake of magnitude 4 may trigger an earthquake with a magnitude of 7.5 given the right conditions).

2.2 BIVARIATE FREQUENCY-MAGNITUDE-INTEREVENT TIME DISTRIBUTIONS: CONSTRUCTION.

The bivariate F-M-T distribution expresses the joint probability of observing an earthquake larger than a given magnitude after a given time lapse (interevent time). In order to construct it, a threshold (cut-off) magnitude M_{th} is first set, on the basis of which a bivariate frequency –

magnitude - interevent time table (histogram) is constructed, representing the observed incremental distributions. The observed *cumulative distribution* is then obtained by backward bivariate summation, according to the scheme (Efstathiou et. al, 2016; Tzanis et. al, 2013; Efstathiou et. al, 2015)

$$N_{m\tau} = \sum_{j=D_T}^{\tau} \sum_{j=D_M}^m \{H_{ij} \Leftrightarrow H_{ij} \neq 0\}, \quad \tau = 1, \dots, D_T, \quad m = 1, \dots, D_M \quad (2.1)$$

where H is the incremental distribution, D_M is the dimension of H along the magnitude axis and D_T is the dimension of H along the Δt axis. The cumulative frequency (earthquake count) can be written as: $N(\{M \geq M_{th}, \Delta t: M \geq M_{th}\})$. Then, the empirical probability $P(>\{M \geq M_{th}, \Delta t: M \geq M_{th}\})$ is simply

$$\frac{N(>\{M \geq M_{th}, \Delta t: M \geq M_{th}\})}{N_0}, \quad N_0 = N(M = M_{th}, 0) = ||N||_{\infty} \quad (2.2)$$

An example of cumulative FMT distribution constructed according to Eq. 2.1 is presented in Fig. 2.1; it is based on the unified catalogue of Japan for the period 2002 - 2016 and $M_{th} \geq 4$ (10,855 events). The distribution is illustrated both in linear and logarithmic frequency scales (Figs. 2.1a and 2.1b respectively). Apparently, it comprises a well-defined and structured surface, with the end-member at $(M \geq M_{th}, \Delta t = 0)$ comprising the one-dimensional Gutenberg - Richter law and the opposite end member at $(M = M_{th}, \Delta t)$ comprising the one-dimensional F-T distribution.

As stated in Section 2.1 (as well as in the introduction) it is very important to study the effect of spatial separation on earthquake size distribution and temporal dynamics. To this effect, it is possible to construct bivariate F-M-T distributions on the basis of catalogue subsets grouped according to the distance between consecutive events (interevent distance), following the rule:

$$C \supset \{C_D : M > M_c \wedge \Delta d_L \leq \Delta d \leq \Delta d_U\} \quad (2.3)$$

where C is the catalogue, C_D is the subset catalogue, Δd is the interevent distance and $\Delta d_L, \Delta d_U$ are the upper and lower group limits. . Eq. 2.3 leads to the construction and modelling the conditional bivariate cumulative distribution

$$P(>\{M \geq M_{th}, \Delta t: [M \geq M_{th} \wedge \Delta d_L \leq \Delta d \leq \Delta d_U]\}) \quad (2.4)$$

as a proxy of a trivariate F-M-T-D distribution. As a result, one may obtain the variation of the entropic indices with respect to distance group

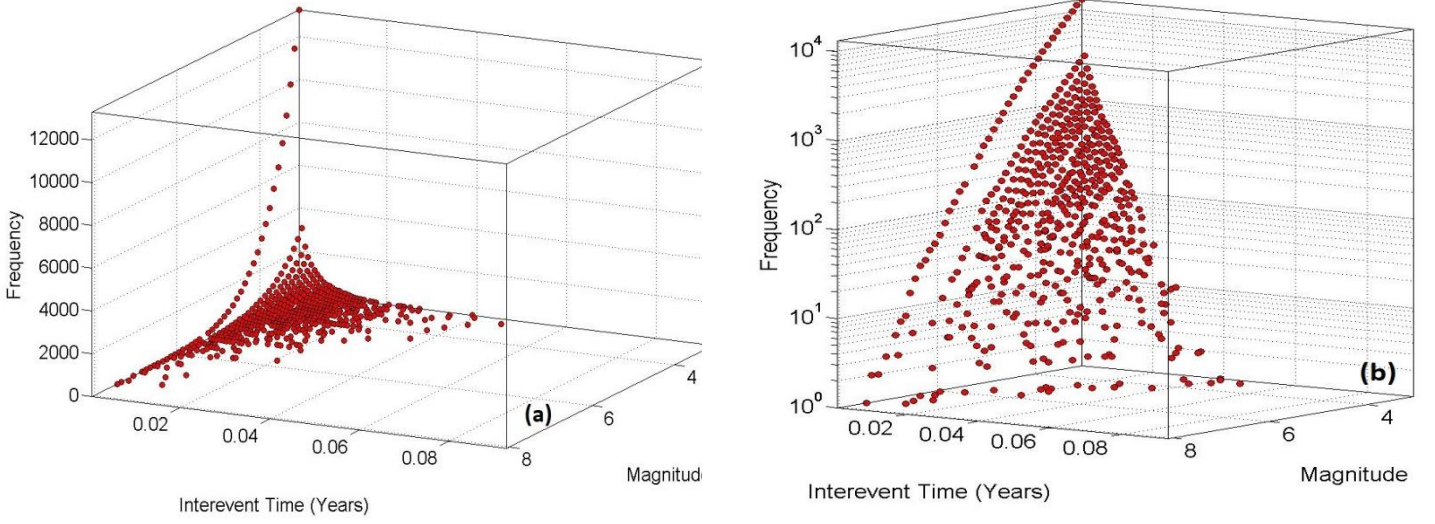


Figure 2.1: (a) The bivariate cumulative frequency-magnitude-interevent time distribution constructed according to Eq. (2.1) for the period 2002-2016 and $M_{th} = 3$ on the basis of the JMA Unified Catalogue (103.696 events). (b) As per (a) but in logarithmic frequency scale.

2.3 IMPLEMENTATION

Assuming that the magnitude and interevent time are statistically independent (Efstathiou et al, 2016; Tzanis et. al, 2013; Efstathiou et., al, 2015), namely that the hierarchy of the active fault network does not influence the sequence of events, the joint probability $P(M \cup \Delta t)$ may factorize into the probabilities of M and Δt in the sense $P(M \cup \Delta t) = P(M) P(\Delta t)$. Then, by implicitly identifying the empirical and escort probabilities one obtains

$$\frac{N(>\{M \geq M_{th}, \Delta t: M \geq M_{th}\})}{N_0} = \left(1 - \frac{1 - q_M}{2 - q_M} \frac{10^M}{a^{2/3}}\right)^{\frac{(2 - q_M)}{(1 - q_M)}} \left(1 - (1 - q_T) \frac{\Delta t}{\Delta t_0}\right)^{\frac{1}{1 - q_T}} \quad (2.5)$$

where q_M and q_T are the entropic indices for the magnitude and interevent times respectively and Δt_0 , is the q -relaxation time, analogous to the relaxation (characteristic) time often encountered in the analysis of physical systems. On taking the logarithm and setting $a = \log(N_0)$ Eq. 2.2 becomes

$$\log N(>\{M \geq M_{th}, \Delta t: M \geq M_{th}\}) = a + \frac{(2 - q_M)}{(1 - q_M)} \log\left(\frac{1 - q_M}{2 - q_M} \frac{10^M}{a^{2/3}}\right) + \frac{1}{1 - q_T} \log(1 - \Delta t_0^{-1} (1 - q_T) \Delta t) \quad (2.6)$$

Eq. 2.6 is a generalized bivariate law of the Gutenberg-Richter king in which

$$b_q = \frac{(2 - q_M)}{(q_M - 1)} \quad (2.7)$$

is the NESP equivalent of the b value (e.g. Telesca, 2012). Accordingly, Eq. 2.6 is the general model to be implemented in the ensuing analysis. If the seismogenetic process is non-extensive (earthquakes occur in correlated space-time), then b_q should be equivalent to the b value computed by conventional methods because the distribution of magnitudes does not relate the energy released by a given earthquake to the energy released by its successor events, but only conveys information about the geometry of the active fault system. However, q_M should differ from unity, thus revealing the interdependence of successive events in the correlated space-time of the seismogenetic system. On the other hand, if seismogenesis is Poissonian, b_q should still be equivalent to the b value computed by conventional methods but $q_T \rightarrow 1$ and the third term in the RHS of Eq. 2.5 should reduce to the logarithm of the exponential distribution. In

both cases, the favourable comparison of b_q (that is q_M) to the results of well-established methods of b value estimation should be a rather robust means of ensuring the validity of the numerical procedure used in approximating Eq. 2.6 and the robustness of the results and conclusions.

An example of an empirical distribution constructed according to Eq. 2.1 and Eq. 2.2 and modelled according to Eq. 2.6 is shown in Fig. 2.2. Because the parameters of Eq. 2.6 are all positive and the entropic indices are bounded ($1 < q < 2$), a following (Efstathiou et al., 2015), it was decided to deploy a least squares solver implementing the *trust-region reflective* algorithm (e.g. Moré and Sorensen, 1983; Steihaug, 1983), together with *Least Absolute Residual minimization* so as to down-weight possible outliers.

The quality of the approximation is very good (Fig. 2.2a), with the correlation coefficient (R^2) being 0.99. The magnitude entropic index $q_M = 1.55$ so that $b_q \approx 0.8$, which compares very well with conventionally estimated b -value (Chapter 4). The temporal entropic index $q_T = 1.2$ indicating very weak correlation, possibly randomness. An appraisal of the results is summarized in Fig. 2.2b and is based on the analysis of the statistical distribution of the residuals. The observed cumulative probability of the sorted residuals (r) is fitted with a normal location-scale distribution (dashed line) and a Student-t location-scale distribution (solid line). Evidently, 95% of the residual population, for which $|r| \leq 0.15$, is normally distributed. A very short tail appears to form at $r < -0.1$; it comprises 7 residuals or approximately 3% of the population and does not deviate significantly from normality. A tail forms at $r > 0.15$, which comprises only 23 out of 244 residuals, or 2%, and represents *outliers* that have been effectively suppressed by the LAR procedure: the solution is determined by the remaining 97.13% of the observations.

The outliers mainly occur at larger magnitudes and longer interevent times. They may be anomalies of the catalogue, (e.g. missing events or sequences of events, errors in magnitude reporting etc.). On the other hand, some may be genuine: for instance, they may correspond to infrequent, externally triggered events. Such details will not be investigated here, but it is interesting to point out that they may appear as outliers in multivariate distributions.

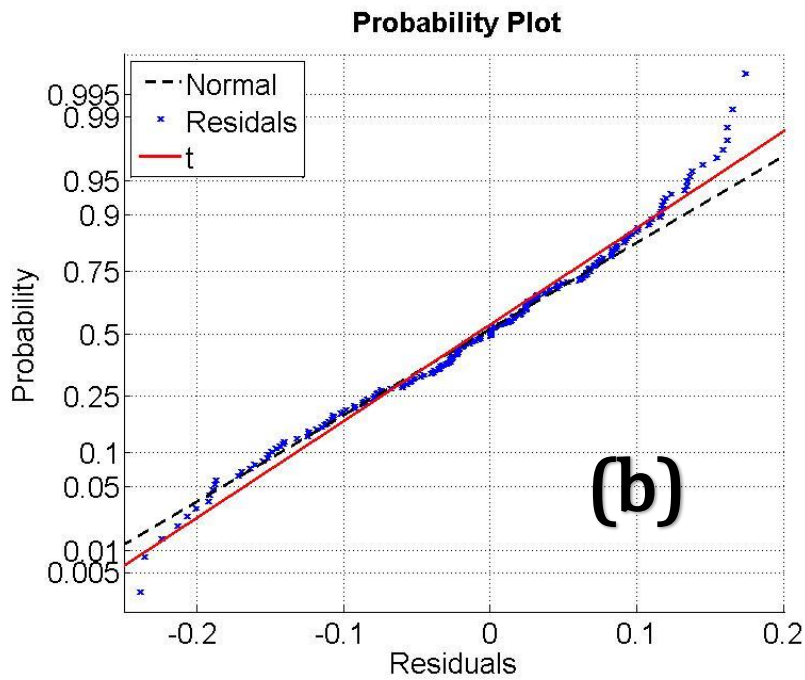
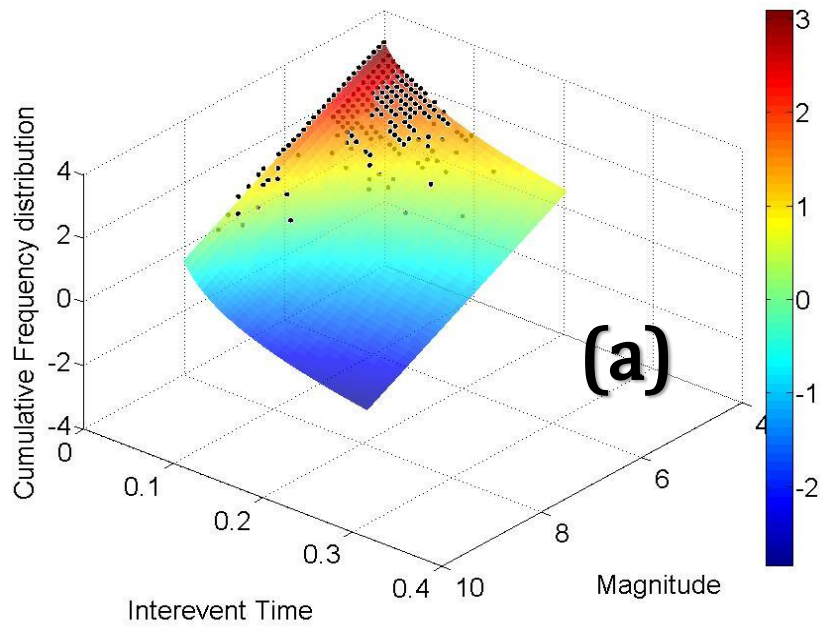


Figure 2.2: (a) F-M-T distribution of a catalogue with the predicted (fitted) distribution based on Eq.1.19 (b) is a probability analysis of the residuals

2.4 MOHOROVICIC DISCONTINUITY

The necessity to separate seismicity into crustal and sub-crustal was noted above. It has been pointed out that the characteristics of crustal and mantle (sub-crustal) seismicity are different. Crustal earthquakes are shallow and occur above the Mohorovicic discontinuity due to deformations of the crust, whilst, sub-crustal earthquakes are located beneath the discontinuity, in the mantle, and are generated by the subduction process. The depth of the discontinuity was estimated by sampling various data from previous studies (see Chapter 2 overview) and then plotted the overall results on a map with the method of natural neighbour interpolation using a grid (219x282). The results are depicted in the following figure (Fig. 2.3). Lowest values are observed in the oceanic plates of the Pacific and Philippines, with average depths 5 to 9 km. As it was expected the continental plates of Eurasia and Okhotsk have crust thickness ranging from 30 – 44 km. beneath mountains and mountain ranges the crust becomes thicker and reaches the maximum value of 44 km (central Japan, southern Ryukyu Arc and northern Hokaido).

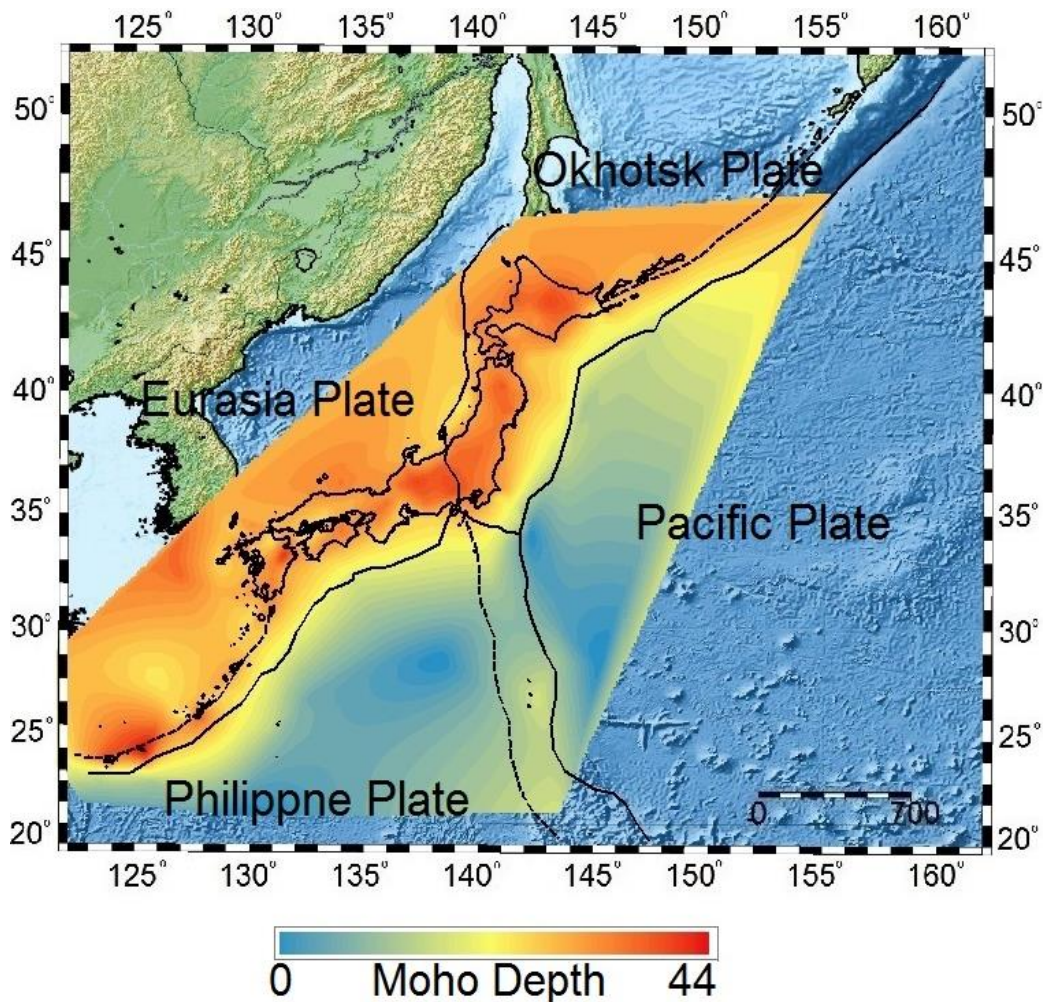


Figure 2.3: The Mohorovicic discontinuity distribution along Japan and Philippine plate.

As it is well portrayed in the Fig. 2.4 and 2.5, the subduction of the oceanic plates is the main cause of seismogenesis. The sub-crustal seismic catalogue of the entire study area consists of 69,982 earthquakes, whilst, the crustal seismic catalogue consists of 33,714 earthquakes. More than half of the earthquakes occurring in the area are generated by the submerged oceanic plates.

Most sub-crustal events (Fig. 2.4) are located along the plate boundaries and on the volcanic arcs of Ryukyu (southern Japan) and Kuril (northern Japan). On the north – Okhotsk plate – seismicity is intense. Earthquakes are present not only along the Kuril Arc, but also on the central-east coast, where a big swarm is located that is related to the 2011 Tohoku earthquake and its aftershock sequence. In Pacific plate there are clusters of earthquakes, showing that they're part of aftershock sequences. Some of these clusters (on the northern part of the Pacific-Okhotsk boundary) are possibly connected with the 2011 Tohoku sequence, judging from their spatial location. Philippine's plate seismic events are located along the Nankai, Suruga and Okinawa Trough (Philippine-Eurasia plate boundary) and along the Izu-Bonin Mariana trough (Philippine-Pacific plate boundary). Eurasia's sub-crustal seismic events are mostly located on Ryukyu Arc, and are a lot less than those of other plates.

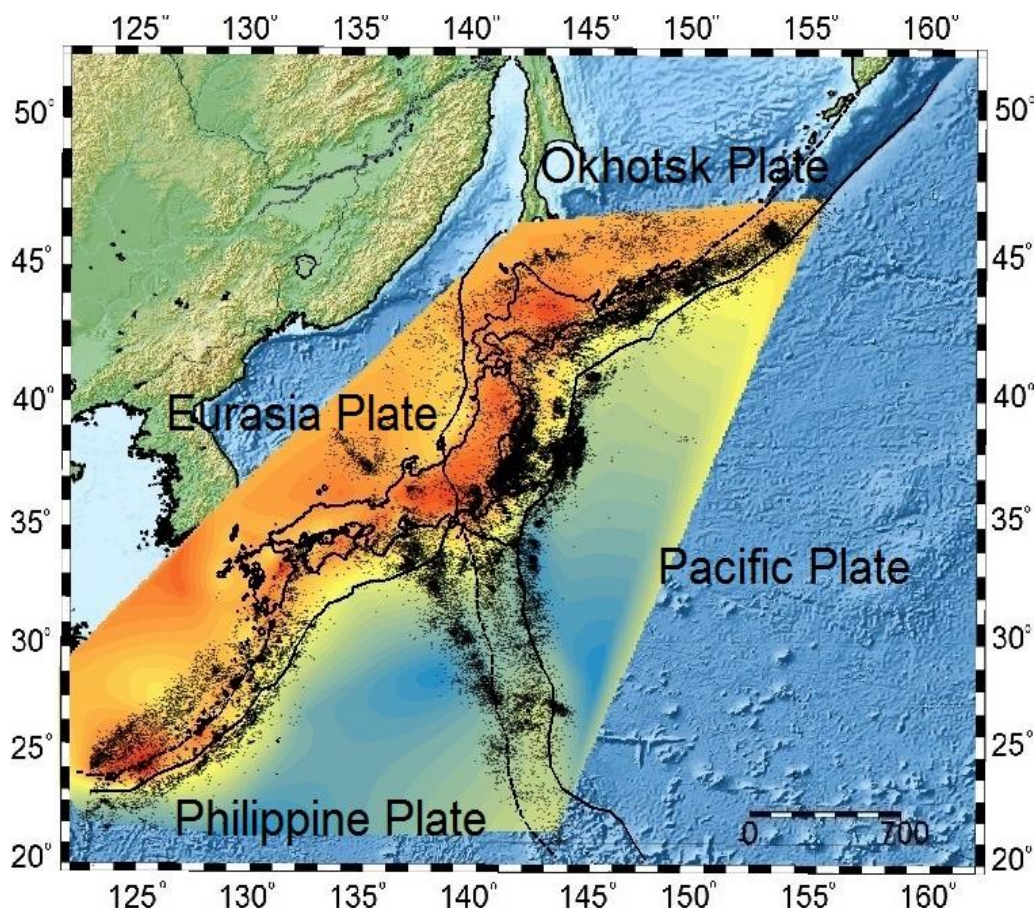


Figure 2.4: Sub-crustal seismicity of the study area.

Crustal seismicity (Fig. 2.5) is less than sub-crustal's half. The presence of earthquake clusters is evident along the entire study area. Here too Okhotsk plate has the most events, with big swarms located on the central-east and northern part. Some swarms are also noticeable in

Pacific plate, whereas, seismicity in Eurasia and Philippine is dispersed without the appearance of earthquake clusters.

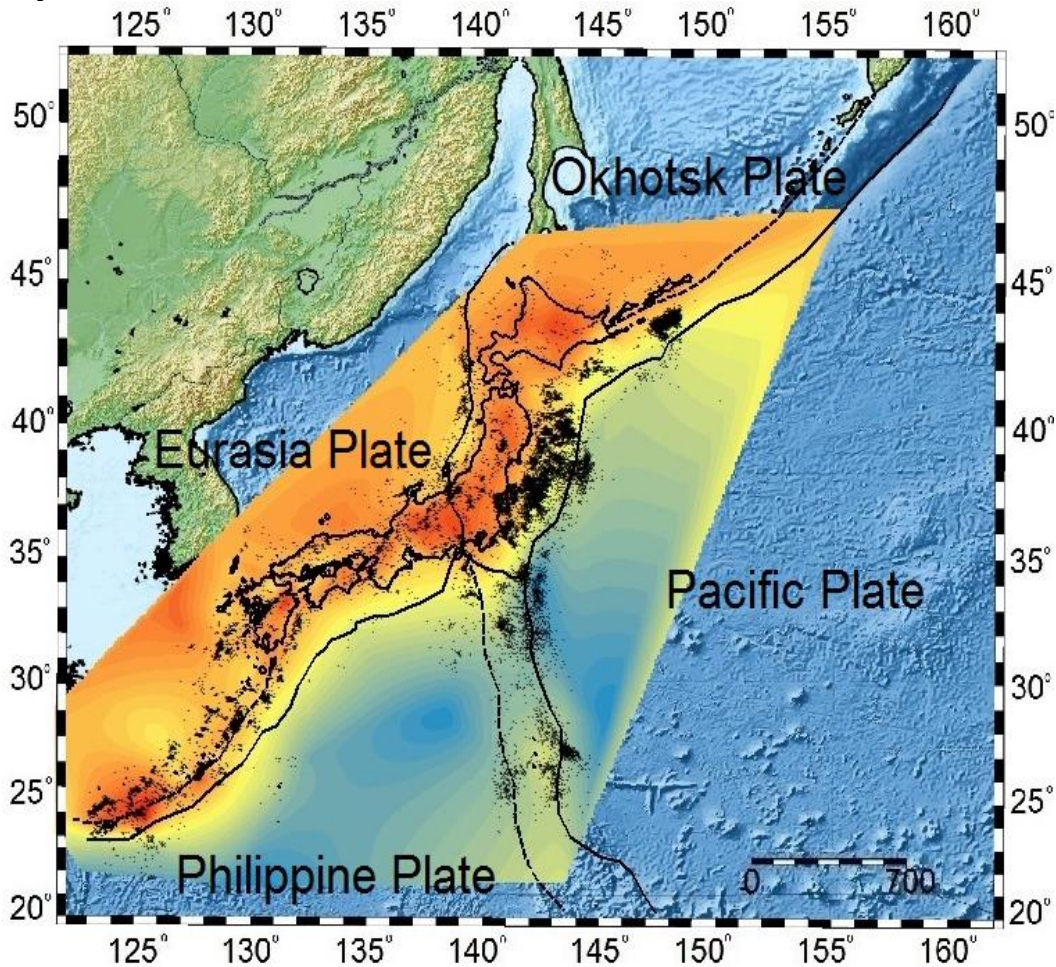


Figure 2.5: Crustal Seismicity of the study area.

2.5 DECLUSTERING

For the purposes of this study, the space-time ETAS model was used (Zhuang 2002; Zhuang et al., 2004, 2008; Helmstetter and Sornette, 2003; Hainzl and Ogata, 2005; Lombardi et al., 2010). This algorithm identifies first order events that are parental to higher order earthquake sequences. To put it simply, it identifies events which, at a certain probability level have triggered aftershock sequences. According to ETAS and the Poisson worldview of seismicity, the triggering (background) events may not be major at all; for example, an earthquake of magnitude 4 may trigger an earthquake with a magnitude of 7.5 given the right conditions.

There is no difference in triggering seismicity among foreshocks, mainshocks and aftershocks. Each parental event triggers its own filial sequence independently according to some probability rules (Zhuang, 2012). The time-varying seismicity rate of this model assumes the form of:

$$\lambda(t, x, y, m) = \mu(x, y, m) + \sum_{i: t_i < t} \kappa(m_i) g(t - t_i) f(x - x_i, y - y_i | m_i) \quad (2.8)$$

where

- i) $\mu(x, y)$ represents the background seismicity rate

- ii) The term $\kappa(m_i)g(t - t_i)f(x - x_i, y - y_i | m_i)$ is the contribution to the seismicity rate by the i^{th} event occurring previously, and $\kappa(m) = Ae^{a(m-m_c)}$ with $m \geq m_c$, is the mean number of direct offspring from an event sized m , m_c being the magnitude threshold, $g(t) = \frac{p-1}{c}(1 + \frac{t}{c})^{-p}$ for $t > 0$ and $f(x, y; m) = \frac{q-1}{\pi D e^{\gamma(m-m_c)}} (1 + \frac{x^2+y^2}{D e^{\gamma(m-m_c)}})^{-q}$ represents the probability density function for the occurrence times and locations of direct offspring, respectively. A, a, c, p, D, γ and γ are constant parameters.

To forecast seismicity by using the model specified by eq. (2.8) it is required to address the following:

- i) Obtain an empirical estimate of background seismicity rates.
 ii) Estimate the ETAS model parameters, $(A, a, c, p, D, \zeta, \gamma)$.

If the catalogue is arranged in chronological order, then the probability of an event j to have been triggered by an event $i < j$ can be estimated from the occurrence rate at its occurrence time and location as

$$p_{i,j} = \frac{\kappa(m_i) \cdot g(t_j - t_i) \cdot f(x_j - x_i, y_j - y_i | m_i)}{\lambda(t_j, x_j, y_j)}$$

and the probability that event j is aftershock is given by

$$p_j = \sum_{i=1}^{j-1} p_{i,j}$$

Conversely, the probability that event j is background is given by

$$\varphi_j = 1 - p_j = \frac{\mu(x_j, y_j)}{\lambda(t_j, x_j, y_j)}$$

The algorithm runs iteratively through the catalogue and by assigning probabilities $p_{i,j}$, p_j and φ_j to the j^{th} event, generates the foreground sub-process associated with the i^{th} event (i.e. its aftershock sequence). It thus separates the catalogue into a number of sub-processes whose initiating events comprise the background. As a general rule, events with $\varphi_j \leq 50\%$ are considered to be foreground.

3. GEOLOGY AND SEISMICITY OF THE STUDY AREA

3.1 GEOLOGY AND TECTONICS OF THE STUDY AREA

The Japanese Islands are located in the midst of the plate convergence zone at the north-western margin of the Pacific Ocean where two oceanic plates are being subducted beneath two continental plates. North – east Japan is considered to be on the North American plate, or the Okhotsk microplate, and south – west Japan on the Eurasian plate or the Amurian microplate. Although the plate geometry and kinematics of these two blocks remain controversial, there is general agreement that these two parts of Japan have been converging with each other in an east – west direction at the rate of 1 to 2 cm/yr, roughly, since the late Pliocene or the early Pleistocene, and the juvenile convergence boundary between the two plates runs along the west coast of northeast Japan and crosses the middle of Honshu toward the Suruga trough (Fig. 3.2 and 3.3).

The Philippine Sea Plate is being subducted beneath the southern part of northeast Japan and beneath southwest Japan. The convergence directions and rates are north – north-westward and 4 to 6 cm/yr at the Suruga – Nankai trough and the Ryukyu trench. The Pacific plate is being subducted beneath northeast Japan west – north –westward at the Kuril and Japan trenches at the rate of about 8 cm/yr and beneath the Philippine Sea plate west – north – westward at the Izu Bonin trench at the rate of about 6 cm/yr (Fig. 3.2 and 3.3). The geology of the four Home Islands (Kyushu, Shikoku, Honshu, and Hokkaido) of Japan is so extremely complicated that it is not easy to obtain an overall view even from small – scale geological maps such as the 1:1,000,000 scale issued by the Geological Survey of Japan (Hirokawa et al., 1978). However, when we try to form a generalised picture, it seems reasonable to consider the geology of the Japanese Islands to be comprised of the following five elements (Hashimoto M., 1991).

1. Pre – Neogene sedimentary and regional metamorphic rocks.
2. Granites and rhyolites mostly of Late Mesozoic to Early Tertiary age.
3. Neogene sediments and associated volcanics.
4. Quaternary sediments.
5. Plio – Pleistocene volcanics (figure 3.1).

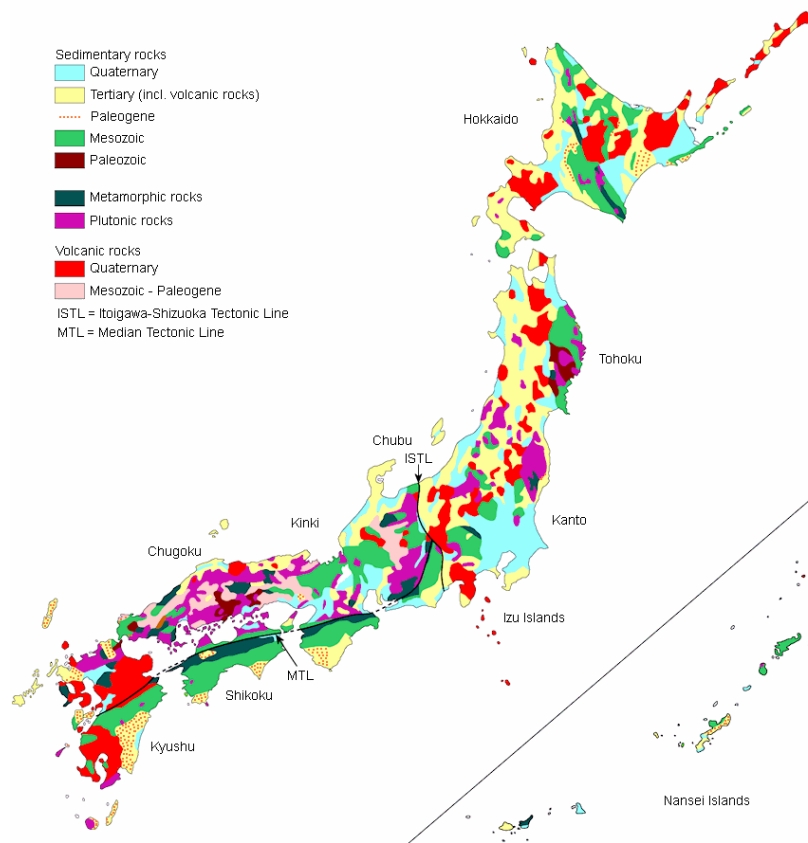


Figure 3.1: Simplified geologic map of Japan. Introduction to the landforms and geology of Japan

Japanese tectonics is controlled by two subduction zones that intersect in a T. A trench – trench – trench triple junction southeast of Tokyo. The four islands of Japan are primarily the result of several large oceanic movements occurring over hundreds of millions of years from the mid-Silurian to the Pleistocene as a result of the subduction of the Philippine Sea Plate beneath the continental Amurian Plate and Okinawa Plate to the south, and subduction of the Pacific Plate under the Okhotsk Plate to the north. They are curved in map view, convex toward the Pacific Ocean. This is probably due to the opening of the Sea of Japan in the Miocene as a backarc basin (Taira, 2001; Barnes, 2008). At the present time, however, the island arcs and trenches off Japan forming the western boundary of the Pacific Plate are convex toward the northwest, toward the Eurasian continent.

The Japan Trench is an oceanic trench, a part of the Pacific Ring of Fire, in the floor of the northern Pacific Ocean off northeast Japan. It extends from the Kuril Islands to the Bonin Islands. It is an extension of the Kuril-Kamchatka Trench to the north and the Izu-Ogasawara Trench. This trench is created when the oceanic Pacific plate subducts beneath the continental Okhotsk Plate. The subduction process causes bending of the downgoing plate, creating a deep-sea trench. Continuing movement on the subduction zone associated with the Japan Trench is one of the main causes of tsunamis and earthquakes in northern Japan, including the megathrust Tōhoku earthquake and resulting tsunami that occurred on 11 March 2011.

The Izu-Bonin-Mariana (IBM) arc system stretches over 2800 km, from south Tokyo, Japan, to beyond Guam, USA, and includes the Izu Islands, Bonin Islands, and Mariana Islands. The IBM arc system lies along the eastern margin of the Philippine Sea Plate in the Western Pacific

Ocean. It is most famous for being the site of the deepest gash in Earth's solid surface, the Challenger Deep in the Mariana Trench (Stern et al., 2003). The IBM arc system now subducts mid-Jurassic to Early Cretaceous lithosphere, with younger lithosphere in the north and older lithosphere in the south, including the oldest (~170 million years old, or Ma) oceanic crust. Subduction rates vary from ~2 cm per year in the south to 6 cm in the north (Miller et al., 2006). The Izu segment is punctuated by inter-arc rifts (Klaus et al., 1992; Taylor et al., 1991) and farther south also contains several submarine felsic calderas (Yuasa and Nohara, 1992). The Bonin segment contains mostly submarine volcanoes and a few island volcanoes, such as Nishino-shima. The highest elevations in the IBM arc (not including Fujiyama on the Izu Peninsula, where IBM comes onshore in Japan) are found in the southern part of the Bonin segment, where the extinct volcanic islands of Minami and Kita Iwo Jima rise almost 1000 meters above sealevel (Stern et al., 2003). The Mariana segment is characterized by an active back arc basin (Fryer, 1995) known as the Mariana Trough.

The Mariana Trough stretches 1300 km from north to south, about the distance from Los Angeles CA to Portland OR, Tokyo, Japan to Seoul, Korea, or London, England to Rome, Italy. The Sagami Trench or Sagami Megathrust or Sagami Subduction Zone (SA) is a westward expansion of the Nankai Trough that meets with the Japan - Izu - Bonin Trenches at about 34°N, 142°E, 200 km west of central Honshu. The Philippine Sea plate (PHS) subducts beneath southwest Japan along Nankai Trough and beneath northeast Japan along the Sagami Trench (Nakamura et al., 1984; Seno, 1977). Megathrust earthquakes associated with the Sagami Trough, known as Kantō earthquakes, are a major threat to Tokyo and the Kantō Region because of the proximity to a population center and the magnitude the Sagami Trough can create.

The Nankai Trough runs off the coast of the southwestern part of Japan, where the Philippine Sea Plate subducts beneath the overriding Eurasian Plate in the northwest direction at a rate of approximately 4.5 cm/yr (Seno et al., 1993). Within the Nankai Trough there is a large amount of deformed trench sediments (Ike, 2004), making one of Earth's best examples of accretionary prism. The state of tectonic coupling between the overriding Eurasian and subducting Philippine Sea Plates has been studied using data from the dense Global Positioning System (GPS) network covering Japan, and it has been estimated to be nearly 100 % over the landward slope of the entire Nankai Trough (complete fault locking) (Mazzotti et al., 2000). Okinawa Trough, also known as the Nansei - Shoto Trough, is the back-arc basin of the Ryukyu trench-arc-back-arc system. It is bounded by the Ryukyu Ridge and Trench to the south and east and by the East China Sea Shelf to the north and west. The entire complex is arcuate, convex toward the Pacific, from Japan to Taiwan (Lee et al., 1980). The Ryukyu Arc extends from Taiwan to south Kyushu. It is an elevated ridge marked by two parallel chains comprising more than 100 islands. Islands along the inner arc are volcanoes of Quaternary age, whereas those along the outer arc are non-volcanic outcrops (Iwasaki et al., 1990). The Ryukyu Arc is divided into three segments by the Tokara Channel and the Kerama Gap, which are considered to be left-lateral strike-slip faults (Wageman et al., 1970; Kobayashi, 1985).

The Ryukyu Trench is usually regarded to be the boundary between the Eurasia plate and the PHS plate. The maximum water depth of the trench is more than 7000 m near the Okinawa Island while most parts of the trench are not deeper than 6500 m. The trench becomes

shallower and broader towards the north, where the trench is with a depth of about 5500 m. Suruga Trough (SU) is a trough that lays off the coast of Suruga Bay in Japan, forming part of the Nankai Trough, the latter being responsible the source of many large earthquakes in Japan's history. Both mark the boundary of the Philippine Sea Plate subducting under the Amurian Plate. The Itoigawa-Shizuoka Tectonic Line Active Fault System (ISTL), in central Japan, is one of the most remarkable active faults on land in Japan for its very high slip rate as an intraplate active fault reaching around 1 cm/yr. Though the high slip rate indicates short recurrence intervals of large earthquakes less than 1,000 years, historic seismicity is quite low during these 1150 years. The ISTL consists of northern (55 km), middle (60 km), and southern (35 km) sections. The estimates of respective average slip rate are 0.3, 1.0, and 0.2 cm/yr (Okumura K. et al., 1998).

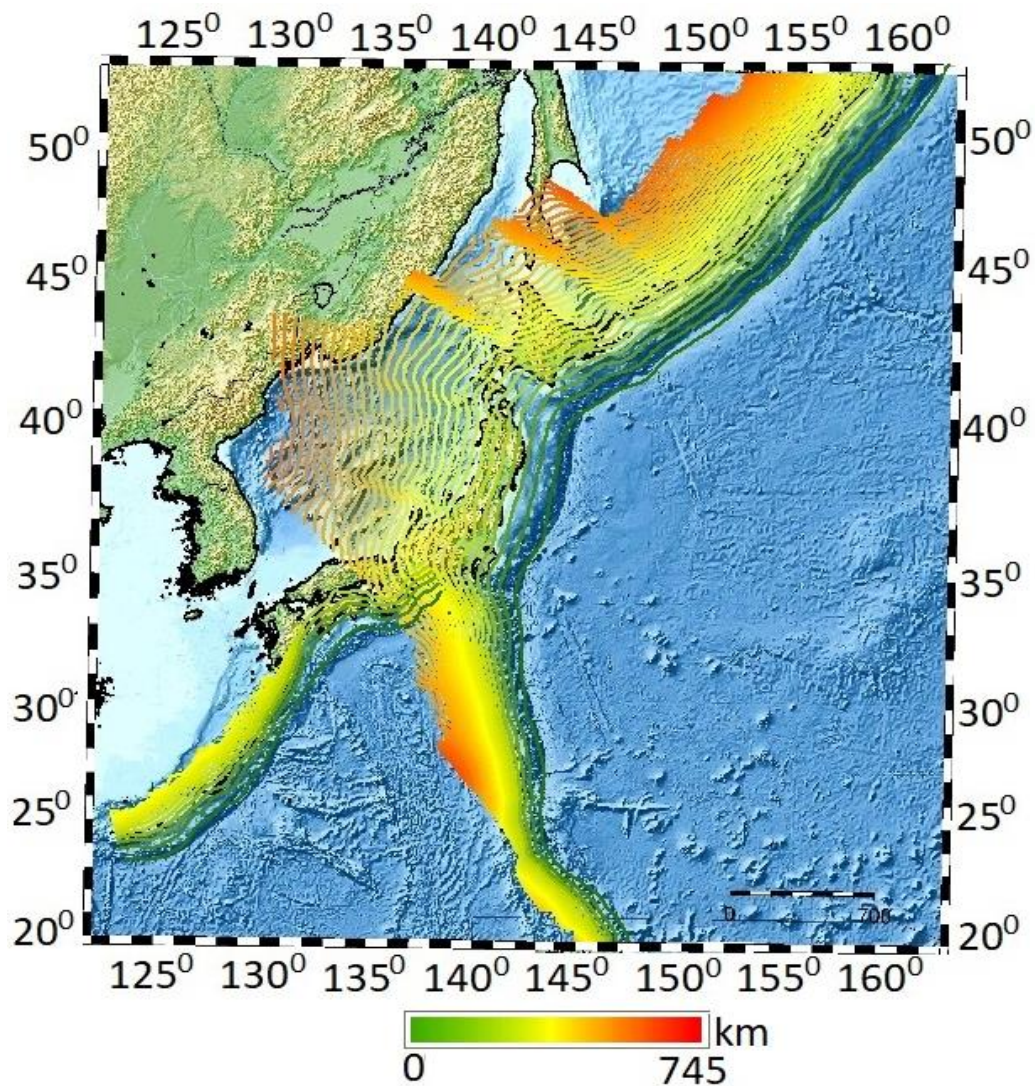


Figure 3.2: Slab depth beneath the Japanese Islands (USGS slab models).

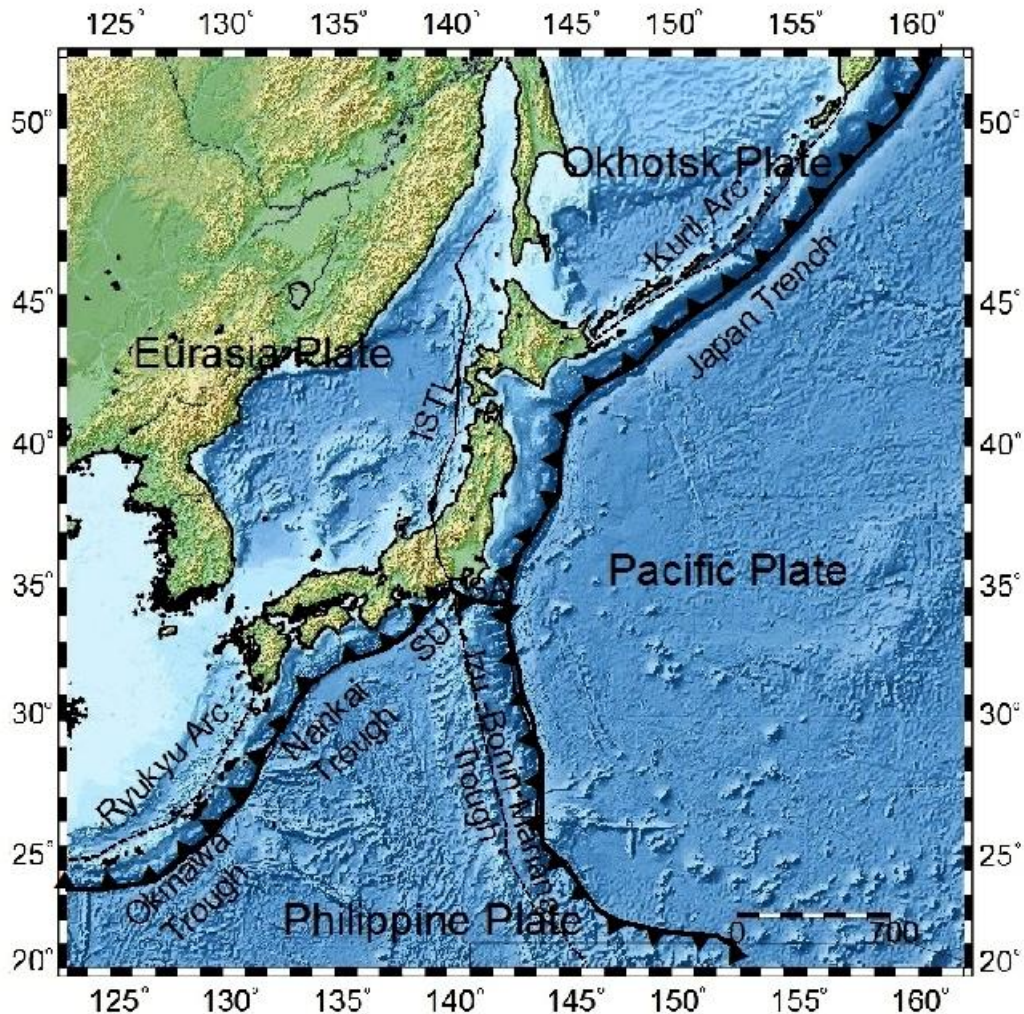


Figure 3.3: Plate-tectonic setting of Japan and surrounding regions. Dashed lines mark volcanic arcs (Kuril Arc, Ryukyu Arc, Izu - Bonin Mariana Arc) and solid lines indicate major fault lines (Japan Trench, Nankai Trough, Suruga Trough (SU), Itoigawa - Shizuoka Tectonic Line (ISTL), Okinawa Trough, Mariana Trough and Sagami Trench (SA)).

3.2 SEISMIC NETWORK AND EARTHQUAKE MONITORING

The seismic activity in and around Japan is high because it is located in an active plate boundary zone where four lithospheric plates converge on one another. Because of these plate interactions the seismic activity in and around Japan is very high. Seismicity covers all depths, in deep seismic zones reaches as deep as about 600 km in the subducted Pacific plate and as deep as 300 km in the subducted Philippine Sea plate along Ryukyu trench. In Japan we have the presence of both intraplate and interplate earthquakes. Interplate earthquakes occur at a plate boundary, whereas, intraplate occur in the interior of a tectonic plate. In general, the last are more difficult to find.

Japan's seismic activity is intense and continuous; the Japanese have suffered great damages and losses. The deadliest earthquake was the 1923 *Great Kantō earthquake*, on the Japanese main island of Honshū (7.9 Mw), with 105,385 deaths, while the strongest and most costly earthquake on record is the 2011 Tohoku earthquake (9.0). After the disastrous 1995 Kobe earthquake, a new national project has started to drastically improve seismic observation

system in Japan. A large number of strong-motion, high-sensitivity, and broadband seismographs were installed to construct dense and uniform networks covering the whole of Japan (Fig. 3.4). The new high-sensitivity seismograph network consisting of 696 stations is called Hi-net, while the broadband seismograph network consisting of 71 stations is called F-net (Fig. 3.5). At most of Hi-net stations strong-motion seismographs are also equipped both at depth and the ground surface. The network of these 659 stations with an uphole/downhole pair of strong-motion seismographs is called KiK-net, while another network consisting of 1034 strong-motion seismographs installed at the ground surface is called K-NET (Okada et al., 2004) (Fig. 3.6).

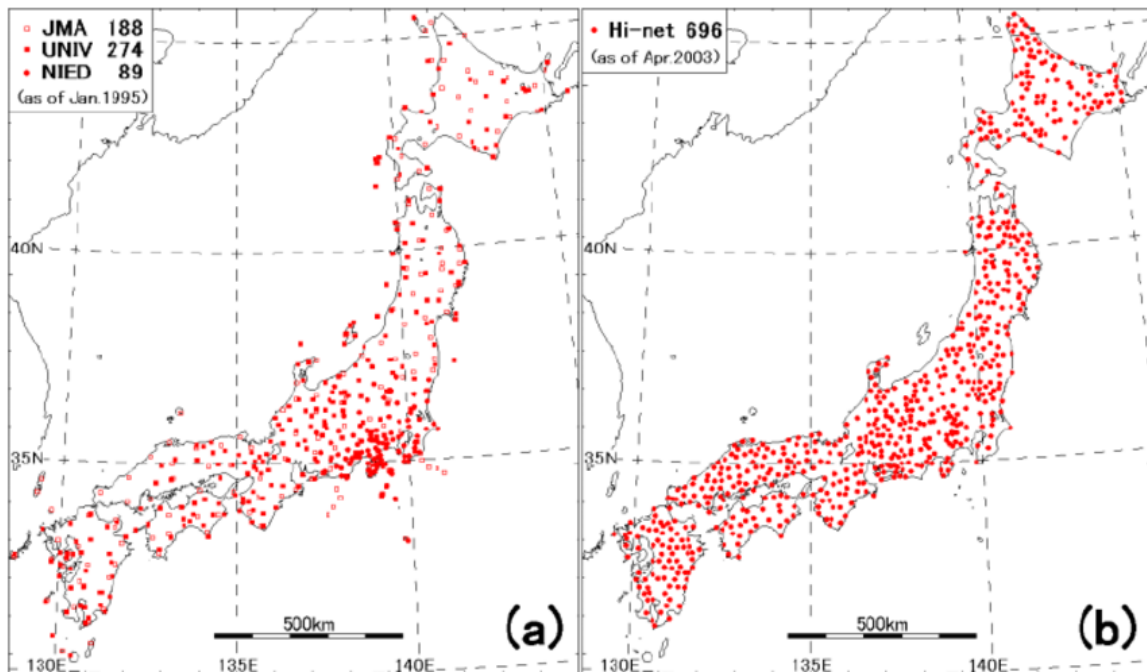


Figure 3.4: Distribution of high sensitivity seismic stations in Japan (a) at the time of 1995 Kobe earthquake and (b) newly added Hi-net stations as of April 2003 (JMA: Japan Meteorological Agency, UNIV: University, NIED: National Research Institute for Earth Science and Disaster Prevention).

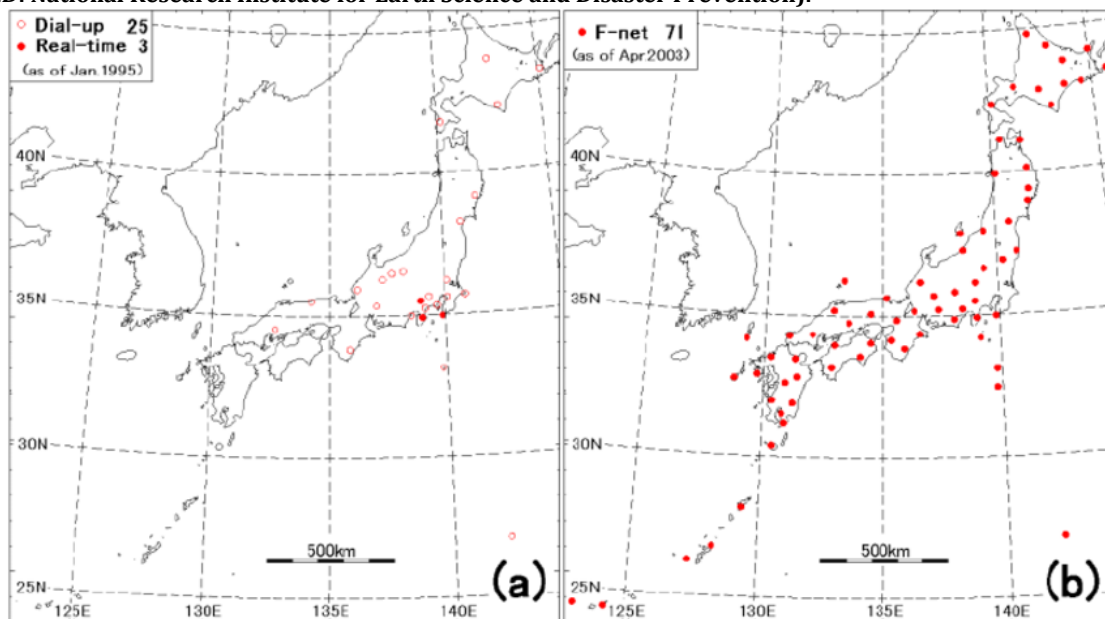


Figure 3.5: Distribution of broadband seismic stations in Japan (a) at the time of 1995 Kobe earthquake and (b) newly added F-net stations as of April 2003. (JMA: Japan Meteorological Agency)

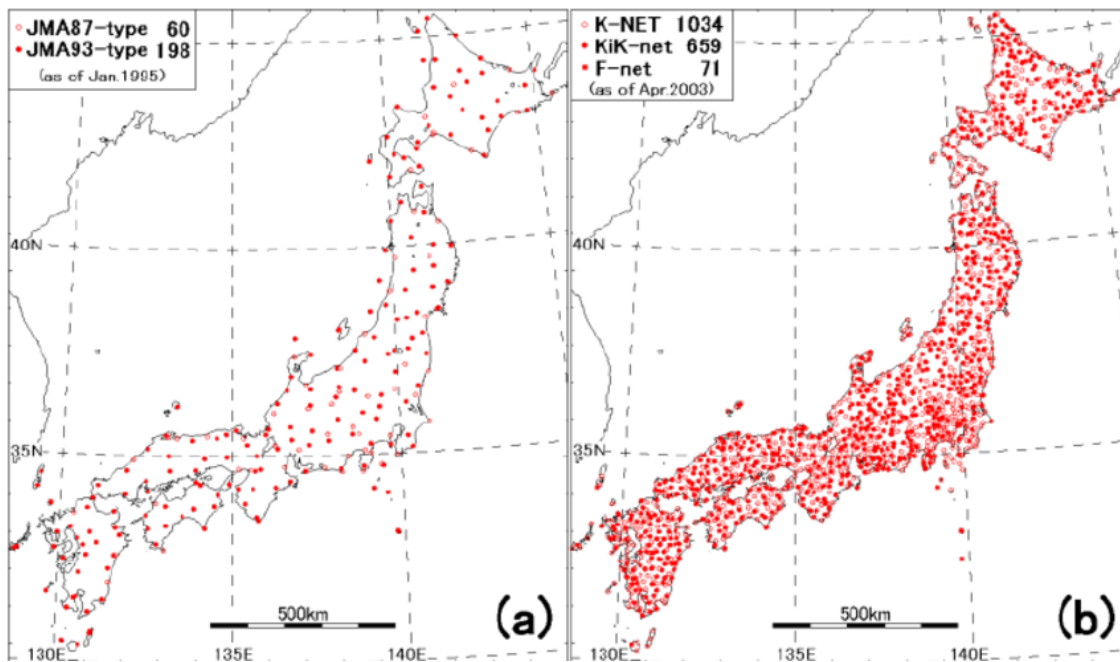


Figure 3.6: Distribution of strong motion seismic stations in Japan (a) at the time of 1995 Kobe earthquake and (b) newly added K-NET, KiK-net and F-net stations as of April 2003. (JMA: Japan Meteorological Agency)

3.2.1 HYPOCENTER DETERMINATION

Hypocenters are calculated using the arrival-times of P-waves and S-waves, and magnitudes are calculated using the maximum seismic-wave amplitudes. An iterative method (Hamada et al., 1983), an extension of Geiger's method (Geiger, 1910), is used to calculate hypocenters. The data weight is given by the following formula, where R denotes the hypocentral distance (Ueno et al., 2002):

For P-waves (W_p)

$$W_p = \frac{R_{min}^2}{R}$$

For S-waves (W_s)

$$W_s = \frac{W_p}{3}$$

R_{min} : Hypocentral distance of the station nearest to the hypocenter (km) (if $R_{min} < 50$, then $R_{min} = 50$; if $W_p > 1$, then $W_p = 1$)

The data of any station with large travel-time residuals are not used for the calculations. The depth of focus is calculated first with no restrictions. If the solution is unstable, then the best solution is searched by changing the depth in 1 km steps. In the case that the focus is located in a region where focal depths are considered to be not well determined, such as in the Kurile Islands region, the focal depth is fixed at 30 km. In principle, the calculation is done only when more than five P or S-wave arrivals have been observed at three or more stations (a criterion used since January 1983). If the number of stations with observations exceeds 40, the nearest 40 stations from the focus are used in the calculation (a criterion used since October 1997).

Procedures for the selection of stations are as follows. A characteristic distance (Δ_{lim}) is defined in terms of the following empirical equation:

$$\Delta_{lim} = \frac{\Delta_3^2}{100 (km)} + H (km) + 100 (km)$$

Here Δ_3 denotes the epicentral distance of the third nearest station from the trial hypocenter; H is focal depth: the unit is kilometre.

The 16 stations nearest to the trial hypocenter are selected without regard to station quality. An additional 24 stations within Δ_{lim} are then selected based on the epicentral distance and station quality, where the station quality is given as an attribute constant derived from seven classes regarding the S/N ratio, data-sending capability and average travel-time residual etc. If the number of selected stations is still not enough for robust estimation in the case of an offshore earthquake or a deep earthquake, for example, additional stations outside Δ_{lim} may be selected until the number of stations becomes sufficient.

3.2.2 MAGNITUDE DETERMINATION

Magnitude M_J : This is calculated only for large and shallow ($H \leq 60$ km) earthquakes using acceleration data from the multi-function seismometers installed at the Local Meteorological Offices. M_J is given by the average of observations of

$$M_J^{OBS} = \log \sqrt{(A_N^2 + A_E^2)} + 1.73 \log \Delta - 0.83$$

using the maximum displacement amplitudes at the stations (Tsuboi, 1954). Here the acceleration data are integrated twice to obtain the displacement data, to which a high pass (6 s) filter is applied to simulate the mechanical strong-motion seismographs.

Displacement Magnitude M_D : This is calculated as the average of observations of

$$M_D^{ST} = \log \sqrt{(A_N^2 + A_E^2)} + \beta_D(\Delta, H) + C_D$$

over stations in the ranges $R \geq 30$ km and $\Delta \leq 700$ km for maximum amplitudes of displacement in the horizontal components (Katsumata, 2004). If the number of stations involved in the average is less than three, Δ is extended out to 2000 km. If the number of the stations used to obtain M_D is two, it is denoted as M_d .

Velocity Magnitude M_V : This is calculated as the average of observations of

$$M_V^{ST} = \log A_Z + \beta_V(\Delta, H) + C_V$$

over stations in range $5 \text{ km} \leq R \leq 400$ km for maximum amplitude of velocity in the vertical component (Funasaki et al., 2004). If the number of stations involved in the average is less than four, Δ is extended out to 1000 km. If the number of the stations used to obtain M_V is two or three, it is denoted as M_v .

First, an initial mean of magnitudes at all the stations is calculated. Then a mean and standard deviation of magnitudes for the stations is calculated, discarding those values deviating more than 0.5 from the initial mean. This mean value is adopted as the magnitude only if the standard deviation is less than 0.35.

The calculated value is adopted as the JMA magnitude according to the priority order $M_j > M_D > M_V > M_d > M_v$, and this is then given as the primary magnitude estimate. The moment magnitude is generally given as the secondary magnitude estimate when CMT solutions are determined; otherwise a secondary magnitude estimate is given according to the priority order. For reference, the meanings of the symbols used in the above formulas are as follows:

Table 3.1: Meanings of the symbols used above.

H	Focal Depth (km)
Δ	Epicentral Distance (km)
R	Hypocentral Distance (km)
α	Constant $1/0.85 = 1.176$
β_D, β_V	Terms showing dependence on Δ and H
C_D	Correlation Value (=0.2) used for accelerometers
C_V	Correction Value depending on types of seismometers
A_N, A_E	Maximum Displacement Amplitude in the horizontal component of accelerometers (mm, 10^{-6} m)
A_Z	Maximum Velocity Amplitude in the vertical component of velocity meters (10^{-5} m/s)

3.3 EARTHQUAKE CATALOGUE

The earthquake catalogue used in this study is produced by the Japan Meteorological Agency (JMA), in cooperation with the Ministry of Education, Culture, Sports, Science and Technology. The catalogue is based on seismic data provided by the National Research Institute for Earth Science and Disaster Resilience, the Japan Meteorological Agency, Hokkaido University, Hirosaki University, Tohoku University, the University of Tokyo, Nagoya University, Kyoto University, Kochi University, Kyushu University, Kagoshima University, the National Institute of Advanced Industrial Science and Technology, the Geographical Survey Institute, Tokyo Metropolis, Shizuoka Prefecture, Hot Springs Research Institute of Kanagawa Prefecture, Yokohama City, and Japan Agency for Marine-Earth Science and Technology.

The catalogue is referring to the time period 01/01/2002 – 31/05/2016 and consists of 103,696 events with a threshold magnitude equal to 3 and depth range 0 - 698.4 (Fig.3.7). The catalogue is homogeneous and for the purposes of this study we used the existing magnitude scale m_V provided by JMA (see below).

The spatial distribution of earthquakes (Fig. 3.6) is mostly constrained on the plate boundaries, across the coastline, and along the volcanic arcs of Kuril (northern Japan), Izu-Bonin Mariana Arc (south-eastern Japan) and Ryukyu (south-western Japan). It is evident that the majority of earthquakes is located in Okhotsk plate, north of the triple junction.

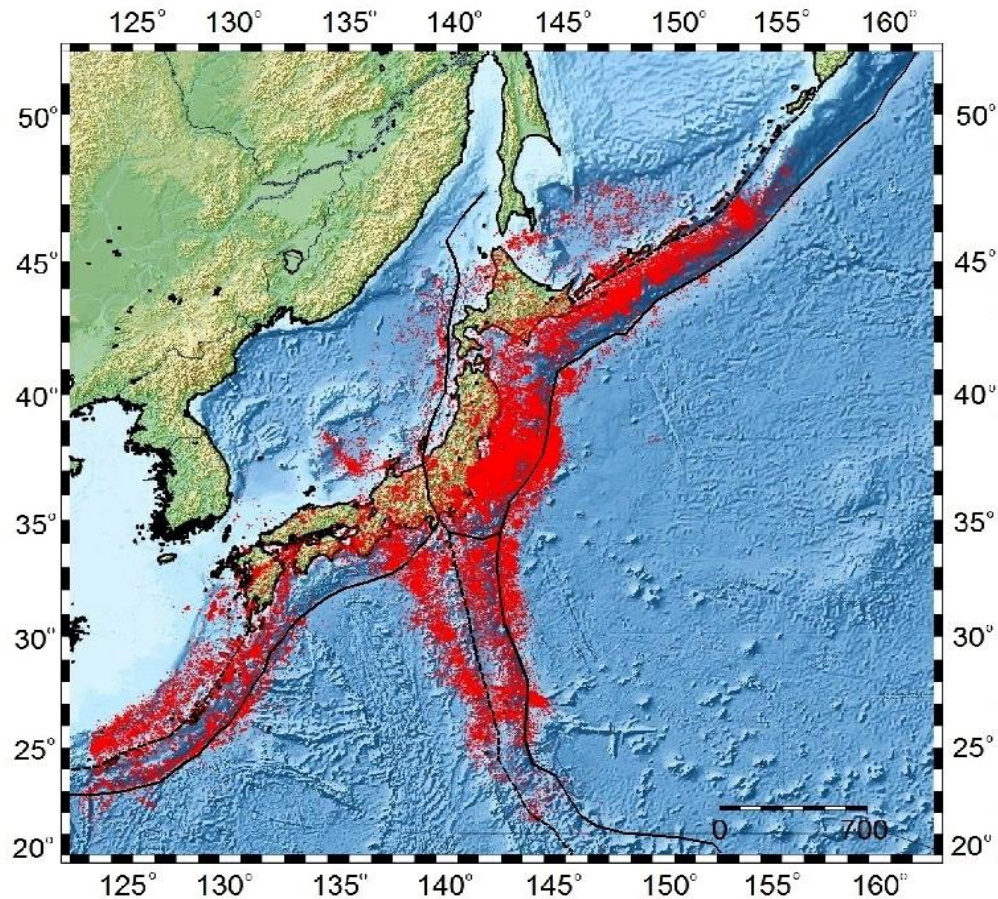


Figure 3.6: Seismic catalogue used in this study. Hypocenters are depicted in red. Solid black lines indicate major tectonic boundaries (Okhotsk, Amurian, Philippine and Pacific) and dashed black lines indicate major arcs.

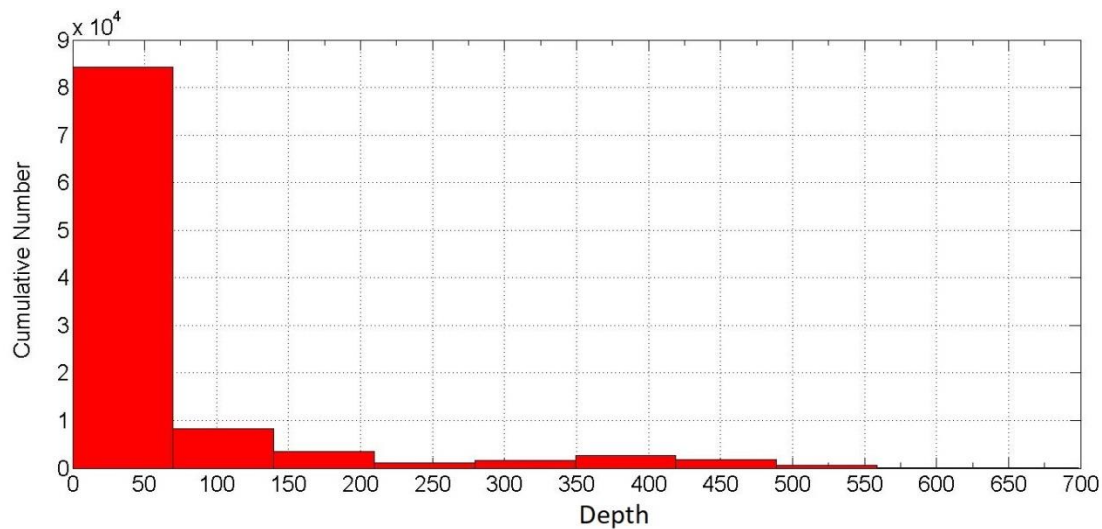


Figure 3.7: Depth histogram of the catalogue. Depth varies from 0 to ~ 700. Most events are below 100 km.

The b - value is among the most widely reported statistics in seismology. Although its globally averaged value is approximately 1, it may vary by as much as a factor of three at both local and region scales (Wiemer and Wyss, 2002). The parameters influencing b -value remain somewhat enigmatic; however, laboratory and numerical models indicated that the parameter scales

inversely with ambient stress conditions (Scholz, 1968; Amitrano, 2003). The dependence of b on stress implies that small ruptures are more likely to grow into large earthquakes in high – stress areas, since the system contains more energy and the rupture can more easily connect across subvolumes with lower stress concentrations (Scholz, 1968). Alternatively, b value patterns may reflect variability in the distribution of fractures within a rock volume (Barton et al., 1999; Henderson et al., 1999; Wyss et al., 2004), whereby higher b values indicate greater structural heterogeneity (Mogi, 1962). Experimental evidence also suggest that increasing thermal gradients or heterogeneous stress conditions generated by nonuniform temperature distributions may result in higher b values (Warren and Latham, 1970). Some studies have discussed the spatial and temporal variations of the b -value before large earthquakes and the spatial variation of the aftershocks. Aftershocks have large b -value, foreshocks, on the other hand, present low value (Suyehiro et al., 1964). This conclusion is supported by numerous field observations such as those in Taiwan (Wang, 1988) and along the Circum – Pacific subduction zones (Carter and Berg, 1981). Measurements of well – pressure, number of triggered earthquakes, and b -values in the Denver waste water injection site revealed that high shear stress corresponds to low b -values and high seismic moment release (Evans, 1966; Healy et al., 1968; Wyss, 1973). This mechanism for the temporal variations of b – values has been used to explain b -value changes prior to major earthquakes in Japan and elsewhere (Imoto, 1991).

The correct estimate of the b , and a -values depends critically on the completeness of the sample under investigation. The frequency magnitude distribution of our catalogue was estimated with the method of robust regression (Fig. 3.8) using the MatLab application. Robust regression works by assigning a weight to each data point. Weighting is done automatically and iteratively using a process called iteratively reweighted least squares. In the first iteration, each point is assigned equal weight and model coefficients are estimated using ordinary least squares. At subsequent iterations, weights are recomputed so that points farther from model predictions in the previous iteration are given lower weight. Model coefficients are then recomputed using weighted least squares. The process continues until the values of the coefficient estimates converge within a specified tolerance.

In order to complete the fitting we use four steps. The first step includes the data preparation, the second, the fitting of the linear model to the data using robustfit, the third step, the estimation of residuals and step four, the removal of outliers from the standard model.

The difference with least squares is that the latter aims to minimize the sum of squares of residuals (L2 norm) from the data to the line (or curve, or surface) being fit. The only problem is primarily due to the squaring, data values with large residuals could have a large amount of influence on the position of the fitted line. Simple tossing away outliers based solely on the fact that they are outliers is a huge "do not do" in statistics, so therein lies a problem. Most robust regression procedures don't work with the L2 norm. Robust regression based on M - estimation obtains estimates by minimizing a non-negative function of the residuals.

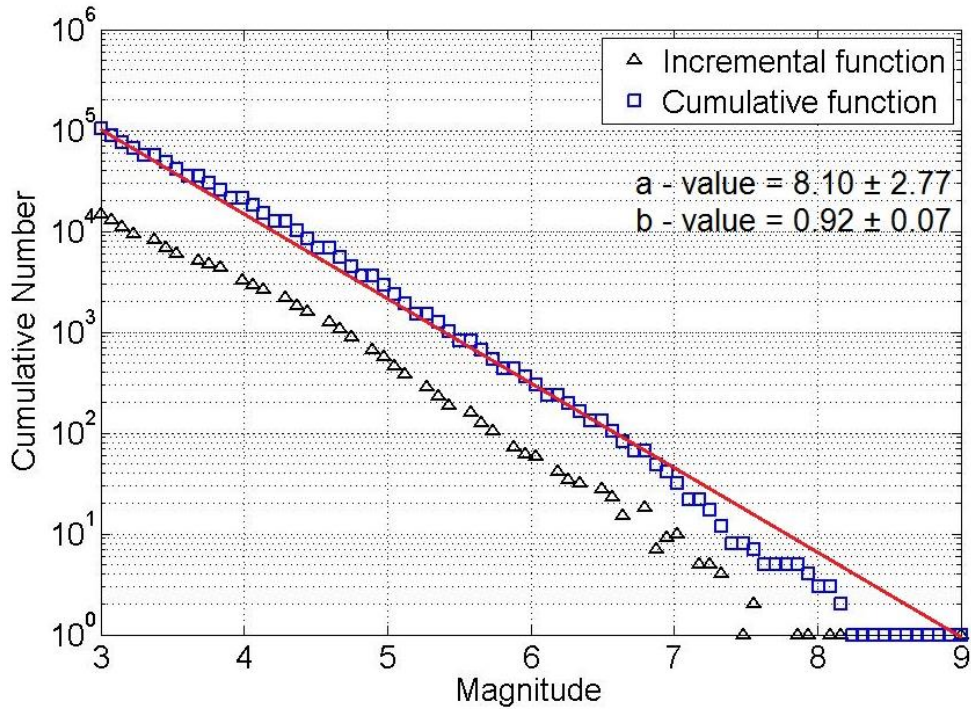


Figure 3.8: Frequency - Magnitude distribution of the entire seismic catalogue. The magnitude of completeness (M_c) is 3, a - value = 8.10 ± 2.77 and b - value = 0.92 ± 0.07 .

The form of the cumulative function is changing for magnitudes ≥ 7 . It is evident that the catalogue mostly contains small magnitudes and as they increase the frequency occurrence is decaying rapidly. As a result we have very few earthquakes with magnitudes larger than 7. That in fact proves that our catalogue is divided into two. For magnitudes ≤ 7 GR's coefficients a , and b are 7.7 and 0.87 respectively, whilst, for magnitudes ≥ 7 b -value is 0.98 and a - value is 8.3.

It is of great importance to map the spatial distribution of the Gutenberg-Richter coefficients. Their variations in space and time can provide useful information about seismogenesis and tectonics. In the following figures (Fig. 3.9 and 3.10), the GR's coefficients, a -value and b -value, along with the variations of magnitude of completeness in time are depicted for both crustal and sub-crustal catalogues.

For crustal events (Fig. 3.9a) b -value ranges from 0.6 to 1.2 and a -value (Fig. 3.9b) from 5 to 7.5. The maximum values for both a and b are located in south-eastern Japan, within the Pacific plate, whilst, the minimum values are located in north-eastern Japan, in Honshu island and Kuril arc, within Okhotsk plate. The magnitude of completeness (Fig. 3.9c) doesn't present any significant changes in time ($M_c \sim 3$), with one small exception in 2011.

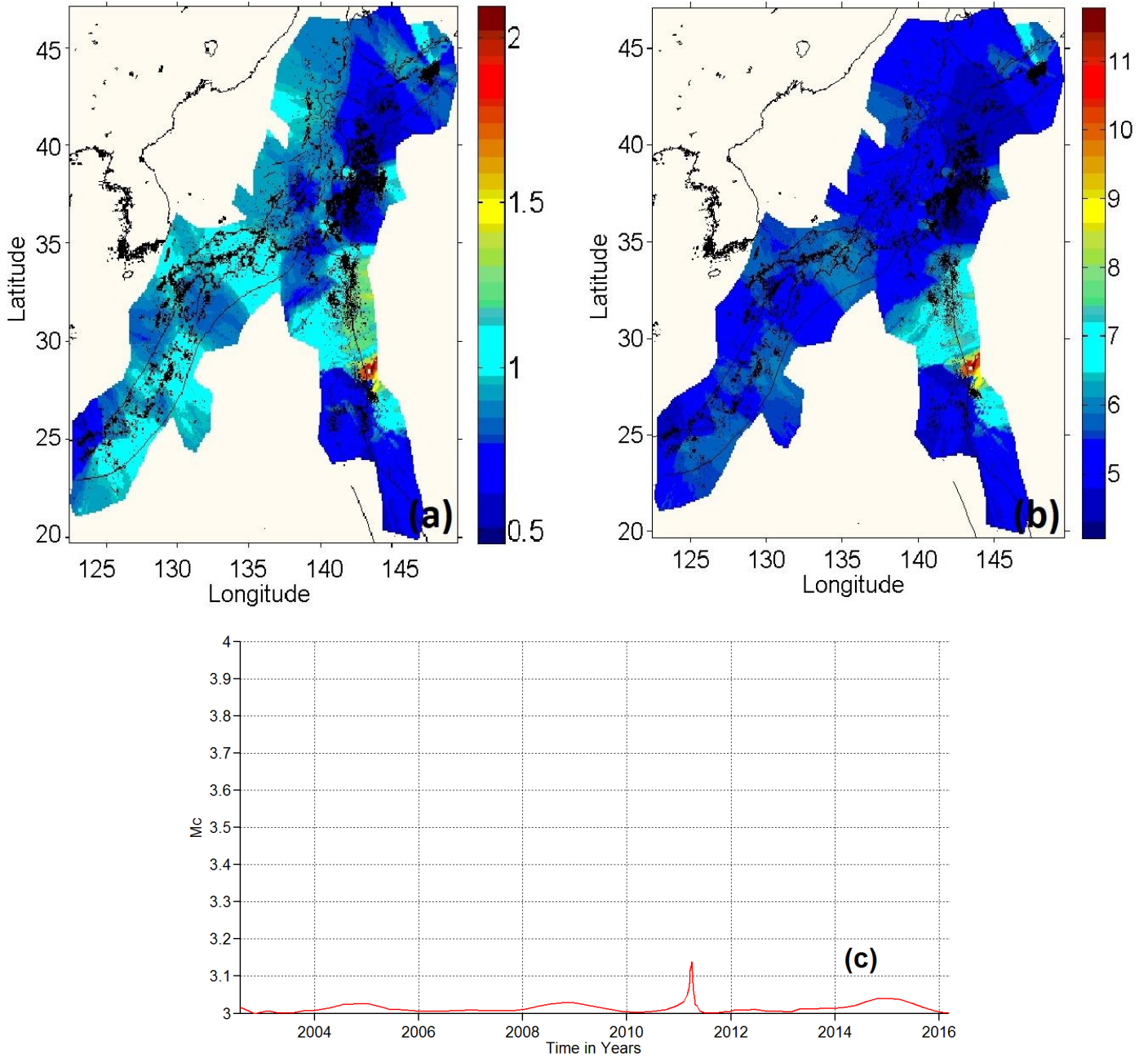


Figure 3.9: Spatial distribution of (a) a-value and (b) b-value for crustal events along the study area. (c) Magnitude of completeness variations in time.

For sub-crustal events the GR coefficients spatial distribution are depicted in Figures 3.10(a) and 3.10(b). *b*-value is around 1 for the entire study area. It increases in the north-eastern and south-eastern Japan, in Kuril arc and Pacific plate. The magnitude of completeness (Fig. 3.10c) presents small variations in time, specifically in 2011, that reaches 3.2. But in general it doesn't exceed 3.1.

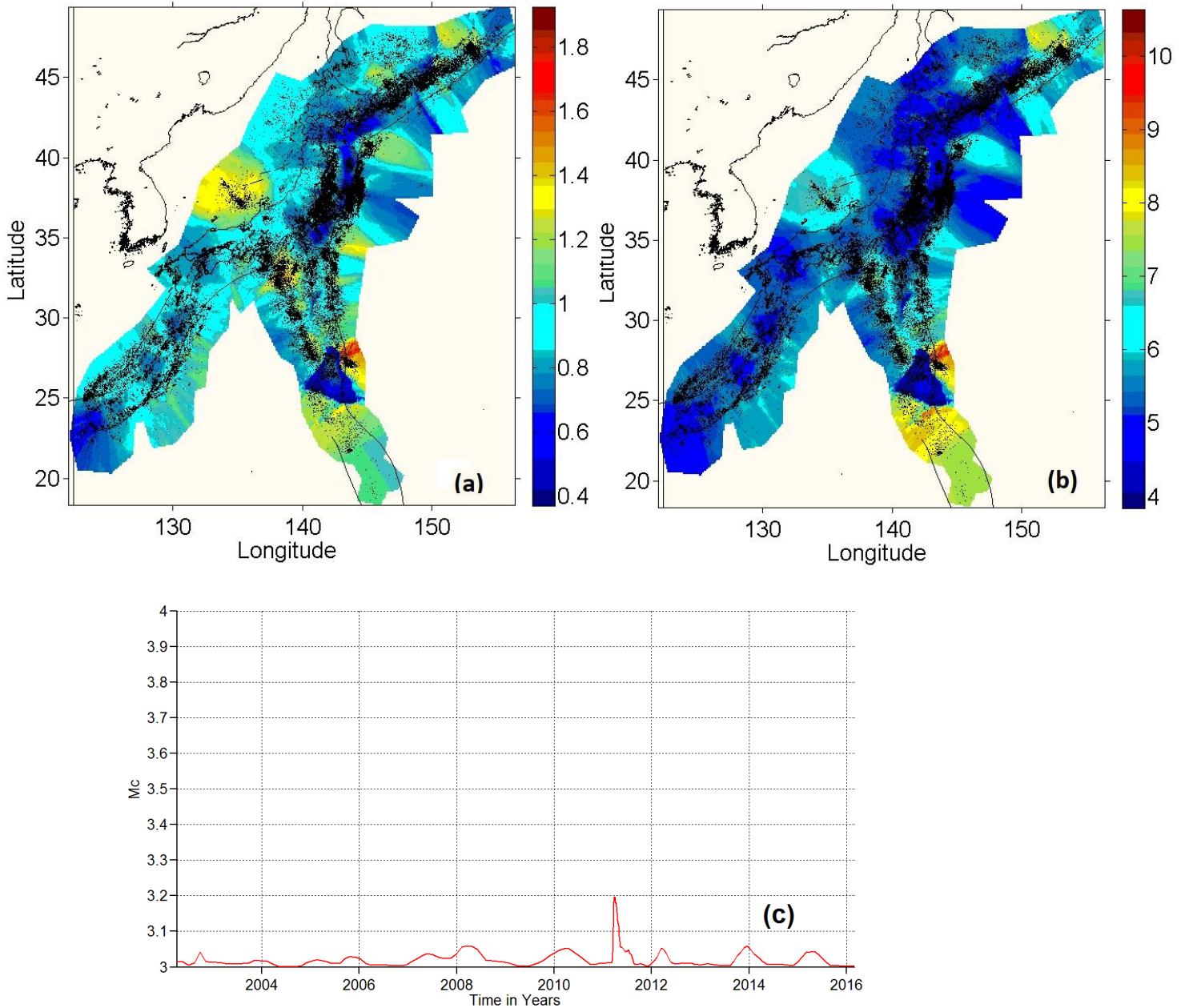


Figure 3.10: Spatial distribution of (a) b-value and (b) a-value for sub-crustal events along the study area. (c) Magnitude of completeness variations in time.

As already mentioned, the total number of events is 103.696 with magnitude of completeness, M_c , 3. The following figure (figure 3.11) shows the cumulative number of earthquakes - seismicity's evolution over the years - for the entire area. It is well known that seismicity is intense and strong earthquakes generate intense and continuous aftershock sequences that affect the seismic process by releasing more energy and triggering neighbouring fault zones. This is well depicted below. In 2011 we observe a steep increase on the number of events, showing that a large earthquake and a strong aftershock sequence took place. Comparing this result to the above analysis of the GR's coefficients we see that in the area, where the epicentre of the 2011 quake is located, we have low b - values and maximum density of events.

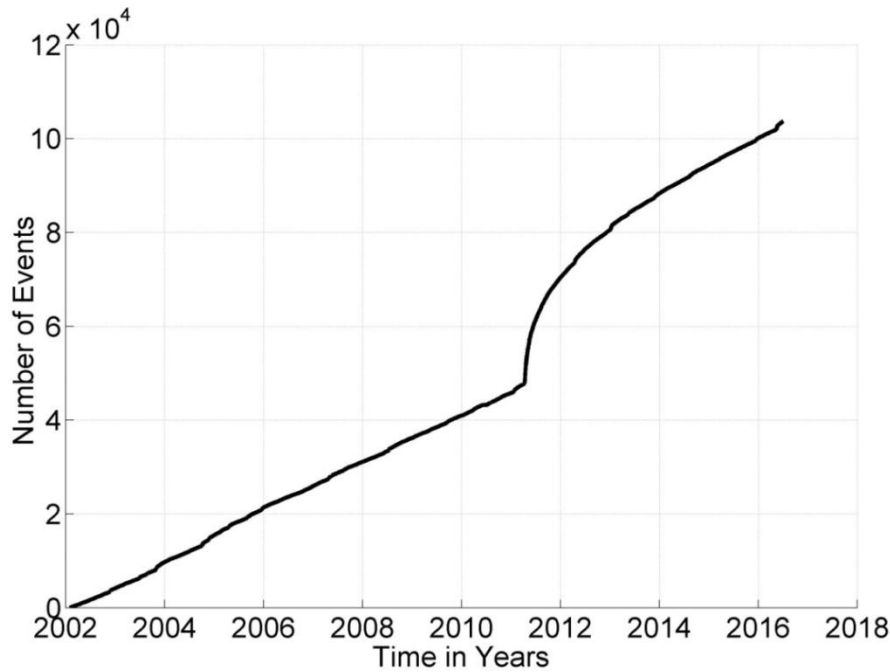


Figure 3.11: Cumulative number of events. The catalogue contains 103.696 seismic events. It is evident that seismicity is intense, due to the steep increase of the curve that indicates the occurrence of a strong earthquake with its aftershock sequence.

3.3.1 Catalogue Declustering

One of the primary objectives of this analysis is to investigate and interpret the characteristics of background seismicity. For that the space-time ETAS model was used, which is an algorithm that identifies events which, at a certain probability level have triggered aftershock sequences. As aforementioned, according to ETAS background events may not be major at all; for example, an earthquake of magnitude 4 may trigger an earthquake with a magnitude of 7.5 given the right conditions.

The output of stochastic declustering is not unique, it is useful to use the probabilities ϕ_j to generate different realizations of the declustered catalogue at different probability levels and use them to test hypotheses associated with background seismicity and/or aftershock clustering. Our analysis herein will be based on the assumption that events with probability $\phi_j \geq 70\%$ are likely to be background. The output of the declustering process is illustrated in Fig. 2.6, 2.7, 2.8 and 2.9 where the cumulative number of earthquake events vs. time is plotted for all catalogues (crustal and sub-crustal) of all study areas and for three different background probabilities ($\phi_j=70\%$, $\phi_j=80\%$ and $\phi_j=90\%$). It is apparent that the declustered catalogues are free of the time-local rate surges that indicate the presence of aftershock sequences.

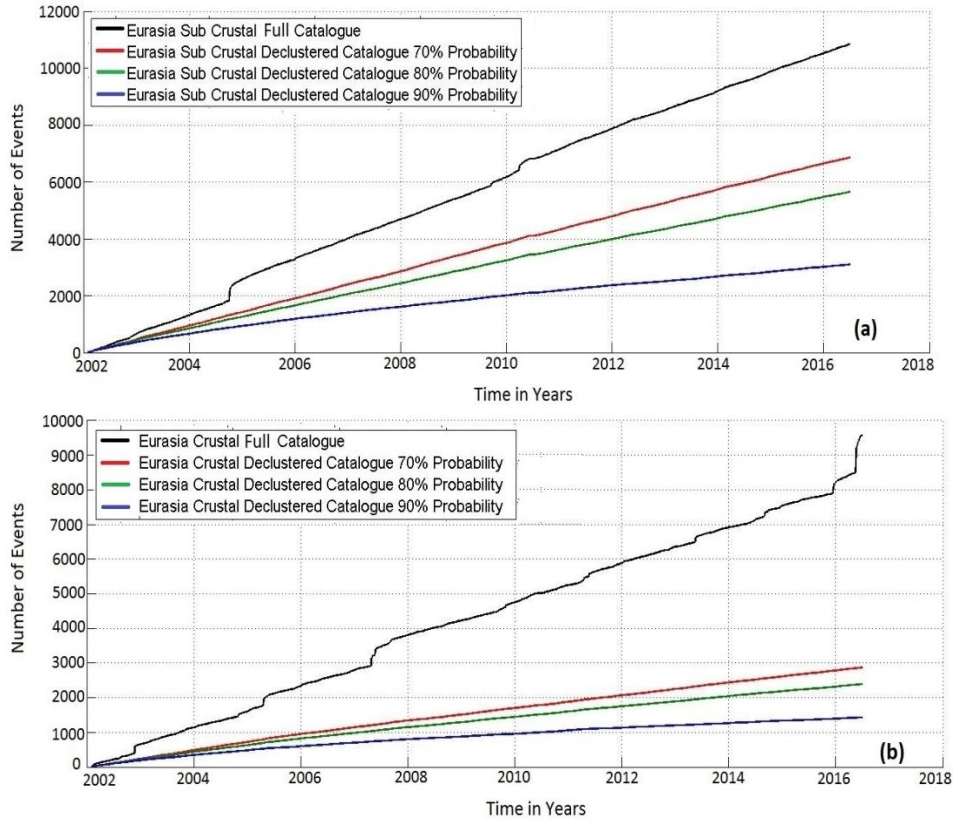


Figure 2.6: Cumulative number of events of Eurasia's a) sub-crustal and b) crustal declustered catalogues. The black solid line indicates the full catalogue. Red, green and blue lines illustrate the three background probabilities that are tested afterwards, 70%, 80% and 90% respectively.

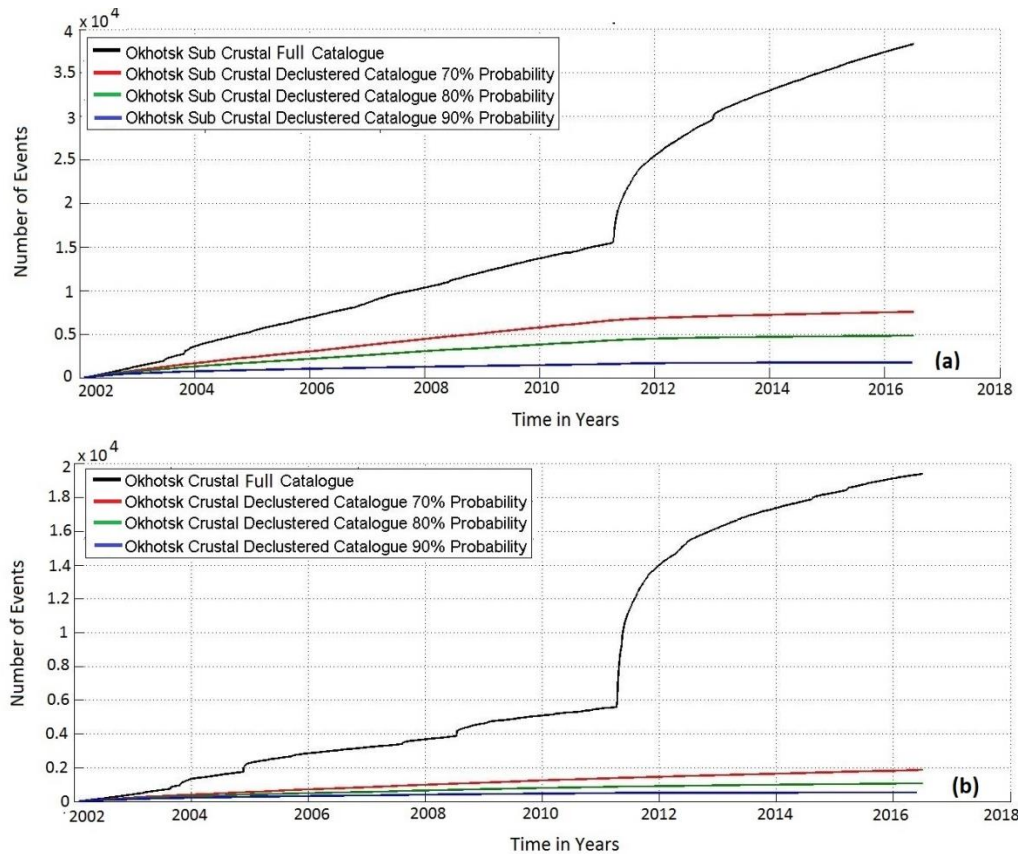


Figure 2.7: Cumulative number of events of the full and declustered catalogues of Okhotsk a) sub-crustal and b) crustal earthquake catalogues. It is well pictured that the declustering process was successful, due to the fact that aftershock sequences have been removed. The black solid line depicts the full catalogue, where the 2011 sequence is shown. Red, green and blue lines illustrate the three background probabilities that are tested afterwards, 70%, 80% and 90% respectively.

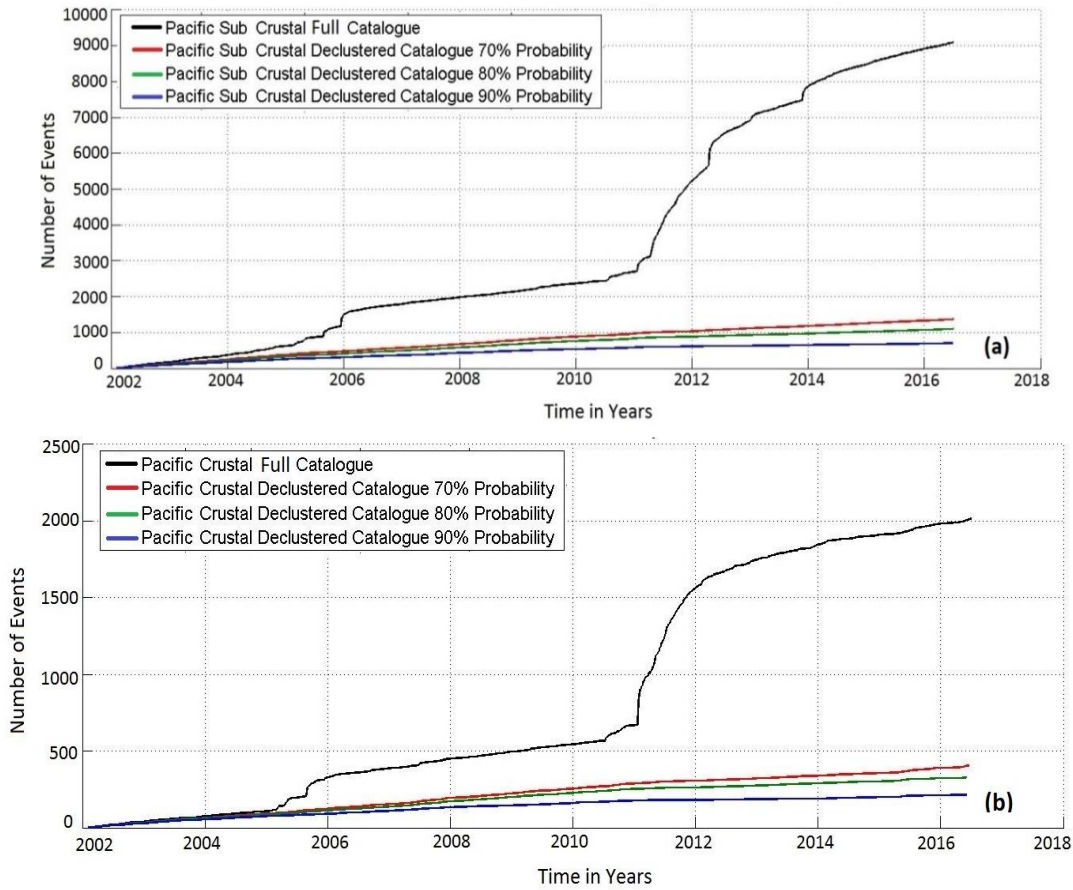
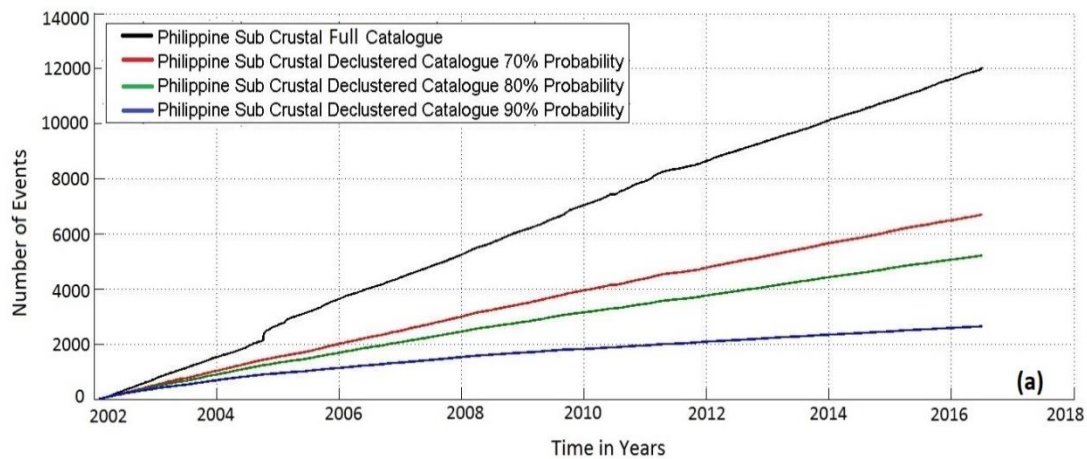


Figure 2.8: Cumulative number of events of the raw and declustered catalogues of Pacific's a) sub-crustal and b) crustal events. The black solid line depicts the raw catalogue. Red, green and blue lines depict the three background probabilities, 70%, 80% and 90% respectively.



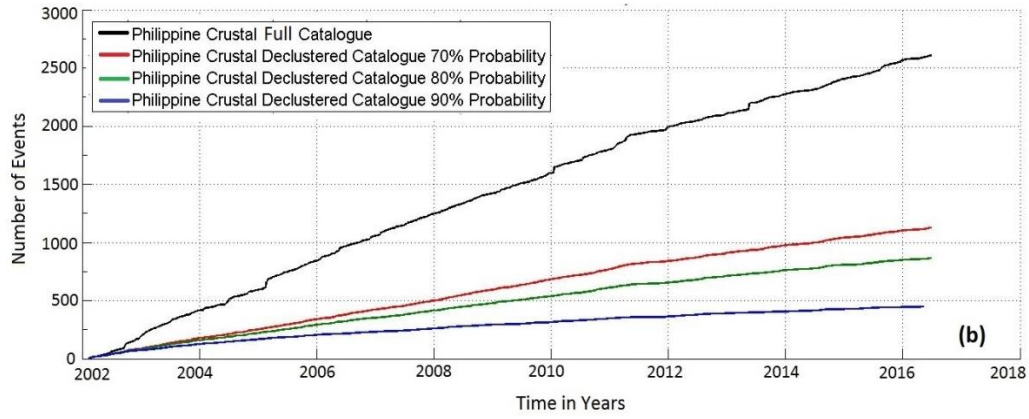


Figure 2.9: Cumulative number of events of the raw and declustered catalogues of Philippine's a) sub-crustal and b) crustal events. The black solid line depicts the raw catalogue. Red, green and blue lines depict the three background probabilities, 70%, 80% and 90% respectively.

4. DETERMINATION AND ANALYSIS OF ENTROPIC INDICES FOR RAW AND DECLUSTERED CATALOGUES AND b - VALUE ANALYSIS

4.1 RAW CATALOGUE ANALYSIS

4.1.1 Eurasian Plate.

The raw catalogue of Eurasian Plate (Fig. 4.1) is first analysed. Earthquakes are located along Ryukyu Arc, Okinawa, Shikoku, southern Honshu and Kyushu islands. The crustal seismicity catalogue consists of 9.595 events, between 0 km and 29 km depth. The catalogue of sub-crustal events consists of 10.855 earthquakes, with depth ranging from 29 km to 621 km.

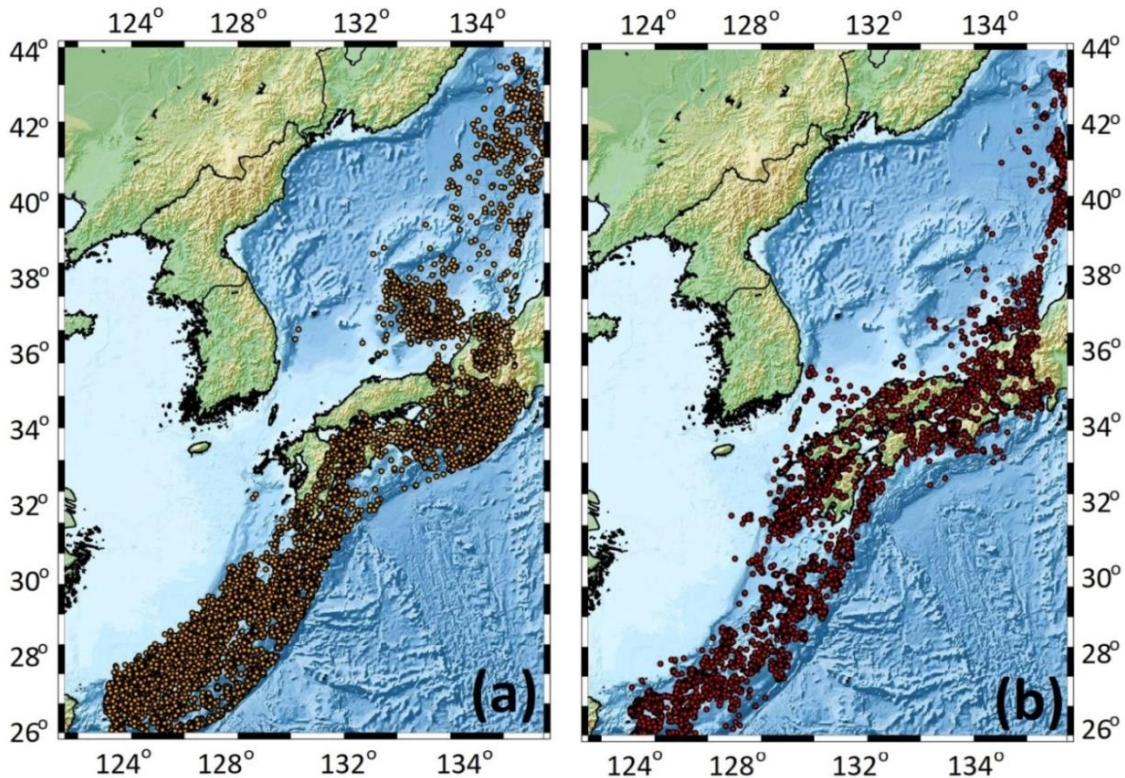


Figure 4.1: Eurasia Plate Seismicity. Two catalogues for different depth ranges are depicted. (a) Sub-crustal seismicity (b) crustal seismicity. Seismic events are distributed along Ryukyu Arc, Honshu and Kyushu islands.

The analysis of sub-crustal seismicity for different cut-off magnitudes is graphically illustrated in (Fig. 4.2a) and shows that the temporal entropic index q_T varies from 1.16 for $M = 3.1$, to 1 for $M = 4.6$ but for the most part, lingers in the interval (1.1, 1.2). Correlation is stronger in crustal seismicity with q_T , varying from 1.23 for $M = 3$ to 1.34 for $M = 4.6$. Therefore, it can be safely deduced that correlation is rather poor, indicating practically random earthquake occurrence, especially for sub-crustal seismicity, with respect to time, at least for cut-off magnitudes of the order of 4.4 – 4.6.

The entropic index q_M for sub-crustal events (Fig. 4.2b) varies from 1.53 for $M = 3.1$, to 1.54 for $M = 4.6$. This yields proxy- b values ranging from 0.89 for $M = 3.1$ to 0.85 for $M = 4.6$. For crustal events q_M , varies from 1.53 for $M=3$ to 1.58 for $M=4.6$ yielding to proxy- b values 0.9 and 0.73 for the same cut-off magnitudes.

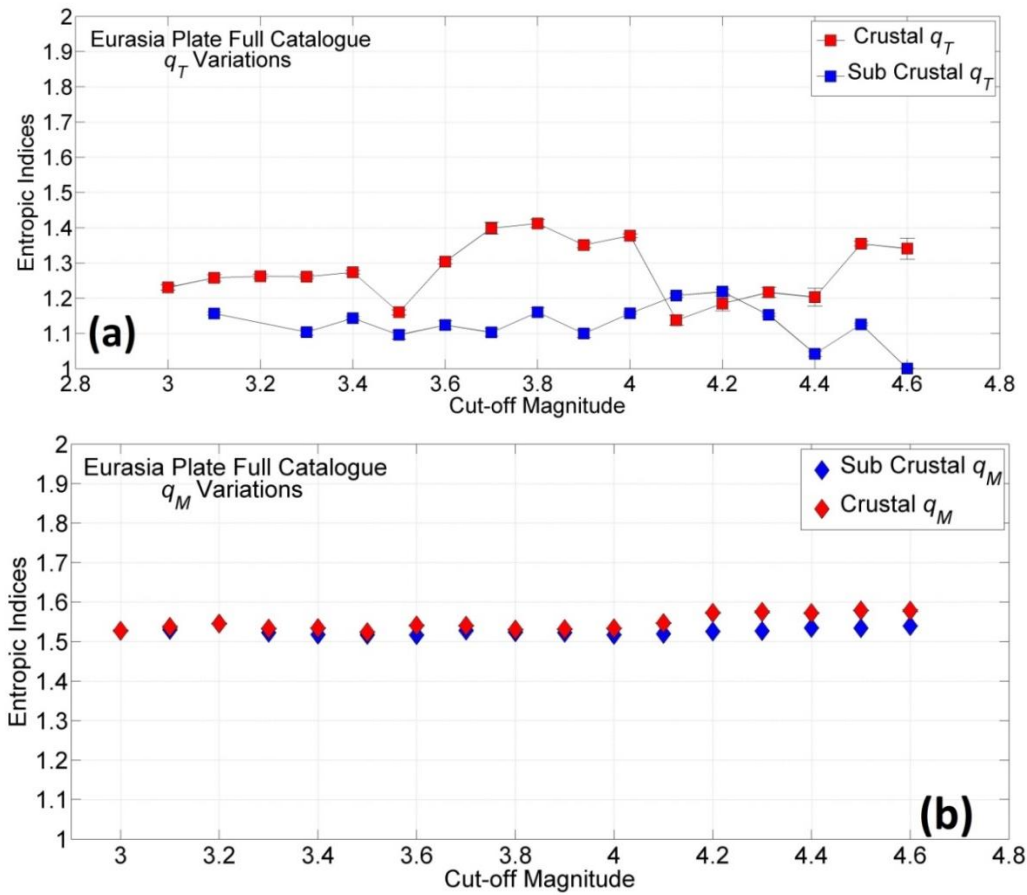


Figure 4.2: Analysis of entropic index dependence on different cut-off magnitudes for sub-crustal (blue) and crustal (red) seismicity. (a) q_T variations, and (b) q_M variations.

The following figure (Fig. 4.3) illustrates the dependence of entropic indices on interevent distance, for a cut-off magnitude of $M=3$. The breadth of interevent distance bins is indicated by the horizontal line segments across the index symbols. For sub-crustal seismicity (Fig 4.3a) correlation is strong up to 100 km, with the temporal index reaching the value of 1.95. Beyond 100km the q_T decreases dramatically and fluctuates in the interval (1, 1.16). For crustal seismicity, correlation is also strong in the first 100 km, where the temporal entropic index reaches the value 1.79, but beyond that interevent distance decreases and fluctuates about 1.2 for distances up to 700km, further dropping to under 1.15 at longer ranges. . The results show that, for a cut-off magnitude of $M=3$, earthquakes are correlated in the first 100 km, due to the presence of earthquake swarms and aftershock sequences. At longer interevent distances, interactions are almost absent for sub-crustal events, and marginal for crustal.

The magnitude entropic index (Fig. 4.3b) for sub-crustal events is very stable and exhibits very small variations between 1.52 and 1.55, leading to proxy- b value variations between 0.8 and 0.9. For crustal events, the magnitude index decreases slightly with distance but lingers in the interval (1.48, 1.55) yielding proxy- b values of 1.05 and 0.83 respectively.

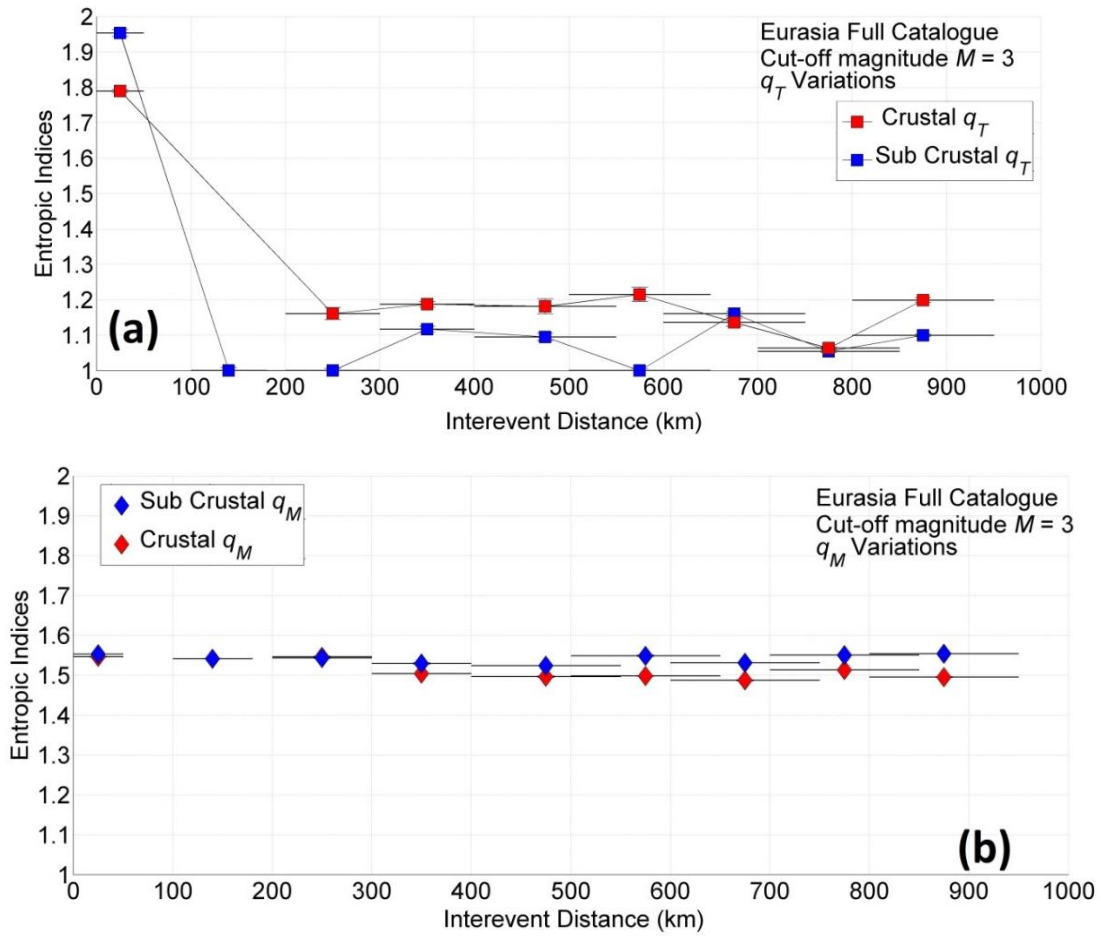
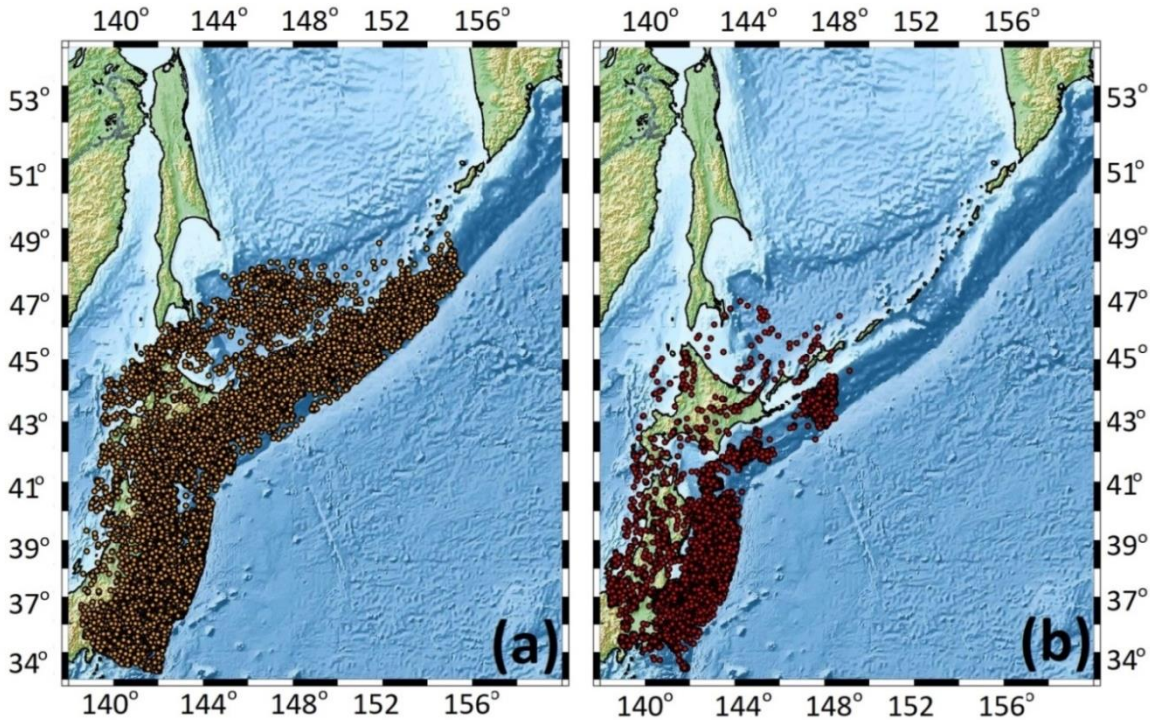


Figure 4.3: Analysis of the variation of entropic indices with interevent distances for sub-crustal (blue) and crustal (red) earthquake catalogues. (a) q_T variations, (b) q_M variations.

4.1.2. Okhotsk Plate

The seismicity of the Okhotsk plate is expressed along the Kuril arc, Hokaido Island and the northern Honshu Island. Correlation again is investigated for two raw catalogues, one for crustal (Fig. 4a) and one for sub-crustal seismicity (Fig. 4.4b).

Figure 4.4: Okhotsk seismicity. Two catalogues for different depth ranges are shown. (a) Sub-crustal



seismicity is depicted in orange and (b) Crustal seismicity is depicted in red.

The analysis of the Okhotsk plate seismicity for different cut-off magnitudes is illustrated in Figure 4.5. For sub-crustal events (Fig. 4.5a), the temporal entropic index, varies from 1.28 at $M=3$, to 1.34 at $M=5.5$, but for the most part lingers in the interval (1.2, 1.3). For cut-off magnitudes larger than $M=5$, q_T increases quasi-linearly and fluctuates between 1.22 and 1.35. Correlation, in general, is weak but increases with magnitude. For crustal seismicity, the temporal entropic index varies from 1.323 at $M=3$ to a surprising level of 2 at $M=5.2$. This would imply that at this magnitude correlation is almost absolute and almost every single event would influence the location and time of the next. Such strong correlation is inevitably related to the 2011 Tohoku earthquake and its aftershock sequence that lasted for almost 2 years and generated large events within the same geographical region.

The variations of the magnitude index q_M (Fig. 4.5b), for sub-crustal events is very stable and exhibits very small variations. For $M=3$ it is equal to 1.5 and for $M=5.5$ is equal to 1.495, this yields to proxy- b ranging from 0.98 to 1.0 for the respective cut-off magnitudes. For crustal seismicity q_M is stable between $M=3$ (1.54) and $M=4.5$ (1.52) and then increases to 1.61 for $M=5.2$. Respectively, for $M=3$ $b_q = 0.88$ and for $M=5.2$ $b_q=0.63$.

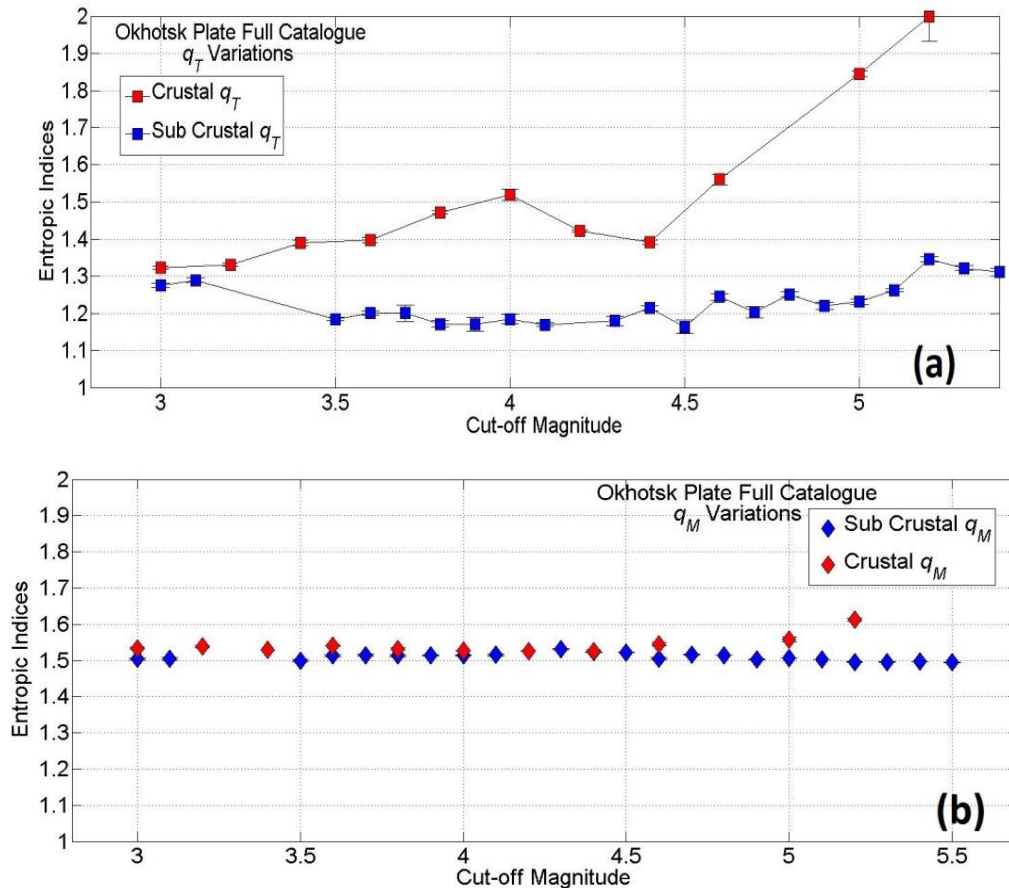


Figure 4.5: Analysis of entropic index dependence on different cut-off magnitudes for sub-crustal and crustal earthquake catalogues. (a) q_T variations, and (b) q_M variations.

Because the seismicity of the Okhotsk plate includes the M9.X Tohoku mega-earthquake of 2011 and its aftershock sequence, it was considered necessary to further divide and study the catalogues into a period leading up to that mega event, and a period following its occurrence. As evident in the following Fig. 4.6, the number of events after this earthquake increases abruptly due to its prolific and extended aftershock sequence.

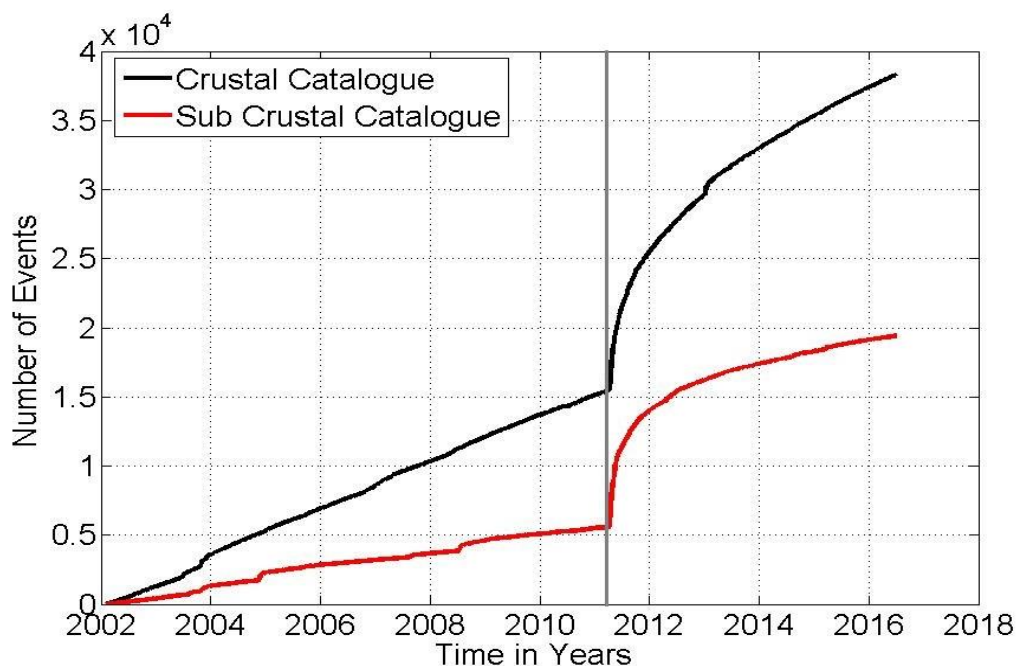


Figure 4.6: Cumulative number of earthquakes of the Okhotsk plate seismicity. The solid black line refers to crustal, and solid red line to sub-crustal seismicity. The vertical solid grey line indicates the occurrence of the 2011 Tohoku mega-earthquake.

The analysis of the sub-crustal seismic catalogues before and after the Tohoku earthquake is depicted in the following figure (Fig. 4.7). Correlation before the earthquake (green squares) is characterized as strong and seems to become stronger as magnitudes increase. The temporal index q_T , varies from 1.3187 for $M=3$, to 1.3208 for $M=5.3$. The entropic index q_M (white rhombus) doesn't exhibit any significant changes, for $M=3$ is equal to 1.512, whereas for $M=5.3$ is equal to 1.5057, yielding to proxy- b values 0.95 and 0.97 for the same cut-off magnitudes. The catalogue referring to earthquakes after the 2011 event (red squares), shows weak correlation that increases dramatically and becomes stronger for magnitudes larger than $M=4.5$. The temporal index q_T , varies between 1.1286 for $M=3$, to 1.5894 for $M=5.2$. The index q_M (grey rhombus), for $M=3$ is equal to 1.5393 and for $M=5.2$ is 1.489 yielding to proxy- b values 0.85 and 1 for the same cut-off magnitudes respectively.

The analysis at different cut-off magnitudes for the crustal seismic catalogues before and after the Tohoku earthquake is depicted in the following figure (Fig. 4.8). Correlation before the earthquake (green squares) is strong and increases as magnitudes increases. The temporal index q_T , varies from 1.1954 for $M=3$, to 1.4141 for $M=4.6$. The entropic index q_M (white rhombus) doesn't exhibit any significant changes, and behaves almost linearly. For $M=3$ is equal to 1.5445, whereas for $M=4.6$ is equal to 1.5164, yielding to proxy- b values 0.84 and 0.94 for the same cut-off magnitudes. The catalogue referring to earthquakes after the 2011 event (red squares), shows weak correlation that increases dramatically and becomes stronger for magnitudes larger than 3.5. The temporal index q_T , varies between 1.1296 for $M=3$, to 1.8818 for $M=5$. The index q_M (grey rhombus) exhibits small variations but in general it fluctuates in the interval (1.5, 1.6). For $M=3$ is equal to 1.5445 and for $M=5$ is 1.5623 yielding to proxy- b values 0.84 and 0.8 for the same cut-off magnitudes respectively.

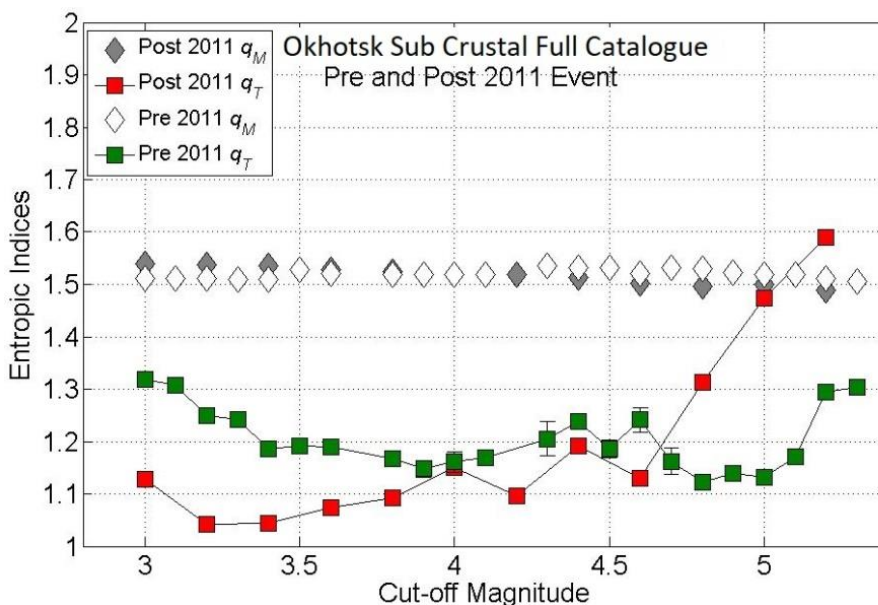


Figure 4.7: Variation of entropic indices with respect to cut-off magnitude analysis for sub-crustal seismicity prior to and after the 2011 Tohoku mega-earthquake.

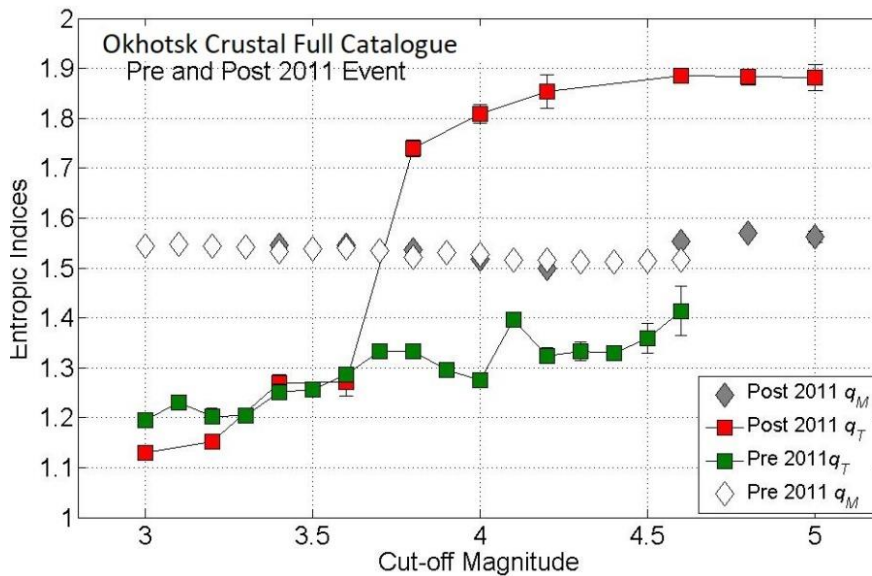


Figure 4.8: Variation of entropic indices with respect to cut-off magnitude analysis for *crustal* seismicity prior to and after the 2011 Tohoku mega-earthquake.

Figs. 4.9 and 4.10 illustrate the variation of the entropic indices with respect to interevent distance, for cut-off magnitudes $M=3$ and $M=4$ and for both sub-crustal and crustal seismicity. The analysis shown therein refers to the entire period of observation (2002-2016) – separate analyses for the periods prior to and after the Tohoku mega-earthquake are not represented due to insufficiency of data for this analysis) The breadth of interevent distance bins is indicated by the horizontal line segments across the index symbols.

The variation of entropic indices on interevent distance for a cut-off magnitude of $M=3$ in both crustal and sub-crustal earthquake catalogues is illustrated in Fig. 4.9. Starting with the sub-crustal seismicity, it is evident that for interevent distances less than 400km, the temporal entropic index varies in the interval (1.23, 1.3) indicating marginal to weak correlation (Fig. 4.9a); thereafter, it decreases below 1.2 and fluctuates between 1.03 and 1.17) indicating Poissonian processes or, equivalently, total absence of long-range interaction. Conversely, for crustal earthquakes (Fig 4.9a), q_T indicates *significant to strong* correlation at interevent distances of up to 650km, ($q_T > 1.4$), which drops to moderate thereafter and up to almost 1000km ($1.2 < q_T < 1.4$). Evidently crustal seismicity exhibits very strong long-range correlation at ranges that are order of magnitude larger than the characteristic dimensions of aftershock zones associated with M_w 6 – 6.7 earthquakes and several times longer than zones associated with M_w 7-7.2 earthquakes (e.g. Kagan, 2002). It follows that interaction at such ranges can hardly be explained in terms of aftershocks; rather it indicates a fault network tightly correlated over very long ranges. The magnitude entropic index for both crustal and sub-crustal earthquakes if shown in Fig. 4.9b).

The variations of entropic indices on interevent distance for cut-off magnitude $M=4$ for the both crustal and sub-crustal earthquake catalogues is illustrated in Fig. 4.10. For sub-crustal earthquakes (blue squares) the index q_T lingers between 1 and 1.65. At 25 km is 1.23 and increases to 1.65 at 140 km. Then it decreases abruptly to 1.17 at 250 km and finally drops to 1.03 at 875 km. The magnitude entropic index varies between 1.5 and 1.6 (blue diamonds), For

crustal earthquakes (red squares) correlation is strong and q_T lingers in the interval [1.23, 1.82]. The magnitude entropic index also varies between 1.5 and 1.6.

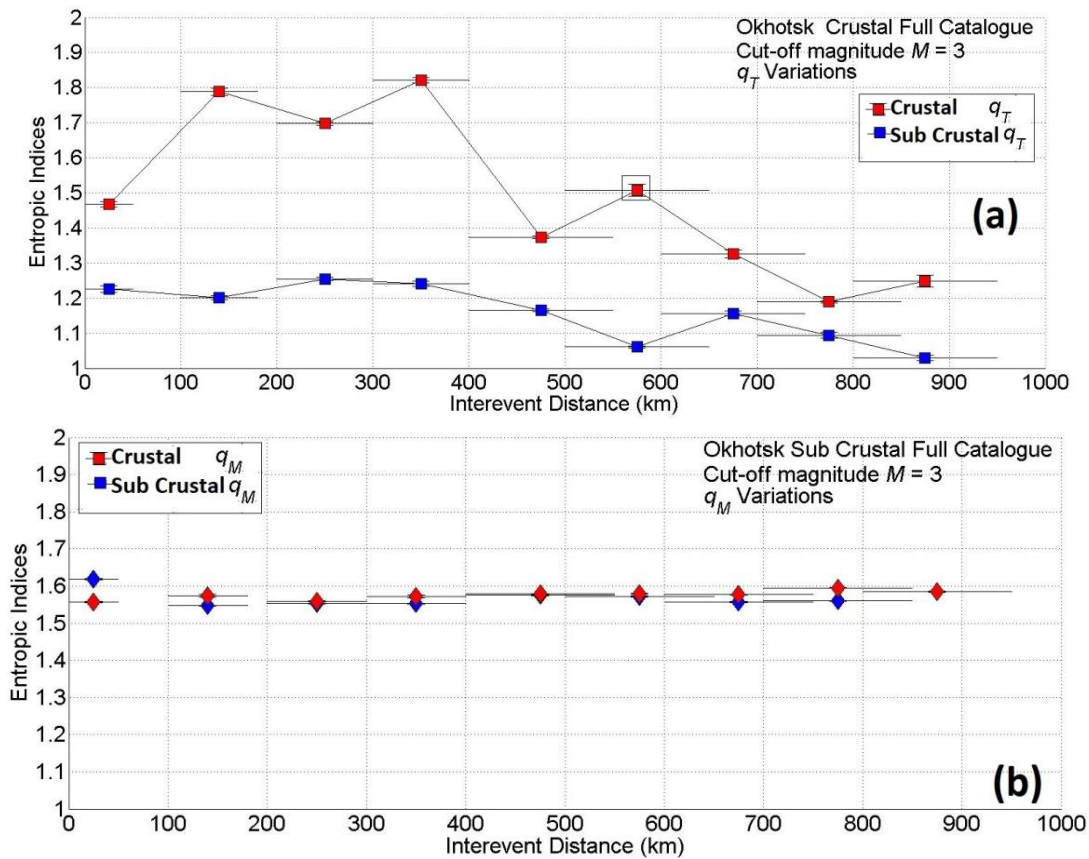
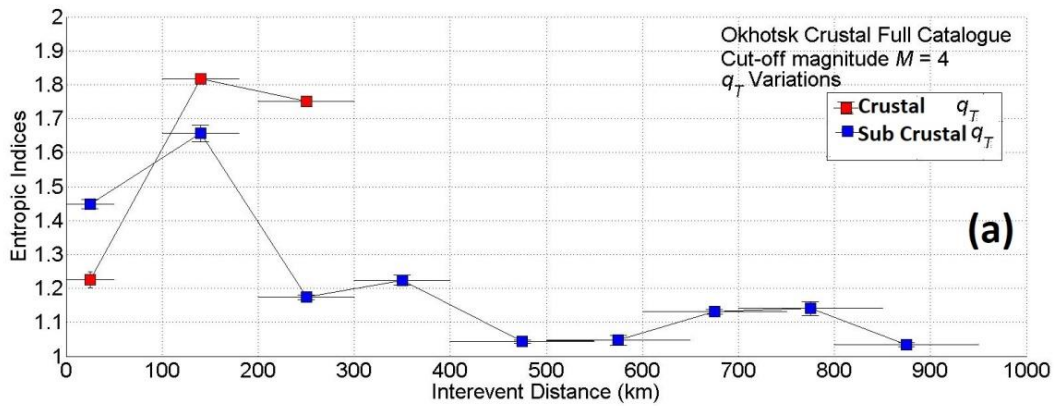


Figure 4.9: Analysis of dependence of entropic indices on interevent distances for sub-crustal and crustal earthquake catalogues for cut-off magnitude 3. (a) q_T variations, and (b) q_M variations.



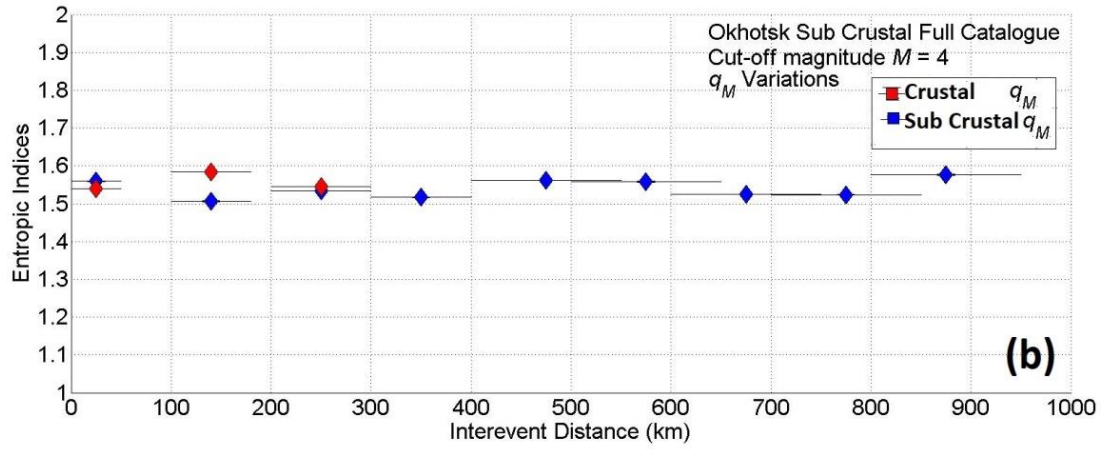


Figure 4.10: Analysis of dependence of entropic indices on interevent distances for sub-crustal and crustal earthquake catalogues for cut-off magnitude 4. (a) q_T variations, and (b) q_M variations.

4.1.3. Pacific Plate

Pacific plate seismicity is distributed along the Japanese Trench. The sub-crustal earthquake catalogue consists of 9,101 events, whilst the crustal earthquake catalogue consists of only 2,014 events.

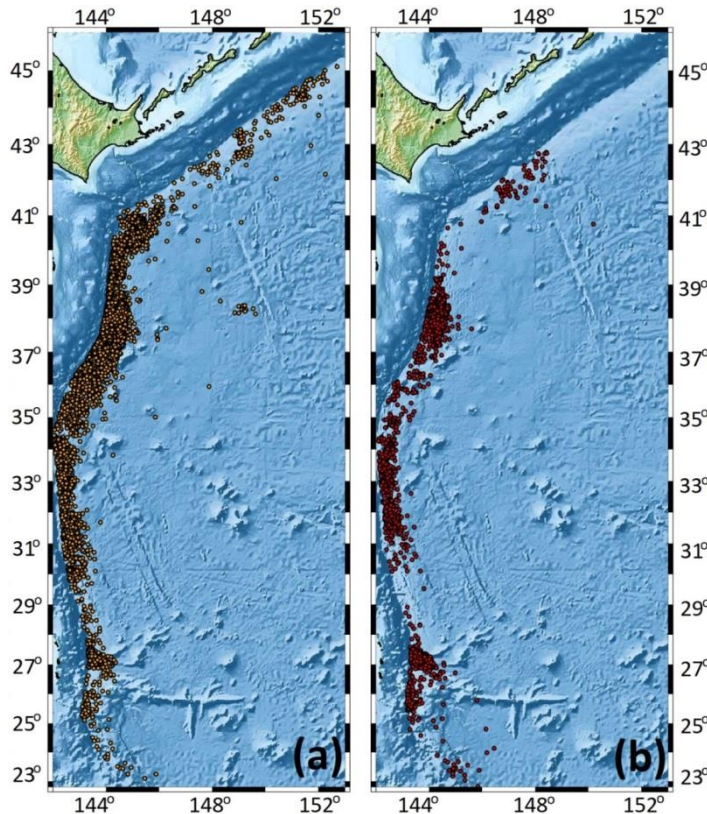


Figure 4.11: Pacific Plate seismicity. (a) Sub-crustal seismicity, (b) Crustal seismicity in red.

The analysis of *sub-crustal* seismicity for different cut-off magnitudes is shown in Fig. 4.12. As evident in Fig. 4.12a, the temporal entropic index q_T increases *linearly* up to $M=4.7$. However, whereas the increase is smooth between $M3.1$ and $M4.2$, it becomes rather erratic thereafter. The linear trend of the sub-crustal q_T can be estimated by fitting a straight line to the q_T data. In this way it can be seen to vary from approximately 1.28 at $M=3.1$ to approximately 1.33 at $M = 4.7$. Therefore, it can be safely deduced that correlation varies from weak to significant; as per Fig. 4.8 (green squares – crustal seismicity prior to the Tohoku mega-earthquake), the quasi-linear upward trend of q_T with magnitude can be interpreted in terms of long-range interaction. Correlation for the crustal earthquake catalogue is also strong. The entropic index q_T lingers between 1.3 and 1.6. For $M=3$ q_T is equal to 1.3, and increases to 1.6 for $M=4.2$.

In sub-crustal seismicity, the entropic index q_M is generally stable and varies between 1.55 and 1.61 with an expectation value of 1.58 ± 0.03 (Fig. 4.12b); this yields b_q values in the range 0.8 to 0.73. In crustal seismicity, q_M is also stable but at markedly higher values than its sub-crustal counterpart (Fig. 4.12b); it varies between 1.60 and 1.63 with an expectation value of 1.62 ± 0.01 , yielding b_q values in the range 0.7 to 0.6. Higher b -values and correlation of crustal seismicity is a result of the Tohoku sequence. Many earthquakes of the west-central Pacific plate are actually a part of the 2011 aftershock sequence. Another reason is the distribution of

faults. Crustal faults tend to be more localized than sub-crustal, resulting to immediate interaction.

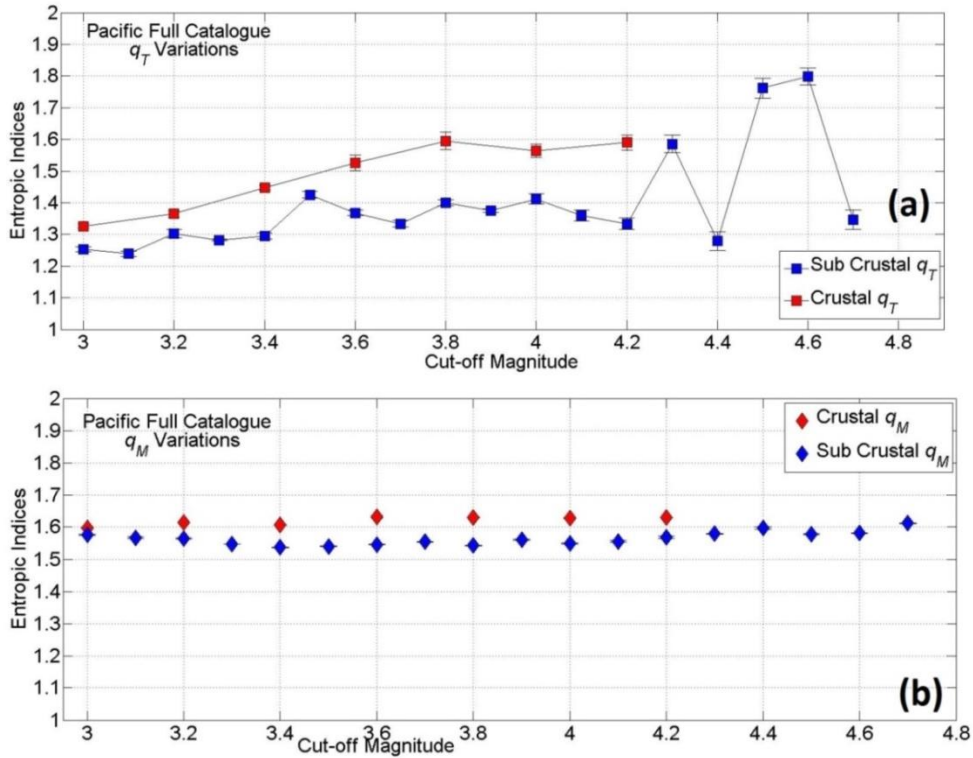


Figure 4.12: Analysis of dependence of different cut-off magnitudes for (a) sub-crustal and (b) crustal earthquake catalogues of Pacific full catalogue.

The analysis of the entropic index dependence on interevent distance is shown in Fig. 4.13. For crustal events there weren't sufficient data to conduct analysis. On the other hand, results for the sub-crustal earthquake catalogue for cut-off magnitude $M=3$ illustrate strong correlation at all distances, The temporal index q_T fluctuates between 1.6 and 1.85 with an expectation value of 1.72 ± 0.1 . These long range interactions prove that an earthquake can be related to another one at greater distances.

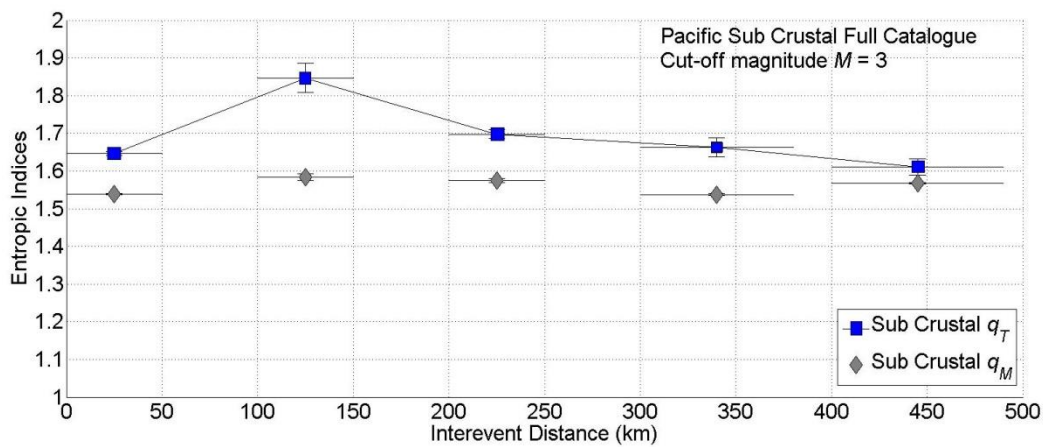


Figure 4.13: Analysis of interevent distances for sub-crustal events at cut-off magnitude $M=3$.

4.1.4. Philippine Plate

The seismicity of the Philippine plate is illustrated in the maps of Fig. 4.14. Crustal seismicity comprises of a total of 2.608 events above a depth of approx. 29km and above the magnitude of completeness ($M_c = 3$), while sub-crustal seismicity comprises 12.036 events between 29km and 700km. The majority of earthquakes is located on the Izu–Bonin–Marianas Trough on the boundary with the Pacific plate in the east, and, along the boundary with the Eurasian plate in the west.

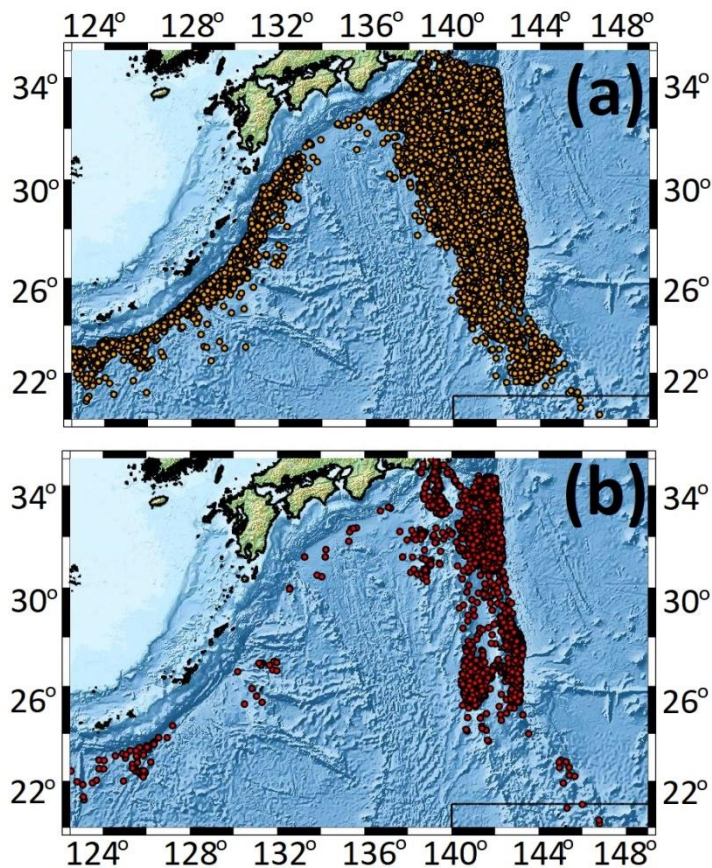


Figure 4.14: Seismicity map of Philippine Plate. Two overlaid catalogues are depicted. Crustal events are depicted in red, and, sub-crustal events in orange.

Herein the analysis of dependence on cut -off magnitude shows a completely different result. Seismicity here is shown to be random. Even though crustal events exhibit higher correlation than sub-crustal, this can still be characterized as weak compared to the other three cases studied so far. Results for the temporal entropic index are illustrated in Fig. 4.15a. For sub-crustal earthquakes q_T is approximately. 1.16 for $M=3$ and slowly decreases towards the larger magnitude scales to approach unity at $M=5$. For crustal earthquakes q_T , in general, lingers in the vicinity of 1.2 and has a mean value of 1.1 ± 0.1 , indicating a *marginally* correlated process.

The magnitude entropic index q_M is almost identical for both sub-crustal and crustal catalogues (Fig. 4.15b); it is very stably determined exhibiting minimal variation about 1.52 ± 0.03 yielding b_q values of 0.8-0.9 very similar to the globally expected value of b .

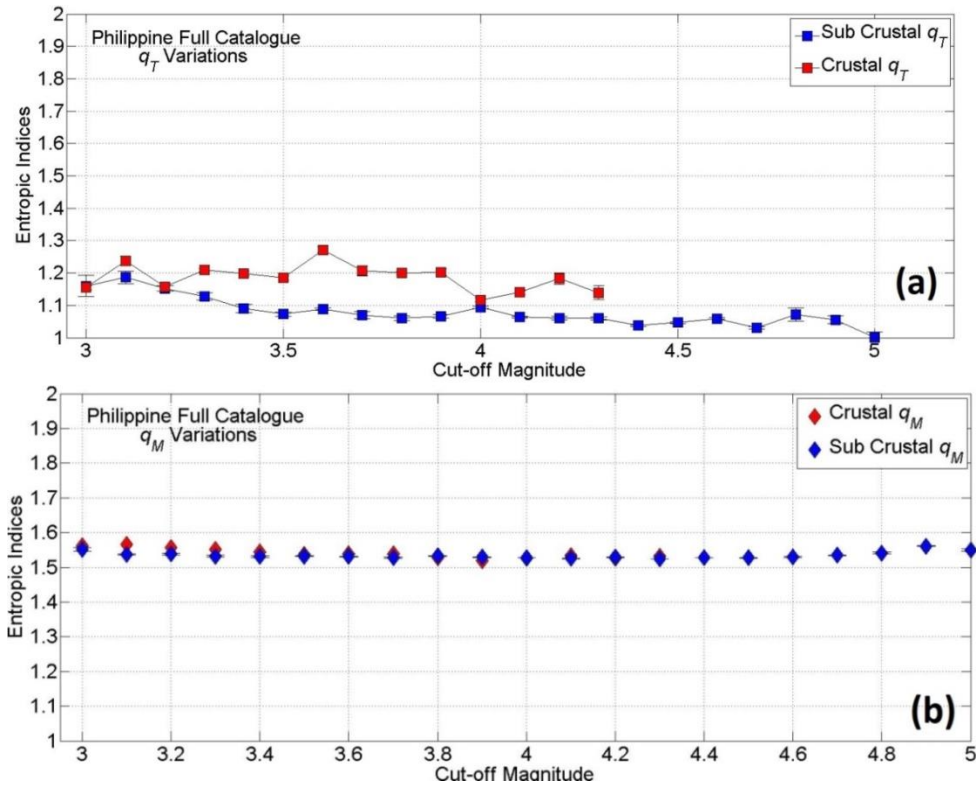


Figure 4.15: Variation of entropic indices with cut-off magnitude for (a) sub-crustal and (b) crustal earthquake catalogues.

The dependence of entropic indices on interevent distance is illustrated in Fig. 4.16 for the sub-crustal earthquake catalogue only. The crustal earthquake catalogue did not contain sufficient data to conduct statistically rigorous analysis. For sub-crustal seismicity, the dependence of entropic indices on interevent distances for cut-off magnitude $M=3$ illustrates very weak correlation, showing that seismicity in this area is a random process, and there is no relation between earthquakes at any distance. That means that the system of seismogenesis is in an equilibrium state

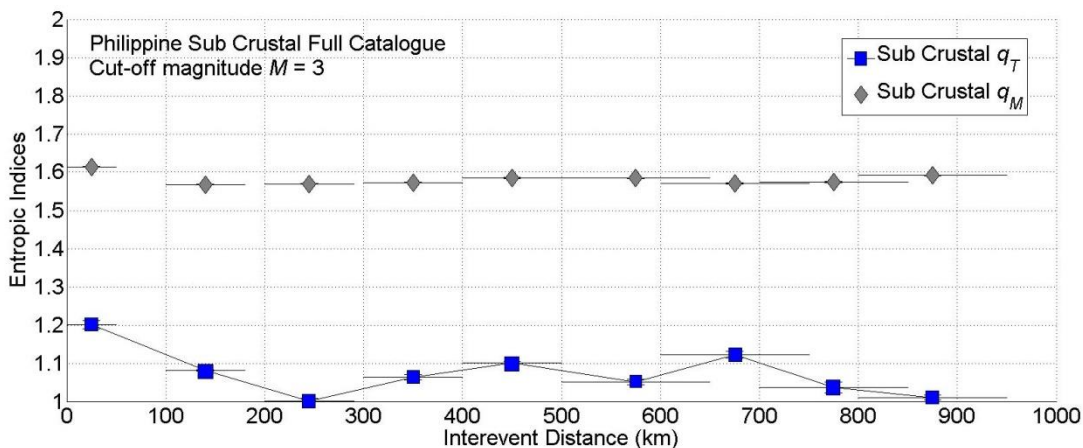


Figure 4.16: Analysis of dependence of entropic indices on interevent distances for sub-crustal events at cut-off magnitude $M=3$.

4.2 DECLUSTERED CATALOGUE ANALYSIS

Herein, the presence of long term interactions and long term memory effects are investigated for the declustered earthquake catalogues. As mentioned in Chapter 2, the purpose of the ETAS declustering algorithm, is to create new catalogues that only contain earthquakes that are considered to be parental to second or third order earthquakes.

For each tectonic plate three earthquake catalogues referring to three different probabilities of background seismicity are analysed ($\varphi_j=70\%$, $\varphi_j=80\%$ and $\varphi_j=90\%$), for both sub-crustal and crustal seismicity, for dependence on different cut-off magnitudes and dependence of the entropic indices on interevent distances.

4.2.1 Eurasia Plate

Eurasia's sub-crustal declustered catalogues are illustrated in the following map (Fig. 4.17).

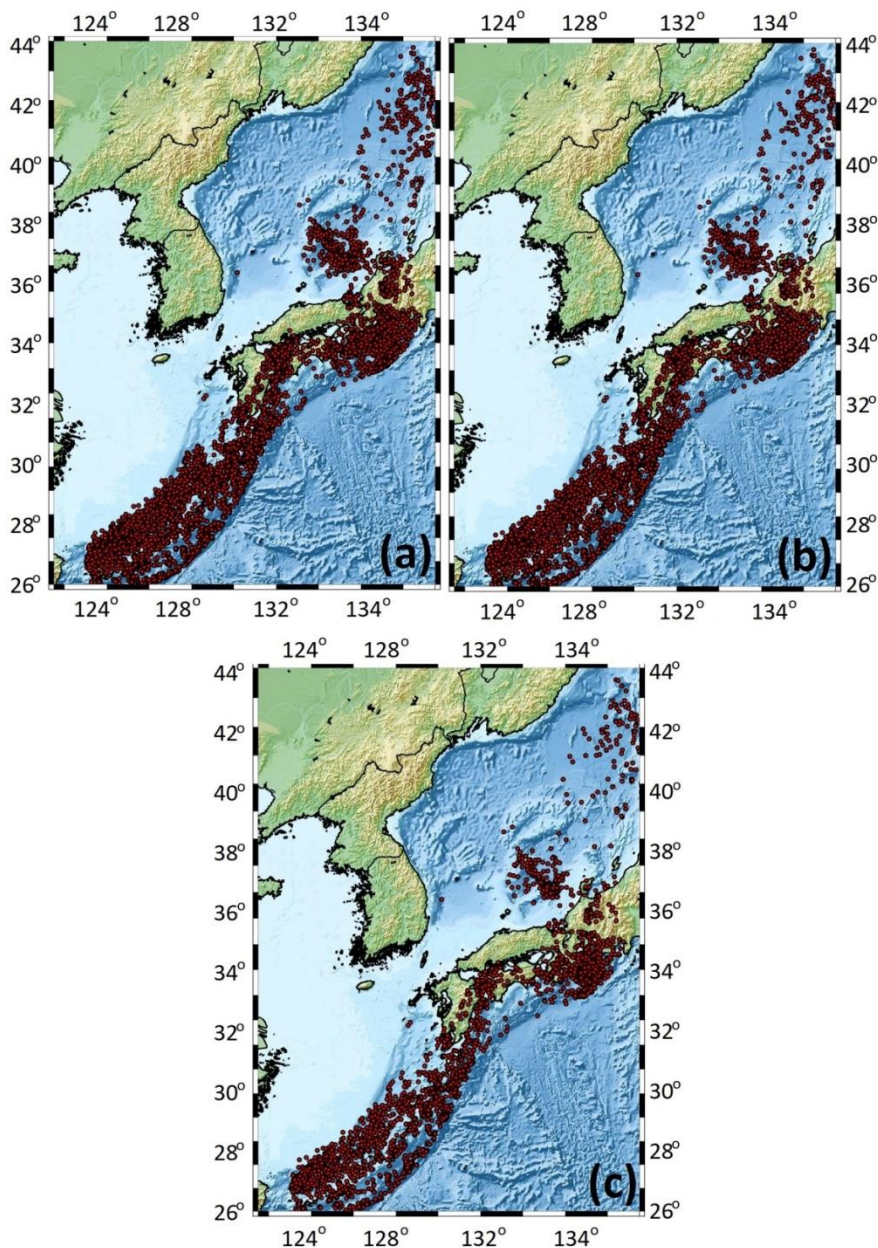


Figure 4.17: Sub-crustal declustered earthquake catalogues of Eurasia. Three background probabilities are depicted (a) 70% probability, (b) 80% probability, and, (c) 90% probability.

The results of the dependence on different cut-off magnitudes analysis for the sub-crustal declustered catalogues of Eurasia Plate are depicted in Fig. 4.18. Correlation, in general, is rather random, in agreement with the full catalogue results. Furthermore, correlation seems to increase as the background probability increases, but still q_T remains low, below 1.2.

For background probability $\varphi_j=70\%$ correlation is random with the temporal index, q_T (4.18a), varying in the interval between 1 and 1.13, suggesting that seismogenesis is a random process. For cut-off magnitude $M=3$ is equal to 1.14 and drops to 1 for cut-off magnitude $M=4.4$. For $\varphi_j=80\%$ results also exhibit randomness with q_T varying between 1 and 1.13. For $\varphi_j=90\%$ correlation increases, but it is still characterized as weak to low. For cut-off magnitude $M=3$ q_T is equal to 1.06 and for cut-off magnitude $M=3.9$ is equal to 1.3.

The magnitude entropic index q_M (4.18b) behaves almost linearly with small variations around 1.5 for all background probabilities. For $\varphi_j=70\%$, is completely linear and equal to 1.49 yielding b_q 's=1. For $\varphi_j=80\%$ the entropic index q_M varies from 1.48 to 1.5, yielding proxy- b values variations between 1 and 1.13, while for $\varphi_j=90\%$ q_M varies between 1.49 and 1.5 yielding proxy- b values variations between 0.98 and 1.03

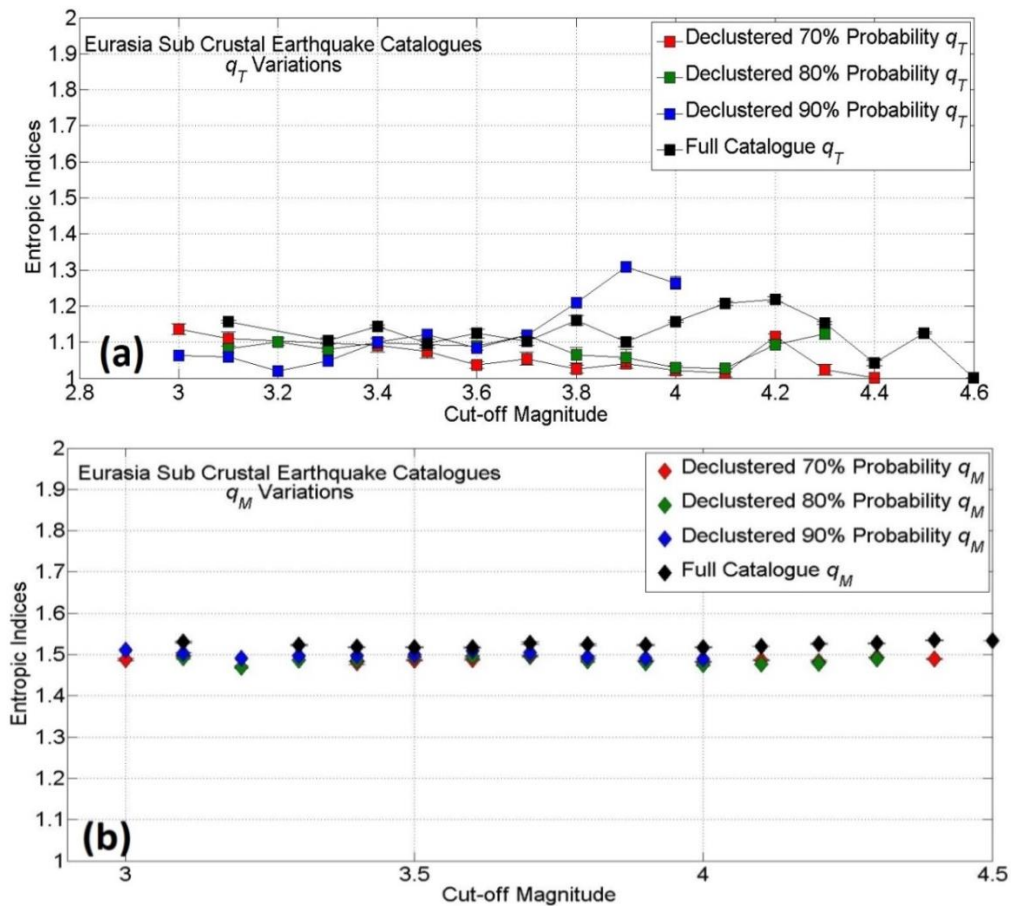


Figure 4.18: Dependence on different cut-off magnitudes analysis for all earthquake catalogues of Eurasia's sub-crustal seismicity. (a) q_T variations, and (b) q_M variations.

The analysis of dependence of the entropic indices on interevent distances for background probabilities $\varphi_j=70\%$ and $\varphi_j=80\%$ is illustrated in Fig. 4.19. For background probability $\varphi_j=90\%$ there weren't sufficient data to conduct analysis.

Correlation for background probability $\varphi_j=70\%$ is rather random (4.19a) with the temporal entropic index q_T varying between 1 and 1.14. For $\varphi_j=80\%$ correlation is even lower with q_T varying between 1.02 and 1.12. The magnitude entropic index (4.19b) varies between 1.5 and 1.55 for all background probabilities.

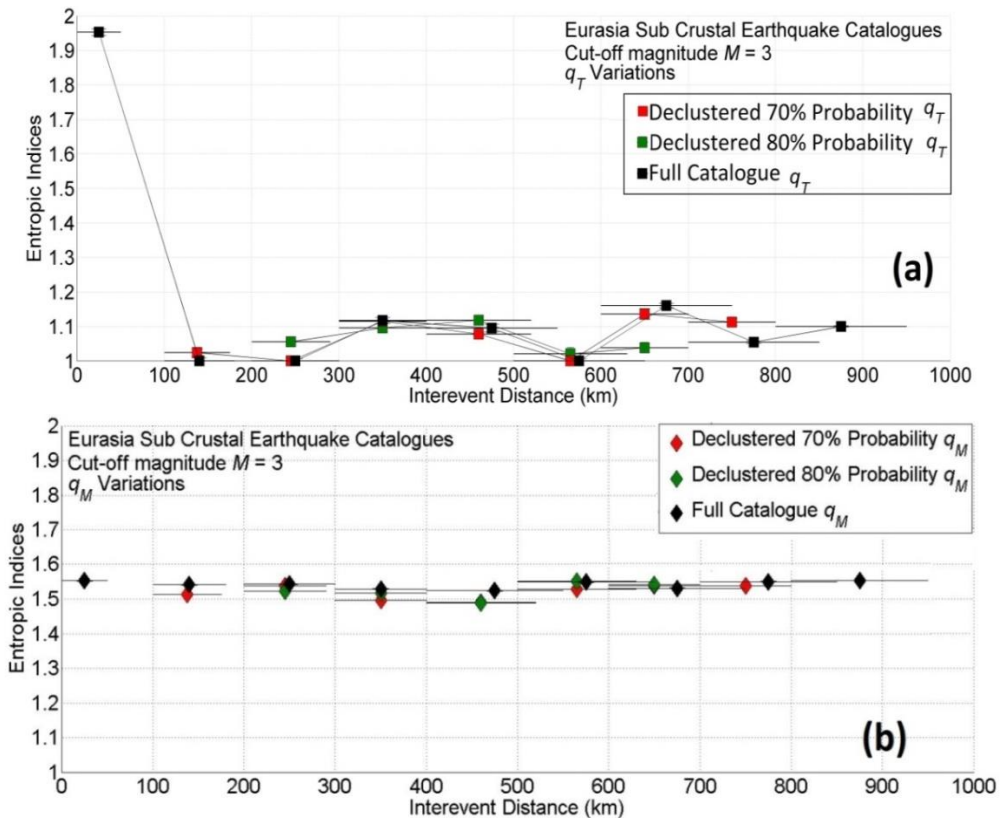


Figure 4.19: Analysis of dependence of the entropic indices on interevent distances at cut-off magnitude 3.0 for different background probabilities (a) q_T variations, and (b) q_M variations.

The declustered crustal earthquake catalogues for Eurasia plate, are illustrated in the following figure (Fig. 4.20).

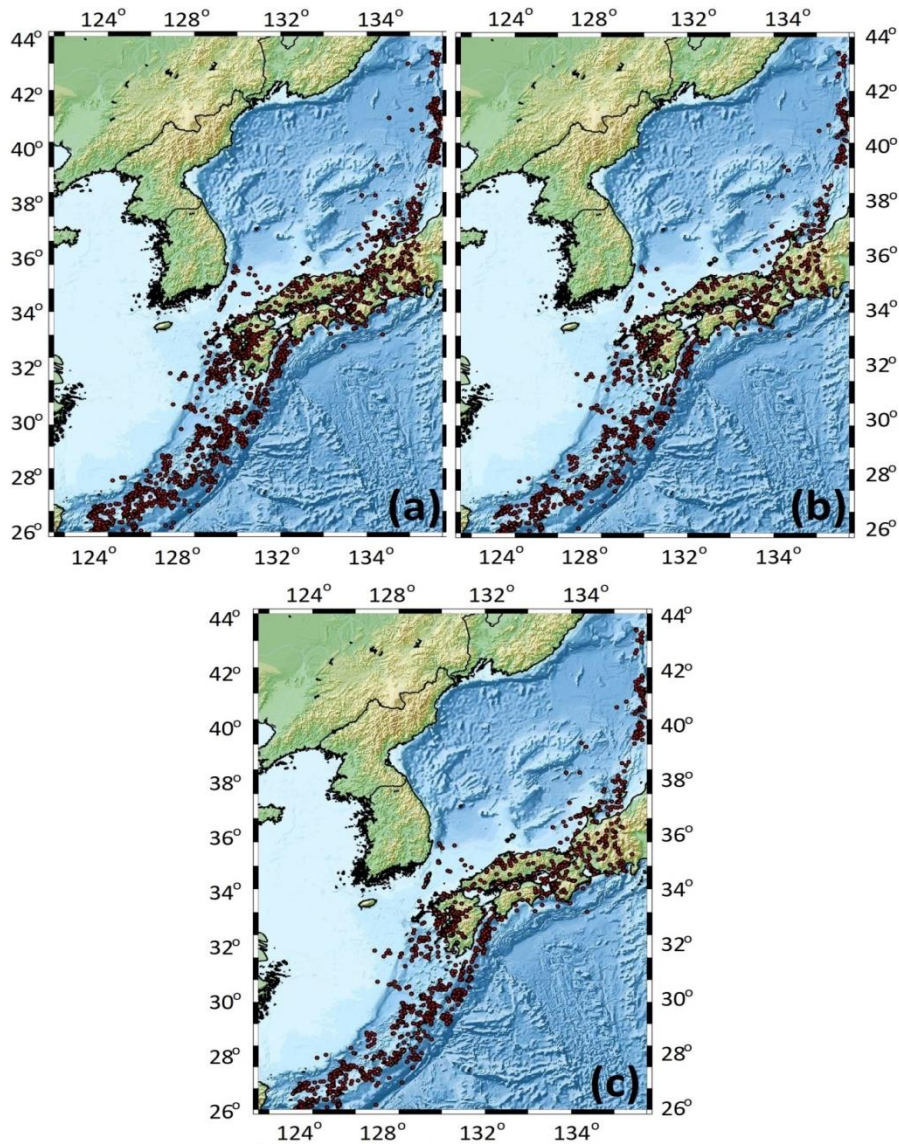


Figure 4.20: Seismicity map of crustal declustered earthquake catalogues of Eurasia Plate. Three catalogues of different background probabilities are depicted. (a) 70% probability (b) 80% probability, and, (c) 90% probability.

The analysis of the crustal declustered earthquake catalogues of Eurasia is illustrated in the following figure (Fig. 4.21). In general correlation is rather low and increases along with background probability. The temporal entropic (Fig. 4.21a) is below 1.3 for all probabilities, while the magnitude entropic index (Fig. 4.21b) varies between 1.4 and 1.5 and has a decreasing trend for all probabilities.

For background probability $\varphi_j=70\%$ q_T exhibits an increasing trend along with the magnitude scale. For cut-off magnitude $M=3$ is equal to 1.07 and for cut-off magnitude $M=3.8$ is equal to 1.21. Therefore, correlation is characterized as random to low. For $\varphi_j=80\%$ q_T is also increasing with the magnitude scale, but is lower than that of $\varphi_j=70\%$ suggesting that seismic process is random. Specifically, for $M=3$ is equal to 1.06 and for cut-off magnitude $M=3.7$ is equal to 1.16. For $\varphi_j=90\%$ q_T varies from 1.14 for cut-off magnitude $M=3$ to 1.3 for cut-off magnitude $M=3.5$.

The magnitude entropic index q_M (Fig. 4.21b) for $\varphi_j=70\%$ behaves almost linearly and varies from 1.44 to 1.48, yielding b_q variations between 1.1 and 1.3. For $\varphi_j=80\%$ q_M varies from 1.44 to 1.45 yielding the same b_q variations. The index q_M for the $\varphi_j=90\%$ probability linear and equal to 1.47 resulting $b_q=1.1$.

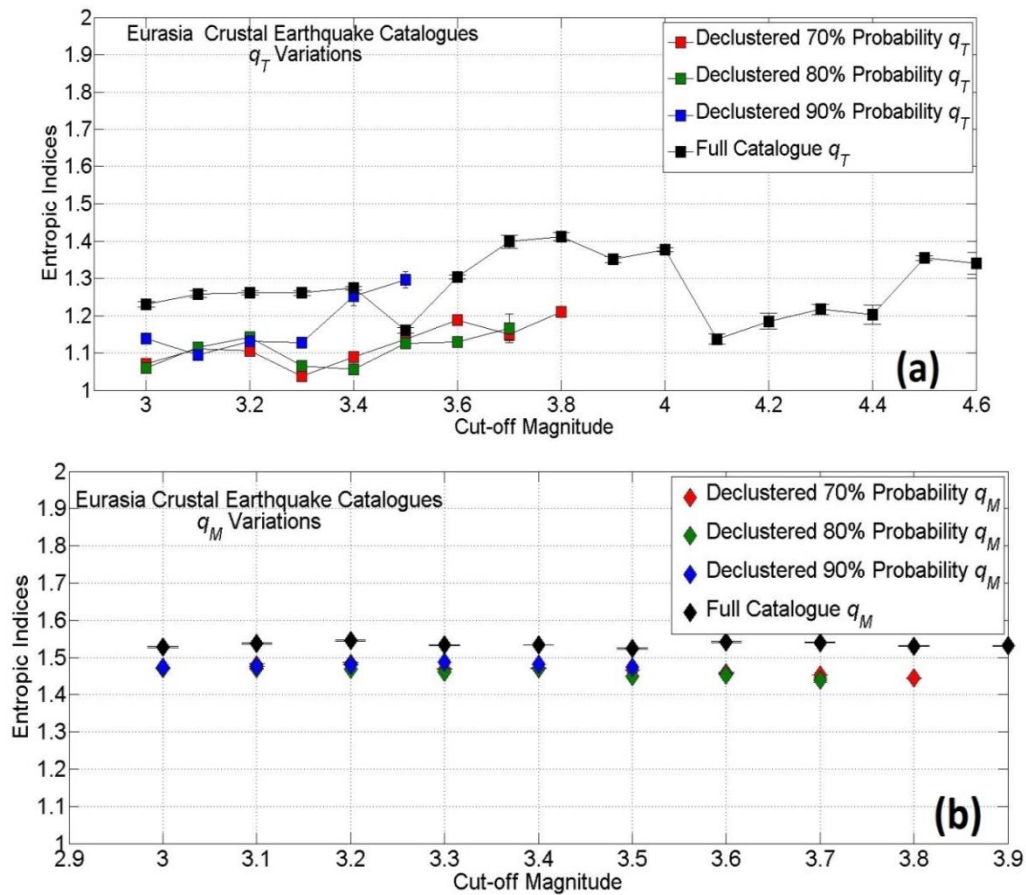


Figure 4.21: Dependence on different cut-off magnitudes analysis for all earthquake catalogues of Eurasia's crustal seismicity. (a) q_T variations, and (b) q_M variations.

4.2.2 Okhotsk Plate

The sub-crustal declustered earthquake catalogues of Okhotsk plate are illustrated in the following figure (Fig. 4.22).

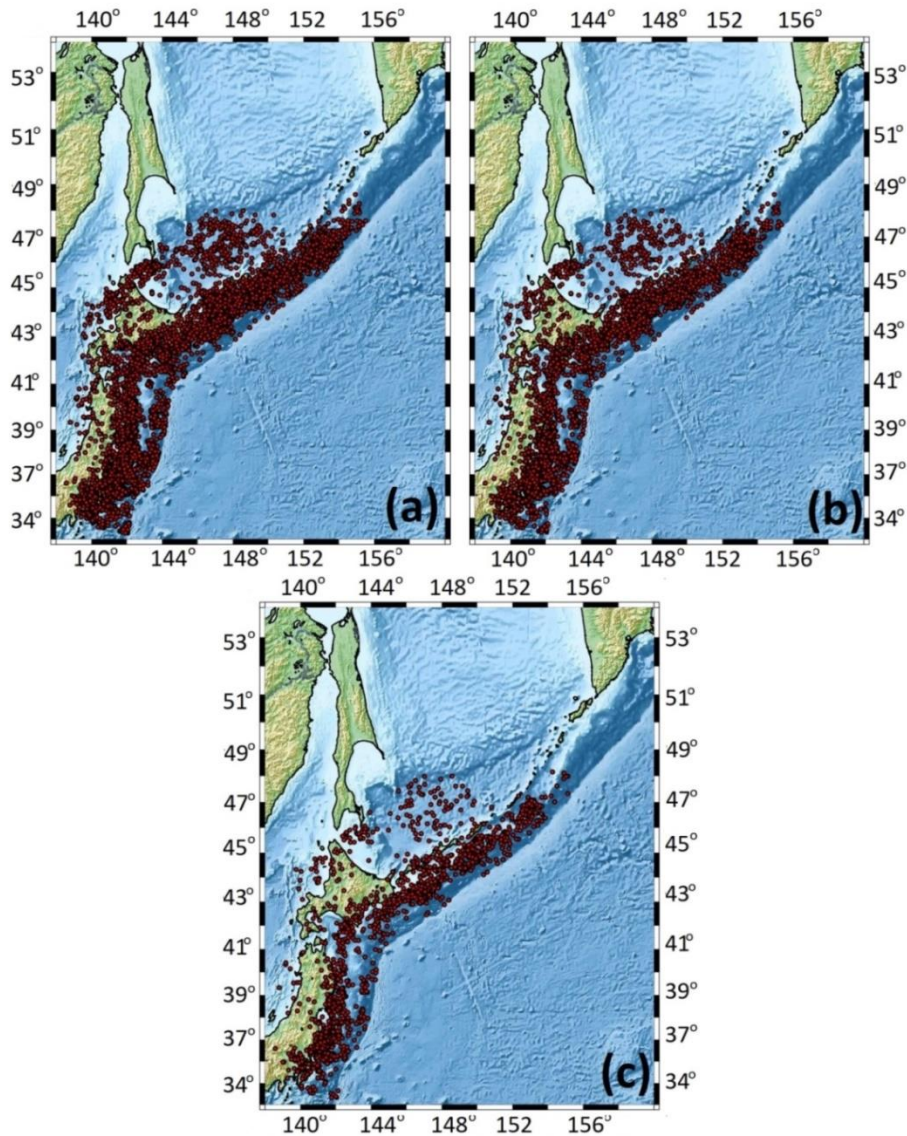


Figure 4.22: Okhotsk plate sub-crustal declustered earthquake catalogues. Three catalogues referring to different background probabilities are depicted. (a) 70% probability, (b) 80% probability, and (c) 90% probability.

The of the sub-crustal declustered catalogues of Okhotsk plate are illustrated in the following figure (Fig. 4.23). In general, the declustered catalogues exhibit strong correlation that increases as background probability increases. The temporal entropic index is above 1.4 for all probabilities (Fig. 4.23a), suggesting the presence of long term interactions and long term memory effects. Background seismicity, as extracted from the declustering process, is characterized by earthquake clusters (Fig. 4.22). Those earthquake clusters may be accountable for the strong correlation values. The magnitude entropic index lingers between 1.4 and 1.6 (Fig. 4.23b).

More specifically, for $\varphi_j=70\%$ the temporal entropic index, q_T , has an increasing trend and varies between 1.4 and 1.6. Therefore correlation is characterized as strong. For $\varphi_j=80\%$ exhibits the same results, with q_T varying between 1.4 and 1.6, while for $\varphi_j=90\%$, even though q_T is decreasing as the magnitude scale increases, it lingers between 1.55 and 1.65 resulting to higher correlation.

The magnitude index, q_M , for $\varphi_j=70\%$ probability is decreasing along the magnitude scale, and varies between 1.47 and 1.5 yielding b_q variations between 0.79 and 1.05. For $\varphi_j=80\%$ q_M exhibits significant changes, and varies between 1.39 and 1.57 yielding b_q variations between 0.76 and 1.5. For $\varphi_j=90\%$ q_M is increasing with magnitudes dor cut-off magnitude $M=3$ is 1.48 and for cut-off magnitude $M=4$ is equal to 1.53, yielding b_q values 1.09 and 0.9 respectively.

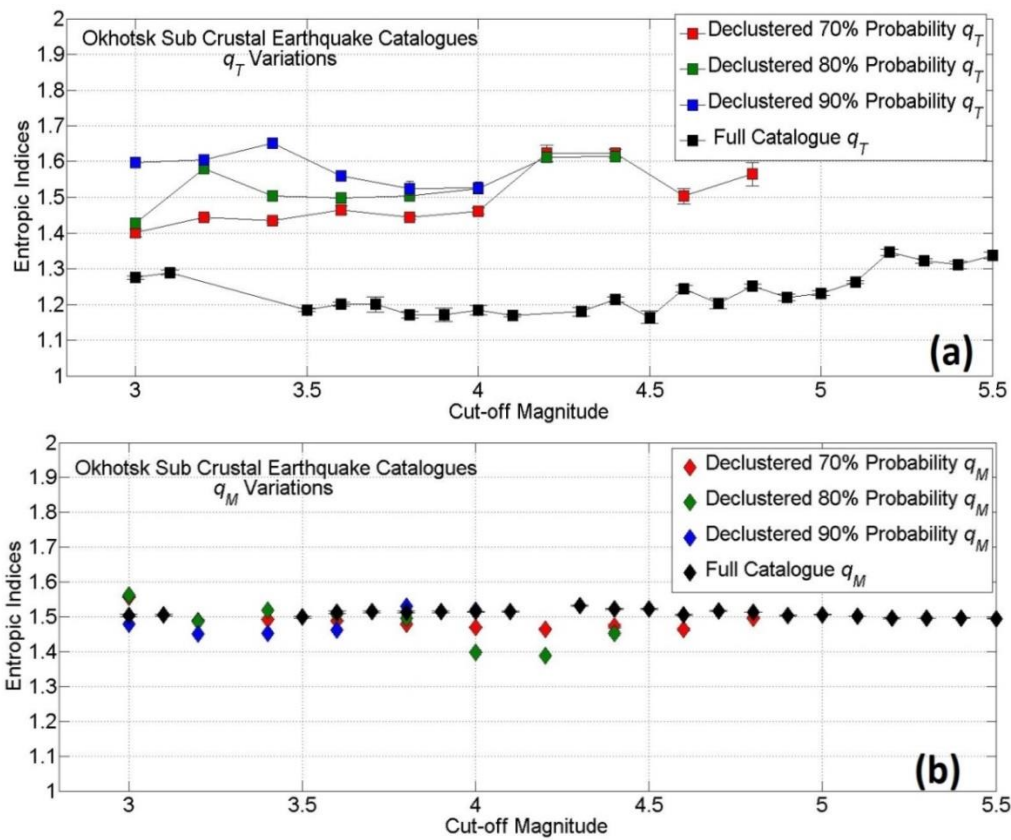


Figure 4.23: Dependence on different cut-off magnitudes analysis for all earthquake catalogues of Okhotsk sub-crustal seismicity. (a) q_T variations, and (b) q_M variations.

The analysis of dependence of entropic indices on interevent distances at cut-off magnitude $M=3$ is illustrated in the Fig. 4.24, for two background probabilities, $\varphi_j=70\%$ and $\varphi_j=80\%$. In general, correlation is increasing with distance, proving that an earthquake can be related to another one at greater distances.

For background probability $\varphi_j=70\%$ correlation is strong (Fig. 4.24a) with q_T varying between 1.28 and 1.65. For distances 137 km to 350 km, q_T lingers between 1.27 and 1.34. After 400 km it increases abruptly and reaches 1.66 at 550 km. After 550 km, it decreases to 1.48 at 830 km. For $\varphi_j=80\%$ q_T has an increasing trend and lingers between 1.34 and 1.65. The magnitude entropic index q_M lingers in the interval (1.5, 1.6) for both background probabilities.

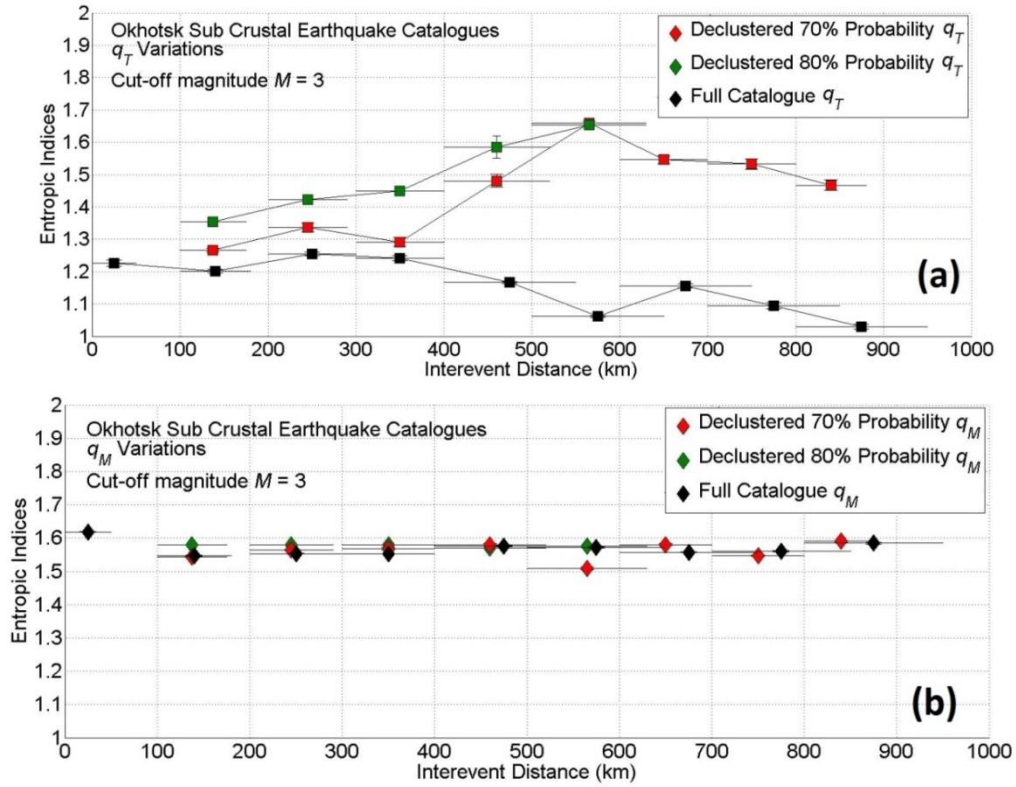


Figure 4.24: Analysis of dependence of the entropic indices on interevent distances at cut-off magnitude 3.0 for different background probabilities (a) q_T variations, and (b) q_M variations.

Okhotsk's crustal declustered earthquake catalogues are illustrated in the following figure (Fig. 4.25).

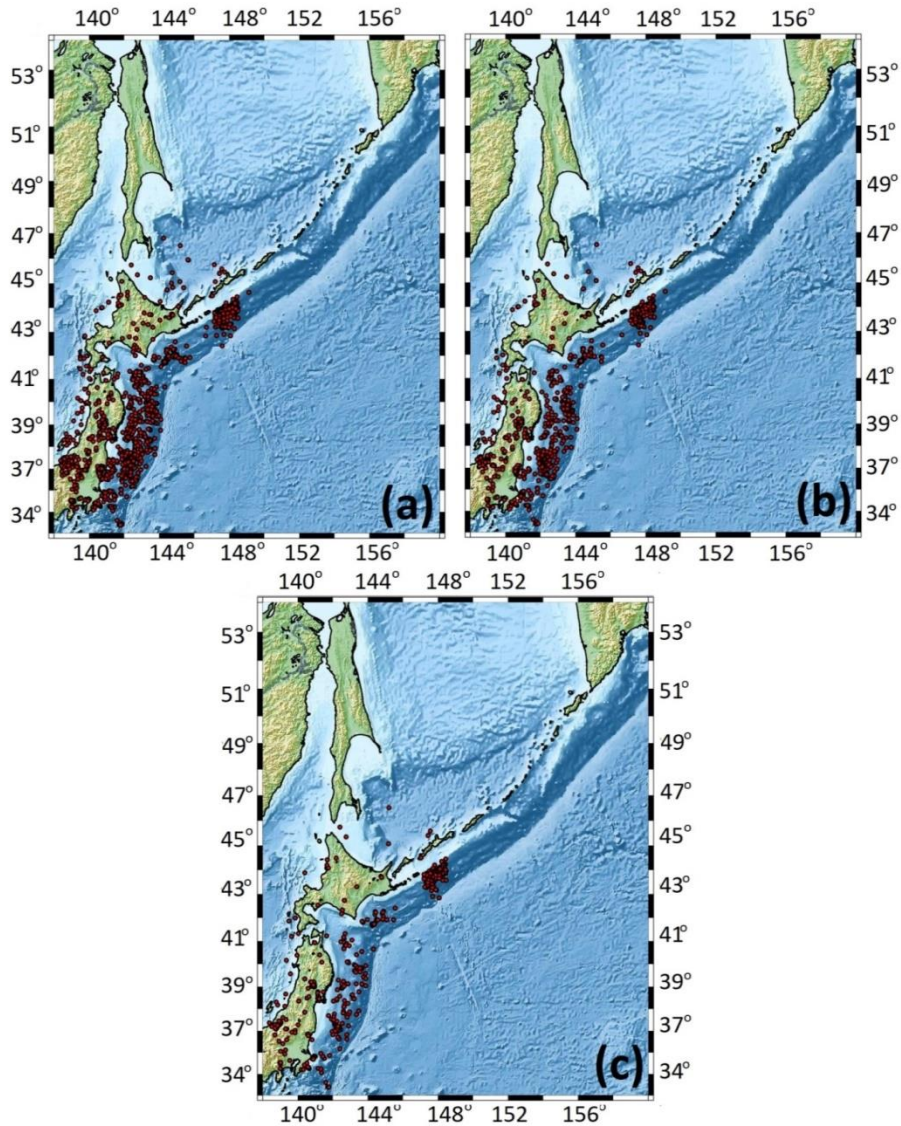


Figure 4.24: Map of declustered crustal declustered catalogues located within Okhotsk plate. Three maps referring to three different background probabilities are depicted (a) 70% probability, (b) 80% probability, and (c) 90% background probability.

The analysis of crustal declustered earthquake catalogues of Okhotsk is illustrated in Fig. 4.25.. In general, the declustered catalogues exhibit significant deviations for the full catalogue's analysis. The temporal entropic index (Fig. 4.25a) increases as background probability increases, and only for probability $\varphi_j=90\%$ correlation can be characterized as strong. The magnitude entropic index (Fig. 4.26b) for probabilities $\varphi_j=70\%$ and $\varphi_j=80\%$ is almost the same, while for probability 90% is increasing.

For background probability $\varphi_j=70\%$ q_T lingers between 1.03 and 1.21. Therefore, correlation is described as random. For probability $\varphi_j=80\%$ correlation is increasing, but it is still characterized as low, with q_T values varying between 1.2 and 1.32. Correlation increases abruptly and becomes strong for $\varphi_j=90\%$. For cut-off magnitude $M=3$ q_T is equal to 1.48, and for cut-off magnitude $M=3.3$ is 1.69.

The magnitude entropic index, q_M , for background probabilities 70% and 80% is almost the same and decreases as magnitudes increase. For probability 70% it varies between 1.49 and 1.52, whilst for 80% it varies between 1.4 and 1.51, yielding to b_q variations 0.89 to 1.08 and 0.9 to 0.99 respectively. For $\varphi_j = 90\%$ q_M lingers between 1.56 and 1.58, yielding b_q variations 0.79 and 0.71.

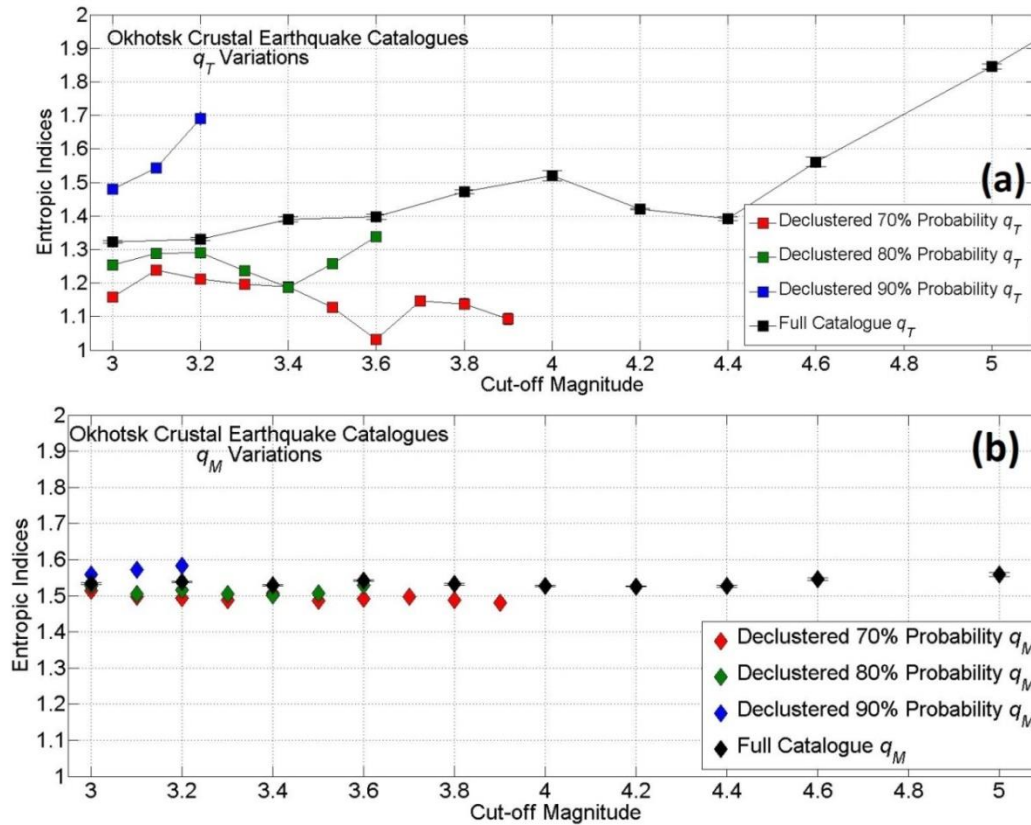


Figure 4.25: Dependence on different cut-off magnitudes analysis for all earthquake catalogues of Okhotsk crustal seismicity. (a) q_T variations, and (b) q_M variations.

4.2.3 Pacific Plate

The sub-crustal declustered earthquake catalogues of Pacific are depicted in the following map (Fig. 4.26). For crustal seismicity there weren't enough earthquakes to conduct analysis.

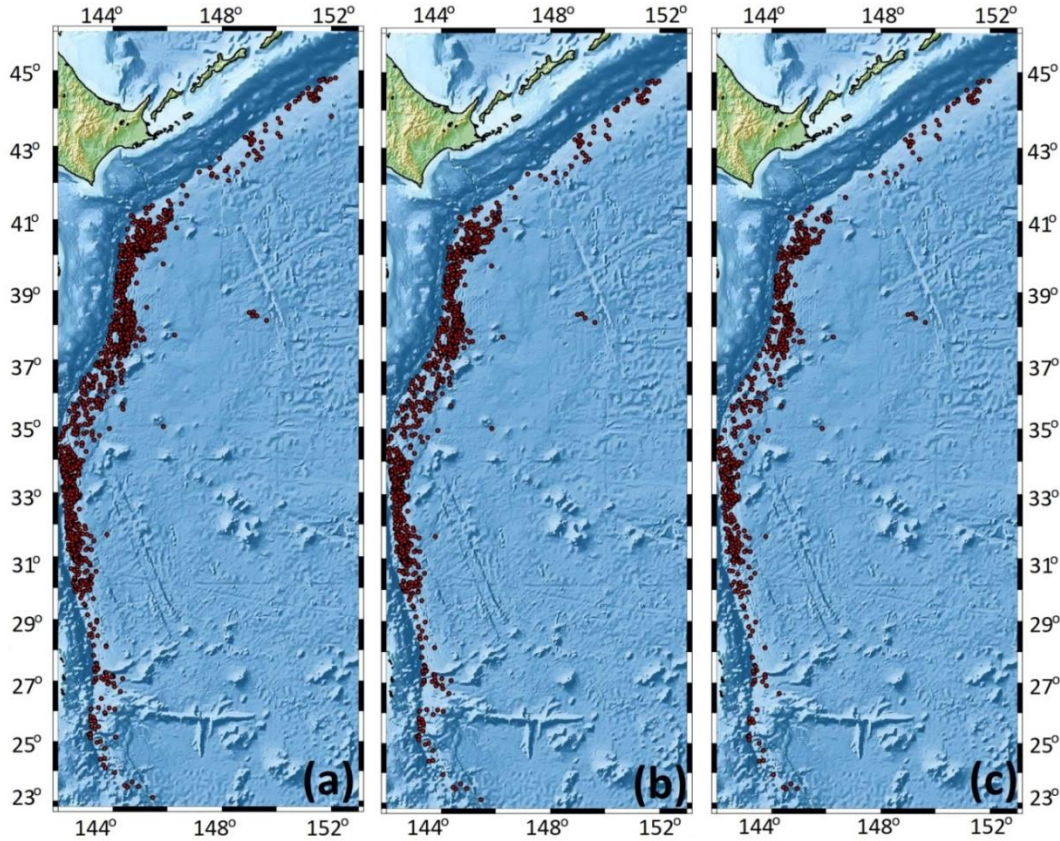


Figure 4.26: Seismicity map of sub-crustal declustered events located in Pacific plate. Three earthquake catalogues are illustrated each referring to a different background probability (a) 70% probability, (b) 80% probability, and, (c) 90% probability.

The analysis of the sub-crustal declustered earthquake catalogues of Pacific is illustrated in the Fig. 4.27. The temporal index q_T (Fig. 4.27a) increases as background probability increases. For probabilities $\varphi_j = 70\%$ and $\varphi_j = 80\%$ is low, below 1.2, therefore seismic process is depicted as random. For $\varphi_j = 90\%$ it increases and becomes strong. The magnitude entropic index q_M (Fig. 4.27b) varies in the interval (1.5, 1.6).

For $\varphi_j = 70\%$, correlation is random with the temporal entropic index, q_T , varying from 1.08 to 1.19. For $\varphi_j = 80\%$, correlation remains weak and q_T lingers between 1.16 and 1.32, but mostly varies around 1.2. For $\varphi_j = 90\%$ correlation is strong. For cut-off magnitude $M=3$ q_T is equal to 1.37, whereas for cut-off magnitude $M=3.4$ is equal to 1.43.

For $\varphi_j = 70\%$ the magnitude entropic index, q_M varies between 1.52 and 1.54, yielding b_q variations between 0.85 and 0.93. For $\varphi_j = 80\%$ q_M varies from 1.53 to 1.55 yielding to b_q values variations from 0.83 to 0.9. For $\varphi_j = 90\%$ q_M linger between 1.51 and 1.54, yielding b_q variations between 0.9 and 0.96.

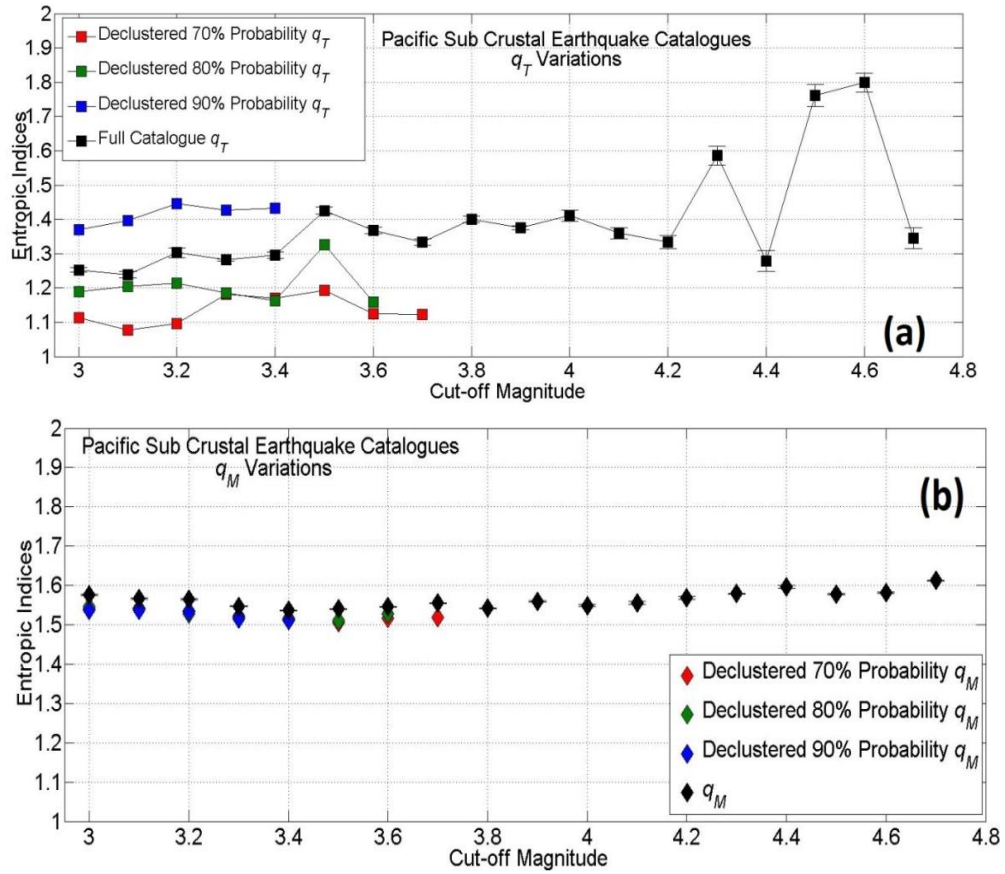


Figure 4.27: Dependence on different cut-off magnitudes analysis for all earthquake catalogues of Pacific sub-crustal seismicity. (a) q_T variations, and (b) q_M variations

4.2.4 Philippine Plate

The declustered sub-crustal earthquake catalogues of Philippine plate are depicted in the following map (Fig. 4.29).

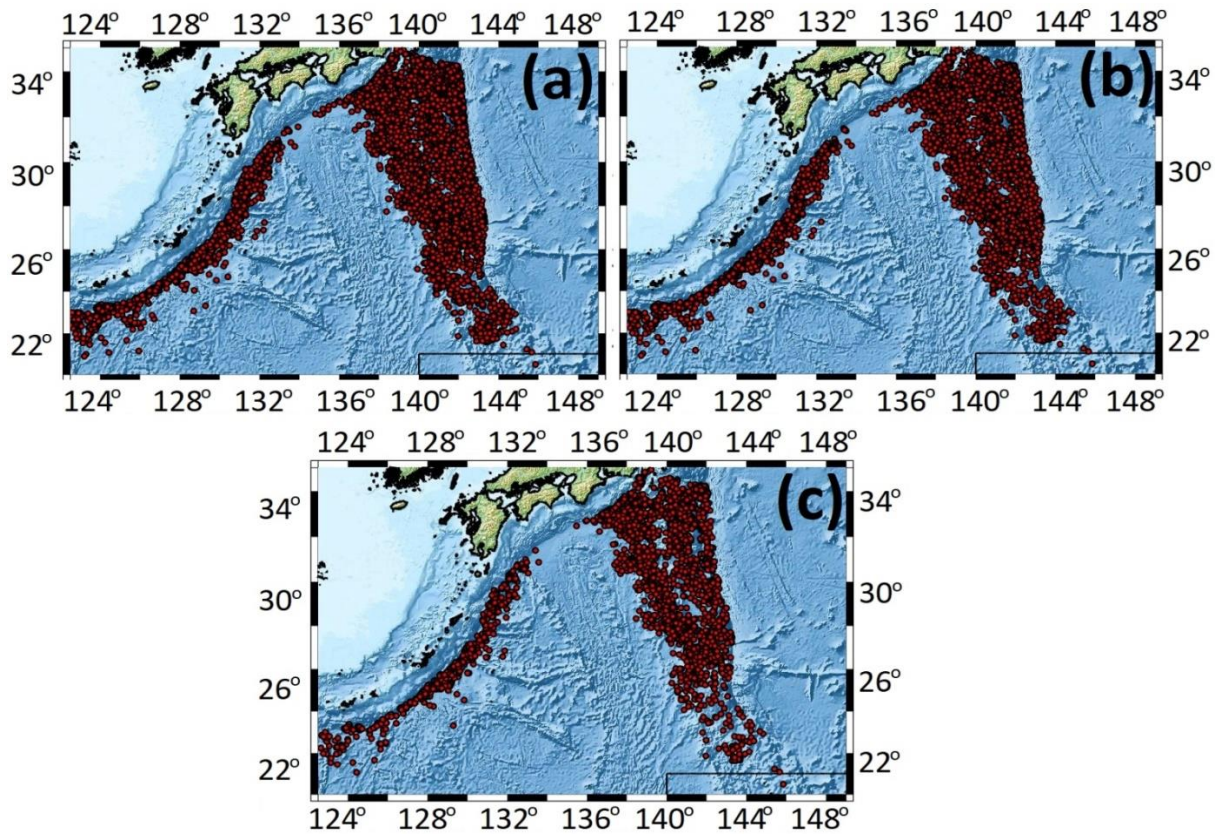


Figure 4.29: Seismicity map of declustered sub-crustal events located within Philippine Plate. Three overlaid earthquake catalogues referring to different background probabilities are depicted. 70% probability in red, 80% probability in and 90% in black.

The analysis of the sub-crustal declustered earthquake catalogues of Philippine is illustrated in Fig. 4.30. In general, the results show that seismogenesis is random. The temporal entropic index q_T (Fig. 4.30a) lingers in the interval (1, 1.2). The magnitude entropic index q_M (Fig. 4.30b) is decreasing with magnitude for all probabilities and lingers between 1.5 and 1.6 for all earthquake catalogues.

Specifically for background probability $\varphi_j = 70\%$ the temporal entropic index, q_T , is decreasing as magnitudes increase. For cut-off magnitude $M=3$ is equal to 1.14, and for cut-off magnitude $M=4.7$ is equal to 1. For background probability $\varphi_j = 80\%$ q_T mostly varies below 1.1. For cut-off magnitude $M=3$ is equal to 1.07 and for cut-off magnitude $M=4.5$ is 1.15. For $\varphi_j = 90\%$, q_T has an increasing trend and varies between 1.13 to 1.3.

For $\varphi_j = 70\%$, the magnitude entropic index, q_M is decreasing and for cut-off magnitude $M=3$ is equal to 1.56 while for cut-off magnitude $M=4.7$ is 1.49, yielding b_q values 0.78 and 1.03 respectively. For $\varphi_j = 80\%$, q_M , for cut-off magnitude $M=3$ is 1.57 and for cut-off magnitude $M=4.5$ is 1.5, yielding b_q variations between 0.75 and 1 for the same cut-off magnitudes, For

$\varphi_j = 90\%$, for cut-off magnitude $M=3$ q_M is equal to 1.57, and for cut-off magnitude $M=4.2$, is equal to 1.54, resulting b_q values 0.76 and 0.86 for the same cut-off magnitudes.

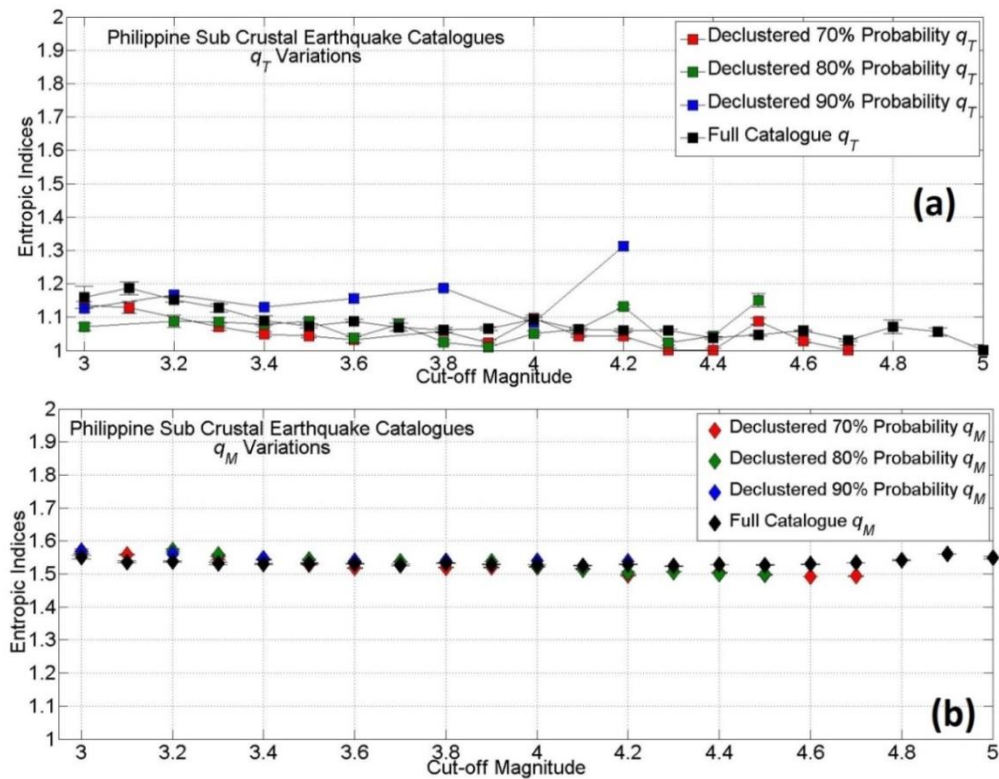
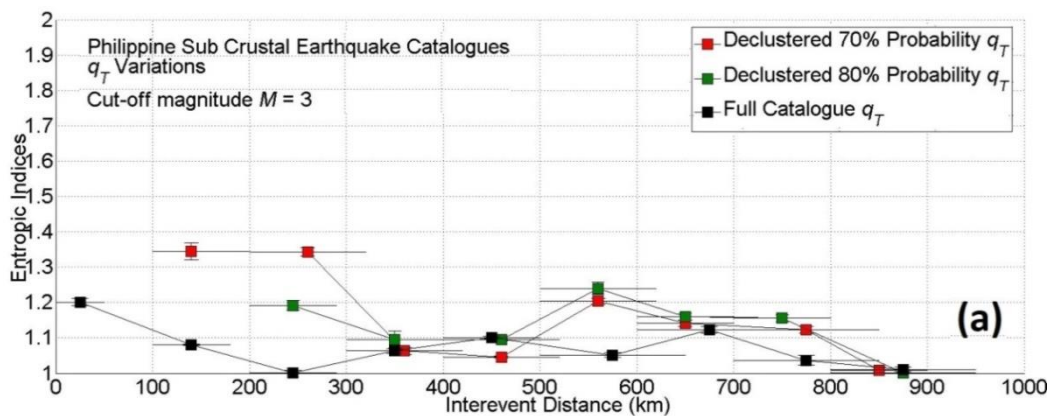


Figure 4.30: Dependence on different cut-off magnitudes analysis for all earthquake catalogues of Philippine sub-crustal seismicity. (a) q_T variations, and (b) q_M variations

Analysis of dependence of the entropic indices on interevent distances was conducted for background probabilities $\varphi_j = 70\%$, and $\varphi_j = 80\%$ (Fig. 4.31). For $\varphi_j = 70\%$ and up to 250 km q_T is above 1.3, meaning that earthquakes are related. After 300 km correlation is random and q_T varies below 1.2 up to 900 km. For $\varphi_j = 80\%$ q_T lingers in the interval (1.1, 1.2). Correlation based on these values is proved to be random for the sub-crustal earthquakes of Philippine. The magnitude entropic index q_M varies between 1.5 and 1.6 for all earthquake catalogues.



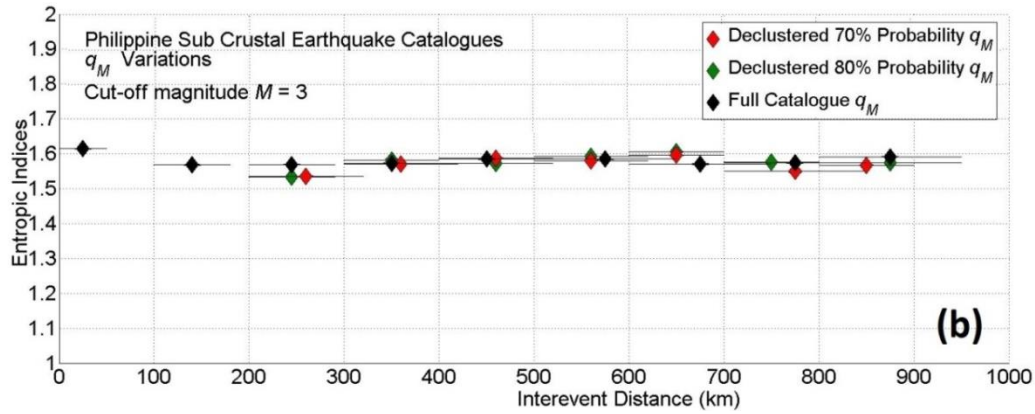


Figure 4.31: Analysis of dependence of the entropic indices on interevent distances at cut-off magnitude 3.0 for different background probabilities (a) q_T variations, and (b) q_M variations

The crustal declustered catalogues of Philippine are depicted in Fig. 4.32.

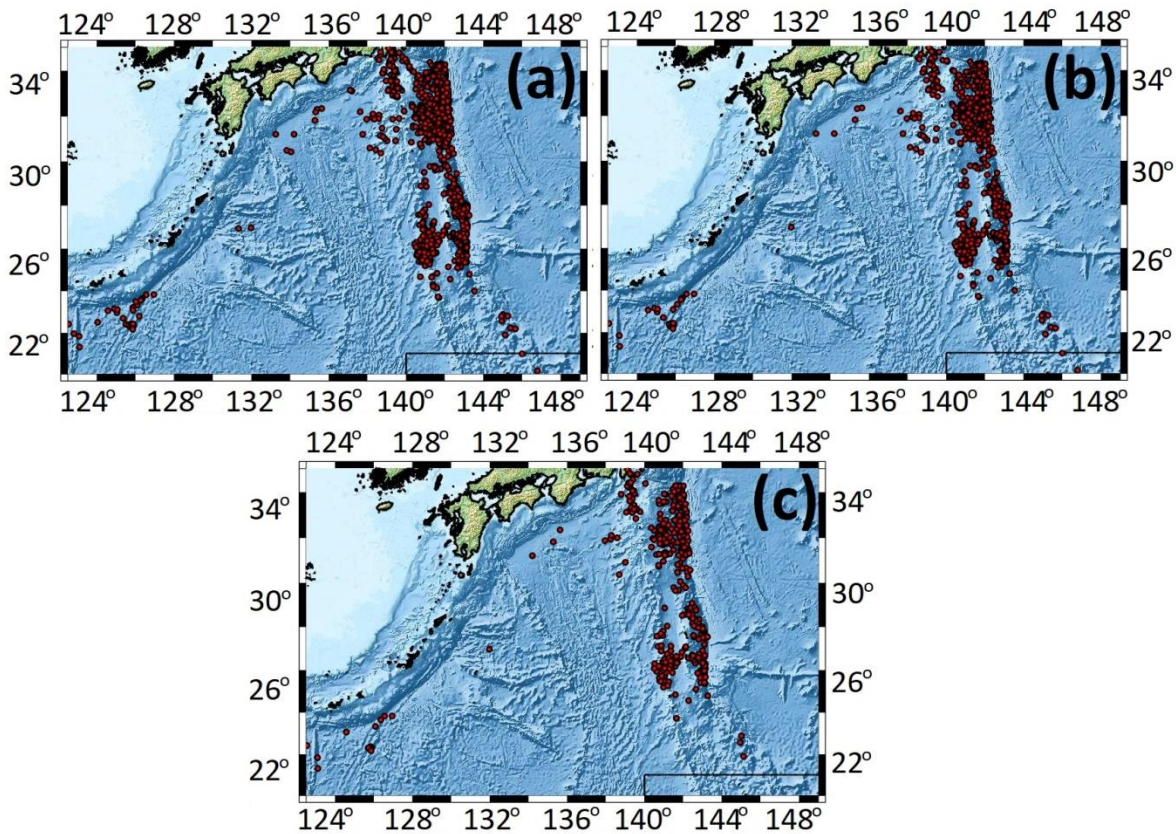


Figure 4.32: Seismicity map of crustal declustered earthquake catalogues of Philippine plate. Three overlaid background probability catalogues are depicted. 70% probability in red, 80% probability in green, and 90% in black.

The analysis of the crustal earthquake catalogue of Philippine is illustrated in the following figure (Fig. 4.33). In general, correlation is low, since q_T varies below 1.3 (Fig. 4.33a). The q_M index varies between 1.5 and 1.6 for all earthquake catalogues (Fig. 4.33b).

For $\varphi_j = 70\%$, and $\varphi_j = 80\%$ correlation is random. The temporal entropic index, q_T , for $\varphi_j = 70\%$ lingers in the interval (1, 1.1). For $\varphi_j = 80\%$ analysis shows that seismogenesis is a

random process, with the temporal index varying below 1.1. For $\varphi_j = 90\%$ correlation seems to increase, and q_T varies between 1.26 and 1.29, but it is still characterized as low to weak.

For $\varphi_j = 70\%$ q_M has a decreasing trend, for cut-off magnitude $M=3$ is equal to 1.57 and for cut-off magnitude $M=3.9$ is equal to 1.51, yielding b_q values 0.76 and 0.96. For $\varphi_j = 80\%$ q_M for cut-off magnitude $M=3$ is 1.57 and for cut-off magnitude $M=3.7$ is 1.53, yielding b_q values 0.76 and 0.88 respectively. For $\varphi_j = 90\%$ the index q_M for cut-off magnitude $M=3$ is equal to 1.57, whereas for cut-off magnitude $M=3.2$ is 1.56, yielding b_q values 0.74 and 0.79 for the same cut-off magnitudes respectively.

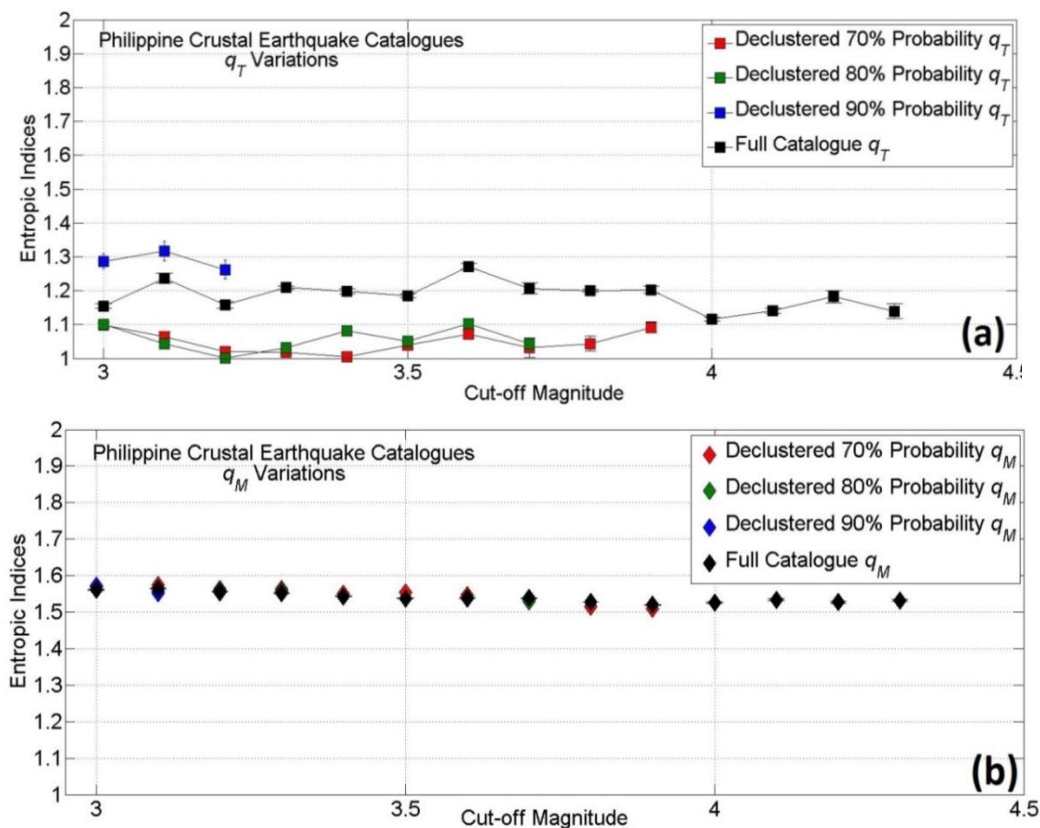


Figure 4.33: Dependence on different cut-off magnitudes analysis for all earthquake catalogues of Philippine crustal seismicity. (a) q_T variations, and (b) q_M variations

4.3 b-VALUE ANALYSIS

In this Section, the behaviour of the proxy- b value computed as a function of cut-off magnitude – $b_q(M)$ – is compared to Gutenberg–Richter b -values (b_{GR}), conventionally estimated on the basis of the univariate frequency-magnitude distribution, also as a function of cut-off magnitude – $b_{GR}(M)$. It is apparent that $b_q(M)$ and $b_{GR}(M)$ are expected to be the same. b_q is calculated from the magnitude entropic index q_M with which it has a hyperbolic relationship (Eq. 2.7). Due to this relationship, b_q is expected to vary rapidly with respect to the conventionally estimated b value. The extent of this variability is a measure of the effectiveness and robustness of the estimation procedure applied to the estimation of entropic indices. In other words, the procedure described in Section 2.3 should produce comparable $b_q(M)$ and

$b_{GR}(M)$. As already mentioned the b_q is estimated through Eq. (2.7); b_{GR} on the other hand is computed with robust regression. The b_q and b_{GR} results from full and declustered catalogues are simultaneously plotted and compared.

4.3.1 Eurasian Plate.

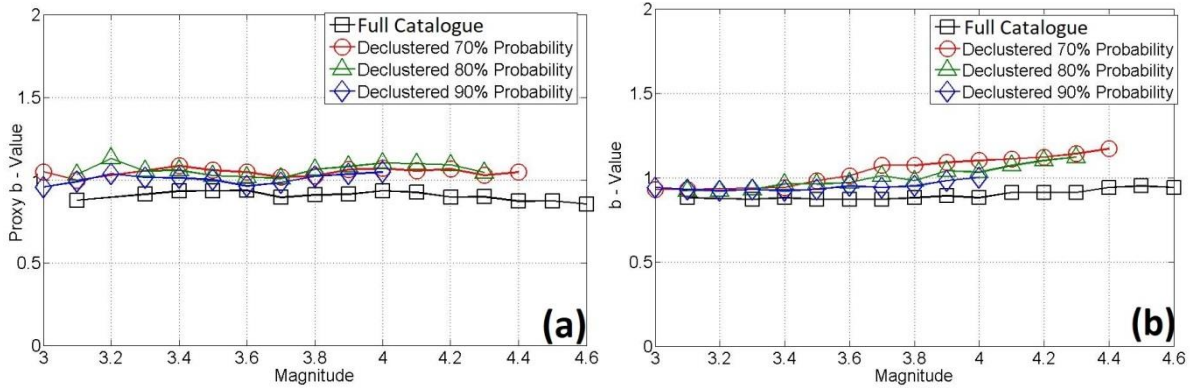


Figure 4.35: Variation of (a) $b_q(M)$ and (b) $b_{GR}(M)$ for the sub-crustal seismicity of Eurasia plate.

The results obtained for the *sub-crustal* and crustal catalogues, of the Eurasia plate are shown in Fig. 4.35 and Fig. 4.36 respectively. As evident in Fig. 4.35, $b_q(M)$ and $b_{GR}(M)$ are very comparable. For the full *sub-crustal* catalogue, b_q fluctuates in the interval (0.85, 0.93), whilst the conventionally estimated b , fluctuates in the interval (0.87, 0.94). In the declustered *sub-crustal* catalogues, b_q determinations are generally tightly clustered in the interval (0.94, 1.26) indicating invariance in the scaling of earthquake (fault) sizes, at least between M_3 and $M_{4.4}$. However, the corresponding b_{GR} determinations exhibit a clear upward trend linear from approx. 0.96 at $M_{3.4}$ to approx. 1.3 at $M_{4.4}$, indicating changes in the scaling of earthquake sizes.

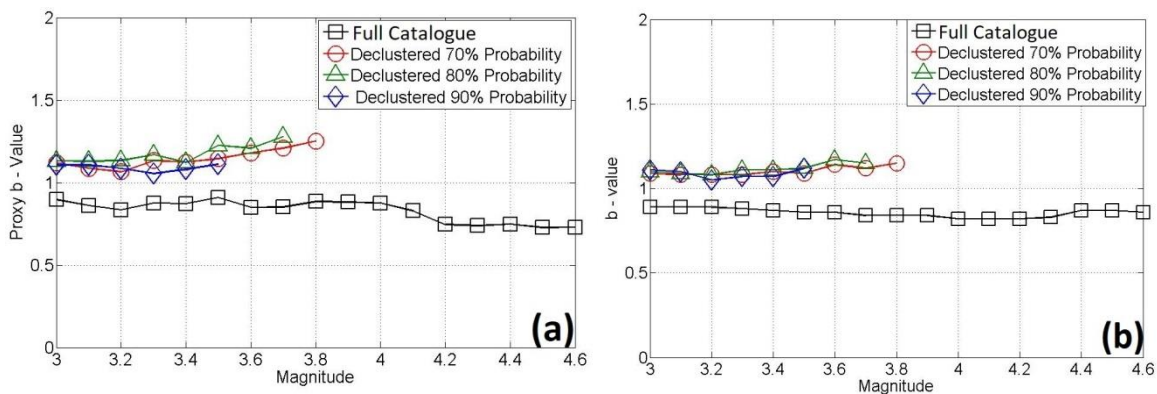


Figure 4.36: Variation of (a) $b_q(M)$ and (b) $b_{GR}(M)$ for the crustal seismicity of Eurasia plate.

Turning to the analysis of crustal seismicity, note that in the full earthquake catalogue of Eurasia, b_q and b_{GR} vary in (0.73, 0.91) and (0.82, 0.9) respectively. In the declustered catalogues, b_q and b_{GR} are both tightly clustered in the intervals (1.05, 1.25) and (1.05, 1.17) respectively and they both exhibit the same slow upward linear trend pointing to changes in the scaling of earthquake (fault) sizes associated with decrease (spreading) in the localization of faulting activity (increase in crustal heterogeneity). The homologous increase and upward trend of b_q and b_{GR} in the declustered catalogues may result from the presence of earthquake

clusters, (Fig. 4.17 and Fig. 4.20), attributed to rock heterogeneity and stress variations due to volcanic activity (see Fig. 4.37). The seismicity of Eurasia (as illustrated in Figs. 4.1, 4.17 and 4.20) develops along southern Japan (Kiushu and southern Honsu islands) and the Ryukyu Arc, areas that are characterized by intense volcanic activity. Volcanic areas are commonly associated with high b -values and variations associated mainly with thermal, mineralogical, petrological and structural complexities (e.g. Lin et al., 2007; Murru et al., 2007; Wiemer and Wyss, 1997; Wiemer and Wyss, 2002; Wiemer et al., 1998; Wyss and Matsumura, 2006; Wyss and Stefansson, 2006; Wyss et al., 2004). Lin et al. (2008), suggest that magma feeding channels, in Ryukyu arc, are characterized by b -values higher than 1.1 suggesting that the magma may rise through numerous conduits, at depth up to 15 km and above the Ryukyu Wadati-Benioff zone, at depths ranging from 90 to 110 km, the high b -values might correspond to the depth of dehydration of the subducting oceanic crust.

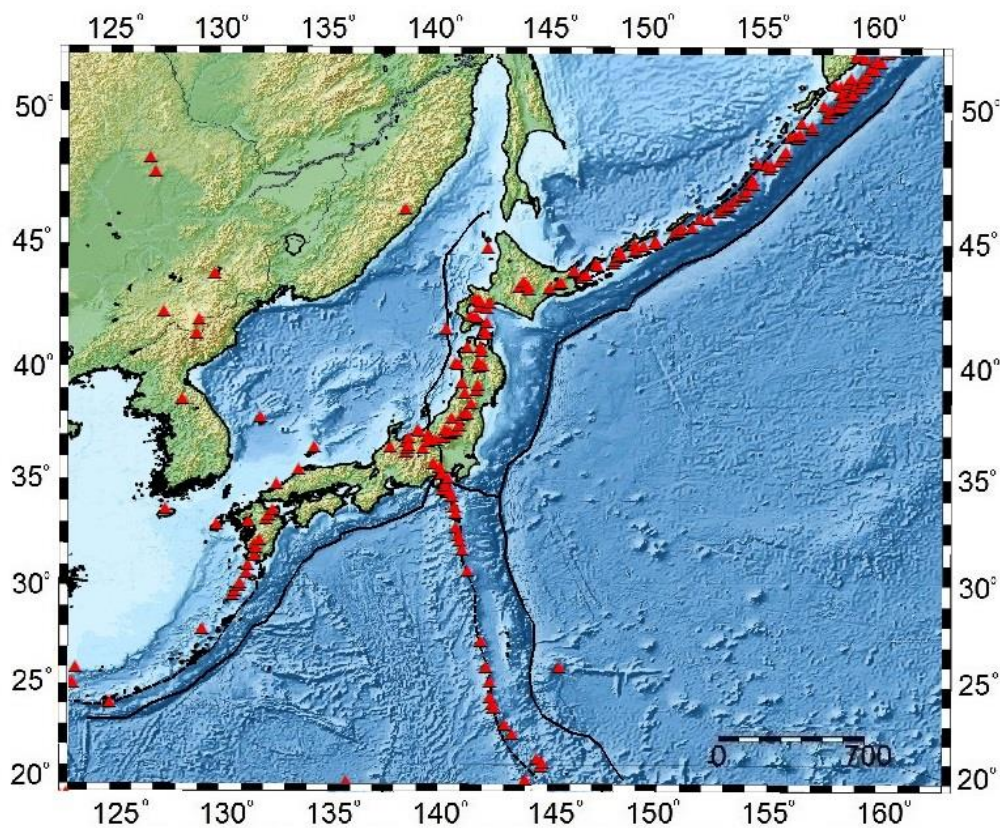


Figure 4.37: Volcanoes of Japan

4.3.2 Okhotsk Plate.

The analysis of b values for the Okhotsk sub-crustal and crustal catalogues is illustrated in Fig. 4.38 and Fig. 4.41.

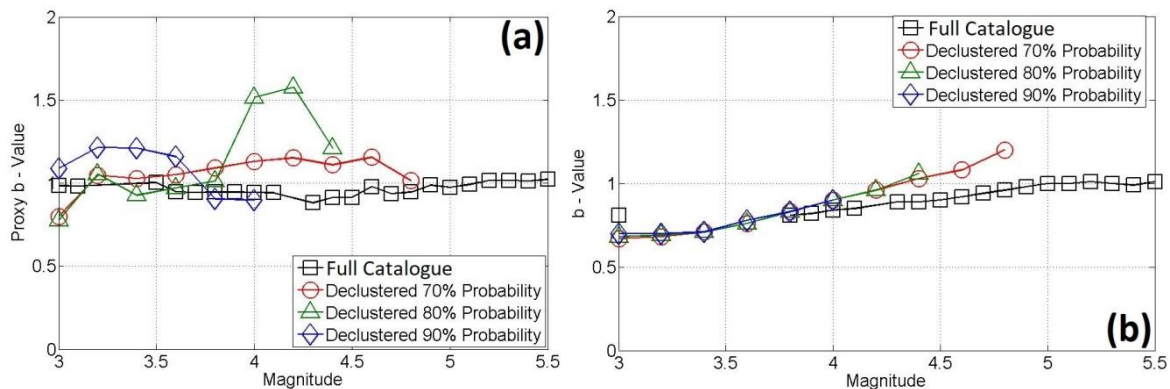


Figure 4.38: Variation of (a) $b_q(M)$ and (b) $b_{GR}(M)$ for the *sub-crustal* seismicity of the Okhotsk plate.

The seismicity of the Okhotsk plate is complicated as it includes the 2011 Tohoku mega-earthquake and its aftershock sequence that lasted for almost two years. b_q and b_{GR} are not consistent, b_q deviates from b_{GR} , especially for background probability 80%. In general, b increases with magnitude and in the declustered catalogues an upward linear trend suggests a corresponding decrease in activity localization, most possibly due to the widespread aftershock sequence.

Prior to the 2011 Tohoku event, the seismicity of the near-coastal part of the northern Tohoku district in NE Japan (also known as the Sanriku area), was characterized by clusters of earthquakes that occurred just above the subduction boundary (Kirby et al., 2005). Similar clusters were previously found by Okada et al. (2004). Uchida et al. (2010) indicated the presence of earthquake clusters (they refer to them as supraslab -events that are within 5–25 km above the Pacific plate subduction boundary), especially near the Sanriku coast. Small repeating earthquakes are also distributed in the same geographic area. Their distribution is not uniform and consists of a number of earthquake clusters whose dimensions are as large as 15 to 30 km (Fig. 4.39).

Given the “complication” of Fig. 4.38 and the properties of seismicity in the study area, it was considered imperative to proceed with a more detailed investigation of the properties of b_q and b_{GR} , with particular reference to the periods before and after the Tohoku event.

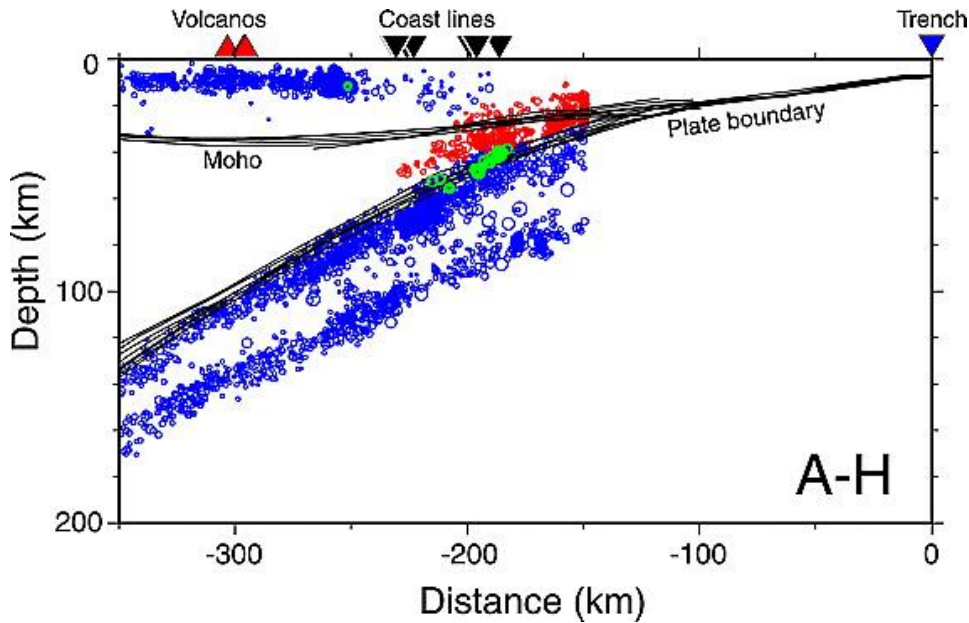


Figure 4.39: Supraslab earthquake clusters above and on the Pacific plate boundary (red and green circles) as depicted in Uchida et al., (2010).

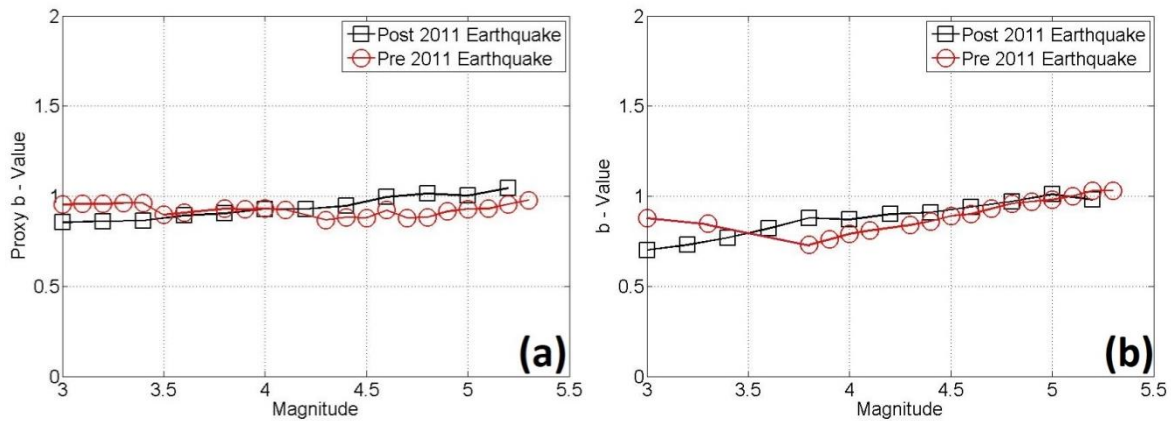


Figure 4.40: Variation of (a) $b_q(M)$ and (b) $b_{GR}(M)$ for the *sub-crustal* seismicity of the Okhotsk plate before and after the Tohoku mega-earthquake. *sub-crustal*

For *sub-crustal* events $b_q(M)$ prior to and after the Tohoku earthquake vary in the intervals (0.84, 1.03). Prior to the 2011 (red circles) earthquake, $b_q(M)$ fluctuates around 0.9, and exhibits a decreasing trend from $M=3$ to $M=4.5$, and after $M=4.6$ increases and reaches 1. After the earthquake (black squares) $b_q(M)$ increases linearly with the magnitude scale and varies from 0.84 to 1.03. Results for $b_{GR}(M)$ are the same. Prior to the 2011 event it decreases at small magnitudes and after $M=3.7$ increases and reaches the value 1 at $M=5.3$. After the earthquake, the $b_{GR}(M)$ curve exhibits increases as the magnitude scale increases and varies in the interval (0.65, 1.02).

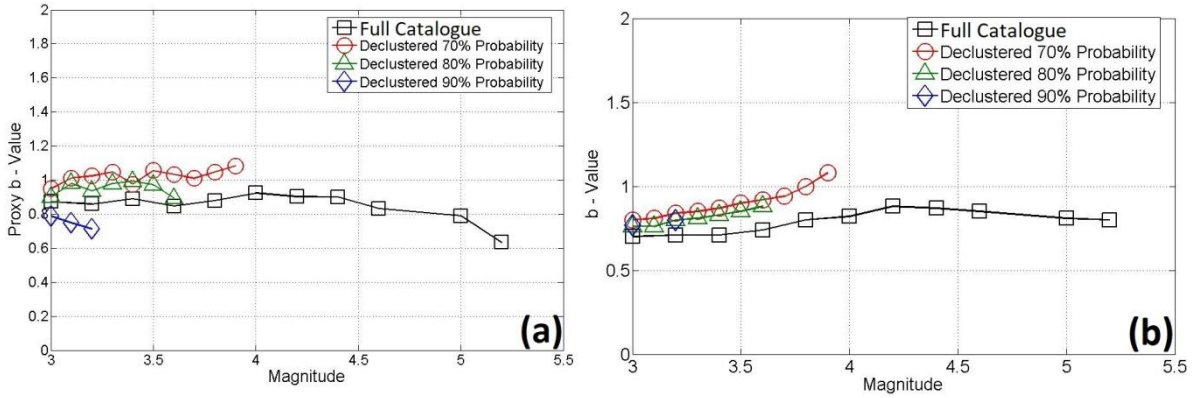


Figure 4.41: Variation of (a) $b_q(M)$ and (b) $b_{GR}(M)$ for *crustal* full and declustered earthquake catalogues of the Okhotsk plate

As for the *crustal* earthquake catalogues of Okhotsk plate b_q and b_{GR} vary in the same intervals (0.6, 1.2). The declustered catalogues exhibit higher b -values than the full. $b_q(M)$ for the full catalogue fluctuates in the interval (0.6, 0.85) and $b_{GR}(M)$ lingers between 0.75 and 0.85. As for the declustered catalogues $b_q(M)$ for background probabilities 70% and 80% has an increasing trend and fluctuates around 1, while for probability 90% decreases and lingers between 0.65 and 0.7. On the other hand, $b_{GR}(M)$ increases for all background probabilities and varies between 0.75 and 1.05.

Based on bibliographic research the concept of earthquake clusters for Okhotsk's *crustal* earthquakes, especially on the northern part and around the Tohoku region has been extensively investigated. Okada et al. (2011) examined the seismic activity in the broader Tohoku region and found that some areas of increased seismicity are located above the edge of the low-velocity zone in the lower crust. This led them to suggest that the observed activity is due to heterogeneity in the lower crust and the presence of over pressurized fluid (Miller et al. 2004). According to Okada et al. (2014) also proved some earthquake clusters are located above the edge of the low-velocity zone beneath the Moriyoshi-zan volcano.

Analysis prior to and after the Tohoku earthquake for *crustal* earthquakes shows that b -values are the same and linger in the interval (0.75, 1.01). Prior to the 2011 (red circles) $b_q(M)$ increase from $M=3$ to $M=4.2$ and then drops until $M=4.8$. After the event (black squares) the $b_q(M)$ curve increases as the magnitude scale increases and lingers in the interval (0.75, 1).

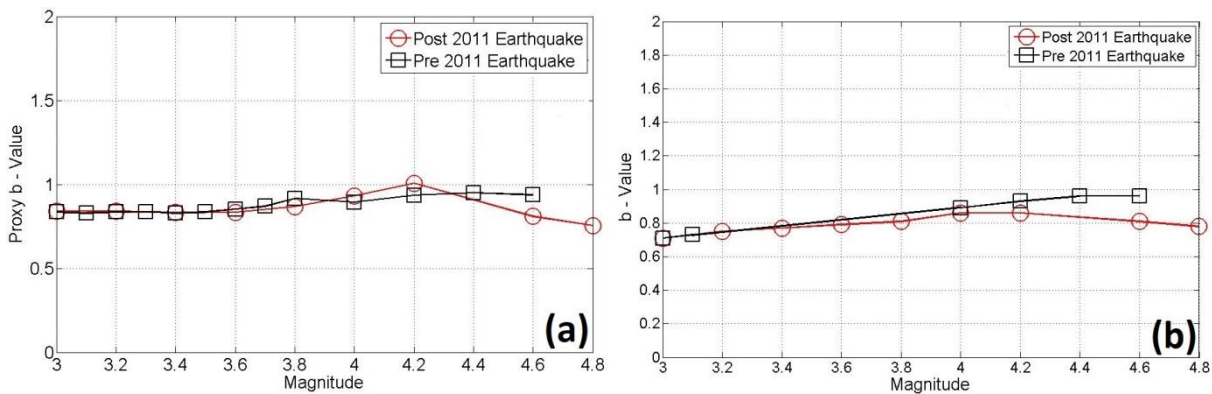


Figure 4.42: Variation of (a) $b_q(M)$ and (b) $b_{GR}(M)$ for the *crustal* seismicity of the Okhotsk plate before and after the Tohoku mega-earthquake

4.3.3 Pacific Plate.

The analysis of the Pacific plate seismicity is shown in Fig. 4.43. Due to insufficiency of data, analysis of b -values wasn't possible for Pacific's crustal events.

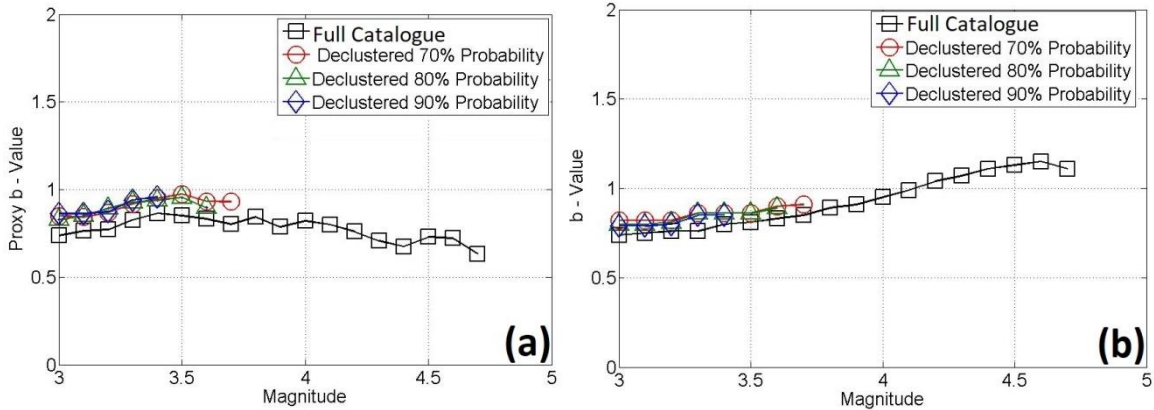


Figure 4.43: Variation of (a) $b_q(M)$ and (b) $b_{GR}(M)$ for the *sub-crustal* seismicity of the Okhotsk plate before and after the Tohoku mega-earthquake. sub-crustal.

It is apparent that the full earthquake catalogues exhibit significant differences: $b_q(M)$ is basically fluctuating around a value of 0.65 ± 0.1 , while b_{GR} is increasing quasi-linearly from 0.69 at $M=3$ to 1.17 at $M=4.5$. However, in the declustered catalogues both $b_q(M)$ and $b_{GR}(M)$ are both self-consistent and mutually consistent and vary in the same interval of (0.8, 1), exhibiting the same upward trend. In addition, they also exhibit higher values, especially at small magnitudes ($M \leq 3.6$).

4.3.4 Philippine Plate.

The analysis of the Philippine plate *sub-crustal* full and declustered catalogues is shown in Fig. 4.50 and 4.51). The analysis of b -values of Philippine's *sub-crustal* events show that b_q and b_{GR} are generally tightly clustered in the interval (0.7, 1.05). $b_q(M)$ for the full catalogue fluctuates around 1.65 ± 0.08 , while for the declustered catalogues it increases and varies in the interval (0.7, 1.03) for all background probabilities. $b_{GR}(M)$ exhibits an increasing trend for all earthquake catalogues and lingers between 0.65 and 1.01.

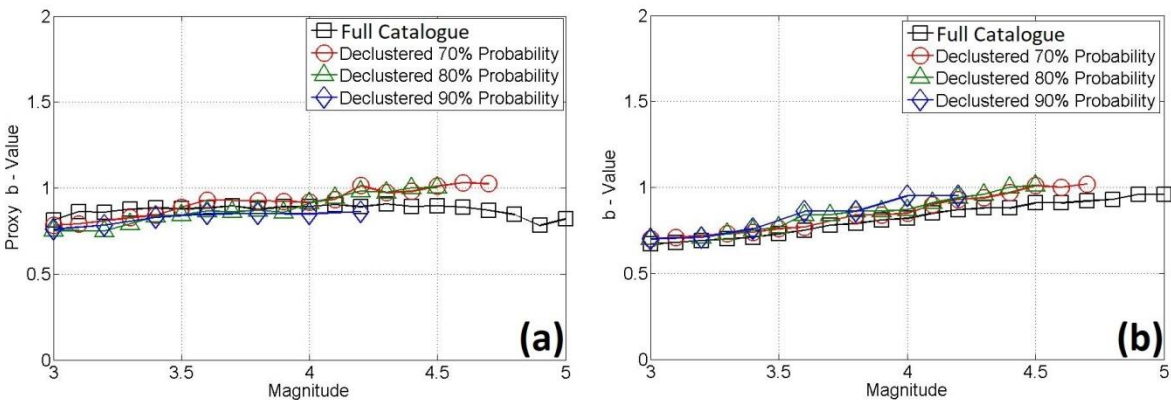


Figure 4.50: Variation of (a) $b_q(M)$ and (b) $b_{GR}(M)$ for the *sub-crustal* full and declustered earthquake catalogues of the Philippine plate.

As for the *crustal* earthquakes of Philippine, results of the b-values analysis show that both $b_q(M)$ and $b_{GR}(M)$ increase quasi-linearly from 0.6 to 1 for all catalogues.

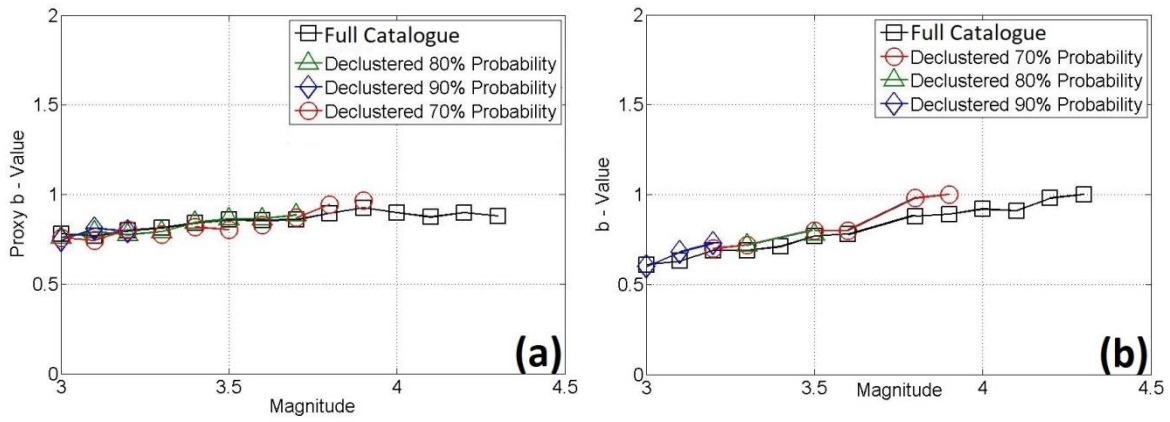


Figure 4.51: Variation of (a) $b_q(M)$ and (b) $b_{GR}(M)$ for the *crustal* full and declustered earthquake catalogues of the Philippine plate

5. TIME DEPENDENCE OF ENTROPIC INDICES VARIATIONS AND b-VALUES

This chapter examines the variations of entropic indices in time, in an attempt to investigate possible time-dependent changes in the (dis)equilibrium state of the seismogenetic systems (fault networks) studied herein. In simple words, the variations of the degree of correlation in time are examined. The temporal index q_T is a measure of this correlation and as stated in the previous chapter is affected by strong earthquakes and aftershock sequences. With this analysis, q_T variations in time are plotted, to scrutinize the behaviour of seismogenesis. In addition, time-dependent changes in the proxy- b value (b_q) are computed on the basis of the magnitude entropic index q_M , and the results are compared to the conventionally estimated Gutenberg–Richter b value (b_{GR}) computed by linear regression using the ZMAP software package (Wiemer, 2001).

5.1 Eurasian Plate

Let us begin, as always, with a presentation of results for the sub-crustal full and declustered catalogues (Fig. 5.1 and 5.2).

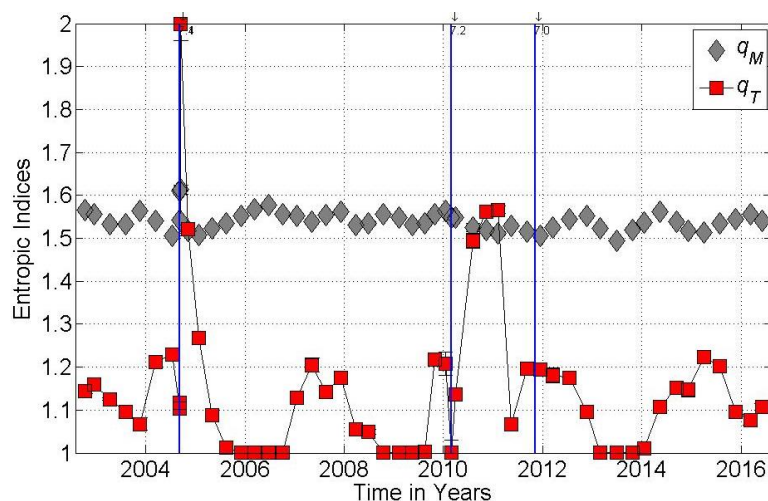


Figure 5.1: Time dependence of the entropic indices for the Eurasia full sub-crustal catalogue. Vertical lines indicate the occurrence of major ($M > 7$) earthquakes.

In general, the temporal index q_T is low (<1.2) but evolves in a structured dynamic fashion, shifting between approx. 1.2 and 1 and at times remaining close to 1 for periods of up to one year. This is consistent with the findings of Section 4.1.1 and indicates a Poissonian seismogenetic system. Note, however, that correlation increases *dramatically* after the occurrence of major earthquakes due to the overwhelming effect of correlated aftershock sequences. Of particular interest is the increase of correlation in the between two $M > 7$ events that have occurred on 2004, 2010 and 2011, whose imprint is also found in the declustered catalogues (see below). The magnitude entropic index q_M is stable around 1.55 ± 0.06 and does not show any significant trend, also in consistency with the findings in Section 4.1.1.

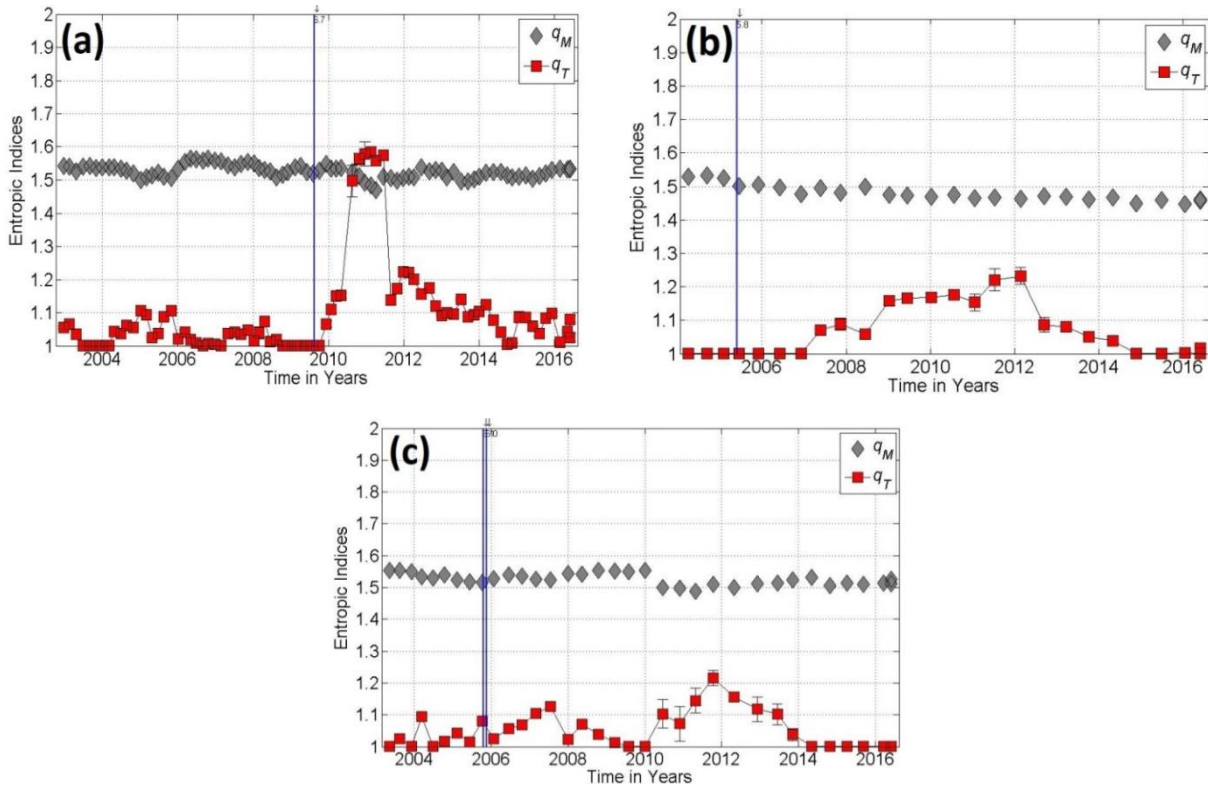


Figure 5.2: Time dependence of the entropic indices for the Eurasia declustered sub-crustal catalogues at the 70% (a), 80% (b) and 90% (c) probability levels. Vertical lines indicate the occurrence times of significant ($M > 5.5$) earthquakes.

The analysis of the declustered sub-crustal catalogues (Fig. 5.2) confirms that seismogenesis in the Eurasian Wadati-Benioff zone is largely Poissonian. A point worth noting is that the declustering algorithm has identified the major ($M=7$) of 2004, 2010 and 2011 shown in Fig. 5.1 to be “foreground” (or “triggered”) and has removed them from the declustered catalogues. A second point of interest is that while the aftershock sequence of the $M7.4$ event of 2004 has been completely suppressed, the correlated activity observed between the $M7.2$ event of 2010 and $M7.0$ event of 2011 has left a significant footprint on the declustered catalogues, indicating that it may not be directly related to aftershock activity associated by these earthquakes, but may comprise a time-local correlated cluster. As with the full catalogue, the magnitude entropic index q_M is stable and featureless and does not exhibit noteworthy traits. The evolution of b -values (b_q and b_{GR}) computed from the full and declustered sub-crustal catalogues of the Eurasia plate is illustrated in Fig. 5.3.

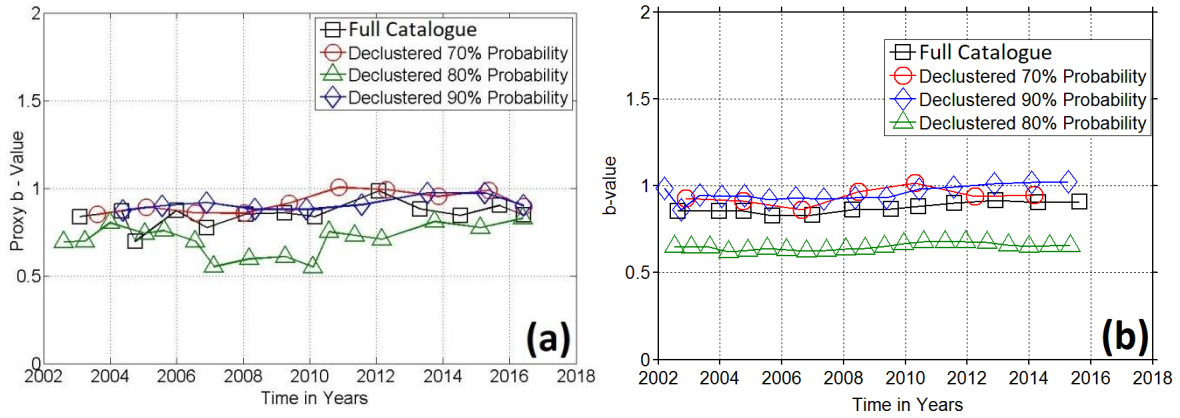


Figure 5.3: Time dependence of b -values for the full and declustered *sub-crustal* catalogues of the Eurasia plate. Pane (a) shows the time dependence of b_q ; panel (b) the time dependence of b_{GR} .

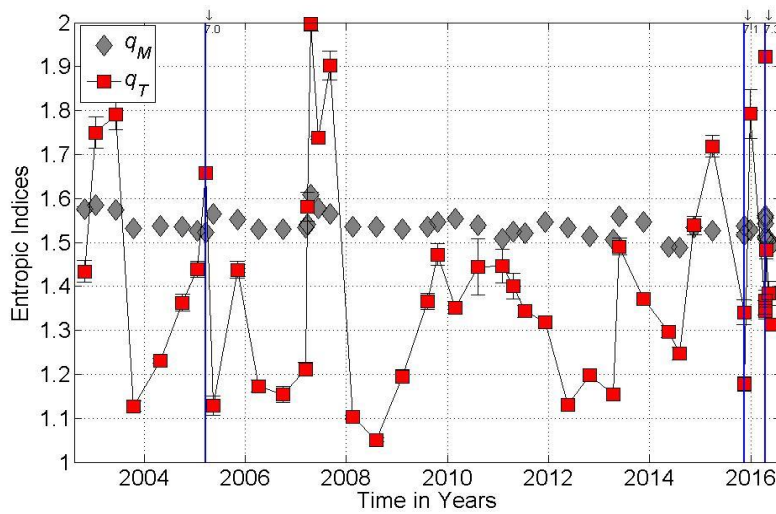


Figure 5.4: Time dependence of the entropic indices for the Eurasia full crustal catalogue. Vertical lines indicate the occurrence of major ($M > 7$) earthquakes.

The time dependence of the entropic indices for the full catalogue is shown in Fig. 5.4. It is evident that the temporal entropic index q_T is both significant and very dynamic, varying in response to changes in the activity of the seismogenetic system. Noteworthy is the elevated state of correlation observed between 2010 and 2012, which coincides with the elevated correlation observed in the sub-crustal data during the same period: it implies that crustal and sub-crustal activity is certainly correlated during this time interval. Interestingly enough, the magnitude entropic index q_M exhibits some variation and increases when q_T increases coherently and concurrently with q_T every time the latter exceeds values of the order of 1.5 (very strong correlation). This implies corresponding decreases in the scaling of earthquake sizes or, equivalently increases in activity localization; it also suggests that the concurrent increase of q_T may result from clustered activity and/or aftershock sequences of significant events.

Fig. 5.5 illustrates the results of the declustered catalogue analysis. It can be immediately seen that the dynamic variation of q_T observed in the full catalogue all but vanishes in the $\varphi = 70\%$ and $\varphi = 80\%$ probability levels (Fig. 5.5a and 5.5b respectively), except for the interval between 2008 and 2012 where, however, it still lingers at a very low to low level (< 1.25). This feature

also disappears in the $\varphi = 90\%$ probability level (Fig. 5.5c). As it turns out, the results of the declustered catalogues all indicate a Poissonian system consistently with the findings of Section 4.2.1. A final point of interest is that the magnitude entropic index q_M exhibits a low-rate albeit steady decrease with time, indicating a corresponding overall increase in b -values, therefore crustal homogeneity (see below).

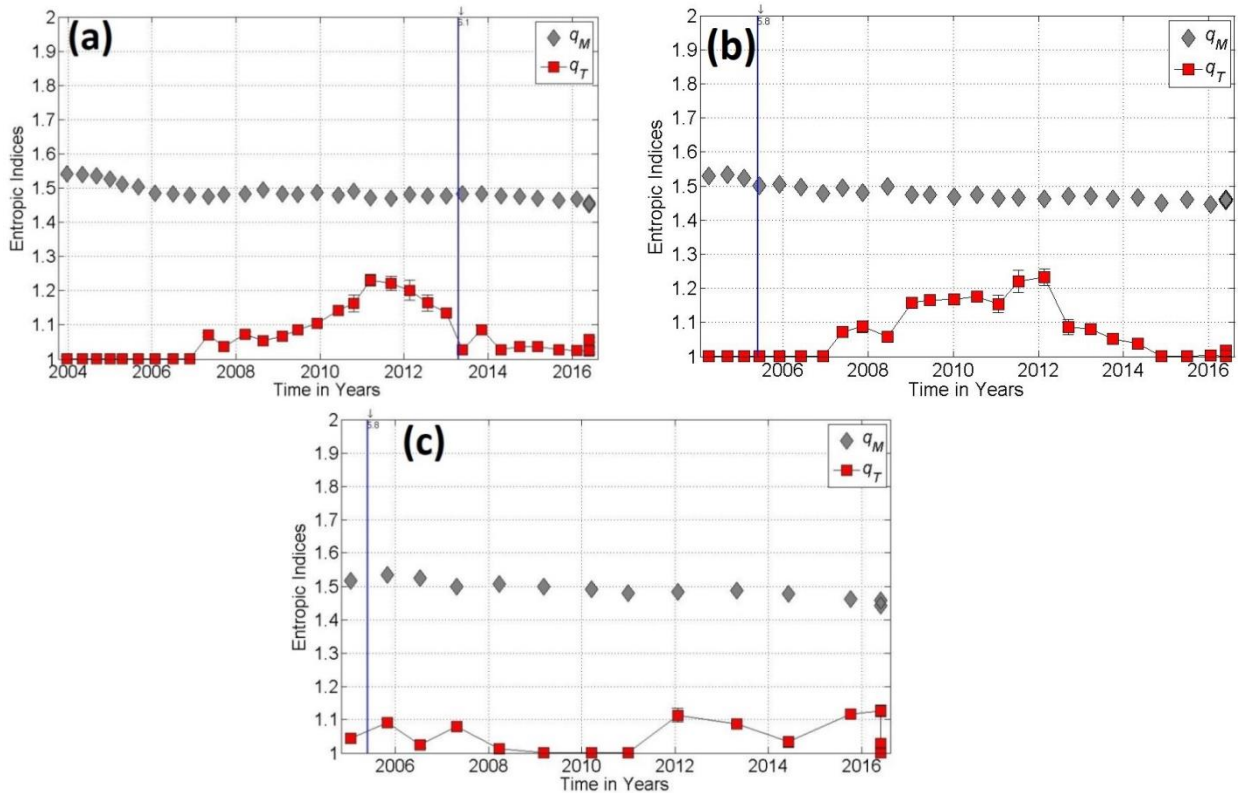


Figure 5.5. Time dependence of the entropic indices for the Eurasia declustered crustal catalogues at the 70% (a), 80% (b) and 90% (c) probability levels. Vertical lines indicate the occurrence times of significant earthquakes

The time dependence of b_q and b_{GR} for the full and declustered catalogues is shown in Fig. 5.6. Three observations can immediately be made: a) both b_q and b_{GR} are very comparable and absolutely compatible. b) b -values obtained from the declustered catalogues are very consistent and markedly higher than those of full catalogues, as often observed in hitherto analysis; it implies a decrease in the localization of background earthquake activity, therefore decreased crustal homogeneity. c) Both b_q and b_{GR} all indicate a low rate albeit clear increase with time, indicating progressive decrease in crustal homogeneity, which is compatible with a Poissonian system.

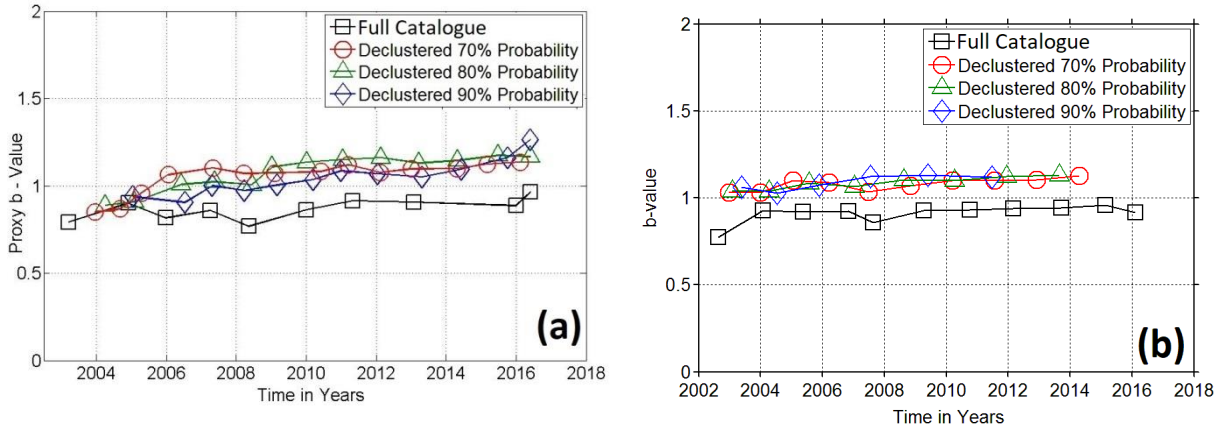


Figure 5.6: Time dependence of b -values for the full and declustered *crustal* catalogues of the Eurasia plate. Panel (a) shows the time dependence of b_q ; panel (b) the time dependence of b_{GR} .

5.2 Okhotsk Plate.

The results of the entropic indices variations in time of the sub-crustal full earthquake catalogue of Okhotsk are depicted in the following figure (Fig. 5.7). In general both entropic indices present significant variations. Correlation in general is weak to moderate ($1 \leq q_T \leq 1.4$) and increases abruptly after the major earthquakes of 2004 (M8), 2006 (M7.9) and 2011 (M7.6). The magnitude entropic index q_M varies around 1.6 ± 0.1 and shows significant changes before and after strong earthquake occurrence.

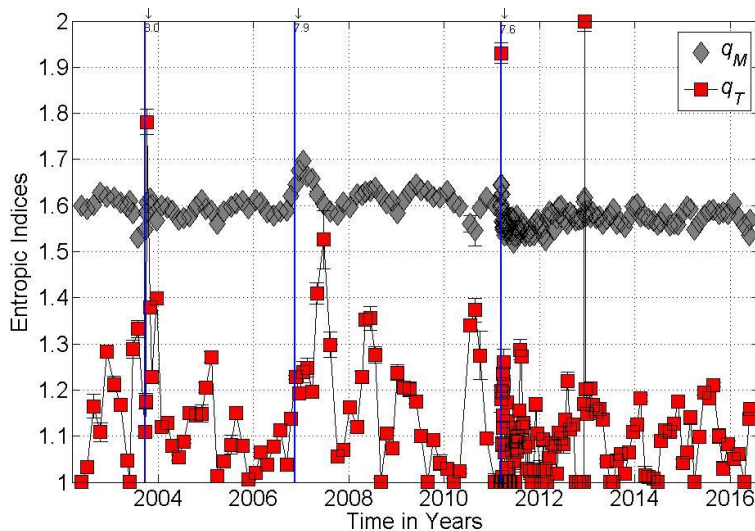


Figure 5.7: Time dependence of the entropic indices for the Okhotsk full sub-crustal catalogue. Vertical lines indicate the occurrence of major ($M > 7$) earthquakes.

Fig. 5.8 illustrates the results of the declustered catalogue analysis. It can be immediately seen that the dynamic variation of q_T observed in the full catalogue completely changes for all background probabilities. For background probabilities $\varphi_j=70\%$ (Fig. 5.8a) and $\varphi_j=80\%$ (Fig. 5.8b) correlation is random with $q_T \leq 1.2$ except after the 2011 earthquake, where correlation increases above 1.2 for a short period. For background probability $\varphi_j=90\%$ (Fig. 5.8c) correlation is also random from 2002-2011. After 2011 and until 2016 q_T varies from 1.2 to 1.8. The magnitude index q_M exhibits significant variations especially for probabilities 70% and 80%. In general, for the time period of 2002 to 2011 it has an increasing trend, but drops

dramatically, below 1.5 for $\varphi_j=70\%$ and around 1.55 for $\varphi_j=80\%$, in 2011, then it returns back to its previous state with a small decreasing trend from 2012 to 2016. For probability 90% it behaves quasi-linearly around 1.6 and exhibits a small decreasing trend.

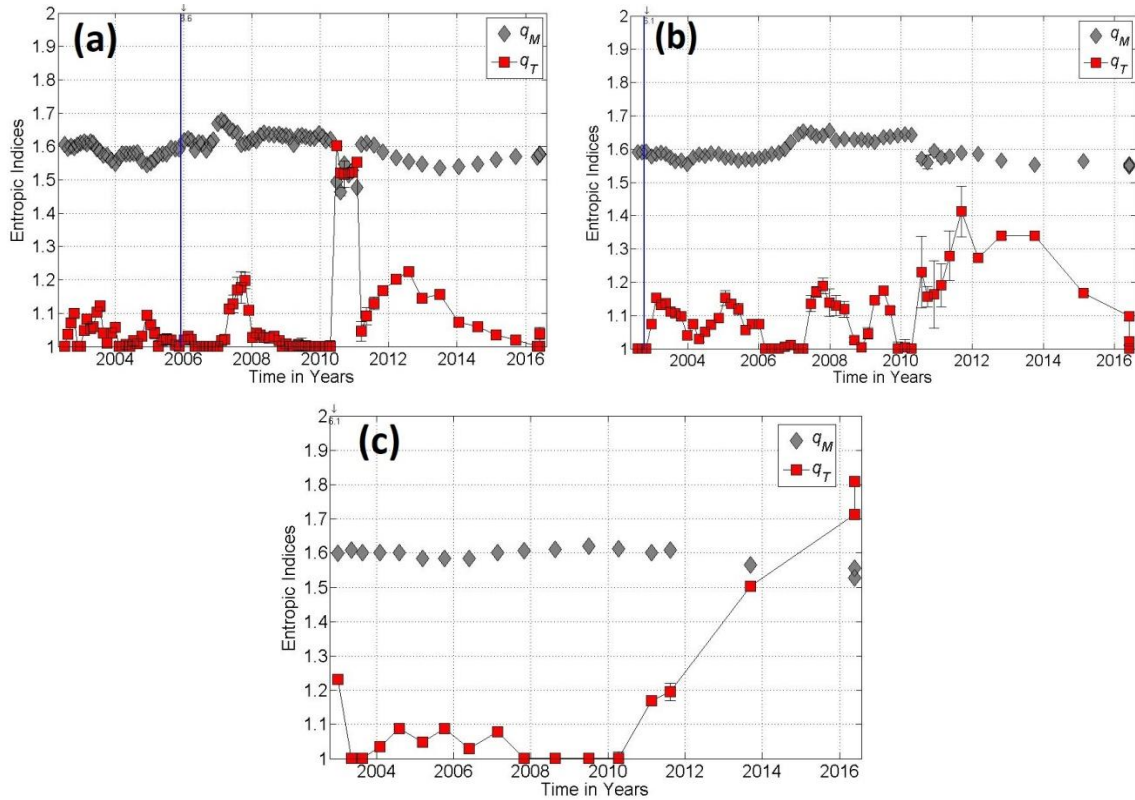


Figure 5.8: Time dependence of the entropic indices for the Okhotsk declustered sub-crustal catalogues at the 70% (a), 80% (b) and 90% (c) probability levels. Vertical lines indicate the occurrence times of significant earthquakes.

The time dependence of b_q and b_{GR} for the full and declustered catalogues is shown in Fig. 5.9. Three observations can immediately be made: a) both b_q and b_{GR} are very consistent and comparable. b) b -values obtained from the declustered catalogues a bit higher than those of full catalogue and c) both b_q and b_{GR} all increase with time, after the 2011 earthquake, indicating progressive decrease in crustal homogeneity and a decrease in the localization of background earthquake activity.

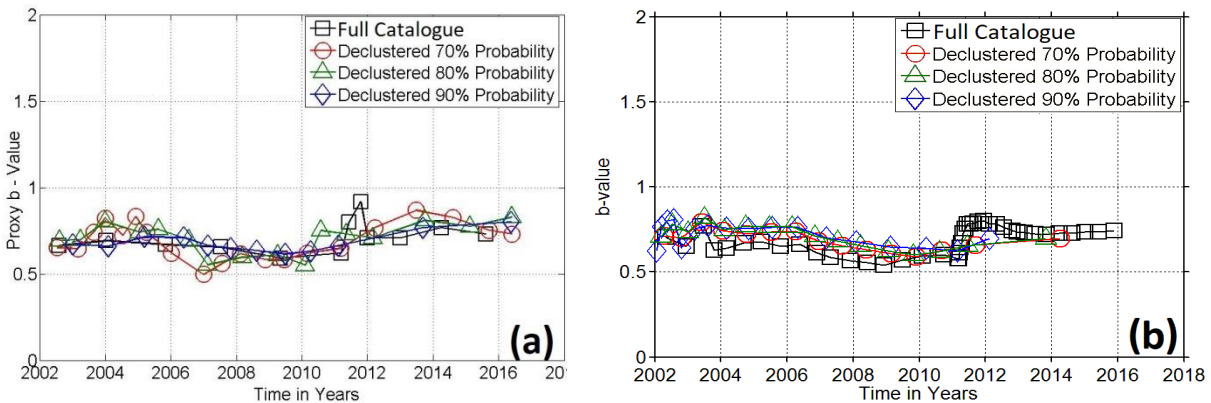


Figure 5.9: Time dependence of b -values for the full and declustered sub-crustal catalogues of the Okhotsk plate. Panel (a) shows the time dependence of b_q ; panel (b) the time dependence of b_{GR} .

Fig. 5.10 shows the variations of entropic indices with time for the crustal earthquake catalogues of Okhotsk.

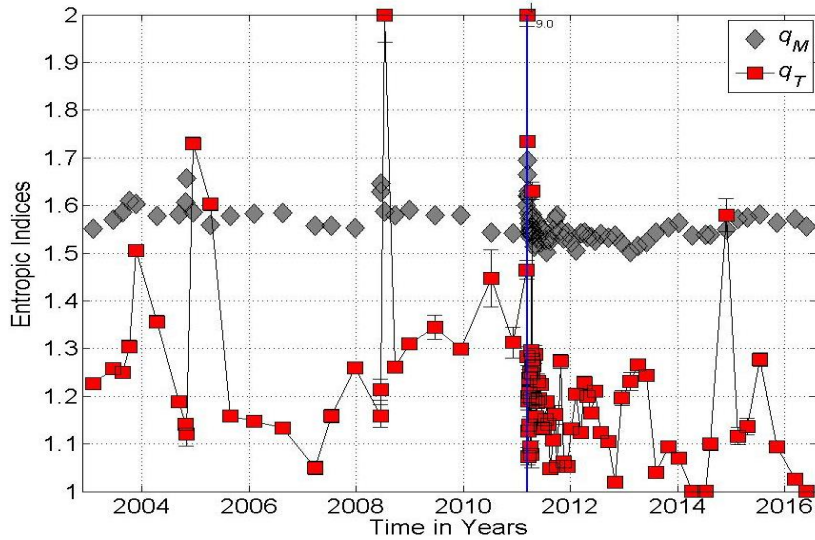


Figure 5.10: Time dependence of the entropic indices for the Okhotsk full crustal catalogue. Vertical lines indicate the occurrence of major ($M \geq 9$) earthquakes.

Correlation for Okhotsk *crustal* full catalogue in general can be characterized as weak, with q_T varying between 1 and 1.3, with some exceptions after strong earthquakes. A distinctive feature of this analysis is the *Tohoku earthquake in 2011* (M_9) where correlation increases dramatically with $q_T=2$. The magnitude entropic index q_M varies around 1.6 ± 0.1 . During the Tohoku earthquake q_M increases abruptly, that implies that earthquake activity is localized, meaning that earthquakes, earthquake energy and stress are confined within a smaller region (a fault).

The declustered catalogues results are depicted in Fig. 5.11. The imprint of the 2011 earthquake is disappeared and correlation becomes random for all background probabilities. The temporal index q_M lingers in the interval (1, 2) with a small increasing trend. The magnitude entropic index q_M fluctuates, for both probabilities, around 1.53 ± 0.03 .

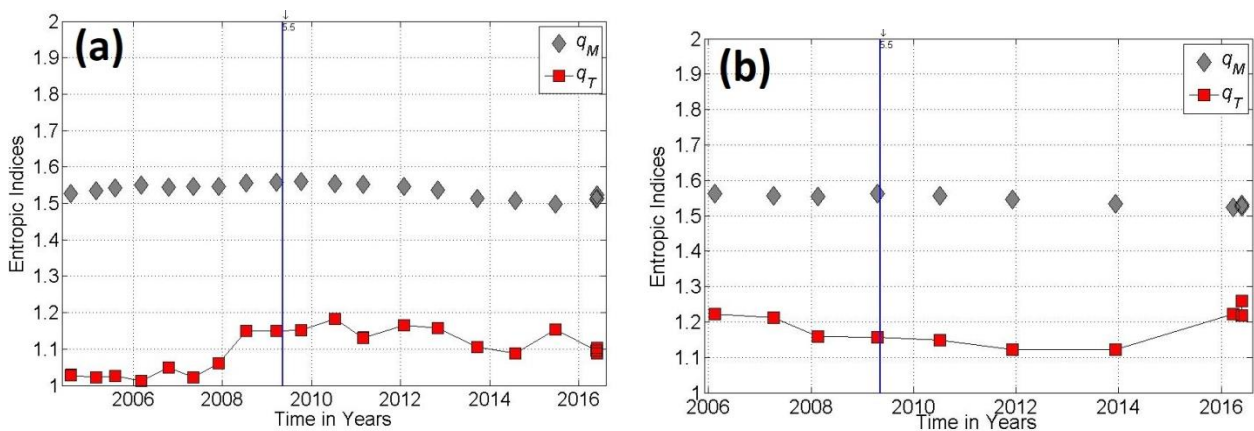


Figure 5.11: Time dependence of the entropic indices for the Okhotsk declustered crustal catalogues at the 70% (a), 80% (b) probability levels. Vertical lines indicate the occurrence times of significant earthquakes.

The time dependence of b_q and b_{GR} for the full and declustered catalogues is shown in Fig. 5.12. For the full catalogue both b_q and b_{GR} are very consistent and comparable, they vary between 0.53 and 1. A very important observation is that b -values decrease to 0.53 before the Tohoku earthquake, during the earthquake they increase abruptly to 1 and after 2012 they slowly decrease. As for the declustered catalogues b_q and b_{GR} are the same and vary around 0.8 ± 0.2 , but they are not affected by the Tohoku earthquake they merely behave quasi-linearly with a tendency to increase.

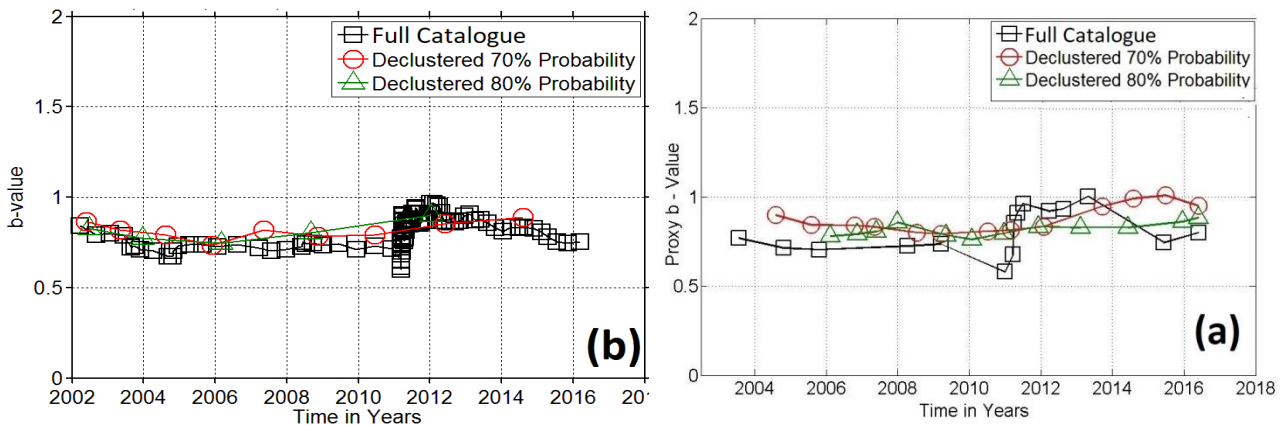


Figure 5.12: Time dependence of b -values for the full and declustered crustal catalogues of the Okhotsk plate. Panel (a) shows the time dependence of b_q ; panel (b) the time dependence of b_{GR} .

5.3 Pacific Plate.

The entropic indices variations with time for Pacific sub-crustal full earthquake catalogue are illustrated in Fig. 5.13. In general, correlation can be characterized as moderate, since the temporal index in most cases is above 1.3. There are, also cases where $q_T=2$ because of strong earthquakes. Another significant observation is that q_T increases without the evidence of strong earthquakes. That can be attributed to crustal seismicity that has affected the entire seismogenetic system. The magnitude entropic index q_M varies around 1.55 ± 0.08 and changes after the earthquakes of 2007 (M8.2) and 2011 (M7.5).

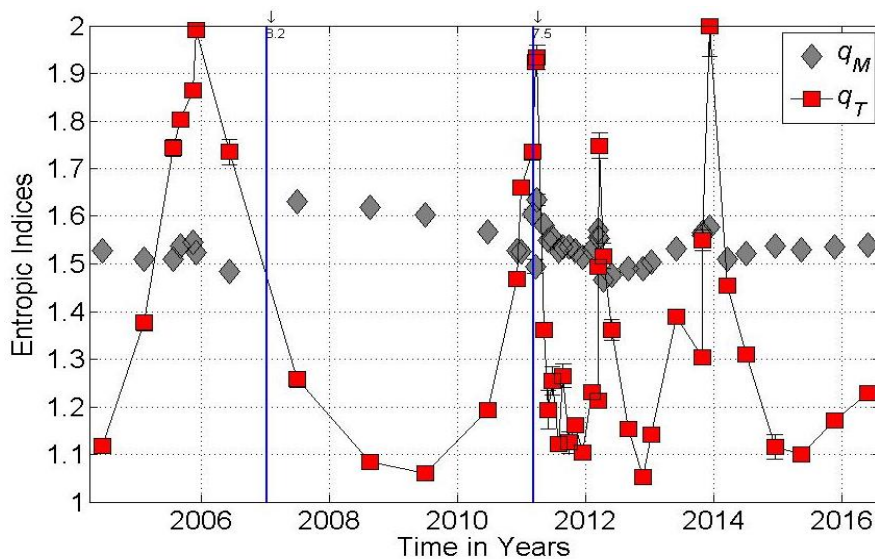


Figure 5.13: Time dependence of the entropic indices for the Pacific full sub-crustal catalogue. Vertical lines indicate the occurrence of major ($M \geq 7$) earthquakes.

Fig. 5.14 shows the variations of entropic indices with time for the declustered earthquake catalogues. Analysis for the $\varphi_j=90\%$ background probability wasn't possible due to deficiency of earthquake data. Correlation for both probabilities is random, with q_T varying in the interval (1, 1.2) for probability 70% and in the interval (1.1 and 1.2) for probability 80%. The magnitude index q_M is the same for both probabilities, it behaves quasi-linearly around 1.55 ± 0.05 .

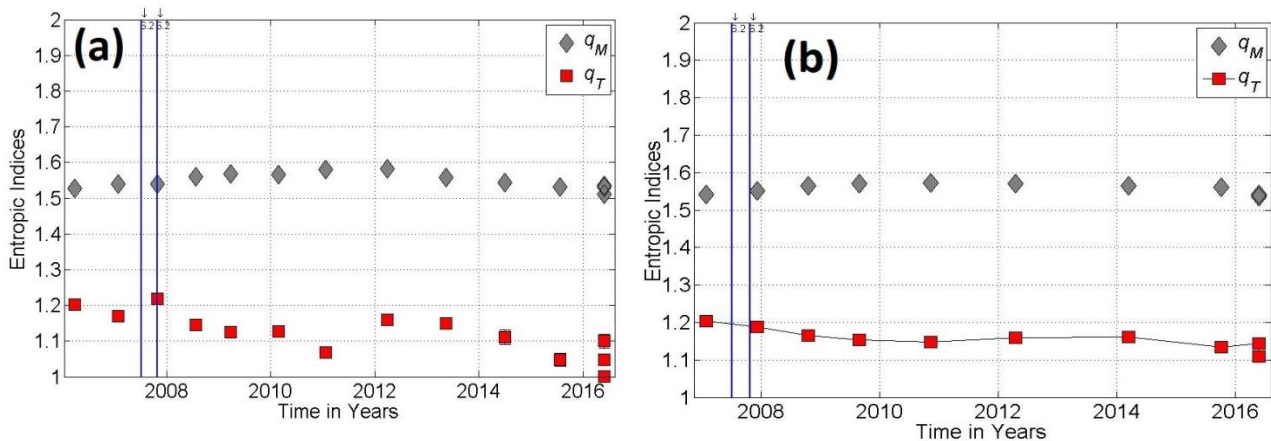


Figure 5.14: Time dependence of the entropic indices for the Pacific declustered sub-crustal catalogues at the 70% (a), 80% (b) probability levels. Vertical lines indicate the occurrence times of significant earthquakes.

The time dependence of b_q and b_{GR} for the full and declustered catalogues is shown in Fig. 5.15. For the full catalogue both b_q and b_{GR} are very consistent and comparable, they vary between 0.6 and 1.2. b -values increase during and after 2011 to 1.2 until the first half of 2012 and then they slowly decrease. As for the declustered catalogues b_q and b_{GR} are the same and vary around 0.8 ± 0.2 , but they are not affected by the earthquakes depicted in the previous panels.

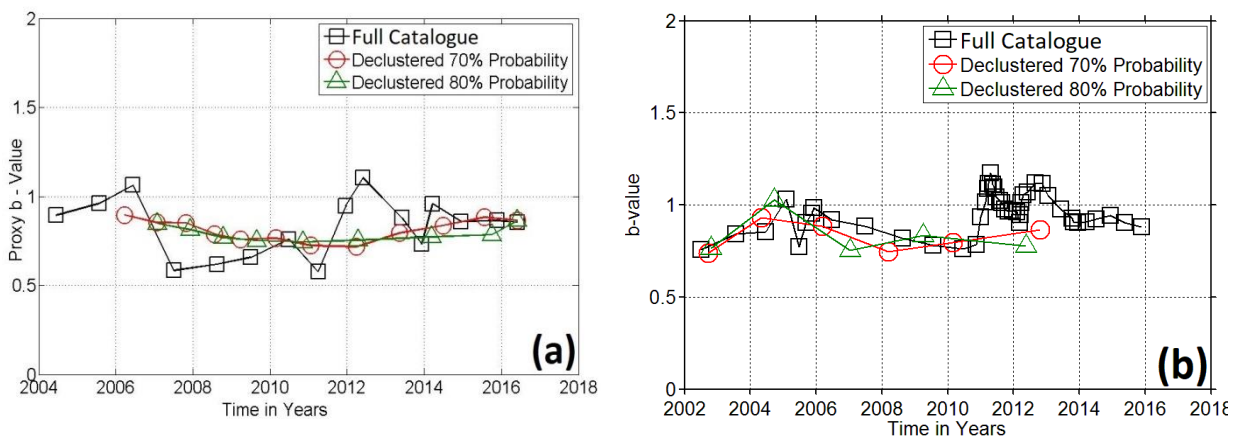


Figure 5.15: Time dependence of b -values for the full and declustered sub-crustal catalogues of the Pacific plate. Panel (a) shows the time dependence of b_q ; panel (b) the time dependence of b_{GR} .

As for the crustal catalogues the results are as followed (Fig. 5.16). The temporal index q_T in general varies between 1.2 and 1.6 and after an earthquake in 2011 ($M7$) it increases to 2.

Thereafter, correlation can be characterized as moderate and in some cases strong. The index q_M exhibits significant variations in the interval (1.48, 1.62) and after 2011 it drops below 1.5.

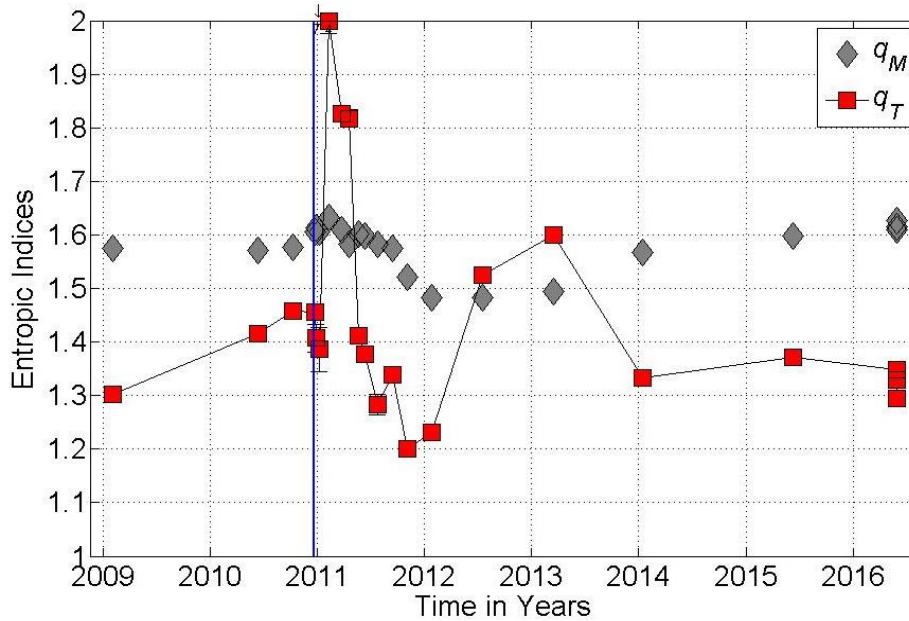


Figure 5.16: Time dependence of the entropic indices for the Pacific full crustal catalogue. Vertical lines indicate the occurrence of major ($M \geq 7$) earthquakes.

The time dependence of b_q and b_{GR} for the full and declustered catalogues is shown in Fig. 5.17. They exhibit the same variations with time between 0.51 and 1.01. From 2002 to 2010 they decrease and after 2011 until 2013 they increase abruptly. Then again they decrease until 2016.

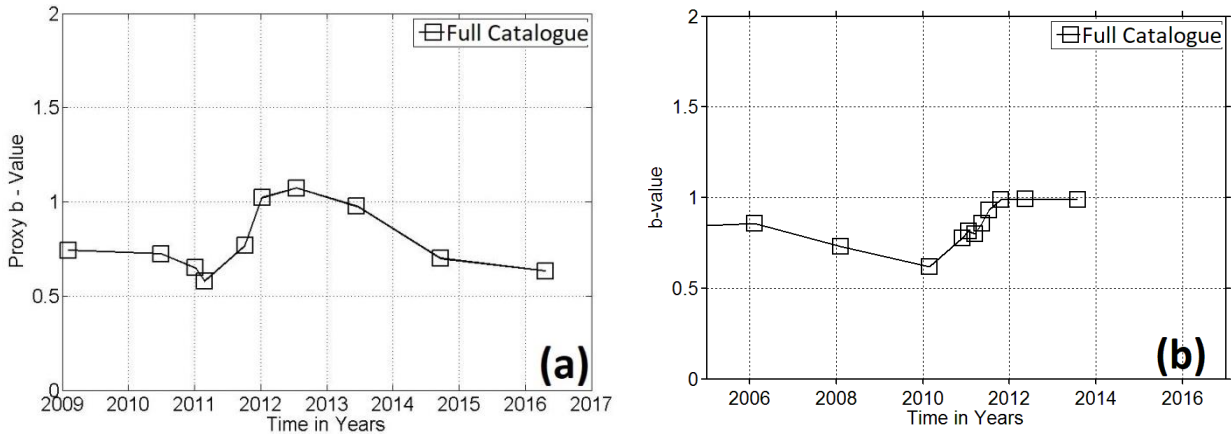


Figure 5.17: Time dependence of b -values for the full and declustered crustal catalogues of the Pacific plate. Panel (a) shows the time dependence of b_q ; panel (b) the time dependence of b_{GR} .

5.4 Philippine Plate.

The variations of the entropic indices in time of the sub-crustal full earthquake catalogue of Philippine plate are illustrated in Fig. 5.18. In general, the temporal index q_T lingers in the interval (1, 1.3) except three times between 2010-2011, that varies between 1.5 and 1.7. Correlation in general is characterized as weak and sometimes even random since it reaches unity many times. The index q_M fluctuates around 1.57 ± 0.04 .

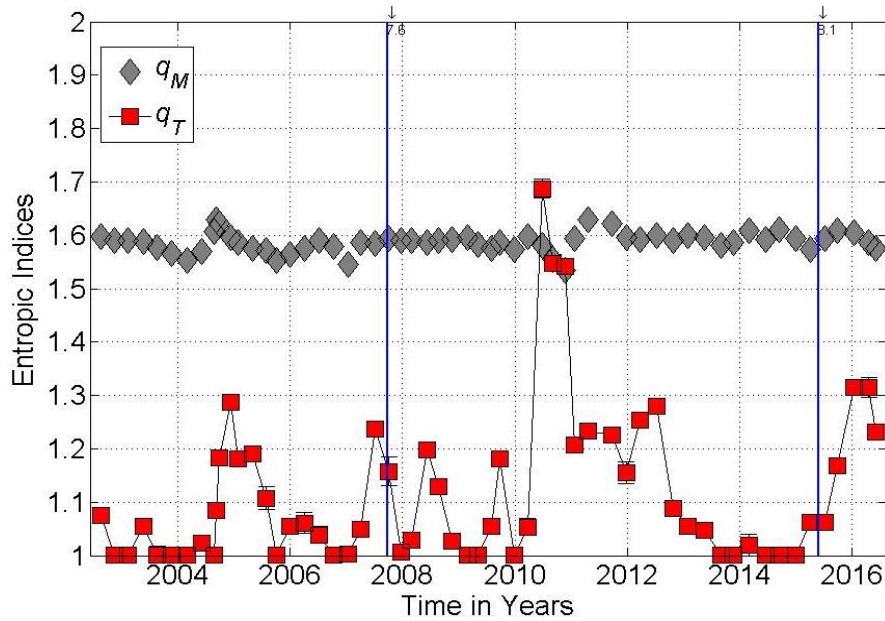


Figure 5.18: Time dependence of the entropic indices for the Philippine full sub-crustal catalogue. Vertical lines indicate the occurrence of major ($M \geq 7$) earthquakes.

The analysis of the declustered earthquake catalogues are depicted in Fig. 5.19 for the sub-crustal earthquakes of Philippine. For background probability $\varphi_j=70\%$ (Fig. 5.19a) correlation is random except 2011 where the entropic index increases above 1.3. After 2011 it drops again below 1.2 and increases after 2016. For background probability $\varphi_j=80\%$ (Fig. 5.19b) correlation is also random with the entropic index varying below 1.2. The imprint of the 2011 earthquake that affected seismogenesis is disappeared. For both probabilities the magnitude entropic index q_M fluctuates around 1.58 ± 0.04 .

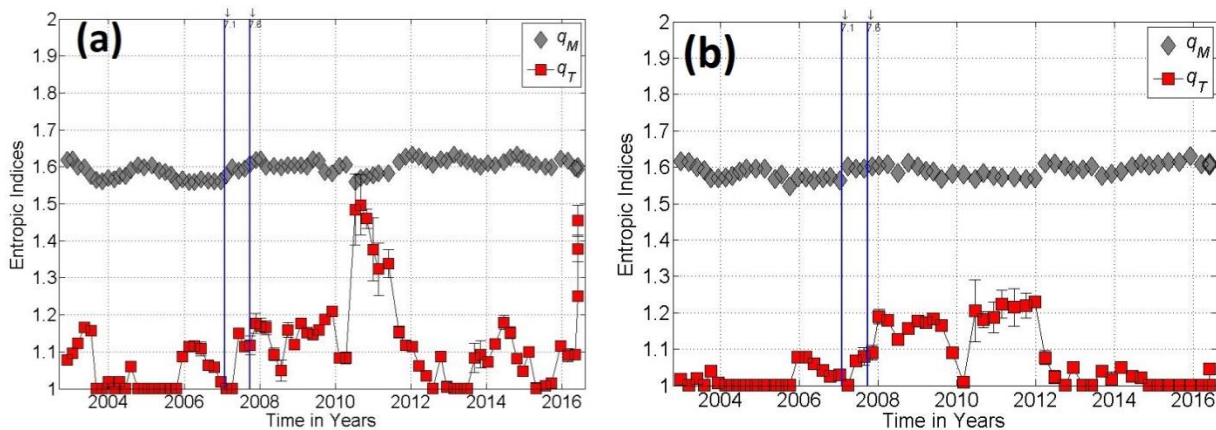


Figure 5.19: Time dependence of the entropic indices for the Philippine declustered sub-crustal catalogues at the 70% (a), 80% (b) probability levels. Vertical lines indicate the occurrence times of significant earthquakes.

The time dependence of b_q and b_{GR} for the full and declustered catalogues is shown in Fig. 5.20. They are extremely consistent between 0.54 and 0.82 and they don't exhibit any significant variations with time. As it turns out, the results of the declustered and full catalogues of Philippine plate indicate a Poissonian system consistently with the findings of Section 4.2.4.

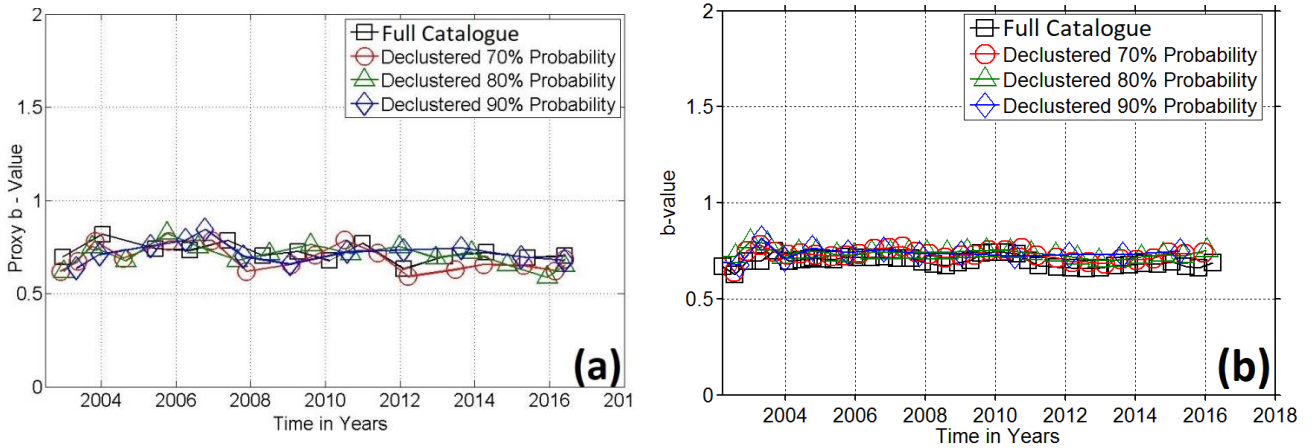


Figure 5.20: Time dependence of b -values for the full and declustered sub-crustal catalogues of the Philippine plate. Panel (a) shows the time dependence of b_q ; panel (b) the time dependence of b_{GR} .

The variations of the entropic indices in time for Philippine crustal full catalogue are depicted in Fig. 5.21. Correlation is weak and the temporal index q_T mostly varies between 1.1 and 1.3, with one exception after 2012 where it increases to 1.48, confirming the fact that seismogenesis of Philippine is Poissonian. The index q_M fluctuates around 1.6 ± 0.02 . Until 2011 it has a decreasing trend, and after 2012 it increases above 1.6.

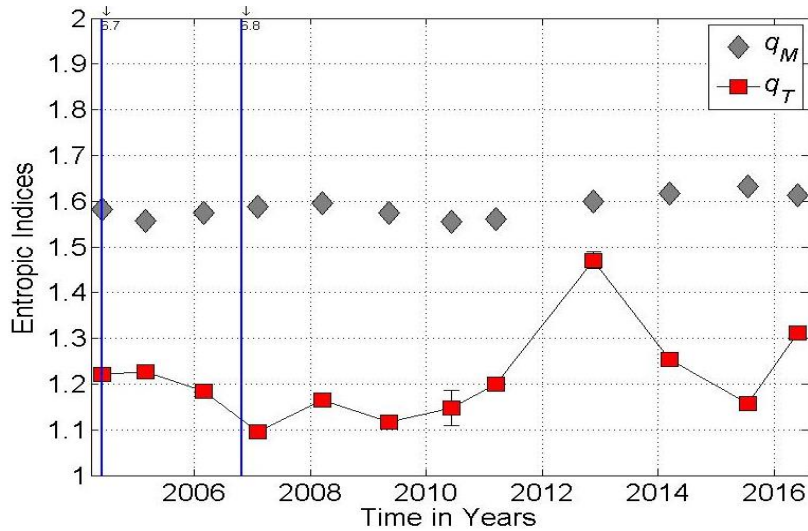


Figure 5.21: Time dependence of the entropic indices for the Philippine full crustal catalogue. Vertical lines indicate the occurrence of major ($M \geq 6$) earthquakes.

In Fig. 5.22 the variations of the entropic indices in time are depicted for $\phi_j = 70\%$. Correlation is random with q_T varying below 1.18. For the period 2008-2011 correlation is completely random with $q_T = 1$. After 2012 it increases and varies between 1.1 and 1.18. The magnitude entropic index q_M behaves linearly and lingers around 1.59 ± 0.02 .

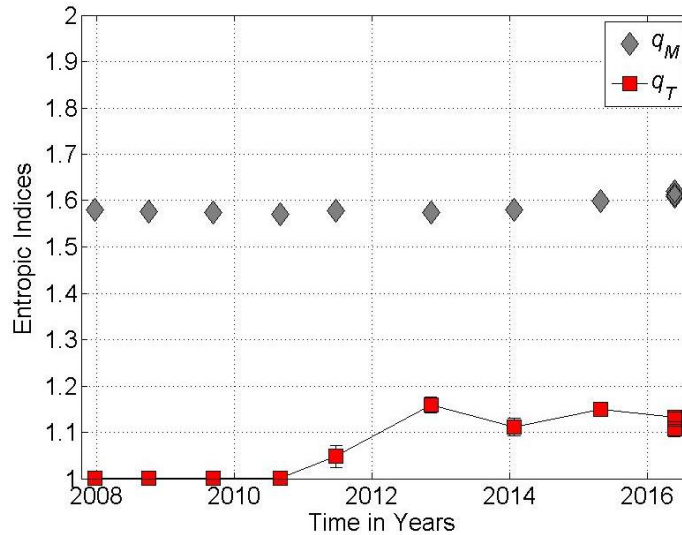


Figure 5.22: Entropic indices variations in time for Philippine’s sub-crustal declustered earthquake catalogue of 70% background probability.

The time dependence of b_q and b_{GR} for the full and declustered catalogues is shown in Fig. 5.23. Three observations can immediately be made: a) both b_q and b_{GR} are absolutely compatible. b) b -values obtained from the declustered catalogues are the same with those of full catalogues,. c) Both b_q and b_{GR} all indicate a low decrease in time.

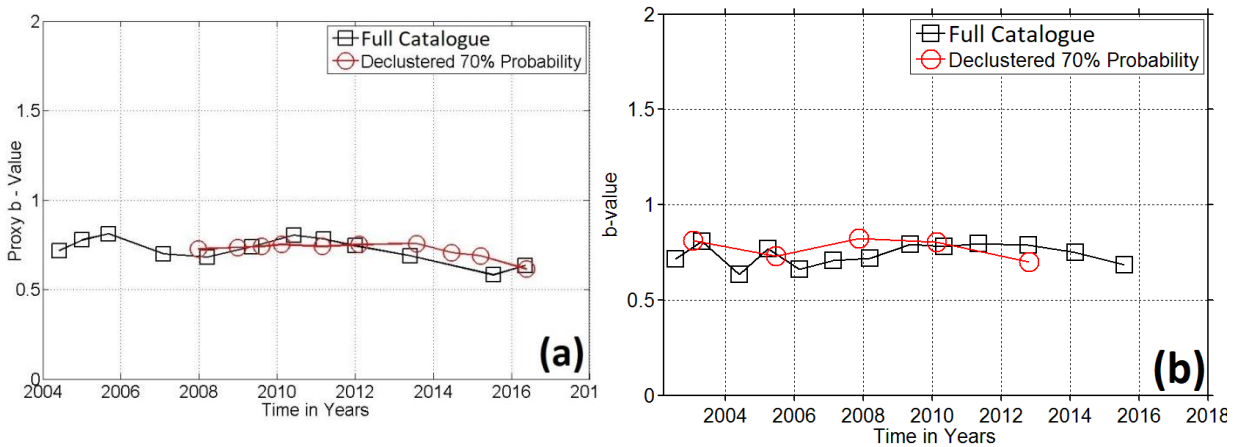


Figure 5.23: Time dependence of b -values for the full and declustered crustal catalogues of the Philippine plate. Panel (a) shows the time dependence of b_q ; panel (b) the time dependence of b_{GR} .

6 .DISCUSSION AND CONCLUSIONS

The objective of this thesis originates in a long-standing discourse between the two principal viewpoints developed by studying the statistical expression(s) of earthquake occurrence and quantifying the expectation of seismic activity. Seismicity comprises the superposition of a background process expressing the continuum of tectonic deformation, and a foreground process of prolific short-term activity associated with earthquake clusters or/and aftershock sequences. The first viewpoint proposes that background seismicity is generated by a self-excited conditional Poisson (point) process whose entropy is assumed to obey the Boltzmann-Gibbs formalism; background earthquakes are spontaneously and independently generated in the fault network and there is no interaction between faults, such that would influence their time and place of occurrence. The second viewpoint posits that background seismicity is generated by a non-equilibrating fault network (system) in which background events are dependent due to *correlation* (interactions) developing and evolving between nodes (faults) of the network, which may extend over long spatiotemporal distances and influence their time and place of occurrence. Correlation effectively confers memory to the fault system and is evident in the form of power laws in the temporal and spatial statistics of earthquake occurrence (seismicity). Both Poisson and Complex/Critical viewpoints, albeit from different perspectives, consider aftershock sequences to comprise dependent events.

This thesis attempts to explore the statistical nature of seismicity by: a) using the generalized formalism of Non Extensive Statistical Physics, (described in Chapters 1.3 and 2), as a universal context for the statistical description of earthquake occurrence, and b) trying to detect and verify the existence and degree of correlation in active fault networks or, equivalently, the level of non-equilibrium. The results of this exercise are reported in Chapters 4 and 5. The existence of correlation is assessed by evaluating the entropic index q appearing in the q -exponential distribution predicted by NESP for the dynamic parameters of non-equilibrating systems; q is bounded as $0 \leq q \leq 2$, with $q = 1$ corresponding to the pure exponential distribution expected for Poissonian processes and $q > 1$ indicating Complexity/Criticality in non-conservative systems. The main focus is placed on the evaluation of two entropic indices: one labelled q_M and associated with the distribution of earthquake magnitudes, which conveys information about the size and space distribution of fault activity and is genetically related to the *b-value* of the Gutenberg-Richter law, and one labelled q_T and associated with the distribution of the lapse between consecutive events (interevent time), which indicates the extent of interaction between faults in a network.

The entropic indices are computed by modelling bivariate empirical distributions of earthquake frequency vs. magnitude *and* interevent time (F-M-T for short) and express the joint probability of observing earthquakes larger than a given magnitude after a given lapse time; details are given in Chapter 2, Sections 2.2 and 2.3. The rigour of the experimental procedure is evaluated, not only by computing 95% confidence limits, but also by evaluating the NESP generalization of the well-known *b*-value, which is related to the entropic index q_M as $b_q = (2 - q_M)(q_M - 1)^{-1}$ – see Chapter 2 for details. It is evident that b_q should be equivalent to the *b* value computed on the basis of the univariate frequency-magnitude distribution of Gutenberg and Richter, labelled b_{GR} . The equivalence arises from the fact that the distribution of magnitudes does not relate the energies released by consecutive events, but only conveys information about the hierarchy and spatial characteristics of the active fault system. Thus, in

all cases b_q should be equivalent to b_{GR} and their comparability should be a strong, albeit indirect means of ensuring the validity of the estimation procedure used in estimating q_M and q_T . The results of this exercise are reported in Chapters 4.3 and 5 and generally *demonstrate* the rigour of the estimation procedure.

The thesis focuses on the analysis of seismogenetic systems along the NW Pacific Rim, which comprises four major convergent plate margins. The Pacific and Philippine oceanic plates subduct beneath the continental plates of Okhotsk (North America) and Eurasian plates. Details about the geodynamics and seismicity of the NW Pacific Rim are provided in Chapter 3. It is important to note that *crustal* and *sub-crustal* earthquakes are separately examined by approximately distinguishing them according to the depth of the Mohorovičić discontinuity (see Chapter 2.4), so as to inquire whether environmental (e.g. temperature, pressure) or/and boundary conditions affect the dynamics of a fault network. The analysis is applied to homogeneous and complete earthquake catalogues in which aftershocks sequences are included (full catalogues) or have been removed (declustered catalogues). If background seismicity is Poissonian, the removal of aftershocks should reduce the earthquake catalogue to an uncorrelated set of events; if it does not, Complexity/Criticality is evident. Herein, the efficient stochastic declustering method of Zhuang et al (2002) has been implemented and details are provided in Chapters 2.5, 3.3.1 and 4.2.

To begin the discussion of the results, one might suggest that they comprise an “expected” and an “interesting” parts. The “expected” part is the behaviour of the magnitude entropic index q_M , which after conversion to b_q turns out to be consistent with expectation from the Gutenberg–Richter Law (Chapter 4.3). Naturally, q_M exhibits differences between seismogenetic systems as well as between full and declustered catalogues, (Chapter 4.1 and 4.2; Tables 7.1 – 7.4), generally exhibiting lower values in the former vs. higher in the latter and thus pointing to a higher level of organization and increased localization in background faulting activity. At any rate, in the general context of NESP, the Gutenberg-Richter law can be almost naturally derived from the q -exponential distribution (Chapter 1.3.3). Thus, a most significant outcome of q_M analysis is that active fault networks can be classified as *sub-extensive* with a high degree of self-organization.

Results from the analysis of the *full crustal and sub-crustal catalogues* (including b_q) are summarized in Table 7.1, in the form of mean values $\bar{q}_T(M)$, $\bar{q}_M(M)$, together with their respective standard deviations $\sigma(q_T)$, $\sigma(q_M)$. Since there is little question as to whether frequency-magnitude distributions (i.e. the time-honoured of Gutenberg and Richter) emerge from non-extensive fault networks, the remaining discussion will be more biased towards the analysis of the temporal entropic index q_T . The pie charts of Fig. 7 comprise a compact presentation and colour-coded classification of all $q_T(M)$ functions obtained in Chapter 4.1 and summarized in Table 7.1, providing a succinct picture of the existence, extent and relative strength of correlation in the seismogenetic systems studied herein. In the classification scheme, all values of $q_T < 1.2$ are shown in red and are considered to indicate insignificant correlation and are taken to demonstrate *randomness*. Values higher than 1.2 are generally taken to indicate statistically significant correlation rated as “*random*” (red, $1 \leq q_T \leq 1.2$), “*weak*” (red, $1.2 < q_T < 1.3$), “*moderate*” (green, $1.3 \leq q_T < 1.4$), “*strong*” (dark green, $1.4 \leq q_T \leq 1.5$), and “*very strong*” (blue, $1.5 \leq q_T$). The pie chart of Fig. 7.1a summarizes the proportions of q_T classes

determined from the *full sub-crustal* catalogues; the pie chart of Fig. 17b is as per Fig. 17a but for the *full crustal* catalogues.

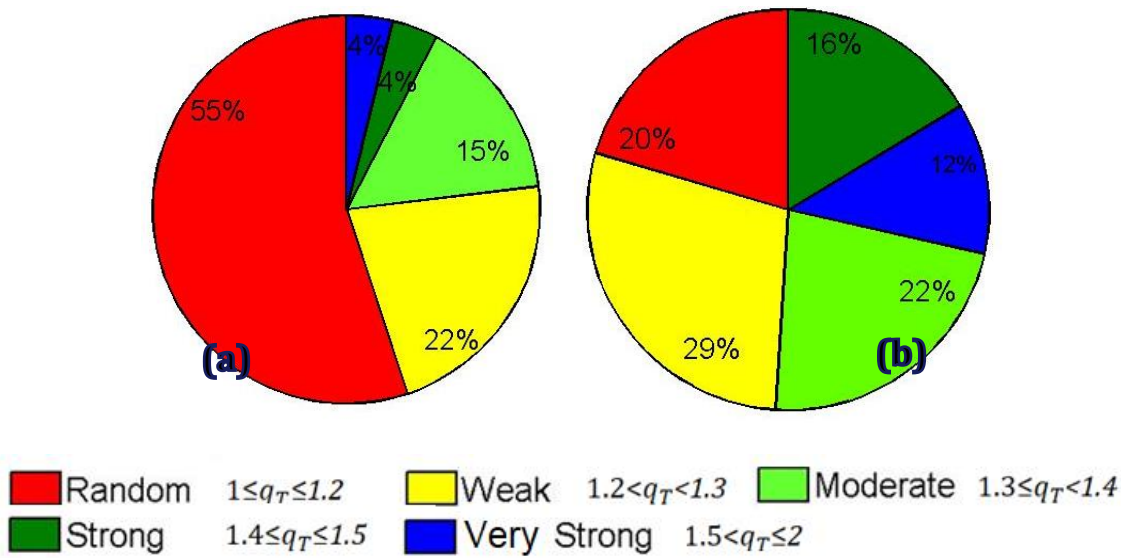


Figure 7.1: Percentage of q_T values obtained from the analysis of (a) all sub-crustal, and (b) all crustal earthquake catalogues.

Table 7.1: Summary of the variation of the magnitude (q_M) and temporal (q_T) entropic indices with respect to cut-off magnitude for all *full* sub-crustal and crustal catalogues considered herein.

Seismic Catalogue	N^a Events ($M \geq 3$)	$q_T(M)$ Range	$\bar{q}_T(M)$	$\sigma(q_T)$	$q_M(M)$ Range	$\bar{q}_M(M)$	$\sigma(q_M)$	$b_q(M)$ Range
Eurasia Plate								
<i>Sub-crustal</i>	10,855	1.0-1.22	1.13	0.056	1.51-1.54	1.53	0.007	0.85-0.93
<i>Crustal</i>	9,595	1.15-1.41	1.28	0.084	1.52-1.57	1.55	0.019	0.73-0.91
Okhotsk Plate								
<i>Sub-crustal</i>	38,333	1.16-1.35	1.23	0.055	1.49-1.53	1.51	0.009	0.88-1.02
<i>Crustal</i>	19,412	1.32-2.00	1.513	0.217	1.52-1.61	1.54	0.025	0.63-0.90
Pacific Plate								
<i>Sub-crustal</i>	9,101	1.23-1.79	1.54	0.025	1.53-1.61	1.57	0.026	0.63-0.86
<i>Crustal</i>	2,004	1.32-1.59	1.49	0.109	1.59-1.63	1.62	0.013	0.58-0.67
Philippine Plate								
<i>Sub-crustal</i>	12,036	1.00-1.18	1.08	0.044	1.52-1.56	1.53	0.009	0.78-0.90
<i>Crustal</i>	2,608	1.11-1.27	1.19	0.041	1.51-1.56	1.54	0.014	0.77-0.92

A first significant observation to make in both Table 7.1 and Fig. 7.1 is that, correlation, as manifested by the temporal entropic index, overall higher in crustal seismicity (Fig. 7.1b), than in sub-crustal (Fig. 7.1a). It is also evident that the characteristic of correlation differ between plates. For example, the Pacific and Okhotsk plates exhibit significant to strong correlation in both crustal and sub-crustal seismicity. However, the seismicity of these plates treated herein, includes the 2011 M9 Tohoku mega-earthquake whose lengthy (>2 years) and spatially extended aftershock sequence is expected to significantly influence the estimation of q_T . As a consequence, it was considered necessary to divide the Okhotsk plate catalogue into a pre- and

a post-Tohoku earthquake parts. The analysis of the two subset catalogues shows that prior to the earthquake, the temporal entropic index was significant and increasing with magnitude (long-range correlation), but after the earthquake it jumped to values in excess of 1.6 indicating very strong correlation in the aftershock sequence. On the other hand, the fault network of the Eurasian Plate is definitely less correlated and might be Poissonian of nature. For the Eurasian plate, the $\bar{q}_T(M)$ of sub-crustal events is 1.13 whilst for crustal events, it is 1.28. Finally, the earthquake activity in the Philippine Plate, is likely Poissonian of nature, inasmuch the mean $\bar{q}_T(M)$ is only 1.08 for the sub-crustal process and as low as 1.19 for the crustal.

As explained in Chapter 2.2, a direct method of evaluating the existence of long range correlation is to analyse bivariate F-M-T distributions constructed by grouping (binning) earthquakes in a catalogue according to interevent distance. The results of this analysis are summarized in Table 7.2. It must be emphasized that for Pacific and Philippine plates catalogues, the *crustal* earthquake subsets did not contain a population of events sufficient as to perform statistically rigorous analysis.

Table 7.2: Summary of the variation of the magnitude (q_M) and temporal (q_T) entropic indices with respect to interevent distance for all full sub-crustal and crustal catalogues considered herein.

Catalogue	N ^o Events	q_T Range			\bar{q}_T	$\sigma(q_T)$	q_M Range	\bar{q}_M	$\sigma(q_M)$	b_q Range
		$\Delta d \leq 100$	$100 < \Delta d \leq 500$	$\Delta d > 500$						
Eurasia Plate										
<i>Sub-crustal</i>	10,855	1.95	1.00-1.11	1-1.16	1.47	0.671	1.52-1.55	1.54	0.011	0.80-0.90
<i>Crustal</i>	9,595	1.78	1.16-1.18	1.06-1.21	1.42	0.509	1.48-1.54	1.51	0.023	0.83-1.05
Okhotsk Plate										
Cut-off Magnitude = 3										
<i>Sub-crustal</i>	38,333	1.22	1.20-1.25	1.02-1.15	1.13	0.162	1.54-1.61	1.56	0.022	0.61-0.82
<i>Crustal</i>	19,412	1.46	1.37-1.80	1.18-1.50	1.49	0.438	1.55-1.59	1.58	0.012	0.68-0.79
Cut-off Magnitude = 4										
<i>Sub-crustal</i>	38,333	1.44	1.04-1.65	1.03-1.14	1.34	0.438	1.50-1.57	1.54	0.024	0.73-0.97
<i>Crustal</i>	19,412	1.22	1.75-1.81	---	1.51	0.417	1.53-1.58	1.56	0.024	0.71-0.85
Pacific Plate										
<i>Sub-crustal</i>	9,101	1.64	1.61-1.84	---	1.72	0.162	1.53-1.58	1.56	0.021	0.71-0.85
Philippine Plate										
<i>Sub-crustal</i>	12,036	1.2	1-1.1	1.01-1.12	1.1	0.141	1.57-1.61	1.58	0.014	0.62-0.75

In general, for all catalogues, correlation is strong for earthquakes up to 100 km due to the overwhelming effect of near-field aftershock sequences. Beyond that range, Okhotsk and Pacific earthquakes are strongly or very strongly correlated over interevent distances of at least 500km and, in some cases, longer. For the seismicity of the Okhotsk plate in particular, and because earthquake populations proved to be sufficient, the analysis was carried out for two cut-off magnitudes, $M=3$ and $M=4$. In both cases, correlation was shown to be significant for

interevent distances of at least 500 km and that correlation in crustal seismicity is considerably stronger than correlation in sub-crustal seismicity. Conversely, in the sub-crustal seismicity of the Eurasia and Philippine plates and for $\Delta d > 100$ km, $q_T(\Delta d)$ decreases below 1.2 and, in most cases, stays below 1.1, indicating absence of correlation at intermediate and long interevent distances

Results from the analysis of the *declustered* crustal and sub-crustal catalogues (including b_q) are summarized in Table 7.2, in the form of mean values $\bar{q}_T(M)$, $\bar{q}_M(M)$, together with their respective standard deviations $\sigma(q_T)$, $\sigma(q_M)$. Furthermore, results from the analysis of q_T for the *declustered* catalogues are again compactly presented in the form of pie charts using the same classification and colour-coding scheme employed in Fig. 7.1. As a general observation, declustering appears to have eliminated all correlation at the 70% probability level (Fig. 7.2a and 7.3a). Nevertheless, this may be a statistical fluke of undeterminable origin since at the 80% probability level correlation appears to increase and at the 90% level to increase even more, indicating that the core of the seismogenetic processes in all plates is likely non-Poissonian. Moreover, at the 90% probability level the background process appears to be statistically comparable both in the crust and in the Wadati-Benioff zones of the NW Pacific Rim.

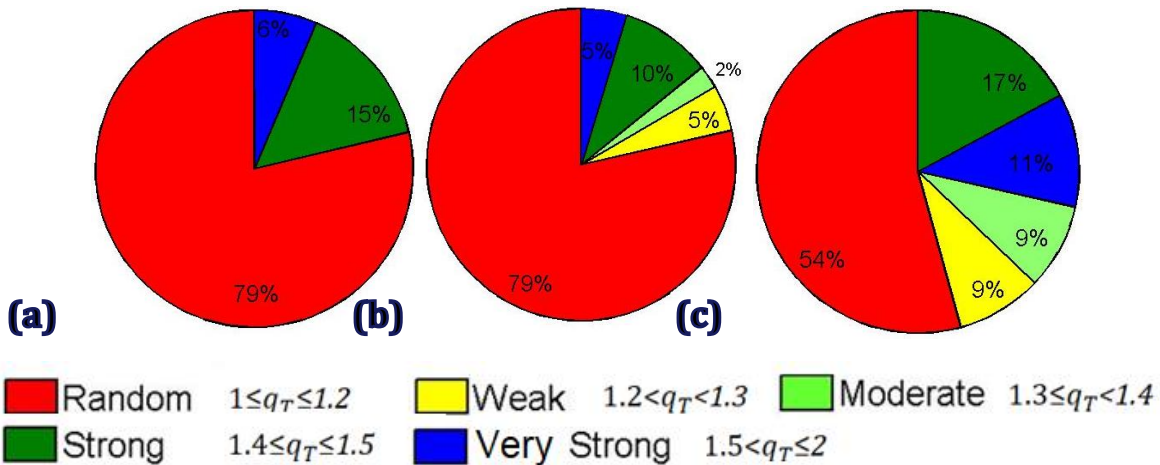


Figure 7.2: Percentage of q_T obtained from the analysis of all *declustered sub-crustal* earthquake catalogues and for probability levels (a) 70%, (b) 80% and (c) 90%.

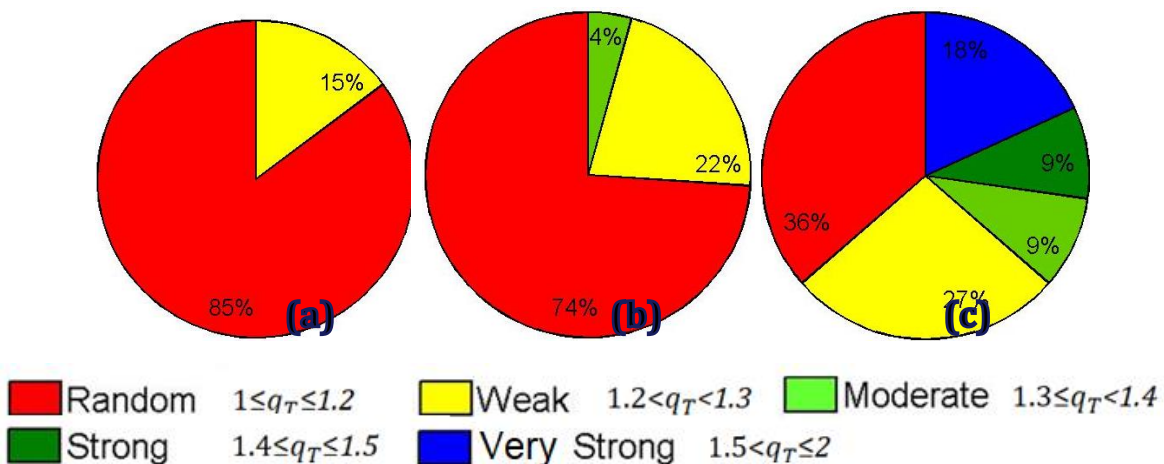


Figure 7.3: Percentage of q_T obtained from the analysis of all *declustered crustal* earthquake catalogues and for probability levels (a) 70%, (b) 80% and (c) 90%.

The seismicity of the Eurasian plate (both crustal and sub-crustal) turns out to be practically Poissonian with respect to time: the temporal entropic index rests below 1.2 for all background probability levels. In the case of Okhotsk, the declustered catalogues yield results that are not fully consistent with those of the full catalogue. Specifically, correlation appears to be strong in declustered sub-crustal seismicity ($\bar{q}_T > 1.5$ throughout). For the 70% background probability the declustered *crustal* catalogues would appear to be practically Poissonian ($\bar{q}_T = 1.15$) but correlation rises by little at the 80% level ($\bar{q}_T = 1.26$) and by far in the 90% probability level $\bar{q}_T = 1.57$. It is important to mention that after declustering, the crustal catalogues contain fewer earthquakes than the sub-crustal... In general terms, correlation appears to be low in the magnitude scales Analysis is conducted for magnitudes $M=3-3.8$ and rises significantly thereafter.

Table 7.3: Summary of the variation of the magnitude (q_M) and temporal (q_T) entropic indices with respect to cut-off magnitude for all *declustered* sub-crustal and crustal catalogues considered herein.

Catalogue	N ^a Events	q_T Range	\bar{q}_T	$\sigma(q_T)$	q_M Range	\bar{q}_M	$\sigma(q_M)$	b_q Range
Eurasia Plate								
φ_j 70%								
<i>Sub-crustal</i>	6860	1.00-1.13	1.05	0.043	1.47-1.50	1.49	0.005	0.99-1.08
<i>Crustal</i>	2855	1.03-1.20	1.12	0.055	1.44-1.48	1.47	0.013	1.06-1.26
φ_j 80%								
<i>Sub-crustal</i>	5650	1.02-1.11	1.10	0.029	1.46-1.49	1.49	0.008	1.0-1.13
<i>Crustal</i>	2385	1.05-1.16	1.11	0.041	1.43-1.47	1.46	0.011	1.12-1.27
φ_j 90%								
<i>Sub-crustal</i>	3090	1.02-1.3	1.16	0.093	1.48-1.51	1.50	0.007	0.95-1.03
<i>Crustal</i>	1425	1.09-1.29	1.17	0.080	1.47-1.48	1.48	0.004	1.05-1.07
Okhotsk Plate								
φ_j 70%								
<i>Sub-crustal</i>	7552	1.40-1.62	1.50	0.08	1.46-1.55	1.49	0.026	0.79-1.05
<i>Crustal</i>	1863	1.03-1.23	1.15	0.061	1.47-1.51	1.49	0.009	0.94-1.08
φ_j 80%								
<i>Sub-crustal</i>	4809	1.42-1.61	1.53	0.064	1.38-1.56	1.48	0.060	0.77-1.5
<i>Crustal</i>	1066	1.18-1.33	1.26	0.047	1.50-1.52	1.51	0.010	0.89-0.99
φ_j 90%								
<i>Sub-crustal</i>	1727	1.52-1.65	1.58	0.049	1.45-1.52	1.48	0.034	0.9-1.21
<i>Crustal</i>	529	1.48-1.69	1.57	0.108	1.55-1.58	1.58	0.124	0.71-0.77
Pacific Plate								
φ_j 70%								
<i>Sub-crustal</i>	1369	1.07-1.19	1.14	0.042	1.50-1.54	1.52	0.013	0.84-0.97
φ_j 80%								
<i>Sub-crustal</i>	1098	1.16-1.32	1.21	0.056	1.51-1.54	1.53	0.013	0.82-0.95
φ_j 90%								
<i>Sub-crustal</i>	697	1.37-1.44	1.41	0.030	1.51-1.53	1.53	0.012	0.86-0.95
Philippine Plate								
φ_j 70%								
<i>Sub-crustal</i>	6702	1-1.13	1.05	0.042	1.49-1.56	1.52	0.022	0.78-1.03
<i>Crustal</i>	1126	1-1.09	1.05	0.032	1.50-1.57	1.55	0.021	0.74-0.96

φ_j 80%								
<i>Sub-crustal</i>	5218	1.01-1.15	1.07	0.043	1.49-1.57	1.53	0.023	0.75-1.0
<i>Crustal</i>	865	1-1.1	1.06	0.035	1.53-1.56	1.55	0.014	0.76-0.88
φ_j 90%								
<i>Sub-crustal</i>	2642	1.12-1.31	1.17	0.072	1.53-1.56	1.55	0.012	0.75-0.88
<i>Crustal</i>	447	1.26-1.31	1.29	0.027	1.55-1.57	1.56	0.010	0.74-0.81

In the case of the Pacific plate, correlation in sub-crustal seismicity is rather low at the 70% level ($\bar{q}_T = 1.14$), rises at the 80% level ($\bar{q}_T = 1.21$) and becomes significant at the 90% level ($\bar{q}_T = 1.41$); the overall state is difficult to characterize but taken at face value, it would appear that the background process, which is expectedly best represented at the 90% probability level, is non-Poissonian. Finally, in the case of the Philippine plate, all declustered catalogues yield ($\bar{q}_T \leq 1.17$) with the sole exception of the 90% *crustal* catalogue for which $\bar{q}_T = 1.29$, which even at the 3σ confidence level indicates a weakly correlated process. The Philippine plate does not allow for confident inferences and if the background process is correlated, it is only marginally so.

The results of the direct method employed in the detection of long-range correlation, namely the analysis of F-M-T distributions constructed by grouping (binning) earthquakes according to interevent distance, are summarized in Table 7.4. Notably, *only* the sub-crustal declustered catalogues contained earthquake populations sufficient to conduct this type of analysis with adequate spatial resolution! It is straightforward to see that at the 70% and 80% probability levels the sub-crustal Eurasia and Philippine plates seismicity is assessed to be Poissonian over all interevent distances and to all intents and purposes, consistently with the findings of hitherto analysis. Unfortunately, results could not be obtained at the 90% level. Conversely, the sub-crustal Okhotsk seismicity turns out significantly to strongly correlated over all resolvable distances at the 70% and 80% levels, as also expected from hitherto analysis.

Table 7.4: Summary of the variation of the magnitude (q_M) and temporal (q_T) entropic indices with respect to interevent distance for all declustered sub-crustal and crustal catalogues considered herein.

Catalogue	№ Events	$q_T(\Delta d)$ Range		\bar{q}_T	$\sigma(q_T)$	$q_M(\Delta d)$ Range	\bar{q}_M	$\sigma(q_M)$	$b_q(\Delta d)$ Range
		$\Delta d \leq 500$ km	$\Delta d > 500$ km						
Eurasia Plate									
$\varphi_j = 70\%$									
<i>Sub-crustal</i>	6860	1.00-1.11	1.00-1.13	1.06	0.091	1.49-1.53	1.52	0.020	0.85-1.04
$\varphi_j = 80\%$									
<i>Sub-crustal</i>	5650	1.05-1.11	1.02-1.03	1.06	0.063	1.48-1.55	1.52	0.020	0.81-1.05
Okhotsk Plate									
$\varphi_j = 70\%$									
<i>Sub-crustal</i>	7552	1.26-1.48	1.46-1.65	1.44	0.138	1.54-1.59	1.57	0.035	0.69-0.96
$\varphi_j = 80\%$									
<i>Sub-crustal</i>	4809	1.35-1.58	1.65	1.49	0.122	1.57-1.58	1.58	0.004	0.72-0.75
Philippine Plate									

$\varphi_j = 70\%$									
Sub-crustal	6702	1.06-1.34	---	1.19	0.12	1.56-1.57	1.57	0.004	0.74-0.78
$\varphi_j = 80\%$									
Sub-crustal	5218	1.09-1.19	1.00-1.24	1.13	0.078	1.53-1.60	1.58	0.022	0.65-0.87

As a general result, it is safe to say that seismogenesis in the NW Circum-Pacific belt (rim) is complex and its catalogue has its own characteristics. Eurasia and Philippine plates exhibit randomness, while Okhotsk and Pacific plates show high correlation. The declustered earthquake catalogues exhibit the same results for each tectonic plate. From the analysis of dependence on different cut-off magnitudes not only measures the correlation between earthquakes, but a statistical b -value (proxy- b value) was estimated.

The results presented above have been obtained through a physics-based approach (NESP) and *not* through any type of model-based (or model-driven) consideration, as usually is the case in earthquake statistical studies. They provide evidence that background seismicity in the seismogenetic systems of the NW Pacific Rim is complex sub-extensive of nature, although it exhibits significant differences between systems (plates): Correlation, i.e. complexity, is certainly pronounced in the Okhotsk and Pacific plates and definitely less evident in the Eurasia and Philippine plates where the system appears to verge on randomness. In the Okhotsk and Pacific plates background seismicity exhibits strong long-range interaction as evident by the overall high correlation observed in highly declustered catalogues (80% and 90% probability level) and, primarily, in the correlation observed in earthquakes separated by long interevent distances. The increase of correlation after declustering can be neatly explained by the exposition of long(er) range interactions after curtailing the effect of short-range interactions associated with aftershock sequences. It is also highly probable –but will not be investigated herein– that the elevated complexity (sub-extensivity) of the Okhotsk and Pacific seismicity is closely related to the 2011 M9 Tohoku mega-earthquake whose preparation phase and aftermath has organized the seismogenetic systems over long ranges.

In a final comment power-laws and long-range interaction are characteristic of self-organization and criticality. Although this may be a likely explanation of the complexity observed in the background seismicity of Okhotsk and Pacific plates, the question is still very far from having been answered. As comprehensively discussed by Sornette and Werner (2009), complexity may not only emerge from inherent non-linear dynamics of the active fault system as required by Criticality: their model-driven analysis suggests that quenched heterogeneity in the stress field and production rates may also be of great importance. It is also noteworthy that using the non-critical Coherent Noise Model, Celikoglu et al. (2010) showed that it is possible to obtain q -exponential distributions of interevent times when extended external stresses act simultaneously and coherently on all the elements of a fault system, although their simulation was incomplete in the sense that it did not include some spatial (geometric) configuration of interacting faults and could not assess the differences with an actual fault network. It is therefore clear that additional work is required before a complexity mechanism of the background seismicity can be proposed with confidence.

BIBLIOGRAPHY

- Abe S., Okamoto Y., (Eds.) (2001). "Nonextensive Statistical Mechanics and Its Applications", Springer, Heidelberg, 2001.
- Abe, K., (1981). "Magnitudes of large shallow earthquakes from 1904 to 1980", *Phys. Earth Planet. Intr.* 27, 72-92.
- Abe, S., Suzuki, N., (2003) "Itineration of the Internet over Nonequilibrium Stationary States in Tsallis Statistics". *Phys. Rev. E* 67 (2003) 016106
- Antonopoulos C.G., Michas G., Vallianatos F. and Bountis T., 2014. Evidence of q-exponential statistics in Greek seismicity. *Physica A: Statistical Mechanics and its Applications*, 409, 71-77; doi: 10.1016/j.physa.2014.04.042
- Amitrano, D. (2003). "Brittle-ductile transition and associated seismicity: Experimental and numerical studies and relationship with the b value", *J. Geophys. Res.*, 108(B1), 2044, doi:10.1029/2001JB000680.
- Bak P., Tang C., & Weisenfeld K., (1988). "Self - organized criticality", *Phys. Rev. A* 38, 364 - 374.
- Bak, P., (1996). "How Nature Works", Springer-Verlag, New York.
- Bak, P., Christensen, K., Danon, L. and Scanlon, T., 2002. Unified scaling law for earthquakes, *Phys. Rev. Lett.*, 88, 178501; doi:10.1103/PhysRevLett.88.178501.
- Bakar, B. and Tirnakli, U., 2009. Analysis of self-organized criticality in Ehrenfest's dog-flea model, *Phys. Rev. E*, 79, 040103; doi:10.1103/PhysRevE.79.040103.
- Batak R. C and Kantz H., 2014. Observing spatio-temporal clustering and separation using interevent distributions of regional earthquakes, *Nonlin. Processes Geophys.*, 21, 735-744; doi:10.5194/npg-21-735-2014.
- Barnes G. L., (2008). "The making of the Japan Sea and the Japanese mountains: understanding Japan's volcanism in structural context". *Japan Review* 20: 3-52.
- Barton, D., G. Foulger, J. Henderson, and B. Julian (1999). "Frequency- magnitude statistics and spatial correlation dimensions of earthquakes at Long Valley caldera, California" , *Geophys. J. Int.*, 138, 563-570.
- Benoit Mandelbrot (1967). "How Long Is the Coast of Britain? Statistical Self-Similarity and Fractional Dimension", *Science, New Series*, Vol. 156, No. 3775.
- Benoit Mandelbrot., (1983). "The Fractal Geometry of Nature"
- Burridge R., and Knopoff L., (1967). "Model and Theoretical Seismology" *Seismological Society of America*, Vol. 57 No.3 p.341 - 371.
- Carbone, V., Sorriso -Valvo, L., Harabaglia, P., Guerra, I., (2005). "Unified scaling law for waiting times between seismic events", *Europhys. Lett.*, 71 (6), p. 1036 (2005) doi: 10.1209/epl/i2005-10185-0
- Carnap R., (1977). "Two Essays on Entropy". University of California Press, Berkeley, California.

- Carter, J. A., and E. Berg,(1981). "Relative stress variations as determined by b-values from earthquakes in Circum-Pacific subduction zones",*Tectonophysics*, 76, 257–271.
- Caruso F., Tsallis C., (2008). "Nonadditive entropy reconciles the area law in quantum systems with classical thermodynamics". *Phys. Rev. E* 78,021102
- Chen Yanguang., (2011). "Modeling Fractal Structure of City - Size Distributions Using Correlation Functions"
- Chou H.C., Juo B.Y., Chiao L.Y., Zhao D.,and Hung S. H., (2009). "Tomography of the Western Ryukyu subduction zone and serpentinization of the fore - arc mantle". *Journal of Geophysical Research: Solid Earth* · December 2009, DOI: 10.1029/2008JB006192
- Culling W. E. H., (1960). "Analytical Theory of Erosion", *The Journal of Geology*, Vol. 68, No. 3 (May, 1960), pp. 336 - 344. The University of Chicago Press
- Efstathiou A., Tzanis A., Valliannatos F., (2015). " Evidence of non-extensivity in the evolution of seismicity along the San Andreas Fault, California, USA: An approach based on Tsallis statistical physics. *Physic and Chemistry of the Earth, Parts A/B/C*, doi:10.1016/j.pce.2015.02.013
- Efstathiou A., Tzanis A., Valliannatos F., (2016). " On the nature and dynamics of the seismogenetic systems of North California, USA: An analysis based on Non-Extensive Statistical Physics.
- Evans, M. D., (1966). "Man made earthquakes in Denver",*Geotimes*, 10, 11–18.
- Fletcher, R., and M. J. D. Powell (1963). "A rapidly convergent descent method for minimization",*Comput. J.*6,no. 2, 163–168, doi:10.1093/comjnl/6.2.16
- Fryer P., Mottl M. J., Phipps S., and Maekawa H. (1995). " Serpentine bodies in the forearcs of Western Pacific Convergent Margins; Origin and Associated Fluids, in *Active Margins*" Edited by Taylor B., and Natland J., pp 259 - 270, AGU Geophysical Monograph 88, American Geophysical Union, Washington DC.
- Funasaki, J. and Earthquake Prediction Information Division (2004). "Revision of the JMA Velocity Magnitude(in Japanese)", *Quart. J. Seis.*, 67, 11 – 20
- Geiger(1910). *Nachr.KoeniglichenGes. Wiss.Göttingen*, 4, 331pp.
- Gell - Mann, M. and Tsallis, C. (eds.), (2004)."*Nonextensive Entropy – Interdisciplinary Applications*". Oxford University Press, New York
- Goodchild M. F., (1980). " Fractals and the accuracy of the geographical measures", *Mathematical Geology* 12 85 - 98.
- Gutenberg, B., and Richter, C.F., (1944). "Frequency of earthquakes in California", *Bull. Seismol. Soc. Am.*, 34-4, 185-188
- Hainzl, S., and Y. Ogata (2005)."+A61Detecting fluid signals in seismicity data through statistical earthquake modeling", *J. Geophys. Res.*110B05S07, doi: 10.1029/2004JB003247.
- Hamada, N., A. Yoshida and H. Hashimoto (1983). "Improvement of the Hypocenter Determination Program of the Japan Meteorological Agency (Reanalyses of the Hypocenter Distribution of the 1980 Earthquake Swarm off the east coast of the Izu Peninsula and the Matsushiro Earthquake Swarm)" (in Japanese), *Quart. J. Seis.*, 48, 35 – 55

- Hasegawa A., Nakajima J., Umino N., and Miura S., (2005). "Deep structure of the northeastern Japan arc and its implications for crustal deformation and shallow seismic activity".
- Hashimoto, M. (ed), (1991). "Geology of Japan". Terra Scientific Publishing Company, Tokyo.
- Healy, J. H., W. W. Rubey, D. T. Griggs, and C. B. Raleigh, (1968). "The Denver earthquakes", *Science*, 161, 1301–1310.
- Helmstetter, A. and D. Sornette, (2003). "Importance of direct and indirect triggered seismicity in the ETAS model of seismicity", in press in *Geophys. Res. Lett.*
- Helmstetter, A., Y. Y. Kagan, and D. D. Jackson (2006). "Comparison of short-term and time-independent earthquake forecast models for Southern California", *Bulletin of the Seismological Society of America*, 96(1), 90–106, doi:10.1785/0120050067.
- Henderson, J.R., Barton, D.J. & Foulger, G.R., (1999). "Fractal clustering of induced seismicity in the Geysers geothermal area, California", *Geophys. J. Int.*, 139, 317–324
- Hirokawa O., T. Yoshida, I. Imai, N. Yamada, M. Hata, S. Iigi, M. Ishida, H. Isomi, T. Nozawa, K. Ono, A. Ozawa, T. Sakamoto, K. Tanaka, Y. Teraoka, K. Tsushima, S. Yamaguchi, C. Ono, and T. Enda (1978). "Geological Map of Japan, 1:1,000,000 (2nd Ed.)", Geological Survey, Japan.
- Ike, T., More, G., Okano, T., Kuramoto, S., Taira, A., (2004). "Along strike changes in basement topography and sediment thickness in the northern Shikoku Basin: Variable inputs to the Nankai Trough Seismogenic Zone", *EOS Transaction, American Geophysical Union*, vol. 85, Fall Meeting Supplements.
- Imoto, M., (1991). "Changes in the magnitude-frequency b-value prior to large ($M > 6.0$) earthquakes in Japan", *Tectonophysics*, 193, 311–325.
- Iwasaki, T., N. Hirata, T. Kanazawa, J. Melles, K. Suyehiro, T. Urabe, L. Moller, J. Makris, and H. Shimamura, (1990). "Crustal and upper mantle structure in the Ryukyu Island Arc deduced from deep seismic sounding", *Geophys. J. Int.*, 102, 631–651.
- Iwasaki, T., Yoshii, T., Ito, T., Sato, T., Hirata, N., (2002). "Seismological features of island arc crust as inferred from recent seismic expeditions in Japan". *Tectonophysics* 355, 53–66
- Kagan, Y.Y., 2002. Aftershock zone scaling, *Bull. Seismol. Soc. Am.*, 92 (2), 641-655.
- Katsumata, A. (2004). "Revision of the JMA Displacement Magnitude (in Japanese)", *Quart. J. Seis.*, 67, 1 – 10.
- Klaus A., Taylor B., Moore G. F., Murakami F., and Okamura Y., (1992) "Back - arc rifting in the Izu - Bonin Island Arc; Structural Evolution of Hachijo and Aoga Shima rifts" *The Island Arc*, 1, 16 - 31.
- Kirby, S., T. Okada, N. Uchida, A. Hasegawa, T. Matsuzawa, and R. Hino (2005), "Supraslab earthquakes above the Pacific-plate slab in NE Japan: A possible graveyard of detached seamounts and volcanic ridges?" *Eos Trans. AGU*, 86(52), Fall Meet. Suppl., S21C-06
- Kobayashi, K., (1985). "Sea of Japan and Okinawa Trough". In Nairn, A.E.M., Stehli, F.G., Uyeda, S., eds., *The Ocean Basins and Margins*, Vol. 1 A. Plenum, New York, pp. 419 - 458.
- Lavenda H. B., (1991). "Statistical Physics: A Probabilistic Approach"
- Lay T., and Wallace T. C., (1995). "Modern Global Seismology", Academic Press, San Deigo, CA.

- Lee, C.-S., Shor, G. G., Bibee, L. D., Lu, R. S., and Hilde, T. W. C. (1980). "Okinawa Trough: Origin as backarc basin". *Mar. Geology*, 35, pages 219–241
- Lombardi, A. M., M. Cocco, and W. Marzocchi (2010). "On the increase of background seismicity rate during the 1997 – 1998 umbria-marche, central Italy, sequence: Apparent variation or fluid - driven triggering?", *Bull.Seismol. Soc. Am.*,100, 1138–1152, doi:10.1785/0120090077
- Lomnitz-Adler J., Knopoff L., & Martinez-Mekler G., (1992)."Avalanches and epidemic models of fracturing in earthquakes", *Phys. Rev. A*, 45, 2211-2221.
- Michas, G., Vallianatos,F. and Sammonds, P., 2013. Non-extensivity and long-range correlations in the earthquake activity at the West Corinth rift (Greece), *Nonlinear Proc. Geoph.*, 20, 713-724
- Miller, M. S., Gorbatov, A., and Kennet, B. L. N. (2006). "Three- dimensional visualization of a near vertical slab tear beneath the southern Mariana arc" *Geochem. Geophys.Geosyst.*, 7 Q06012, doi:10.1029/2005GC001110 , 2006a.
- Mogi K., (1962). "Magnitude-frequency relation for elastic shocks accompanying fractures of various materials and some related problems in earthquakes", *Bull. Earthquake Res. Inst., Univ. Tokyo*, 40, pp. 831–853.
- Moré, J.J. and Sorensen, D.C., (1983). "Computing a Trust Region Step", *SIAM Journal on Scientific and Statistical Computing*, 3, 553–572.
- Musmeci, F., and D. Vere-Jones (1986). "A variable-grid algorithm for smoothing clustered data", *Biometrics* ,42,483–494.
- Nakamura K., Shimazaki N., and Yonekura A., (1984)." Subduction, bending and eduction - Present and Quaternary tectonics of the northern border of the Philippine Sea Plate", *Bulletine of SocieteGeologie de France*, v. 26, p. 221 - 243.
- Nakamura M, Umedu N (2009). "Crustal thickness beneath the Ryukyu arc from travel-time inversion". *Earth Planet Space*, 61: 1191–1195. 10.1186/BF03352971
- Nakamura, M., Yoshida, Y., Zhao, D., Katao, H., Nishimura, S., (2003). "Three-dimensional P- and S-wave velocity structures beneath the Ryukyu arc". *Tectonophysics* 369, 121–143.
- Ogata Y., (2011). "Significant improvements of the space - time ETAS model for forecasting of accurate baseline seismicity".*Earth Planets Space*, 63, 217–229, 2011
- Ogata, Y. (1998). "Space-time point-process models for earthquake occurrences", *Ann. Inst. Stat. Math.*50,no. 2, 379–402, doi:10.1023/A:1003403601725.
- Ogata, Y., (1988). "Statistical models for earthquake occurrences and residual analysis for point processes", *J. Am. Statist. Assoc.*, 83, 9–27
- Ogata, Y., and J. Zhuang (2006). "Space-time ETAS models and an improved extension "Tectonophysics,413(1-2),13–23
- Okada Y., Kasahara K., Hori S., Obara K., Sekiguchi S., Fujiwara H., and Yamamoto A., (2004). "Recent progress of seismic observation networks in Japan —Hi-net, F-net, K-NET and KiK-net—", *Earth Planets Space*, 56, xv - xxviii.

- Okada, T., T. Matsuzawa, and A. Hasegawa (2003), Comparison of source areas of M4.8+–0.1 earthquakes off Kamaishi, NE Japan—Are asperities persistent feature? *Earth Planet. Sci. Lett.*, 213, 361–374.
- Okada, T., K. Sakoda, T. Matsuzawa, R. Hino, A. Hasegawa, S. Sakai, and T. Kanazawa (2004), Characteristic seismic activity in the subducting plate boundary zone off Kamaishi, northeastern Japan, revealed by precise hypocenter distribution analysis using ocean-bottom seismometers, *Geophys. Res. Lett.*, 31, L19604, doi:10.1029/2004GL020366.
- Okumura K., R. Imura, T. Imaizumi, M. Togo, H. Sawa, K. Mizuno, Y. Kariya (1998). "Recent surface faulting events along the northern part of the Itoigawa-Shizuoka tectonic line: trenching survey of the Kamishiro Fault and East Matsumoto basin faults, central Japan", *J. Seismol. Soc. Jpn. (Zisin)*, 50, pp. 35–51
- Pacheco, J. F., Scholz, C. H. & Sykes, L. R. (1992). "Changes in frequency size relationship from small to large earthquakes", *Nature* 355, 71–3.
- Papadakis, G., Vallianatos, F. and Sammonds, P., 2013. Evidence of Nonextensive Statistical Physics behaviour of the Hellenic Subduction Zone seismicity, *Tectonophysics*, 608, 1037–1048.
- Papadakis, G., Vallianatos, F. and Sammonds, P., 2015. A Nonextensive Statistical Physics Analysis of the 1995 Kobe, Japan Earthquake, *Pure and Applied Geophysics*, 172 (7), 1923–1931.
- Parsons, T., Segou, M. and Marzocchi, W., 2014. The global aftershock zone, *Tectonophysics*, 618, 1–34; doi: 10.1016/j.tecto.2014.01.038
- Picard, R. R., and Cook, R. D. (1984). "Cross-Validation of Regression Models," *Journal of the American Statistical Association*, 79, 575–583
- Plastino A., Plastino A. R., (1994). "From Gibbs microcanonical ensemble to Tsallis generalized canonical distribution", *Phys. Lett. A* 193 (1994) 140
- Rundle J. B., Klein, W., Gross, S. & Turcotte, D. L. (1995). "Boltzmann fluctuations in numerical simulations of nonequilibrium lattice threshold systems", *Phys. Rev. Lett.* 75, 1658–61.
- Scholz C.H., (1968). "The frequency-magnitude relation of microfracturing in rock and its relation to earthquakes", *Bull. Seismol. Soc. Am.*, 58, pp. 399–415
- Seno T., (1977). "The instantaneous rotation vector of the Philippine Sea plate relative to the Eurasian Plate", *Tectonophysics*, 42, 209 - 226.
- Shiomi, K., Obara, K. & Sato, H., (2006). "Moho depth variation beneath southwestern Japan revealed from the velocity structure based on receiver function inversion", *Tectonophysics*, 420, 205–221.
- Sotolongo - Costa O., and Posadas A., (2004). "Tsallis's entropy: A non - extensive frequency - magnitude distribution of earthquakes". *Phys. Rev. Letters*, 92 (4), 048501; doi:10.1103/PhysRevLett.92.048501
- Steihaug, T., (1983). "The Conjugate Gradient Method and Trust Regions in Large Scale Optimization", *SIAM Journal on Numerical Analysis*, 20, 626–637.

Stern R. J., Fouch M. J., and Klemperer S. L., (2003). "An overview of the Izu - Bonin - Mariana subduction factory. In: Eiler L. (ed.) *Insid+ A44e the Subduction Factory*. American Geophysical Union, Washington DC, Geophysical Monograph 138, 175 - 222.

Suyehiro S. T. Asada and M. Ohtake, (1964). "Foreshocks and Aftershocks accompanying a perceptible earthquake in central Japan". *Paper Meteorol. Geophys.* 15, 17-88.

Taira, A., (2001). "Tectonic evolution of the Japanese island arc system". *Annual Rev. Earth & Planet Sci.* 29, 109-134.

Tamarit F.A., Anteneodo C., (2005). "Relaxation and aging in long - range interacting systems, in *Nonextensive Statistical Mechanics*". *New Trends, New perspectives*, In: Boon, J.P., Tsallis C., (eds.) *Europhysics News* 36, 194 (2005) 24.

Taylor R. N., Klaus A., Brown G. R., Moore G. F., Okamura Y., and Murakami F. (1991). "Structural development of Sumisu Rift, Izu - Bonin Arc, *J. Geophys. Res.*, 96, 113 - 129.

Telesca, L., (2011). "Tsallis - based nonextensive analysis of the Southern California seismicity". *Entropy*, 13, 1267-1280.

Telesca, L., (2012). "Maximum Likelihood Estimation of the Nonextensive Parameters of the Earthquake Cumulative Magnitude Distribution". *Bull. Seismol. Soc. Am.*, 102, 886-891.

Theiler J., (1990). "Statistical Precision of Dimension Estimators", *Phys. Rev. A*, 41, 3038 - 3051

Tsallis C., (1988). "Possible generalization of Boltzmann - Gibbs statistics". *Journal of Statistical Physics*, 52(1-2), 479-487.

Tsuboi, C. (1954). "Determination of the Gutenberg-Richter's magnitude of shallow earthquakes occurring in and near Japan (in Japanese)", *Zisin* 2, 7, 185 - 193.

Turcotte D. L. and Glasscoe M. T., (2004). "A damage model for the continuum rheology of the upper continental crust", *Tectonophysics*, 383, 71

Turcotte D. L., (1993). "Fractal tectonics and erosion", *Fractals* 1, 491-512.

Turcotte D. L., (1994a). "Crustal deformation and fractals, a review, in *Fractals and Dynamic Systems in Geoscience*", J. H. Kruhl, ed., pp. 7-23, Springer-Verlag, Berlin.

Turcotte D. L., (1995). "Scaling in geology: Landforms and earthquakes". *Proc. Natl. Acad. Sci. USA*, 92, 6697-704.

Turcotte D.L., (1997). "Fractals and Chaos in Geology and Geophysics". Second Edition, Cambridge University Press, Cambridge, 398 p.

Tzani A. and Makropoulos K., (2002). "Did the 7/9/1999 M5.9 Athens Earthquake Come with a Warning?", *Natural Hazards* 27: 85-103/

Tzani A., Vallianatos F., and Efstathiou A., (2013). "Interdependence of Magnitude, interevent time and interevent distance in North California". *Bul. Of the Geological Society of Greece*, vol. XLVII 2013

Uchida N., Kirby S. H., Okada T., Hino R., Hasegawa A., (2010). "Supraslab earthquake clusters above the subduction plate boundary offshore Sanriku, northeastern Japan: Seismogenesis in a graveyard of detached seamounts?". *Journal of Geophysical Research*. doi: 10.1029/2009JB006797

- Ueno, H., S. Hatakeyama, T. Aketagawa, J. Funasaki and N. Hamada (2002). "Improvement of hypocenter determination procedures in the Japan Meteorological Agency (in Japanese)", *Quart. J. Seis.*, 65, 123 – 134.
- Vallianatos, F. and Sammonds, P., (2013). "Evidence of non-extensive statistical physics of the lithospheric instability approaching the 2004 Sumatran-Andaman and 2011 Honshu mega-earthquakes", *Tectonophysics* doi:0.1016/j.tecto.2013.01.009
- Vallianatos, F. and Telesca, L. (Eds.), 2012. *Statistical Mechanics in Earth Physics and Natural Hazards*, *Acta Geophysica*, 60, 499–501.
- Vallianatos, F., Michas, G., Papadakis, G. and Tzanis, A., (2013). "Evidence of non- extensivity in the seismicity observed during the 2011–2012 unrest at the Santorini volcanic complex, Greece". *Nat. Hazards Earth Syst. Sci.*, 13, 177–185;0.5194/nhess-13-177-2013.
- Vallianatos, F., Michas, G., Papadakis, G., Sammonds, P., (2012). "A non - extensive statistical physics view to the spatiotemporal properties of the June 1995, Aigion earthquake (M6.2) aftershock sequence (West Corinth rift, Greece)". *ActaGeophysica* , 60, 3, 758-768.
- Vere-Jones, D. (2005). "A class of self-similar random measure, *Advances in Applied Probability*", 37(4), pp. 908–914
- Wageman, J.M., Hilde T. W. C., and Emery K.O., (1970). "Structural framework of the East China Sea and Yellow Sea", *Am. Assoc. Petrol. Geol. Bull.*, 54, 1611-1643.
- Wang, J. H., (1988). "b-values of shallow earthquakes in Taiwan", *Bull. Seismol. Soc. Am.*, 78, 1243–1254.
- Warren N.W. and Latham G.V., (1970). "An experimental study of thermally induced microfracturing and its relation to volcanic seismicity", *J. Geophys. Res.*, 75, pp. 4455–4464.
- Wehrl A., (1978). "General Properties of Entropy". *Reviews of Modern Physics*, 50, 221-260.
- Wiemer S., and Wyss M., (2000). "Minimum magnitude of complete reporting in earthquake catalogs: Examples from Alaska, the western United States, and Japan", *Bull. Seismol. Soc. Am.* 90, 859–869.
- Wiemer, S., 2001. A software package to analyse seismicity: ZMAP, *Seismol. Res. Lett.*, 72 (2), 374-383.
- Wyss, M., Sammis, C.G., Nadeau, R.M. & Wiemer, S., (2004). "Fractal dimension and b-value on creeping and locked patches of the San-Andreas fault near Parkfield, California", *Bull. seism. Soc. Am.*, 94, 410–421
- Wyss, M., (1973). "Towards a physical understanding of the earthquake frequency distribution", *J. R. Astron. Soc.*, 31, 341–359.
- Yeats R., 2013. *Active Faults of the World*, Cambridge University Press.
- Yoshii, T., (1994). "Crustal structure of the Japanese islands revealed by explosion seismic observations". *Zisin* 46, 479–491 (in Japanese with English abstract).
- Yoshimoto, K. et al., (2004). "Moho and Philippine Sea plate structure beneath central Honshu Island, Japan, from teleseismic receiver function", *EarthPlanets Space*, 56, 1271–1277.

Yuasa M., and Nohara M. (1992). " Petrographic and geochemical along - arc variations of volcanic rocks on the volcanic front of the Izu - Ogasawara (Bonin) Arc", Bull. Geol. Surv. Japan, 43, 421 - 426.

Zhuang J., (2011). "Next - day earthquake forecasts for the Japan region generated by the ETAS model". Earth Planets Space, 63, 207–216, 2011

Zhuang, J., (2006). "Second-order residual analysis of spatiotemporal point processes and applications in model evaluation", Journal of the Royal Statistical Society: Series B (Statistical Methodology) ,68(4), 635–653, doi:10.1111/j.1467-9868.2006.00559.x.

Zhuang, J., Y. Ogata, and D. Vere-Jones (2004). "Analyzing earthquake clustering features by using stochastic reconstruction",Journal of Geophysical Research,B5(3), B05,301, doi:10.1029/2003JB002879.

Zhuang, J., (2012). "Long-term earthquake forecasts based on the epidemic-type aftershock sequence (ETAS) model for short-term clustering". Research in Geophysics, 22, e6. doi:10.4081/rg.2012.e8.

Zhuang, J., A. Christophosen, M. K. Savage, D. Vere-Jones, Y. Ogata, and D. D. Jackson (2008). "Differences between spontaneous and triggered earthquakes: their influences on foreshock probabilities",Journal of Geophysical Research,113, B11,302, doi:10.1029/2008JB005579